STUDIES OF GEOLOGIC STRUCTURES WITH THE VLF METHOD

AUTHOR: WARREN FRANK KING

TITLE: STUDIES OF GEOLOGIC STRUCTURES WITH THE VLF METHOD

DEPARTMENT: MINING ENGINEERING AND APPLIED GEOPHYSICS

DEGREE: MASTER OF SCIENCE

ABSTRACT

Very Low Frequency (17.8 KHz) electromagnetic measurements were made with the Geonics EM-16 over several faults (including the Gloucester fault) southeast of Ottawa, and over the Smoky Creek and Lois Lake faults in the Noranda area. Magnetotelluric (wave impedance) measurements on many of the profiles substantiate the EM-16 anomalies. The field results compare favourably with theoretical profiles over vertical two-dimensional contacts.

The investigation indicates that, in many cases, the Geonics EM-16 is a convenient tool to map faults, shear zones, contacts, and other broad two-dimensional features concealed beneath overburden.

Studies in geologic structures with the VLF method

by Warren King

A thesis submitted to the Faculty of Graduate Studies and Research in partial fulfilment of the requirements for the degree of

MASTER OF SCIENCE

Department of Mining Engineering and Applied Geophysics McGill University.

July 1971

ACKNOWLEDGEMENTS

W.M. Telford, is gratefully acknowledged. In addition to his guidance, Professor Telford reviewed the manuscript and made valuable suggestions. Special thanks are due to Dr. A. Becker, of the Geological Survey of Canada, who first conceived of this investigation, and who provided assistance and advice throughout its duration. The theoretical profiles in Chapter III were run on a computer program developed by J.A. Slankis. Helpful discussions were held with L.S. Collett and W.J. Scott. The field work was carried out during the summers of 1969 and 1970, while the author was a graduate assistant with the Geological Survey of Canada.

TABLE OF CONTENTS

		•		
ABS	ABSTRACT			
ACKI	ACKNOWLEDGEMENTS			
TABI	TABLE OF CONTENTS			
I	INTF	RODUCTION	1	
	1.1	General Considerations	ĺ	
	1.2	Historical Background	2	
	1.3	Purpose of Project	6	
II	THEO	DRY	7	
	2.1	Wave Impedance Concepts	7	
	2.2	Maxwell's Equations for Two-Dimensional Structures	12	
		(i) "H Parallel" or "E Perpendicular" Polarization	13	
		(ii) "E Parallel" or "H Perpendicular" Polarization	15	
	2.3	The Polarization Ellipse	20	
III		RETICAL PROFILES OVER TWO-DIMENSIONAL ICAL CONTACTS	27	
	3.1	Method	27	
	3.2	Results	31	
IV	INST	RUMENTS	60 ·	
	4.1	Geonics EM-16	60	

4.2 Westinghouse VLF Wave Impedance Meter.....

V	FIEI	D WOR	K	67
	5.1	Leitr	rim and Russell Areas	67
		(i)	Location and Description of Faults Traversed	67
		(ii)	Description of Geologic Formations	70
		(iii)	Field Procedures	71
	5.2	Noran	nda Area	72
VI	RESU	LTS OF	FIELD WORK	78
	6.1	Leitr	im Area	78
		(1)	Geonics EM-16 Profiles Across Gloucester Fault	78
		(11)	Wave Impedance Profiles Across Gloucester Fault	82
		(iii)	Discussion of Results	92
	6.2	Russe	ll Area	95
		(i)	Geonics EM-16 and Wave Impedance Profiles	96
		(ii)	Discussion of Results	152
	6.3	Noran	da Area	156
		(i)	Geonics EM-16 and Wave Impedance Profiles Across the Smoky Creek Fault	156
		(11)	Geonics EM-16 and Wave Impedance Profiles Across the Lois Lake Fault	177
		(iii)	Discussion of Results	201

-	١
3	
44	,

VII CONC	LUSI	ONS	203
BIBLIOGRA	PHY.	••••••	206
APPENDIX	I-	Conversion of Wave Impedance Dial Reading to Apparent Conductivity	208
APPENDIX	II-	Conversion of Phase Dial Reading to Phase Angle Between $\mathbf{E}_{\mathbf{y}}$ and $\mathbf{H}_{\mathbf{x}}$	210
APPENDIX	III-	DC Resistivity Depth Sounding Profiles for the Smoky Creek Area (Wenner Array)	212

CHAPTER I

INTRODUCTION

1.1 General Considerations

There is a need for geophysical methods to trace faults, contacts, and marker beds in regions that are extensively covered with overburden. All geophysical methods depend upon contrasts in the physical properties of the rocks and minerals involved. A unique and often uniform property of a rock unit is its electrical conductivity. A method capable of detecting conductivity contrasts would therefore be useful in the geologic mapping of faults and contacts, provided such a contrast existed. Such a technique is that of electromagnetic induction.

In electromagnetic induction prospecting methods an alternating primary magnetic field is generated by passing alternating current through a coil or along a long wire. This field is measured with a receiver consisting of a coil connected to an electronic amplifier, meter, or potentiometer bridge. In the absence of conducting zones an insignificant eddy-current field is induced in the ground. If a conductive zone is present, stronger eddy-currents may circulate within it and a secondary magnetic field will be created. If it is large enough, the secondary field may be

detected by the receiver in the presence of the primary field. Prospecting for these conductive zones is carried out by systematically traversing the ground, either with the receiver unit alone or with the source and receiver in combination, depending upon the system employed.

1.2 Historical Background

Since 1957 the United States Geological Survey has been using electromagnetic methods to trace conductive strata beneath glacial drift in Minnesota, Wisconsin and Maine (Frischknecht, 1966), with the object of developing techniques that can be used in mapping bedrock geology in areas of extensive glacial drift or thick residual soil. In most of the studies the horizontal loop (slingram) method was used.

Electromagnetic conductors in metamorphic terrains of Minnesota, Wisconsin, and Maine commonly contain such metallic minerals as specular hematite, various sulphides and graphite (Frischknect and Ekren, 1960). The work done by the U.S.G.S. is concerned with lithologic units that contain concentrations of conductive minerals. Conductive beds comprise only a small part of the total volume of rocks in the areas studied, but they are sufficiently continuous and numerous to be used in tracing bedrock geology.

Electromagnetic methods proved to be a valuable supplement to conventional geologic mapping in northern Maine, where many conductive black slates and black cherts occur in

rocks of lower Paleozoic age (Frischknect, 1966). Black slate zones were traced over distances of several miles by horizontal loop surveys. Most of the black slate zones were highly anisotropic, and both the thickness and conductivity of the zones varied considerably along strike. Black chert zones were also found to be conductive, and several of these were successfully traced for distances up to several miles.

Geophysical mapping of this type was a very useful supplement to surface geologic information. The association of these conductive beds with other rock units such as greywacke, meta-volcanics, siltstone, quartzite, and conglomerate was known, and this permitted extrapolation of outcropping units.

In October of 1967 A. Becker of the Geological Survey of Canada conducted a profile across the Gloucester fault (a fault occurring in Paleozoic sediments) in the vicinity of Leitrim, Ontario using the horizontal loop method. An almost undiscernible response was obtained (Becker, 1970). It must be stressed that for this method to be successfully applied in areas that are covered with overburden, relatively thin horizons of anomalously high conductivity must be present, since the horizontal loop method is not intended to respond to a broad, two-dimensional conductivity contrast such as a fault or other contact. What

is needed is a method which employs a large scale uniform primary magnetic field and a relatively simple receiver, such as the AFMAG method or the VLF method.

The AFMAG method utilizes naturally occurring electromagnetic radiation in the audio frequency range, of which the primary source is atmospheric electrical discharges that occur on a worldwide basis. AFMAG (audio frequency magnetics) is essentially a dip-angle system with the source located at infinity. The nature of the AFMAG fields has been described in detail by Ward et al. (1958) and Ward (1959) while Sutherland (1967) gives a brief description of ground and airborne AFMAG equipment currently in use.

Normally the magnetic field is horizontally polarized, but as a conductor or contact is approached, the plane of polarization is tilted out of the horizontal. By measuring the tilt angle of the magnetic field, it is possible to locate subsurface features.

In 1958 an extensive airborne AFMAG survey was flown in the Lake Abitibi - Noranda area of N.W. Quebec. Shaw (1961, 1962) observed many "fault and shear type AFMAG responses". There was excellent correlation between these responses and the known faults in the area. In particular, the Lois Lake, Manneville, Smoky Creek, Hunter, and Porcupine-Destor faults are well defined by the AFMAG survey, although the Porcupine-Destor fault has a complex anomaly

pattern in certain places due to powerline interference. The well-known Cadillac, Horne, Here, and Davidson faults also fall within areas of strong powerline interference, and responses over these zones cannot be considered reliable.

Upon reviewing this survey and several others, Collett (1967) concludes that the AFMAG technique appears to be very useful for broad reconnaissance mapping of geological features, and states that at least one major exploration company is using AFMAG to map structural features such as faults and shear zones.

In 1966 the Geological Survey of Canada made some trial measurements to determine if VLF waves could be used to map geologic structure (Collett, 1967). Becker conducted a VLF profile across the Gloucester fault and obtained a good response which clearly indicated the presence of the fault (Becker, 1967). This profile can be regarded as the basis for the present study, and the VLF technique will be subsequently described in detail.

It is interesting to note that J. Slankis (also working for the G.S.C. at the tim e) conducted telluric current surveys across the same fault at various times in the spring and summer of 1966, 1967 and 1968. Large, extraneous phase shifts, thought to be due to local power sources, rendered the results largely uninterpretable (Slankis, 1969).

Further discussions of electromagnetic mapping

techniques may be found in Sutherland (1967) and Collett (1967).

1.3 Purpose of the Project

At the outset, the main purpose of the project was to investigate the response of a VLF (Geonics EM-16) electromagnetic unit across the Gloucester fault. These results were to be correlated with wave impedance measurements made across the same fault. Some of the faults in the Noranda area (namely the Smoky Creek, Hunter Creek, and Lois Lake faults) were also to be surveyed, with the hope that the method would prove suitable for tracing faults and similar large scale contacts concealed beneath overburden.

CHAPTER II

THEORY

2.1 Wave Impedance Concepts

1

The magnetotelluric method utilizes the boundary conditions forced on the electric and magnetic fields when an EM wave propagating through air interacts with the earth's surface. The essential measurement is the electromagnetic wave impedance (the ratio of the electric field to the magnetic field, E/H) at the surface. For a homogeneous (or layered) earth, the horizontal electric field is related only to the orthogonal magnetic field, and the impedance is a complex scalar. A homogeneous earth geometry will therefore be considered in developing the basic magnetotelluric relationships from Maxwell's equations:

$$\overline{\nabla} \times \overline{E} = -\frac{\partial \overline{B}}{\partial t}$$
 (2-1)

$$\overline{\nabla} \times \overline{H} = \overline{J} + \frac{\partial \overline{D}}{\partial t}$$
 (2-2)

$$\overline{\nabla} \cdot \overline{D} = \rho = 0$$
 (2-3)

$$\overline{\nabla} \cdot \overline{B} = 0$$
 (2-4)

where $\overline{J} = \sigma \overline{E}$, $\overline{D} = \varepsilon \overline{E}$, $\overline{B} = \mu \overline{H}$

and:

 \overline{E} = the electric field intensity in volts per meter

B = the magnetic induction in webers per square meter

 \bar{H} = the magnetic field intensity in ampere-turns per meter

 \hat{J} = the electric current density in amperes per square meter

 \overline{D} = the electric displacement in coulombs per square meter

 ρ = the volume charge density in coulombs per cubic meter

 σ = the electrical conductivity in mhos per meter

 ε = the permittivity in farads per meter

 μ = the permeability in henrys per meter

By assuming e time dependence, these equations reduce to:

$$\nabla \times \hat{E} = i\omega u \hat{H}$$

$$\nabla \times \widetilde{H} = \sigma \widetilde{E} - i\omega \varepsilon \widetilde{E}$$

Combining these we get the vector Helmholtz equation:

$$\nabla^2 \vec{E} + k^2 \vec{E} = 0$$

$$\nabla^2 \widehat{H} + k^2 \widehat{H} = 0$$

where $k^2 = i\omega\mu\sigma + \varepsilon\mu\omega^2$

The solutions are
$$\widehat{E} = e^{i(k_x x + k_y y + k_z x)}$$

and $\widehat{H} = e^{i(k_x x + k_y y + k_z x)}$

where $k^2 = k_{\chi}^2 + k_{\gamma}^2 + k_{\hat{\epsilon}}^2$

In EM propagation in the earth at frequencies employed by the VLF method (\simeq 20 KHz), the conduction current term (iwµ σ) is much greater than the displacement current term, and the Helmholtz equation becomes the vector diffusion equation.

The solution is a damped wave, which decays exponentially with depth, the decay depending upon conductivity and frequency. The skin depth is that depth at which the fields fall to 1/e of the surface value and is given by $\delta=\sqrt{2/\mu\omega\sigma}$. A useful approximation to the skin depth is given by

$$\delta = 500 \sqrt{\rho/f}$$

where δ is in meters

 $\mu = \mu_a = 4\pi \times 10^{-7}$ henrys per meter

ρ is in ohm meters

σ is in mhos per meter

f is in hertz

This affords a qualitative estimate of the effective depth of penetration.

The propagation constant in the ground is much greater than that in the air:

$$k_{air}^{z} = \mu \epsilon \omega^{z} \simeq \mu_{o} \epsilon_{o} \omega^{z}$$

$$k_{\text{earth}}^{2} = i\omega\mu\sigma >> k_{\text{air}}^{2}$$

The earth therefore has a high refractive index with respect to the air, and incident waves will be refracted almost straight down, regardless of the angle of incidence (Swift, 1967).

The calculation of wave impedance at the earth's surface is straightforward and is given for two polarizations. These are the "E horizontal" polarization, when the electric vector is parallel to the ground and is polarized in the y direction, and the "H horizontal" polarization, when the magnetic vector is parallel to the ground and is polarized in the y direction. Both of these waves will propagate in the x-z plane.

For an incident "E horizontal" wave: $E^{\mathbf{I}} = E_{v}^{\mathbf{I}} e^{\pm i (\mathbf{k}_{x_a} x + \mathbf{k}_{\xi_a} \xi)}$

The refracted (transmitted) wave is given by:

$$E^{\mathsf{T}} = E_{\mathsf{V}} e^{\pm i \left(\mathsf{K}_{\mathsf{X}_{\mathsf{Z}}} \times + \mathsf{K}_{\mathsf{Z}_{\mathsf{Z}}} \right)}$$

where $k_{\mathbf{x}}^{2} = k_{\mathbf{x}_{\mathbf{x}}}^{2} + k_{\mathbf{y}_{\mathbf{x}}}^{2} + k_{\mathbf{z}_{\mathbf{x}}}^{2}$ and $k_{\mathbf{x}}^{2} = k_{\mathbf{x}_{\mathbf{x}}}^{2} + k_{\mathbf{y}_{\mathbf{x}}}^{2} + k_{\mathbf{z}_{\mathbf{x}}}^{2}$ are the propagation constants in the air and ground respectively. If the horizontal wavelength is much greater than the skin depth in the earth (as is normally the case at VLF frequencies), then $k_{\mathbf{x}_{\mathbf{y}}}^{2} + k_{\mathbf{y}_{\mathbf{x}}}^{2} << k_{\mathbf{z}_{\mathbf{x}}}^{2}$, so $k_{\mathbf{z}_{\mathbf{x}}}^{2} \simeq k_{\mathbf{y}}^{2}$ (Madden and Swift, 1969). In this case the refracted wave is given by:

$$E^{\mathsf{T}} = E_{\mathsf{y}}^{\mathsf{T}} e^{\pm i \, k_{\mathsf{d}_{\mathsf{g}}} \mathsf{Z}}$$

The associated magnetic field is found by taking the curl of \mathbf{E}^{T} according to equation (2-1).

$$H_X^T = \frac{k_2}{\mu\omega} E_y^T$$

The wave impedance is obtained from:

$$\eta = \frac{E_y}{H_x} = \frac{\mu \omega}{k_{z_z}}$$

where $k_{\ell}^{2} = i\omega\mu\sigma$

Similarly for an "H horizontal" wave:

$$H^{T} = H_{V}^{T} e^{\pm i (k_{x_{a}} x + k_{z_{a}} z)}$$

The refracted wave is $H^{T} = H_{y}^{T} e^{\pm i (k_{x} \times + k_{t} + k_{t})}$

From equation (2-2), making the same long wavelength approximation as before, the associated electric field is:

$$E_{x}^{T} = \frac{1k_{1}}{\sigma} H_{y}^{T}$$

The impedance is given by $\eta = -\frac{E_x}{H_v} = \frac{-ik_z}{\sigma}$

For sources with relatively long wavelengths, the E parallel and H parallel impedances are equal, and the impedance for a homogeneous halfspace is isotropic (Swift, 1967). This impedance is $\eta = \frac{\mu\omega}{k_2} = -\frac{ik_2}{\sigma} = \sqrt{-i\mu\omega/\sigma}$.

The resistivity is obtained from the impedance by the relation:

$$\rho = - \frac{1}{100} \eta^2$$

This formulation is valid for a homogeneous half-space and for horizontally layered media, in which the problem is one-dimensional.

2.2 Maxwell's Equations for Two-Dimensional Structures

There are many features which cannot be described by horizontal layers of contrasting conductivity; numerous important geological structures are, in fact, two dimensional. These include faults, shear zones, and dikes in which the strike length is large compared to the skin depth. Maxwell's equations will now be formulated utilizing the geometry of Fig. 2.1, with the y axis as the strike direction, and the z axis positive downwards. The two polarizations are once again considered separately.

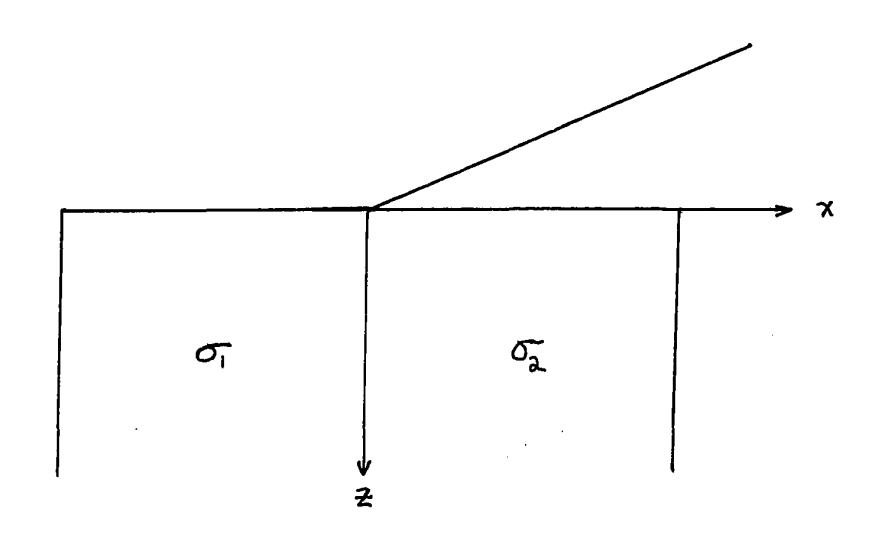


Fig. 2.1 Two-Dimensional Fault with Strike Length Infinite in y Direction

(i) "H Parallel" or "E Perpendicular" Polarization The source field varies as $e^{\frac{i}{k_y} \psi - \omega t}$ along strike. For this polarization $\widetilde{E} = (E_x, E_z)$ $e^{\frac{i}{k_y} \psi - \omega t}$ and $E_y = 0$.

$$\nabla \times \overline{E} = \hat{X} \left(\frac{\partial E_z}{\partial y} - \frac{\partial E_y}{\partial z} \right) - \hat{Y} \left(\frac{\partial E_z}{\partial x} - \frac{\partial E_x}{\partial z} \right) + \hat{Z} \left(\frac{\partial E_y}{\partial x} - \frac{\partial E_x}{\partial y} \right)$$

$$= -\frac{\partial \overline{B}}{\partial t}$$

$$\overline{B} = (B_x, B_y, B_z) e^{i(k_y y - \omega t)}$$
and
$$-\frac{\partial \overline{B}}{\partial t} = (i \omega B_x + i \omega B_y + i \omega B_z) e^{i(k_y y - \omega t)}$$

so
$$\frac{\partial E_{x}}{\partial z} - \frac{\partial E_{z}}{\partial x} = i \omega B_{y} = i \mu \omega H_{y}$$
 (2-5)

$$i k_{y} E_{z} = i \mu w H_{x}$$

$$H_{x} = \frac{k_{y}}{\mu w} E_{z} \qquad (2-6)$$

$$-\frac{\partial N}{\partial E^{X}} = i w B^{2}$$

$$i k_{y} E_{x} = -i \mu \omega H_{z}$$

$$H_{z} = -\frac{k_{y}}{\mu \omega} E_{x} \qquad (2-7)$$

$$\nabla \times \overline{H} = \hat{\pi} \left(\frac{\partial H_z}{\partial y} - \frac{\partial H_y}{\partial z} \right) - \hat{y} \left(\frac{\partial H_z}{\partial x} - \frac{\partial H_x}{\partial z} \right) + \hat{z} \left(\frac{\partial H_y}{\partial x} - \frac{\partial H_x}{\partial y} \right)$$

$$\overline{T} = \sigma \overline{E}_x + \sigma \overline{E}_z$$
So
$$\frac{\partial H_z}{\partial x} - \frac{\partial H_y}{\partial z} = 0 \qquad (2-8)$$

$$\frac{\partial H_z}{\partial y} - \frac{\partial H_y}{\partial z} = \sigma \overline{E}_x$$

$$i \, k_y \, H_z - \frac{\partial H_y}{\partial z} = \sigma \overline{E}_z \qquad (2-9)$$

$$\frac{\partial H_y}{\partial x} - \frac{\partial H_x}{\partial y} = \sigma \overline{E}_z \qquad (2-10)$$

$$\frac{\partial H_y}{\partial x} - i \, k_y \, H_x = \sigma \overline{E}_z$$

Substituting (2-7) into (2-9) and (2-6) into (2-10) to eliminate $H_{\rm x}$ and $H_{\rm z}$:

$$-\frac{i k_{y}^{2}}{\mu w} E_{x} - \frac{\partial H_{y}}{\partial z} = \sigma E_{x}$$

$$\frac{\partial H_{y}}{\partial z} = -\left(\frac{i k_{y}^{2}}{\mu w} + \sigma\right) E_{x} \qquad (2-11)$$

$$\frac{\partial H_{y}}{\partial x} - \frac{i k_{y}^{2}}{\mu w} E_{z} = \sigma E_{z}$$

$$\frac{\partial H_{y}}{\partial x} = \left(\sigma + \frac{i k_{y}^{2}}{\mu w}\right) E_{z} \qquad (2-12)$$

Equations 2-5, 2-11, and 2-12 represent a set of equations for E_x , E_z , and H_y . For wavelengths much longer than the skin depth, k_y = 0 and 2-11 and 2-12 reduce to:

$$\frac{\partial H_{\gamma}}{\partial \tau} = -\sigma E_{\gamma} \qquad (2-13)$$

$$\frac{\partial H_{Y}}{\partial x} = \sigma E_{\pm} \qquad (2-14)$$

(ii) "E Parallel" or "H Perpendicular" Polarization $\frac{i\left(k_{\gamma}\gamma-\omega t\right)}{i\left(k_{\gamma}\gamma-\omega t\right)}$ The source field again varies as e along strike. $H=\left(H_{\chi},\ H_{Z}\right)\text{ e}^{i\left(k_{\gamma}\gamma-\omega t\right)}\text{ and }H_{\gamma}=0.$

$$\nabla \times \overline{H} = \hat{x} \left(\frac{\partial H_2}{\partial y} - \frac{\partial H_{yy}}{\partial z} \right) - \hat{y} \left(\frac{\partial H_2}{\partial x} - \frac{\partial H_{x}}{\partial z} \right) + \hat{z} \left(\frac{\partial H_{yy}}{\partial x} - \frac{\partial H_{x}}{\partial y} \right)$$

$$= \sigma \cdot \overline{E}_x + \sigma \cdot \overline{E}_y + \sigma \cdot \overline{E}_z$$
so
$$\frac{\partial H_x}{\partial z} - \frac{\partial H_z}{\partial x} = \sigma \cdot \overline{E}_y \qquad (2-15)$$

$$i k_{y} H_{z} = \sigma E_{x}$$

$$E_{x} = \underbrace{i k_{y}}_{\sigma} H_{z} \qquad (2-16)$$

$$E_{\pm} = -\frac{i k_{y}}{\sigma} H_{x} \qquad (2-17)$$

$$\nabla \times \hat{E} = \hat{x} \left(\frac{\partial E_{x}}{\partial y} - \frac{\partial E_{y}}{\partial z} \right) - \hat{y} \left(\frac{\partial E_{x}}{\partial x} - \frac{\partial E_{x}}{\partial z} \right) + \hat{z} \left(\frac{\partial E_{y}}{\partial x} - \frac{\partial E_{x}}{\partial y} \right)$$

$$= -\frac{\partial \hat{B}}{\partial x}$$

$$-\frac{\partial \hat{B}}{\partial x} = \left(i \omega B_{x} + i \omega B_{z} \right) e^{i \left(k_{y} y_{y} - \omega t \right)}$$

$$\hat{E} = \left(E_{x}, E_{y}, E_{z} \right) e^{i \left(k_{y} y_{y} - \omega t \right)}$$

$$\frac{\partial E_{z}}{\partial y} - \frac{\partial E_{y}}{\partial z} = i \omega B_{x}$$

$$i k_{y} E_{z} - \frac{\partial E_{y}}{\partial z} = i \omega B_{z}$$

$$\frac{\partial E_{y}}{\partial x} - \frac{\partial E_{x}}{\partial y} = i \omega B_{z}$$

$$\frac{\partial E_{y}}{\partial x} - i k_{y} E_{x} = i \omega H_{z} \qquad (2-19)$$

$$\frac{\partial E_{z}}{\partial x} - \frac{\partial E_{x}}{\partial x} = 0 \qquad (2-20)$$

Substituting (2-16) into (2-19) and (2-17) into (2-18) to eliminate E_x and E_z :

$$\frac{k_{y}^{2}}{\sqrt{5}}H_{x}-\frac{\partial E_{y}}{\partial z}=i\mu\omega H_{x}$$

$$\frac{\partial E_{Y}}{\partial z} = -i \mu \omega H_{X} + i \mu \omega \frac{k_{Y}^{2}}{k^{2}} H_{X}$$

since

(

$$\sigma = \frac{k^2}{i \mu w}$$

$$\frac{\partial E_{Y}}{\partial z} = -i \mu \omega \left(1 - \frac{k_{Y}^{2}}{k^{2}} \right) H_{X} \qquad (2-21)$$

$$\frac{\partial E_{y}}{\partial x} = i \mu \omega H_{z} - i \mu \omega \frac{k_{y}^{2}}{k^{2}} H_{z}$$

$$\frac{\partial E_{Y}}{\partial x} = i \mu \omega \left(1 - \frac{k_{Y}^{2}}{k^{2}} \right) H_{2} \qquad (2-22)$$

Equations (2-15), (2-21), and (2-22) constitute a set of equations for E_y , H_x , and H_z . For wavelengths much longer than the skin depth, k_y = 0 and (2-21) and (2-22) reduce to:

$$\frac{\partial E_{Y}}{\partial z} = -i \mu \omega H_{x} \qquad (2-23)$$

$$\frac{\partial E_{\gamma}}{\partial x} = i \mu \omega H_{z} \qquad (2-24)$$

Therefore the magnetotelluric wave impedance over two dimensional features depends upon the orientation of the field components with respect to the strike. The "H parallel" mode has an anomalous vertical electric field associated with it, whereas the "E parallel" polarization has an associated vertical magnetic field. It is therefore the "E parallel" polarization which is the most convenient from the viewpoint of VLF

electromagnetic measurements.

In addition to the systems of equations for the two polarizations, the following boundary conditions must hold at the contact: Hin = Han

H . + = Hat

Eit = Eat

 $J_{n} = J_{2n}$

where H_{in} , H_{an} = normal components of the magnetic field on opposite sides of the contact

> Hit, Hat = tangential components of the magnetic field on opposite sides of the contact

> Elt, Est = tangential components of the electric field on opposite sides of the contact

Jin, Jan = normal components of the current density on opposite sides of the contact

Since the current density normal to the contact (\mathcal{J}_n) must be continuous, the boundary condition on E_n is $E_{in} = \frac{\sigma_a}{\sigma_i} E_{an}$ and E_n is therefore discontinuous (Fig. 2.2(a)). Thus there will be a discontinuity in the wave impedance (and hence the apparent resistivity) for the "E perpendicular" polarization for the simple geometry of Fig. 2.1 and have found that this is in fact the case (Fig. 2.2 (b)). The wave impedance

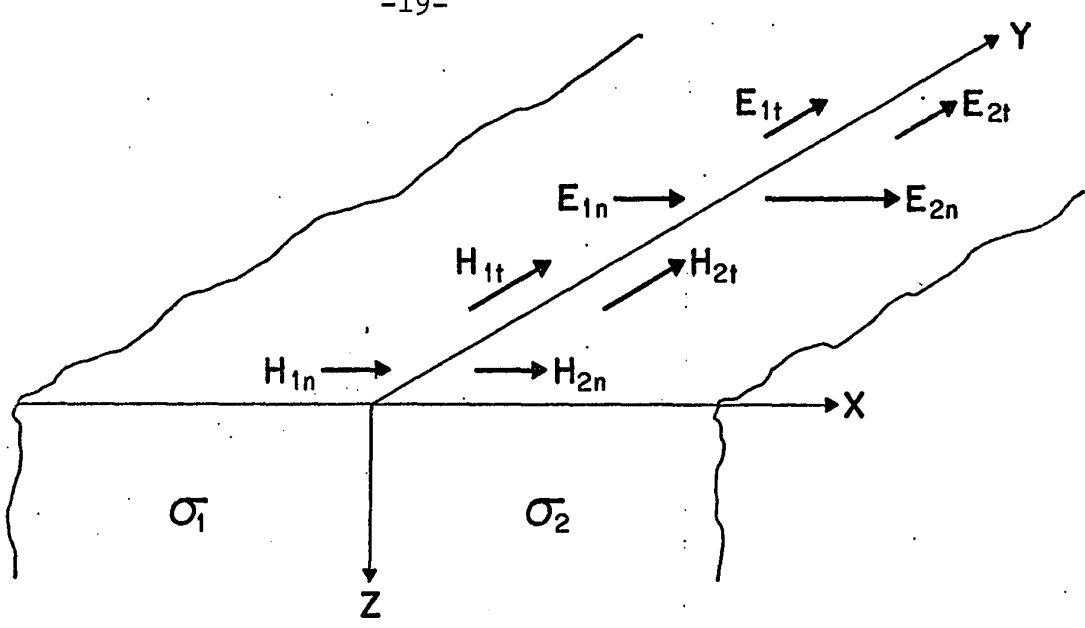


Fig. 2.2(a) Boundary Conditions on the Field Vectors at a Conductivity Interface ($\sigma_1 > \sigma_2$)

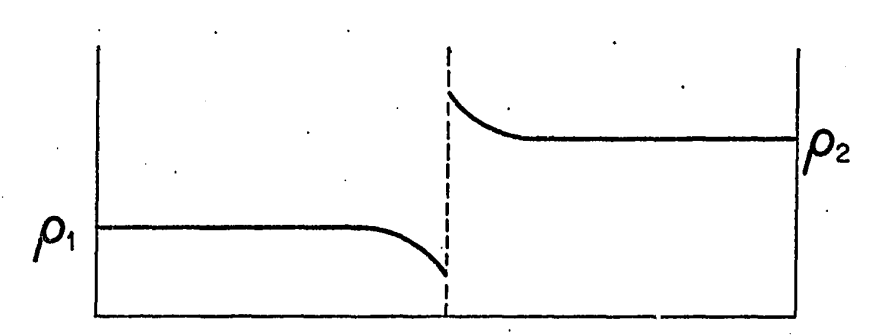


Fig. 2.2(b) Apparent Resistivity Profile for "E Perpendicular" Polarization

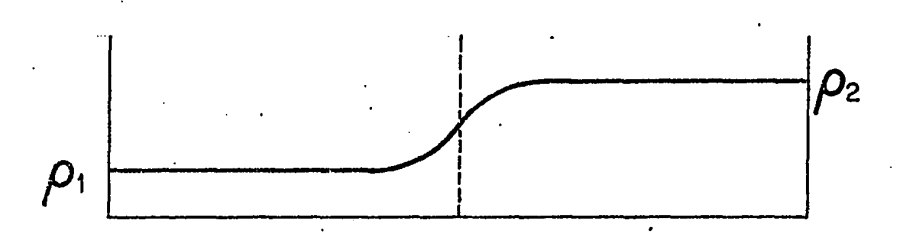


Fig. 2.2(c) Apparent Resistivity Profile for "H Perpendicular" Polarization

(_}

increases above its true isotropic value when approaching the contact from the more resistive side, and decreases when approaching it from the conductive side.

However, for the "H perpendicular" polarization, there is a smooth transition in wave impedance from one side of the contact to the other, since both H_n and E_{\uparrow} are continuous. (Strangway and Vozoff, 1967, and Madden and Swift, 1969). This case is illustrated in Fig. 2.2(c).

2.3 The Polarization Ellipse

The primary field in the air approximately obeys a Laplace type of equation (since $k_{\text{air}}^2 \approx \mathcal{O}$) and suffers little change in phase from point to point. When inhomogeneities (faults, shear zones, dikes, conductors) are present and a secondary field exists, there is generally a phase difference between the primary and secondary fields. In dip-angle systems the receiver responds to the resultant of the primary and secondary fields. With this in mind, we will consider what happens when two vectors, alternating at the same frequency (ω) but having a relative phase difference, are superimposed.

Consider the two vectors $\overrightarrow{A} = \omega t$ and $\overrightarrow{B} = (\omega t + \phi)$ which differ in phase by angle ϕ and in direction by any arbitrary space angle. If we take x and z coordinates in the plane of the two vectors, the vectors can always be resolved into pairs

of rectangular components (see, for example, Grant and West, p. 482). The two components in each direction can then be summed to yield a pair of orthogonal quantities:

$$X = H_x \cos(\omega t + \phi_x) = A_x \cos\omega t + B_x \cos(\omega t + \phi)$$

$$Z = H_z \cos(\omega t + \phi_z) = A_z \cos\omega t + B_z \cos(\omega t + \phi)$$

where X and Ξ are both functions of t, and H_{\star} and $H_{\bar{\star}}$ are constants.

Let
$$\delta = \phi_{x} - \phi_{x}$$

$$\frac{X}{H_{x}} = \cos (\omega t + \phi_{x})$$

$$\frac{Z}{H_{2}} = \cos (\omega t + \phi_{x} + \delta)$$

$$= \cos (\omega t + \phi_{x}) \cos \delta - \sin (\omega t + \phi_{x}) \sin \delta$$

$$= \frac{X}{H_{x}} \cos \delta - \sqrt{1 - \frac{X^{2}}{H_{x}^{2}}} \sin \delta$$

$$\frac{Z}{H_{x}} - \frac{X}{H_{x}} \cos \delta = \sqrt{1 - \frac{X^{2}}{H_{x}^{2}}} \sin \delta$$

Squaring both sides, we obtain:

$$\frac{Z^2}{H_2^2} - \frac{2ZX}{H_2H_X} \cos \delta + \frac{X^2}{H_X^2} = \sin^2 \delta$$

This is an ellipse inclined to the horizontal (Heiland, p. 688) as in Fig. 2.3.

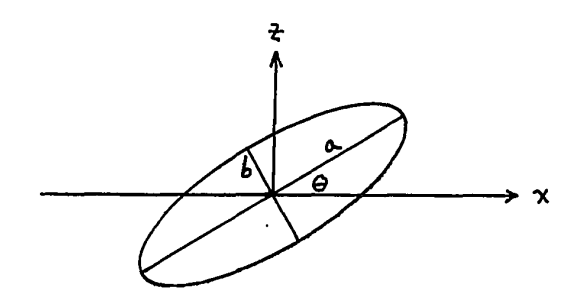


Fig. 2.3 The Polarization Ellipse

From Heiland (p. 689)
$$\tan 2\theta = 2 \frac{H_2 H_X}{H_X^2 - H_2^2} \cos \delta$$

Putting $R = \frac{H_2}{H_X}$, $\tan 2\theta = \frac{2R \cos \delta}{1 - R^2}$

For $\delta = 0$, $\tan 2\theta = \frac{2R}{1 - R^2} = \frac{2 \tan \theta}{1 - \tan^2 \theta}$

and so $\tan \theta = R = \frac{H_2}{H_X}$

From Heiland (p. 690), the lengths of the axes are given by:

$$a^{2}, b^{2} = \frac{2 H_{2}^{2} H_{x}^{2} \sin^{2} \delta}{H_{2}^{2} + H_{x}^{2} + \sqrt{4 H_{x}^{2} H_{2}^{2} \cos^{2} \delta + (H_{x}^{2} - H_{2}^{2})^{2}}}$$

$$= \frac{2 H_{2}^{2} H_{x}^{2} \sin^{2} \delta}{4 H_{x}^{2} + H_{x}^{2}$$

$$a^{2}, b^{2} = \frac{2 H_{2}^{2} H_{x}^{2} \sin^{2} \delta}{H_{3}^{2} + H_{x}^{2} \mp (H_{x}^{2} - H_{2}^{2}) \sec 2^{\Theta}}$$

since
$$\tan^2 \theta = \frac{4 + \frac{H_z^2}{H_x^2} \cos^2 \delta}{\left(1 - \frac{H_z^2}{H_x^2}\right)^2}$$

$$= \frac{4 + \frac{H_z^2}{H_x^2} + \frac{1}{2} \cos^2 \delta}{\left(H_x^2 - H_z^2\right)^2}$$

Now
$$a^{2}$$
, $b^{2} = \frac{2 H_{2}^{2} H_{x}^{2} \cos^{2} \delta \tan^{2} \delta}{H_{2}^{2} + H_{x}^{2}} + \frac{2 H_{x}^{2} \cos^{2} \delta \tan^{2} \delta}{H_{x}^{2} - H_{2}^{2}} \cos^{2} \delta \tan^{2} \delta}$

$$= \frac{H_{x}^{2} - H_{2}^{2}}{2} \times \frac{H_{x}^{2} - H_{2}^{2}}{\left(H_{x}^{2} - H_{x}^{2}\right) \int \left(H_{2}^{2} + H_{x}^{2}\right) + \left(H_{x}^{2} - H_{2}^{2}\right) \cos^{2} 2\theta}$$

$$= \frac{H_{x}^{2} - H_{2}^{2}}{2} \times \frac{\tan^{2} 2\theta \tan^{2} \delta}{H_{x}^{2} - H_{2}^{2}} + \sec 2\theta$$

$$= \frac{H_{x}^{2} - H_{2}^{2}}{2} \times \frac{\tan^{2} 2\theta \tan^{2} \delta}{\frac{1 + R_{x}^{2}}{2} + \sec 2\theta}$$

The ratio of the lengths of the axes is given by:

$$f^2 = \frac{b^2}{a^2} = \frac{\frac{1+R^2}{1-R^2} - \sec 2\theta}{\frac{1+R^2}{1-R^2} + \sec 2\theta}$$

$$\frac{1}{(1 + \sec 2\theta)} + \frac{R^2 (1 + \sec 2\theta)}{(1 + \sec 2\theta)}$$

from which:
$$R^2 = \sec 2\theta (1+n^2) - (1-n^2)$$
sec $2\theta (1+n^2) + (1-n^2)$

$$= \frac{(1+n^2) - (1-n^2) \cos 2\theta}{(1+n^2) + (1-n^2) \cos 2\theta}$$

For
$$\Theta = 0$$
, $R^2 = \frac{2n^2}{2}$

For
$$h = 0$$
, $R^2 = \frac{1 - \cos 2\theta}{1 + \cos 2\theta}$

Now R is the vertical secondary field divided by the primary field plus the horizontal secondary field:

$$R = \frac{H_{k}}{H_{x}} = \frac{\text{vertical secondary field}}{\text{primary field + horizontal secondary field}}$$

A question to ask at this point is whether or not R can be approximated by a quantity T, where:

$$T^2 = r^2 + tan^2 \Theta$$

$$T = \sqrt{R^2 + \tan^2 \theta}$$

since κ and $\hbar \kappa$ Θ are in fact the two quantities which are measured by the Geonics EM-16 (as will be seen later). It so happens that $R \approx T$ is a very good approximation. Figure 2.4 shows the per cent error $\left(\frac{R-T}{R} \times 100 \,\%\right)$ when R is approximated by T for various values of Θ and κ . The error involved in the approximation is only significant when Θ and κ are very large. e.g. for $\Theta = 40^{\circ}$ ($\hbar \kappa = .84$) and $\kappa = 0.3$, the error is only slightly greater than 3%.

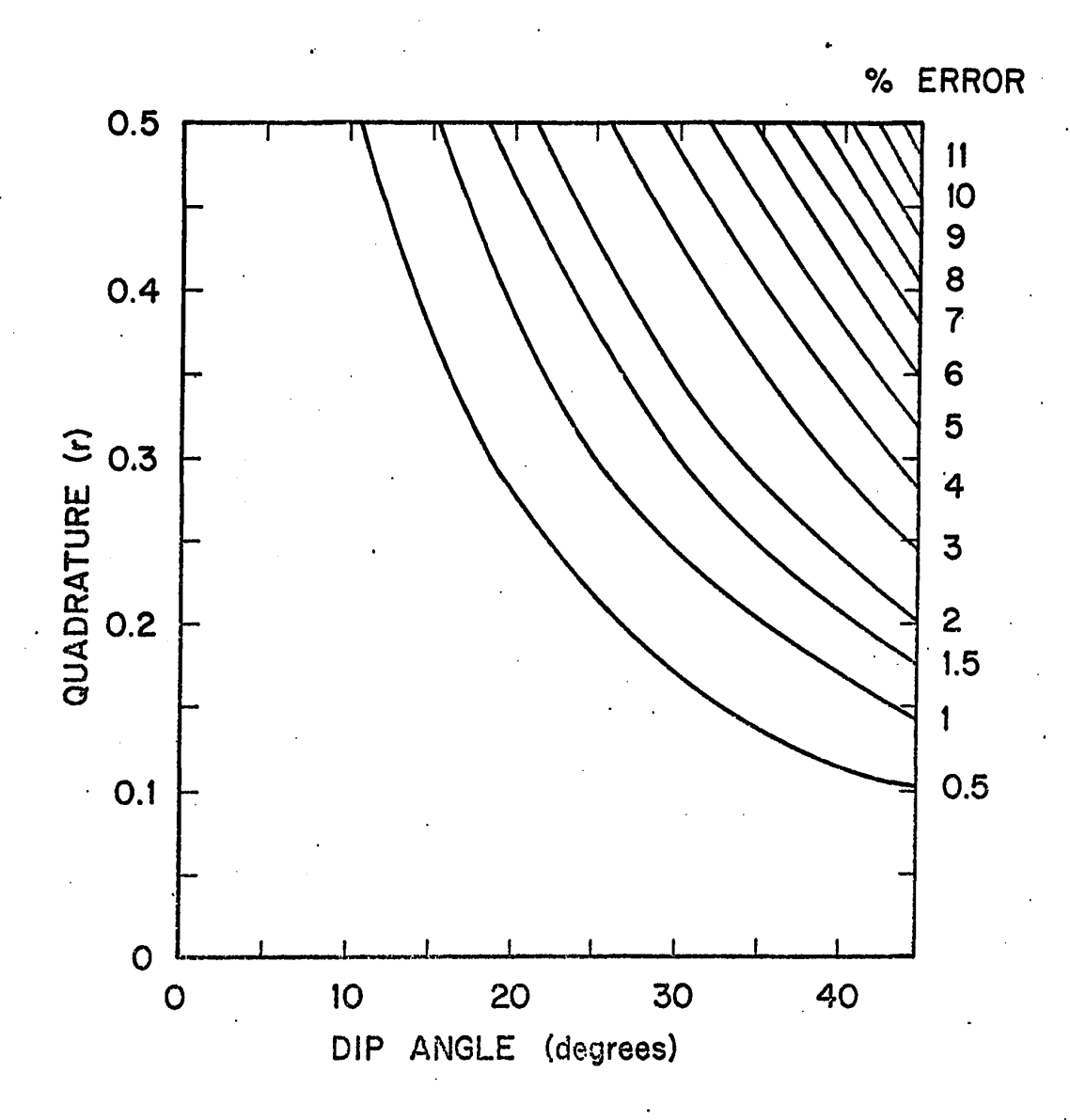


FIG. 2.4 PER CENT ERROR AS A FUNCTION OF DIP ANGLE AND QUADRATURE WHEN R IS APPROXIMATED BY T.

CHAPTER III

THEORETICAL PROFILES OVER TWO-DIMENSIONAL VERTICAL CONTACTS

3.1 Method

Equations (2-15), (2-23) and (2-24) constitute a set of equations for E_y , H_x , and H_z (provided that the wavelength is much longer than the skin depth) for the "H perpendicular" polarization. Swift (1967) and Madden and Swift (1969) have numerically solved these equations using a transmission network analogy, and more recently Slankis (1970) has solved them using a somewhat similar technique.

Using a program developed by Slankis, and an IBM 360-65 digital computer, theoretical profiles have been calculated over a two-dimensional vertical fault.

The effect of a fault was calculated for nine combinations of resistivity on either side of the fault, as shown in Table 3-1. ρ_R denotes the resistivity on that side of the fault with the higher resistivity, while ρ_C denotes the resistivity on the side of the fault with the lower resistivity (i.e. the "more conductive" side of the fault).

$ ho_{ m R}$	PC
(ohm meters)	(ohm meters)
10 ⁵	104
10 ⁵	103
10 ⁵	10 ²
104	10 ³
104	102
104	10
10 ³	102
103	10
102	10

TABLE 3-1 THE COMBINATIONS OF RESISTIVITY USED TO CALCULATE THE EFFECT OF A VERTICAL FAULT

The effect of the fault was to be calculated for each of these nine combinations at various frequencies, with overburden of varying depth and resistivity. (The frequencies selected were 10 Hz (the approximate frequency of telluric current methods), 100 Hz (representative of AFMAG methods), 1,000 Hz (roughly the frequency used in conventional exploration EM methods such as vertical loop and horizontal loop, although these are not infinite source methods), and 10,000 Hz (for VLF methods). Overburden resistivities of 1, 10, and 100 ohm meters were chosen, and depths of overburden were to be 0.5, 1.5, 5, 15, 50, and 150 meters. Fortunately it is

not necessary to calculate the effect of the fault using all the combinations of frequency, overburden resistivity, and overburden depth for each of the nine resistivity combinations. (This would result in 648 separate cases, plus 36 more for the case of no overburden).

Table 3-2 shows the skin depth (δ) in meters for each of the combinations of overburden resistivity (ρ_0) and frequency mentioned above. Table 3-3 shows the ratio d/δ for the various combinations of overburden depth (d) and skin depth (δ) in the overburden. There are only eleven values of d/δ , the ratio of overburden depth to skin depth in the overburden. Ratios of d/δ of 1/100 or less were not used, since the skin depth is very much greater than the overburden depth, and these cases are virtually the same as having no

OVERBURDEN RESISTIVITY

		l Ω m.	10Ωm.	100Ωm.
	10 Hz	150 m.	500	1500
SNCY	100 Hz	50	150	500
FREQUEN	1,000 Hz	15	50	150
FR	10,000 Hz	5	15	50

TABLE 3-2 SKIN DEPTH IN METERS FOR COMBINATIONS OF OVERBURDEN RESISTIVITY AND FREQUENCY

δ →	5	15	50	150	500	1500
d → 0.5	1/10	1/30	1/100	1/300	1/1000	1/3000
1.5	1/3	1/10	1/30	1/100	1/300	1/100
5	1	1/3	1/10	1/30	1/100	1/300
15	3	1	1/3	1/10	1/30	1/100
50	10	3	1	1/3	1/10	1/30
150	30	10	3	1	1/3	1/10
	·					

TABLE 3-3 RATIOS OF OVERBURDEN DEPTH (d) TO SKIN DEPTH IN OVERBURDEN (8).

overburden at all. On the other hand, ratios of d/δ greater than 1 were rejected, since it was considered that overburden more than one skin depth thick would attenuate most of the downgoing energy of the wave before bedrock was reached, and there would be no response whatsoever. This left only four values of d/δ (1/30, 1/10, 1/3, 1).

This means that only a few cases cover a wide range of situations, and changing the thickness of the overburden has the same effect as changing the frequency or resistivity. The nine combinations of resistivity were used with a combination of parameters that yielded the four ratios of d/8 given above, (in this case, we used 5, 15, 50, and 150 m. of 1 ohm m. overburden and a frequency of 10 Hz), resulting in 36 theoretical profiles. By applying scaling relations, theoretical profiles over any of the other 648 cases could be obtained. In addition, theoretical profiles were obtained for the 36 cases with no overburden (nine resistivity combinations and four different frequencies).

The program calculates the ratio of the total vertical secondary magnetic field to the primary horizontal magnetic field $(H_{\rm z}/H_{\rm x})$, the normalized value of the electric field $(E_{\rm y})$, the phase angle between $E_{\rm y}$ and $H_{\rm x}$, the phase angle between $H_{\rm z}$ and $H_{\rm x}$, and the apparent resistivity along the profile over the fault.

3.2 Results

A fault with a resistivity contrast of 1000:100 ohm meters and a response at a frequency of 10 Hz is taken as a representative example. The response in the absence of overburden ($d/\delta = 0$) is compared to responses in the presence of overburden. Values of the parameter $d/\delta = 1/30$, 1/10, and 1/3 were obtained by using an overburden resistivity of 10 ohm

meters and depths of 15, 50, and 150 ohm meters respectively. (Obviously other combinations of overburden resistivity and depths could have been arbitrarily selected to give the same values for d/δ). The response for $d/\delta = 1$ was found to be negligible (about 1%), and will not be examined.

In the following diagrams the fault is located at 0, and horizontal distances (in meters) are numbered right and left of the fault without distinguishing a positive or negative direction away from 0. The block with the higher resistivity is always to the left of 0.

Fig. 3.1 shows the profiles of apparent resistivity over the fault. Remote from the fault, the apparent resistivity is very nearly the true resistivity in the absence of over burden $(d/\delta=0)$. In the vicinity of the fault, there is a smooth transition between the two values of resistivity on either side of the fault, (1000 ohm m. -100 ohm m.) and the apparent resistivity contrast is the true resistivity contrast (10:1 in this case). However, the presence of overburden lowers the apparent resistivity as well as the apparent resistivity contrast. With 15 meters of 10 ohm m. overburden $(d/\delta=1/30)$, the apparent resistivity is down to about 600 ohm m. on one side of the fault and about 90 ohm m. on the other, resulting in an apparent resistivity contrast of slightly less than 7 to 1. With 150 meters of 10 ohm m. overburden $(d/\delta=1/3)$, these apparent resistivities are about

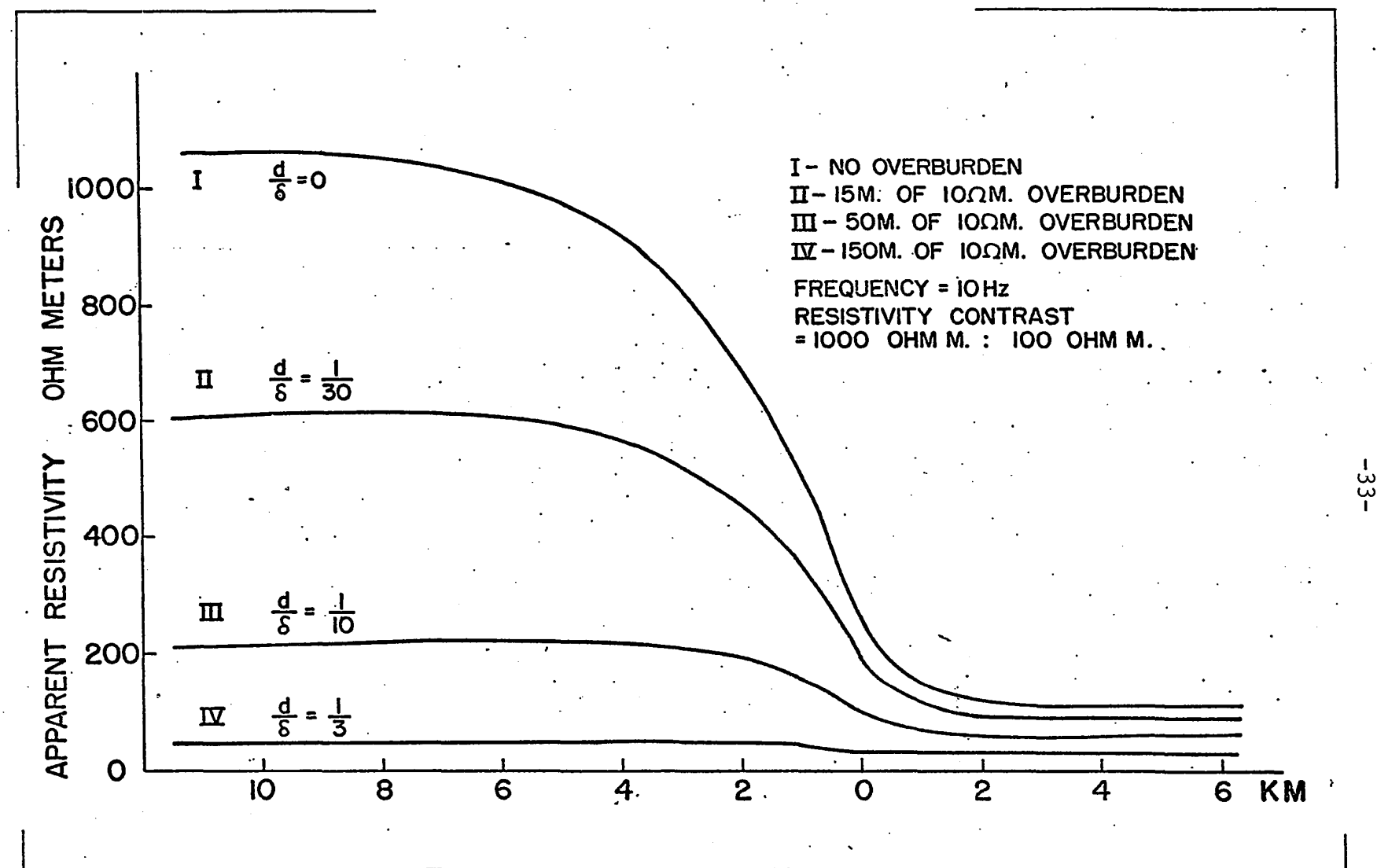
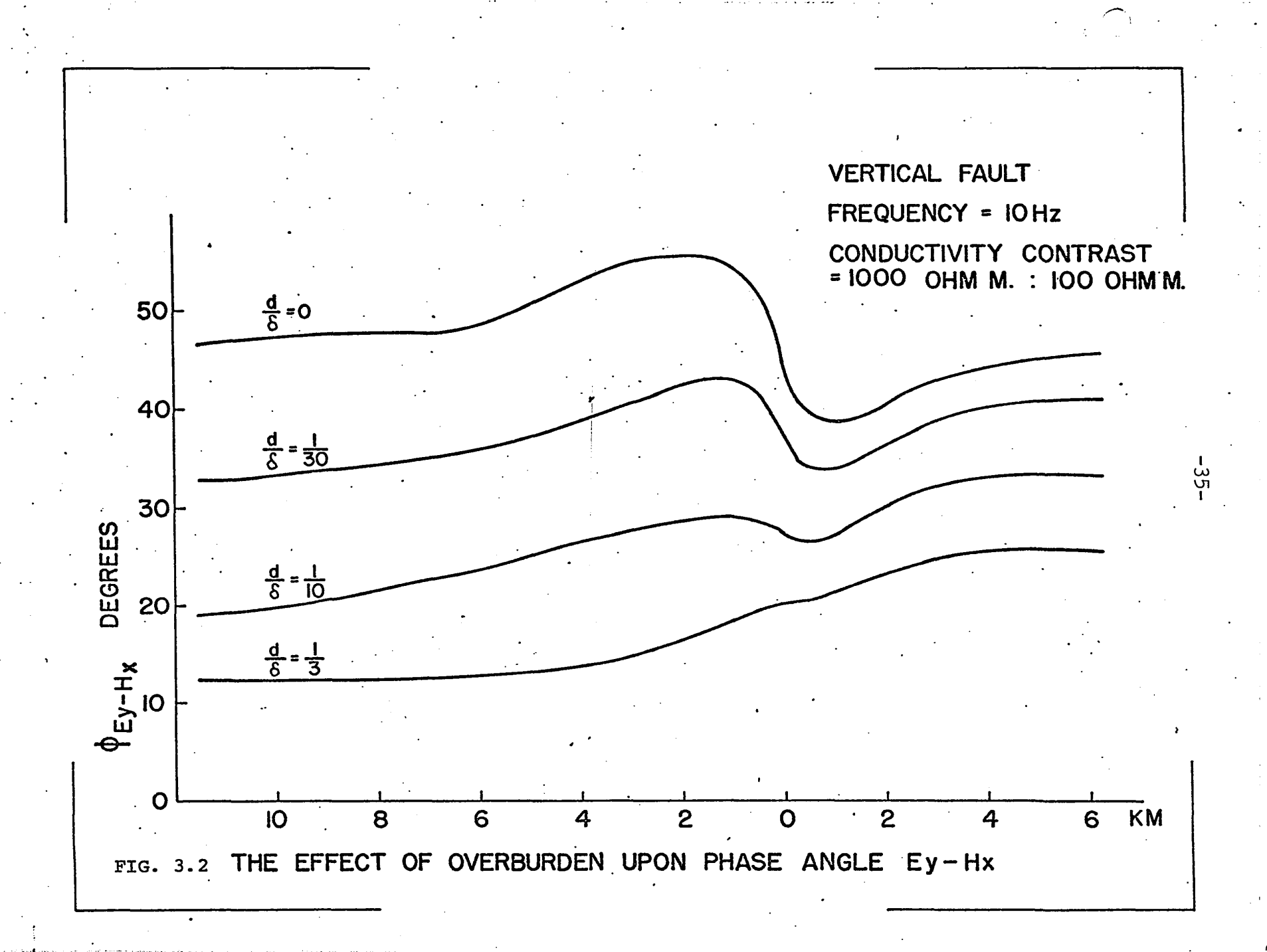


FIG. 3.1 THE EFFECT OF OVERBURDEN UPON APPARENT RESISTIVITY

50 ohm m. and 25 ohm m, resulting in an apparent resistivity contrast of only 2 to 1. These results indicate that, in the presence of overburden, the apparent resistivity contrast will be less than the true resistivity contrast between the bedrock on either side of the fault.

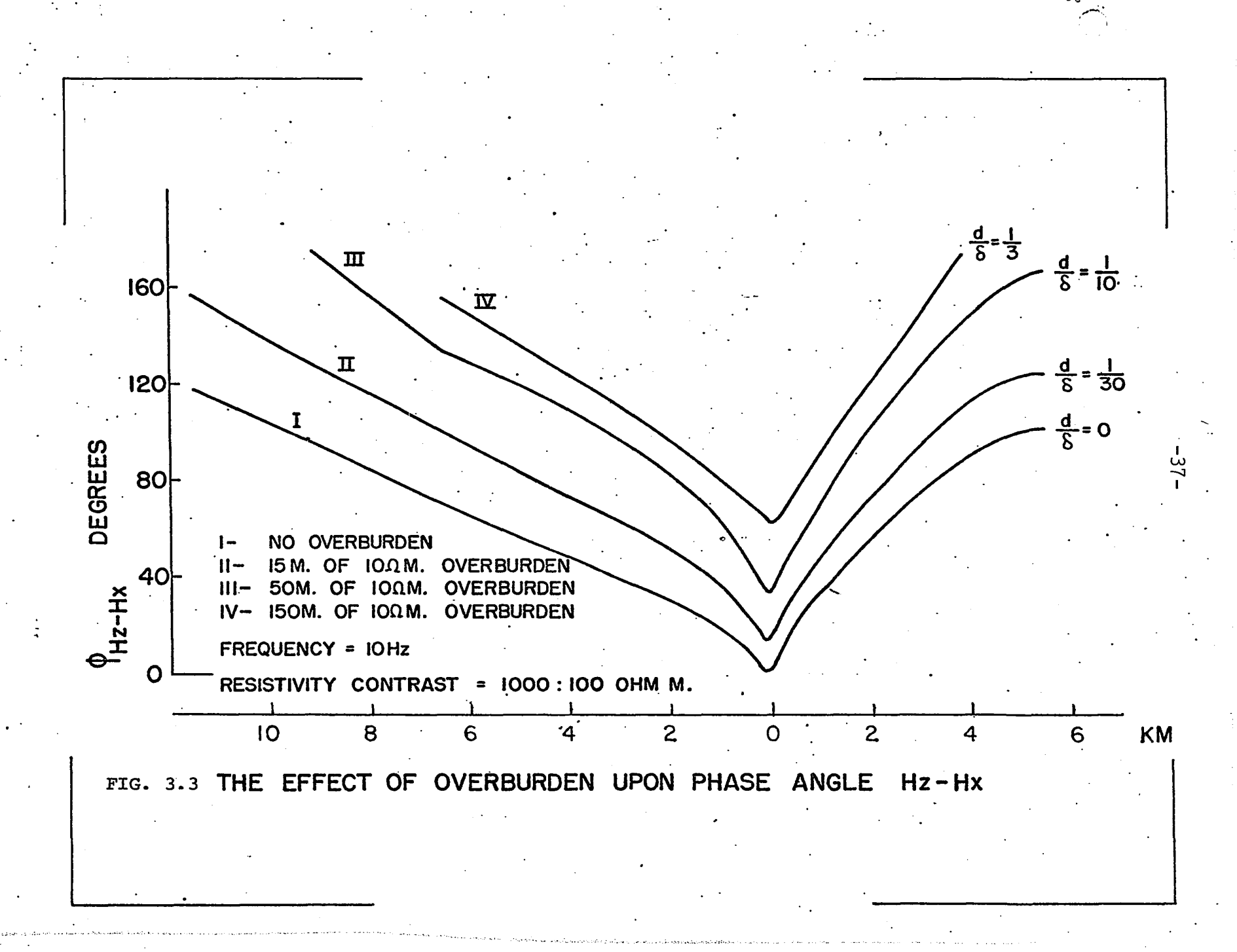
Fig. 3.2. shows the behaviour of the phase angle between the horizontal electric ($\mathbf{E}_{\mathbf{v}}$) and horizontal magnetic (H,) fields for the same four cases. Remote from the fault and on either side of it, the phase angle is about 45 degrees for $d/\delta = 0$. Approaching the fault on the more resistive side, the phase angle increases to slightly more than 55 degrees before it starts to decrease in the immediate vicinity of the fault, until directly over the fault it is once again 45 degrees. On the more conductive side of the fault the phase angle continues to decrease to slightly less than 40 degrees before it gradually increases again to assume the value of 45 degrees remote from the fault. The presence of overburden generally decreases the phase angle, (more so on the resistive side), but also tends to smooth out the profile over the fault. For $d/\delta = 1/30$, the phase angle is about 35 degrees remote from the fault on the more resistive side, and about 40 degrees on the more conductive side. $d/\delta = 1/3$, the phase angle is about 12 degrees on the more resistive side and about 25 degrees on the more conductive side. The latter profile shows almost a smooth transition between



these two values when the fault is crossed. In general, then, one can expect the phase angle in the vicinity of a fault to vary as previously described. Remote from the fault, and in the presence of overburden, the phase angle will be higher on the more conductive side.

The behaviour of the apparent resistivity and phase angle (between the horizontal electric and magnetic fields) will not be discussed in detail, since these are well known from the magnetotelluric method. In fact, the apparent resistivity and the phase angle for almost any depth and resistivity of overburden can be readily obtained from any standard two layer magnetolluric curves. (See, for example, Keller and Frischknecht p. 219-220). However, the previous examples serve to illustrate the behaviour of these two quantities in the presence of a vertical fault.

The effect of overburden upon the phase angle between the vertical magnetic ($\rm H_Z$) and horizontal magnetic ($\rm H_X$) fields is shown in Fig. 3.3. In all cases the phase angle is a minimum directly over the fault, and increases almost linearly on both sides of the fault as the distance from the fault increases. However, the phase angle increases more rapidly on the more conductive side of the fault. For $d/\delta = o$, (the case of no overburden) the phase angle is very nearly zero over the fault. As the depth of overburden increases, the shape of the phase angle curve changes only slightly, but

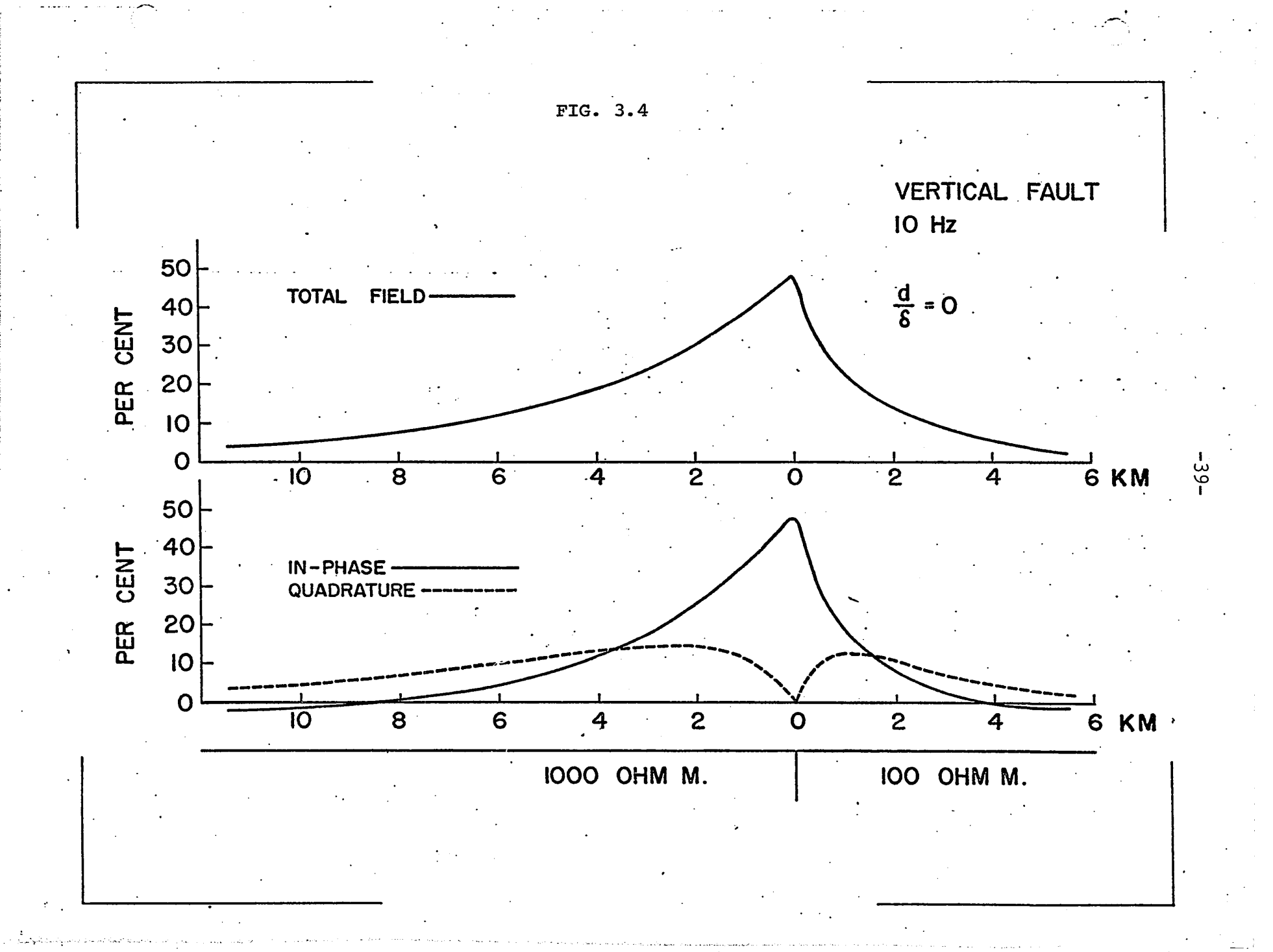


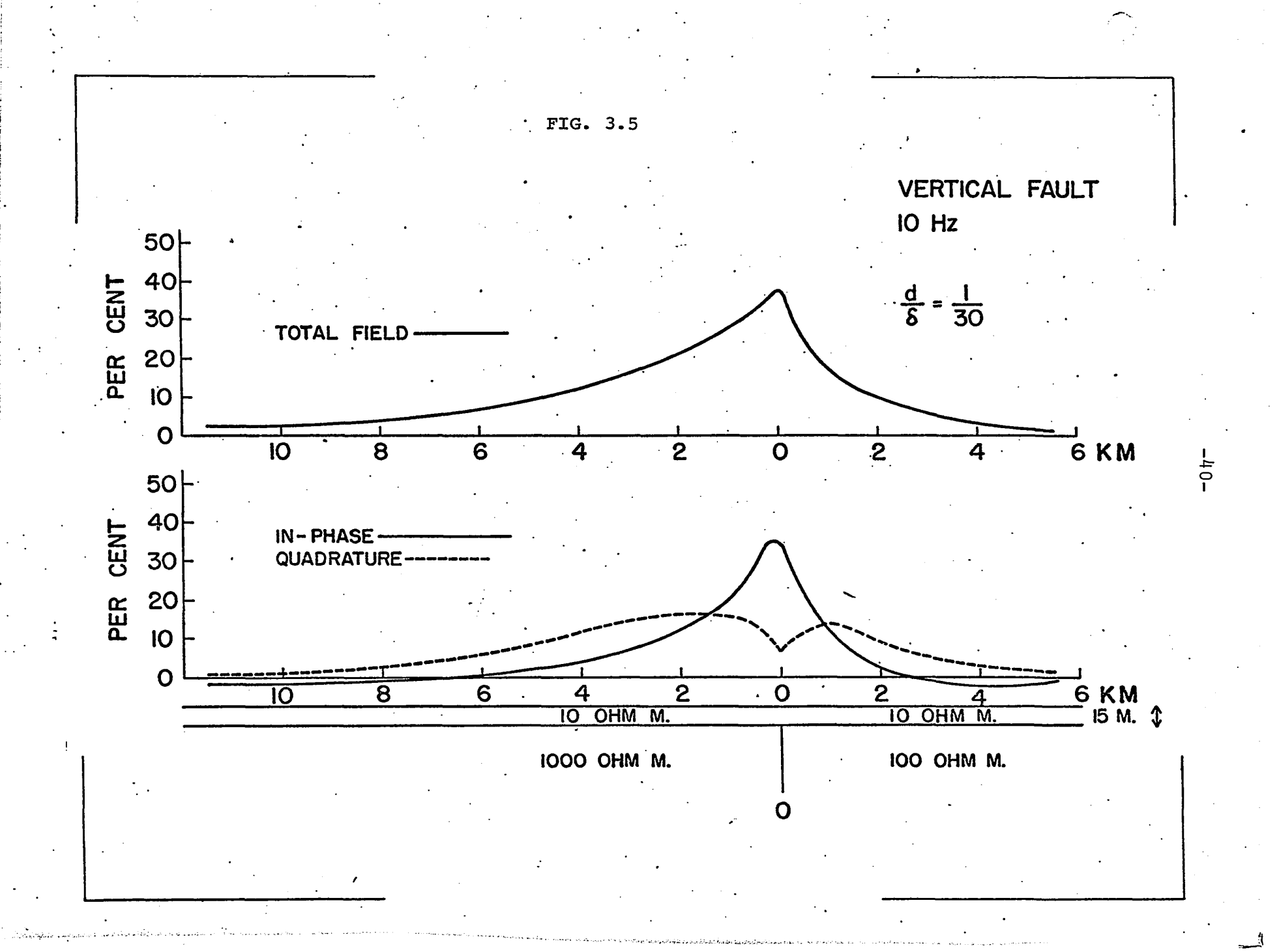
the whole curve shifts upwards. When $d/\delta = 1/30$, the phase angle is about 12 degrees over the fault, while for $d/\delta = 1/10$ it is 32 degrees, and for $d/\delta = 1/3$ it is more than 60 degrees directly over the fault.

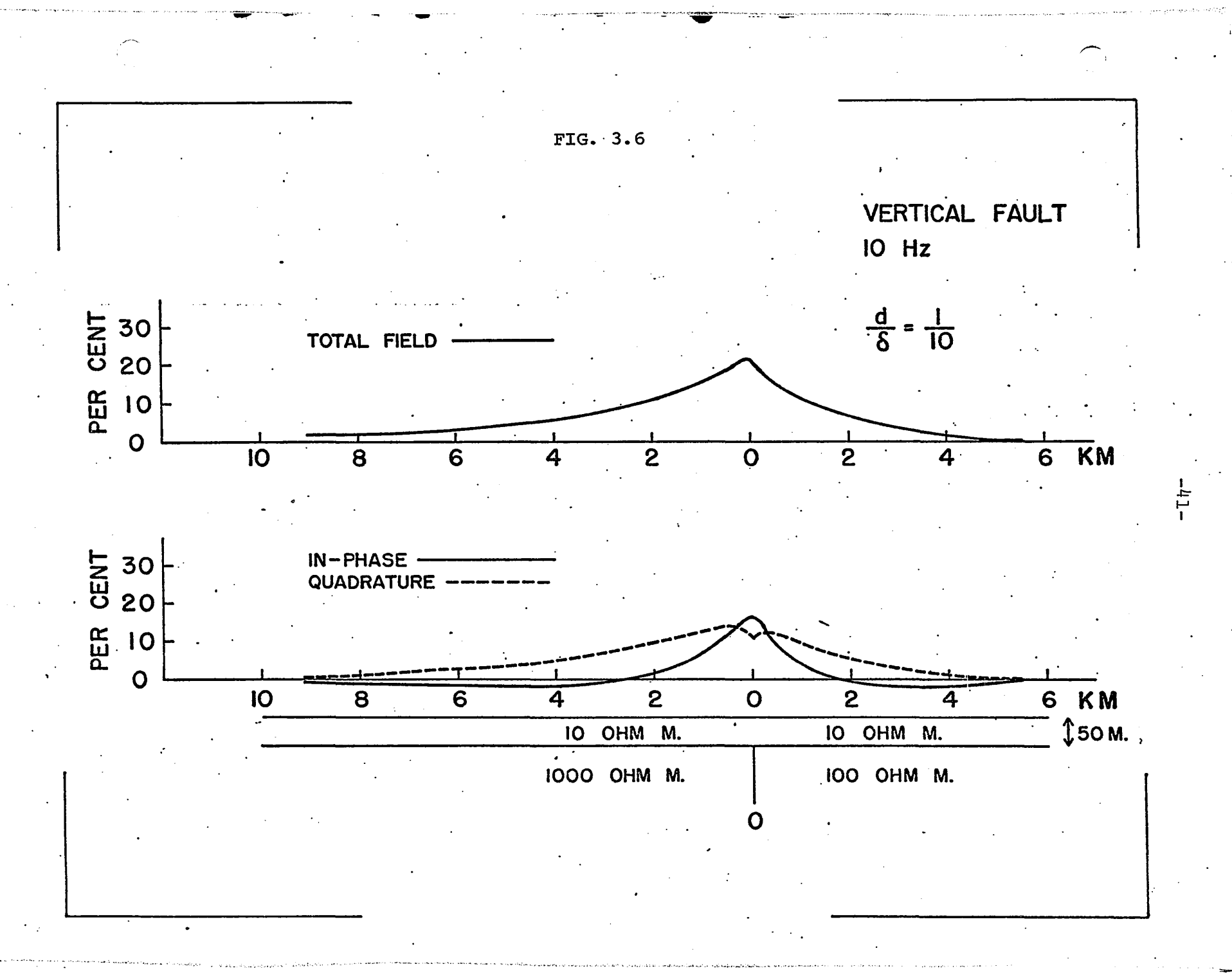
The behaviour of this phase angle is very important, since it determines the nature of the in-phase and quadrature response. The in-phase response is given by $\mathbf{H}_{\mathbf{Z}}$ cos ϕ and that of the quadrature by $\mathbf{H}_{\mathbf{Z}}$ sin ϕ , where $\mathbf{H}_{\mathbf{Z}}$ is the total vertical secondary field expressed as a percentage of the primary, and ϕ is the phase angle between $\mathbf{H}_{\mathbf{Z}}$ and $\mathbf{H}_{\mathbf{X}}$. Therefore, it is to be expected that the in-phase response will decrease and the quadrature response will increase with increasing overburden.

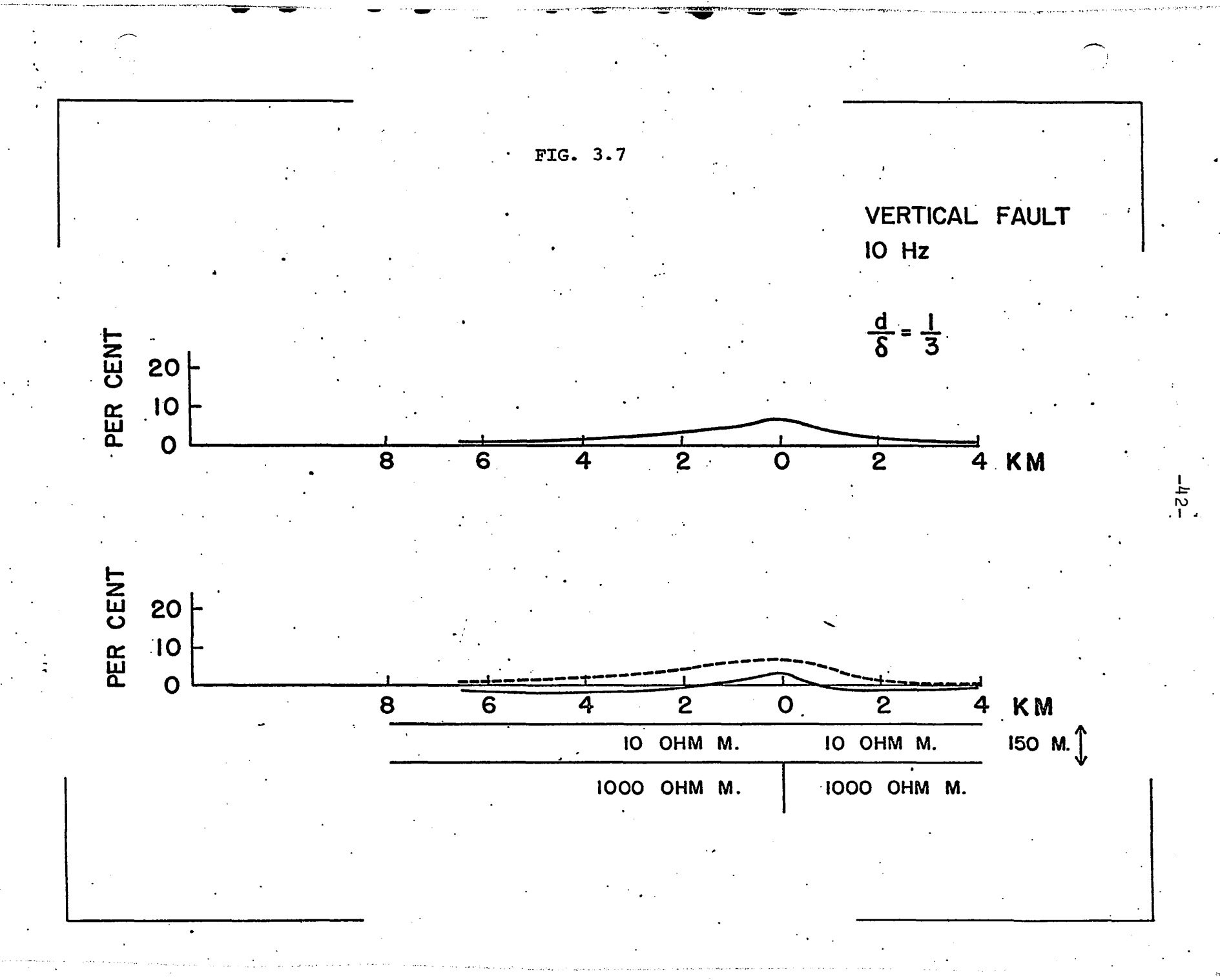
Figs. 3.4 to 3.7 show the total field and the in-phase and quadrature responses for the four cases under consideration. For $d/\delta = 0$ (Fig. 3.4), the total field response is an asymmetric peak over the fault, with the peak being steeper on the more conductive side of the fault. The in-phase response resembles that of the total field very closely.

However, the quadrature response over the fault is almost zero, since the phase angle is about zero. Initially, the quadrature increases away from the fault on both sides (but reaches a maximum more rapidly on the conductive side), then gradually falls off as the distance from the fault increases. The quadrature response becomes greater than that of the in-phase at some distance from the fault, since it falls







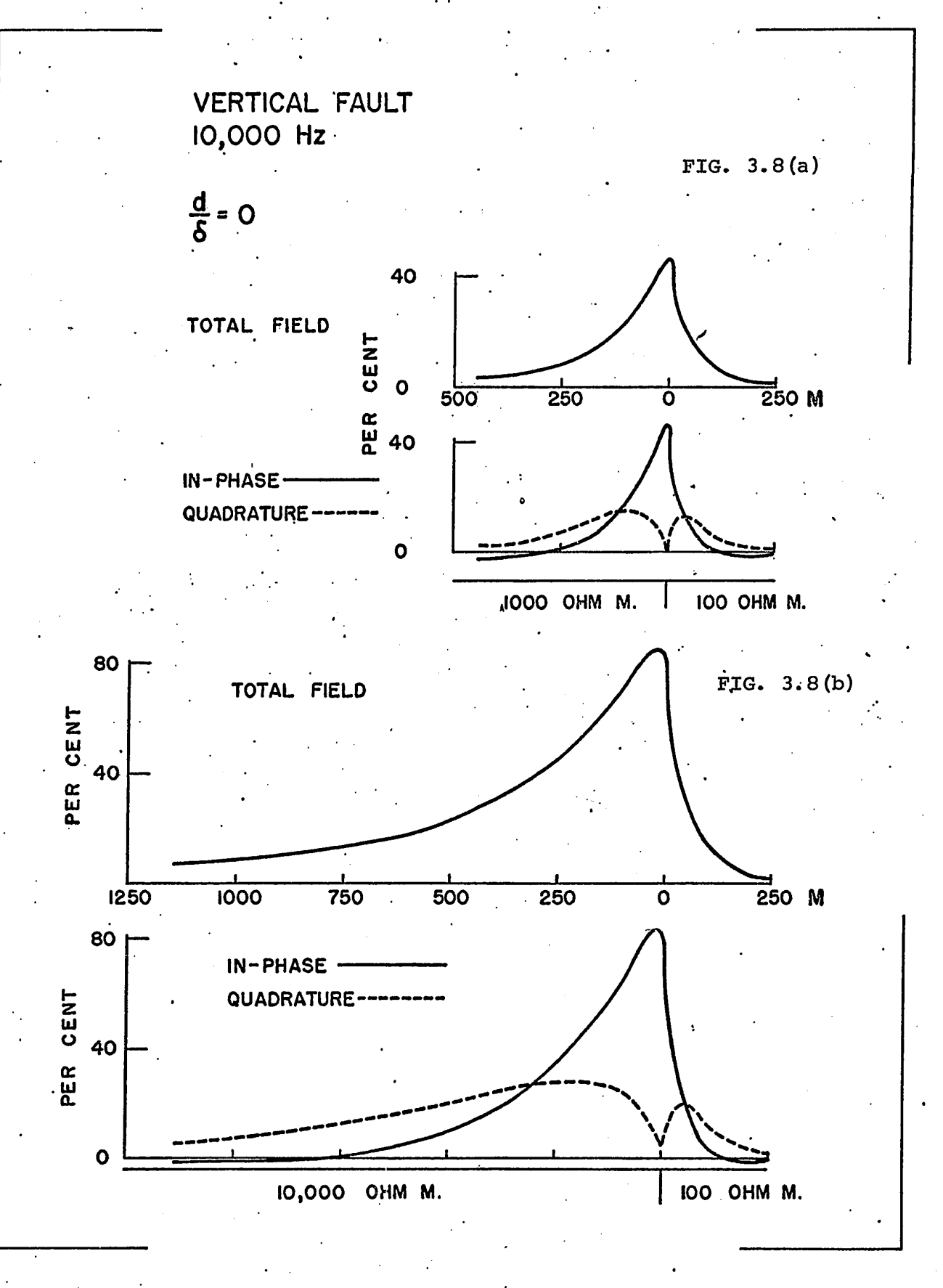


off much more slowly. When $d/\delta = 1/30$ (Fig. 3.5) the quadrature response is much larger over the fault. It still displays the characteristic minimum beneath the in-phase peak, but this minimum now has a value of 12 per cent instead of nearly zero. Directly over the fault, the in-phase response has decreased from nearly 50 per cent (for $d/\delta = 0$) to about 35 per cent.

For $d/\delta = 1/10$ (Fig. 3.6) the in-phase and quadrature responses have almost the same magnitude over the fault; the in-phase response has a maximum value of about 14 per cent, while the quadrature response is about 10 per cent. The quadrature is much broader than the in-phase, but still displays a local minimum directly over the fault, although the minimum is not as well marked as in the previous two cases. The in-phase and quadrature still fall off more rapidly on the more conductive side of the fault.

The in-phase and quadrature response are greatly reduced when $d/\delta = 1/3$ (150 m. of overburden), and the quadrature response is now greater than that of the in-phase (Fig. 3.7). Both responses are in the shape of a rounded peak centered over the fault, and the quadrature no longer displays a local minimum at that point. The responses still fall off more rapidly on the more conductive side of the fault.

Fig. 3.8 (a) shows the effect of increasing the frequency from 10 Hz to 10,000 Hz over the same fault for



d/δ = 0. The reader is cautioned that uniformity of scale has not been preserved from case to case, for the sake of convenience. The in-phase and quadrature response have the same magnitude over the fault at 10,000 Hz as at 10 Hz, but the anomaly has greatly decreased in width. The total half-width at 10,000 Hz is about 250 meters, compared to 3600 meters at 10 Hz. Increasing the frequency decreases the skin depth, with the result that the response falls off much more rapidly at high frequency.

Fig. 3.8 (b) shows the effect of increasing the resistivity contrast from 1,000:100 ohm meters to 10,000:100 ohm meters (also at 10,000 Hz with no overburden). The in-phase response has increased to more than 80 per cent, and is much more skewed because of the higher resistivity contrast. The quadrature response is also larger, but still displays the local minimum over the fault. This minimum seems to be sharper when the resistivity contrast is higher.

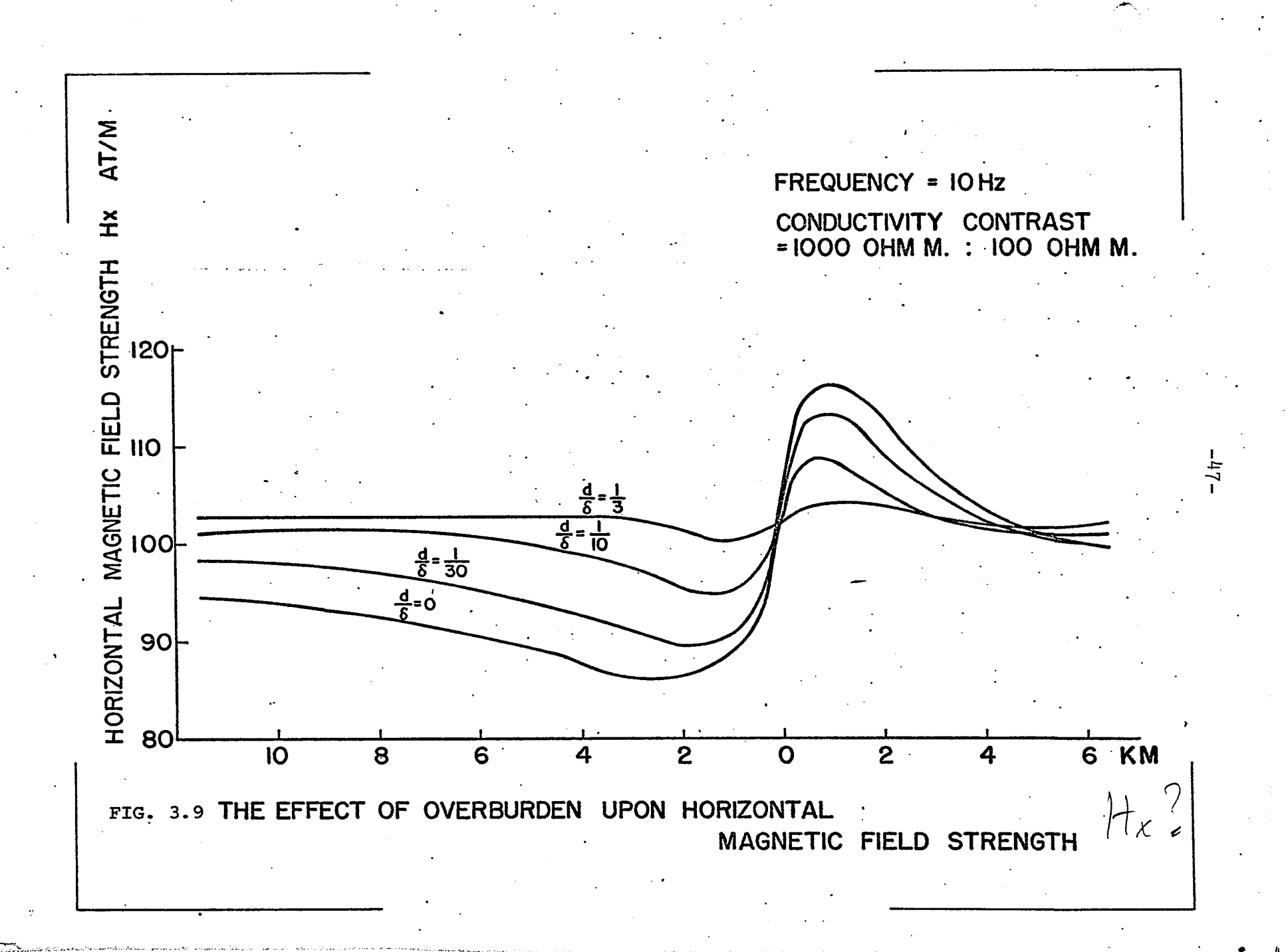
The above results are representative of the behaviour of the field components over a vertical fault and may be summarized as follows:

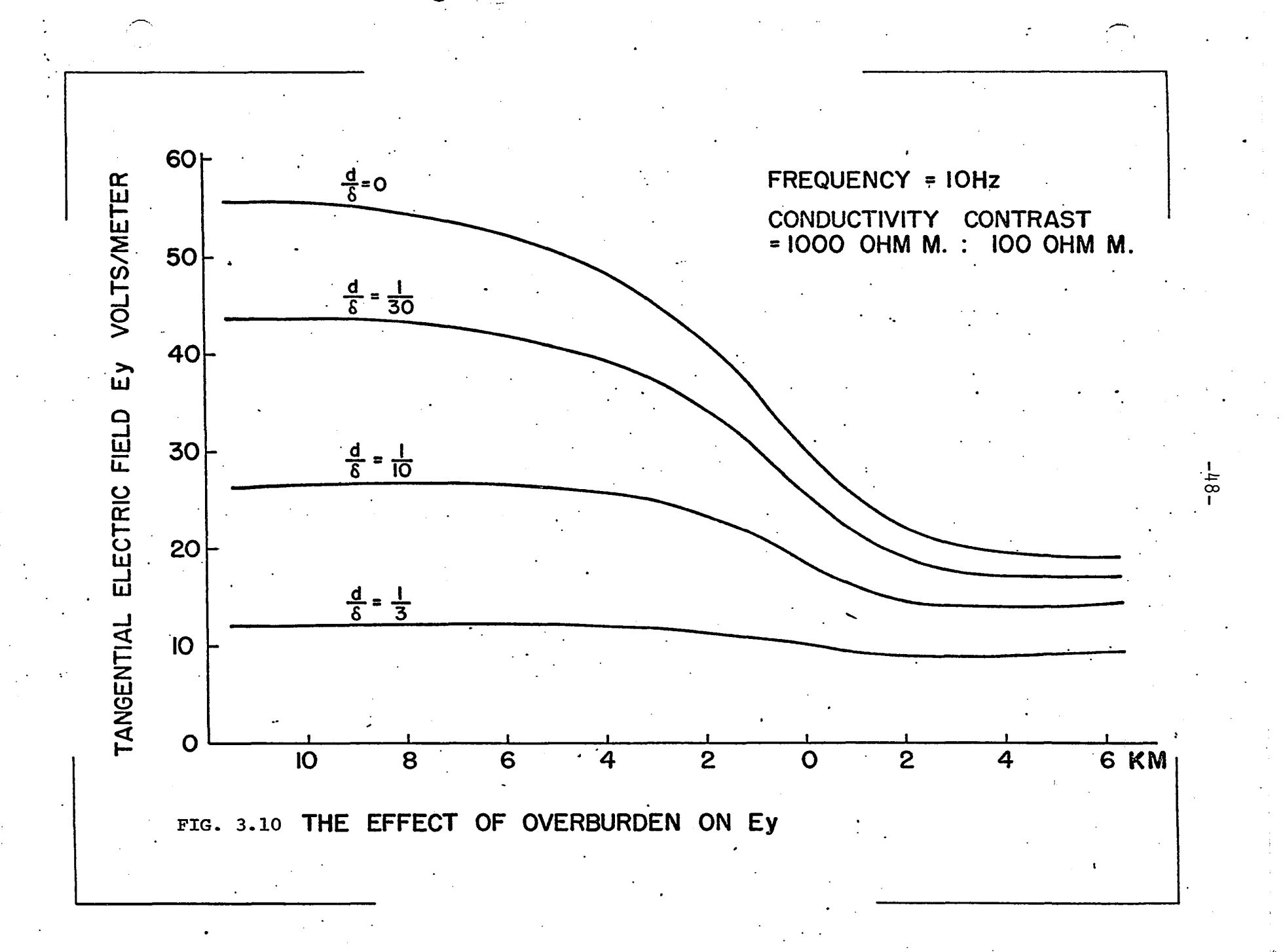
- 1. The total field response is an asymmetric peak over the fault. The response falls off more rapidly on the more conductive side of the fault.
- 2. The in-phase component of the secondary vertical magnetic field is also an asymmetric peak over the fault, and

falls off more rapidly on the more conductive side of the fault.

- 3. The quadrature component displays a local minimum over the fault. This minimum becomes less pronounced as the depth of overburden increases. The quadrature response is broader than that of the in-phase.
- 4. Both the in-phase and quadrature response decrease as the depth of overburden increases. The quadrature response becomes greater than that of the in-phase when the overburden is more than about one-half a skin depth thick.
- 5. The in-phase and quadrature response increase with increasing resistivity contrast across the fault.
- 6. The width of the anomaly decreases with increasing frequency, for a given resistivity contrast.

Fig. 3.9 shows the normalized values of the horizontal magnetic field (H_{χ}) for the four different cases. H_{χ} starts to decrease as the fault is approached on the more resistive side, but increases in the immediate vicinity of the fault. H_{χ} continues to increase as the fault is crossed, and then falls off as the distance from the fault increases on the conductive side, but does not become as low as it originally was on the more resistive side of the fault. This is best illustrated when $d/\delta=0$ (no overburden), for the effect becomes less pronounced as the depth of overburden





increases. In general, then, we can expect the horizontal magnetic field strength in the vicinity of a fault to vary as previously described, but remote from the fault, it will be higher on the more conductive side.

Fig. 3.10 shows how the tangential component of the electric field (E_y) changes over the fault. Remote from the fault E_y assumes a constant value. However, E_y is greater on the more resistive side of the fault than on the more conductive side, and there is a smooth transition between the two values as the fault is crossed. As the depth of overburden increases, this transition becomes less pronounced, (similar to apparent resistivity) and is barely perceptible when $d/\delta = 1/3$.

It is important to note that E_y is greater on the more resistive side of the fault. This means that if the fault is crossed going from the resistive medium toward the more conductive medium, then $\frac{\partial E_y}{\partial x}$ is negative. However, if the fault is crossed going from the more conductive medium to the resistive medium, then $\frac{\partial E_y}{\partial x}$ is positive.

From Section 2.2 (ii)

$$\frac{\partial E_y}{\partial z} = -i\mu\omega H_x \qquad (2-23)$$

$$\frac{\partial E_y}{\partial x} = i\mu\omega H_z$$
 (2-24)

and so

$$\frac{H_{Z}}{H_{X}} = - \frac{\frac{\partial E_{y}}{\partial x^{y}}}{\frac{\partial E_{y}}{\partial z}}$$

This means that when $\frac{\partial E_y}{\partial x}$ is negative, then $\frac{H_z}{H_x}$ is positive. However, when $\frac{\partial E_y}{\partial x}$ is positive, then $\frac{H_z}{H_x}$ is negative.

It is therefore important to keep the orientation of an electromagnetic measuring system constant throughout the course of a survey, for then it is possible to determine the side of the contact which has the higher resistivity. For an infinite source electromagnetic system with the measuring coils kept in a fixed orientation with respect to the source, a fault (or contact) with the higher resistivity on the east side will give exactly the opposite response (with respect to sign) to a fault with the higher resistivity on the west side. i.e. the in-phase, quadrature, and total field response will have the same magnitude and same shape, but they will be opposite in sign in each of the two cases. With this fact in view, now is a convenient time to define the sign convention which will be used in this investigation when a dip angle measuring system (namely the VLF EM-16, to be described later) is employed.

1. On an east-west traverse, the operator will always orient himself so that he is facing east (or as nearly so as

possible, depending upon the azimuth to the transmitter) when taking a measurement. Dip angles toward the east will be recorded as positive.

2. On a north-south traverse, the operator will always orient himself so that he is facing north (or as nearly so as possible) when taking a measurement. Dip angles toward the north will be recorded as positive.

With this convention, a fault or contact with the higher resistivity on the west (on an E-W traverse) or the south (on an N-S profile) will give a positive response (in-phase and quadrature, as well as total field $\rm H_Z/H_X$), and a fault with the higher resistivity on the east or north will give a negative response.

It must be noted that during this investigation the total field will always be plotted as the absolute value of the total field, and therefore will always appear positive.

Now is a convenient time to digress to explain briefly the response to be expected over a good conductor such as a graphite shear, a massive sulfide body, or man-made features such as buried telephone cables, metallic drain pipes, etc. Over the conductive zone E_y decreases, reaching a minimum over the center of the zone (usually the axis of the conductive body). This means that $\frac{\partial E_y}{\partial x}$ is negative as the conductive zone is approached; $\frac{\partial E_y}{\partial x} = 0$ directly over the center of the zone, and $\frac{\partial E_y}{\partial x}$ is positive as the conductive

zone recedes. Using the sign convention already described, this results in the familiar cross-over type response. Approaching a conductor from the south (say, on a north-south traverse) the in-phase and quadrature are both positive, reaching a maximum at some point before the axis of the conductor is crossed. Directly over the axis of the conductor the in-phase and quadrature will be zero (theoretically, at least), while they will both become negative and attain a negative maximum after the conductor axis has been crossed. On the total field profile this will appear as two peaks side by side, separated by a sharp minimum directly over the conductor. Of course, the width and magnitude of the response are determined by the depth, size, and conductivity of the body. i.e. a shallow, narrow body will produce a steep, sharp crossover, while a wide body, buried deeper, will produce a wide cross-over with slow roll-off on both sides. For a further discussion of cross-over responses, the reader is referred to Paterson and Ronka (1969) or to Geonics Limited - "EM-16 Operating Manual".

The remaining results of the theoretical profiles for two-dimensional contacts are presented in Figs. 3.11 and 3.12. In addition to d/δ , there are two other parameters which determine the nature of the response over a vertical contact.

These are Kcr, the ratio of the resistivity on the

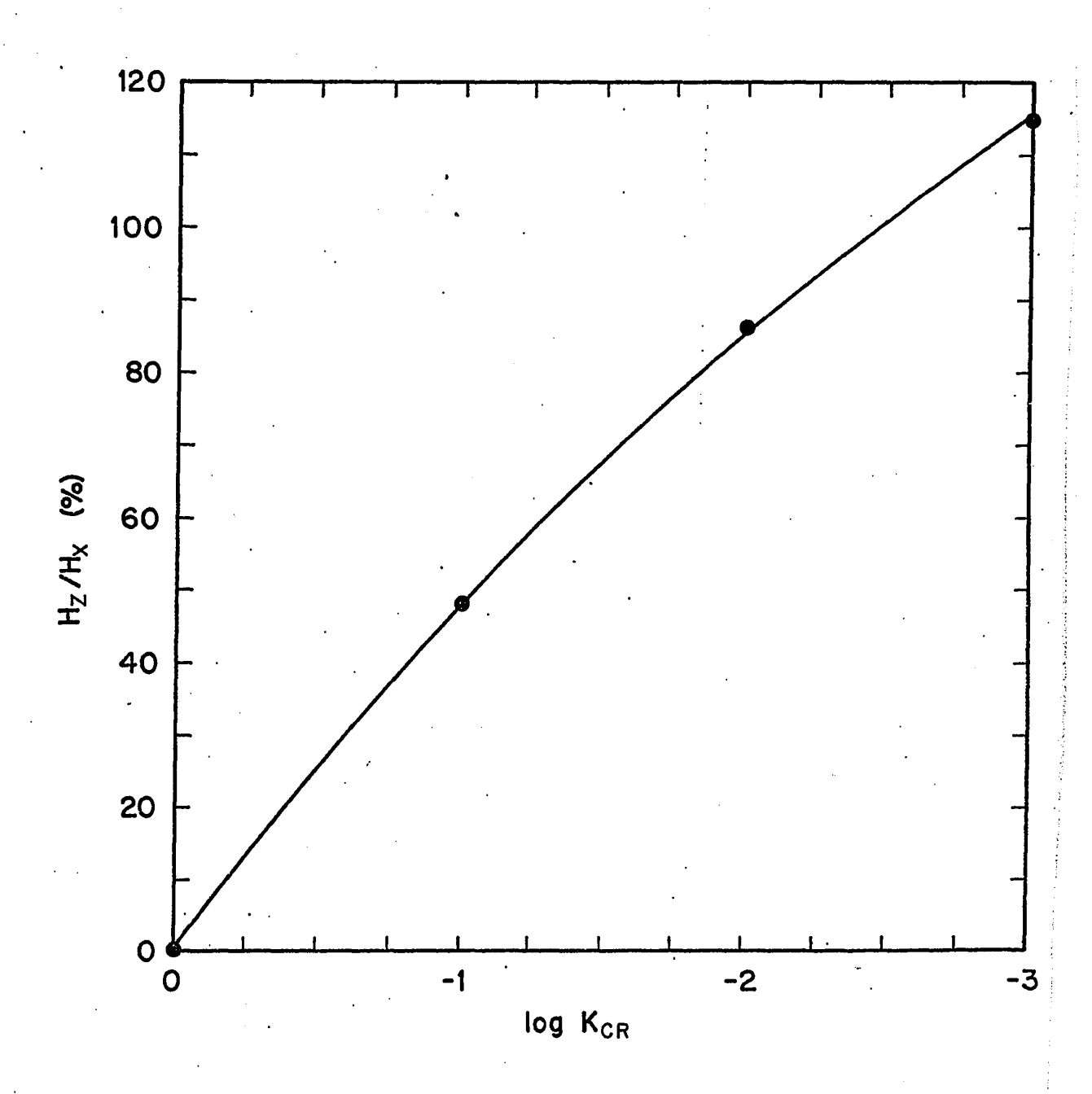
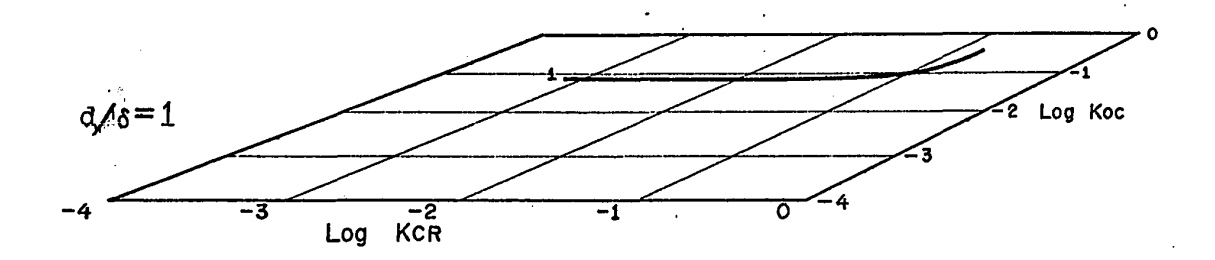
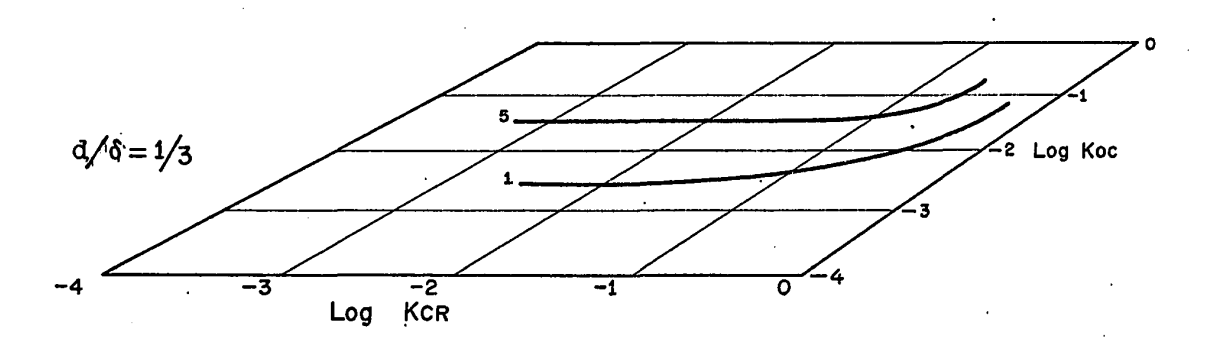
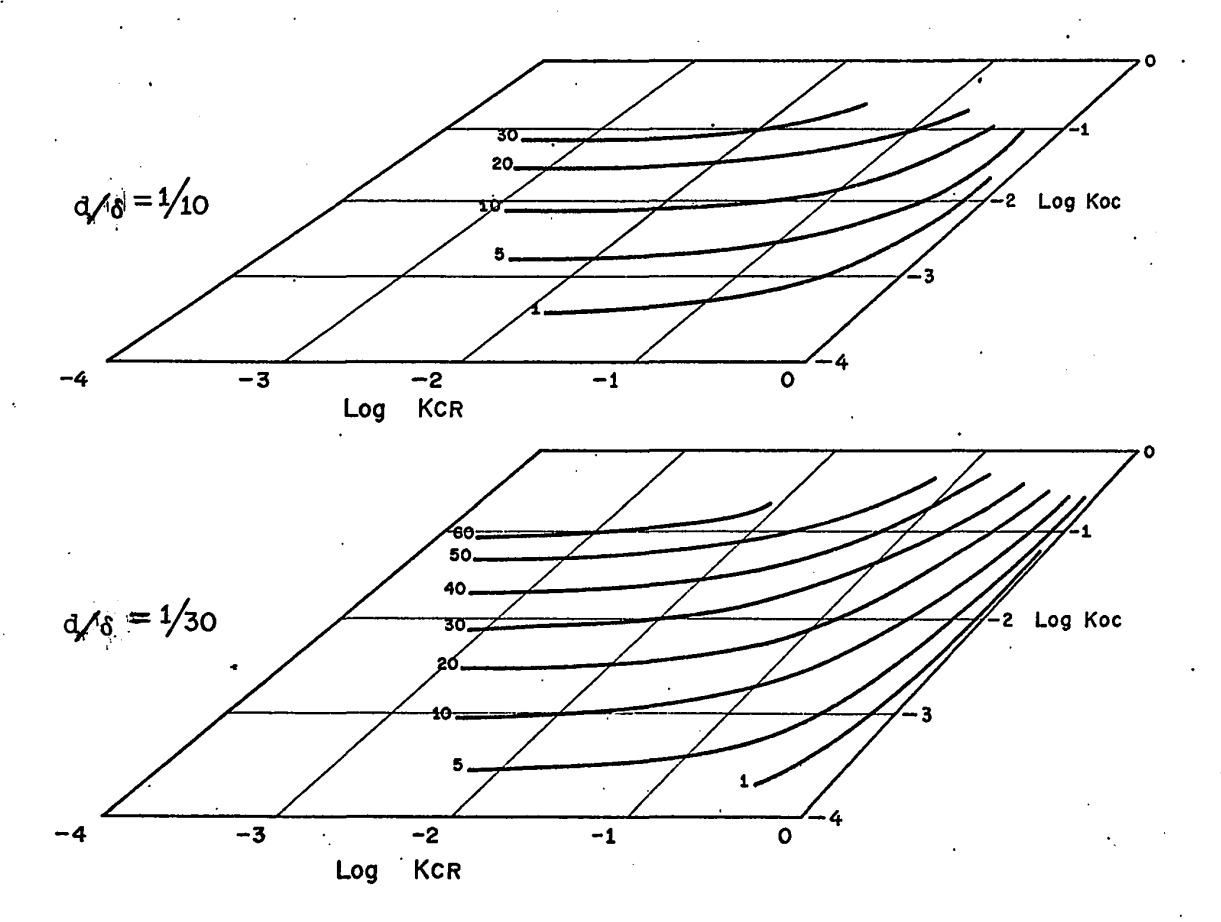


FIG. 3.11 AMPLITUDE OF TOTAL VERTICAL SECONDARY FIELD VS. LOG KCr for d/ δ = 0

FIG. 3.12 AMPLITUDE OF TOTAL VERTICAL SECONDARY FIELD VS. LOG KCT WHEN OVERBURDEN IS PRESENT







more conductive side of the fault to that on the more resistive side (i.e. $\rho_{\rm C}/\rho_{\rm R}$), and Koc, the ratio of the overburden resistivity to the resistivity on the more conductive side of the fault $(\dot{\rho}_{\rm C}/\rho_{\rm C})$.

There is no overburden for the case of $d/\delta = 0$, and the only parameter which determines the amplitude of the response is Kcr. (i.e. a resistivity contrast of 1000:100 ohm m. gives a response of the same amplitude (although not the same width) as a contrast of 10,000:1000 ohm m. Fig. 3.11 shows the total vertical secondary field (as a percentage of the primary) as a function of log Kcr.

The magnitude of the response increases almost linearly as the resistivity contrast increases. For a resistivity contrast of 10:1 (Kcr = 1/10) the vertical secondary field has an amplitude of about 48 per cent over the fault, while for a contrast of 1000:1 (Kcr = 1/1000) the amplitude is about 115 per cent.

Fig. 3.12 shows the amplitude of the total vertical secondary field (in per cent) over a vertical fault when overburden is present. The cases for $d/\delta = 1/30$, 1/10, 1/3, and 1 are shown and the results (some of which have been mentioned already) may be summarized as follows:

- 1. The amplitude of the response decreases as the ratio of overburden depth to skin depth (d/ δ) increases.
- 2. The amplitude increases as the resistivity contrast between the two sides of the contact increases.

3. The amplitude decreases as the resistivity contrast between the overburden and the bedrock increases (assuming that the overburden is less resistive than the bedrock).

The amplitude of the response for many cases may be read directly off the graphs of Fig. 3.12; e.g. at a frequency of 10,000 Hz, consider a contact between two rocks with resistivities of 10,000 ohm m. and 1000 ohm m (Kcr = 1/10, log Kcr = -1) covered by 5 meters of 100 ohm m. overburden ($d/\delta = 1/10$, Koc = 1/10, log Koc = -1). From the graph for $d/\delta = 1/10$, it can be seen that the amplitude of the response will be very nearly 20 per cent. Now consider the same contact covered by 1.5 meters of 10 ohm m. overburden, so that d/δ is still 1/10, but now Koc is 1/100 and log Koc is -2. The amplitude of the response is now slightly less than 10 per cent.

Tables 3-4 to 3-7 show the half-width of the anomaly for the same four cases of d/ δ . The half-width is shown in terms of skin depth in the more conductive medium (i.e. ρ_C), as this seemed to be the best way to summarize the results. Therefore, in order to obtain the half-width of the anomaly for a given case from the table, it is first necessary to determine the skin depth in the medium on the more conductive side of the fault (and not the skin depth in the overburden). The results may be summarized as follows:

- 1. For a given resistivity contrast across the fault (Kcr) and a given resistivity contrast between the overburden and the more conductive side of the fault (Koc), the anomaly becomes wider as the overburden becomes thinner. (i.e. as d/δ decreases).
- 2. For a given resistivity contrast between the overburden and the more conductive side of the fault (Koc) and a given d/δ , the anomaly becomes wider as the resistivity contrast across the fault (Kcr) increases.
- 3. For a given Kcr and a given d/δ , the anomaly becomes narrower as the resistivity contrast between the overburden and the more conductive side of the fault (Koc) increases.

Using Tables 3-4 to 3-7 in conjunction with Fig. 3.12 allows one to determine the half-width, as well as the amplitude of the response, for any case under consideration.

Table 3-4

 \bigcirc

(_)

Half width of anomaly in terms of Skin Depths (δ) in the more conductive medium ($\rho_{\rm C})$ for d/δ = 1/30

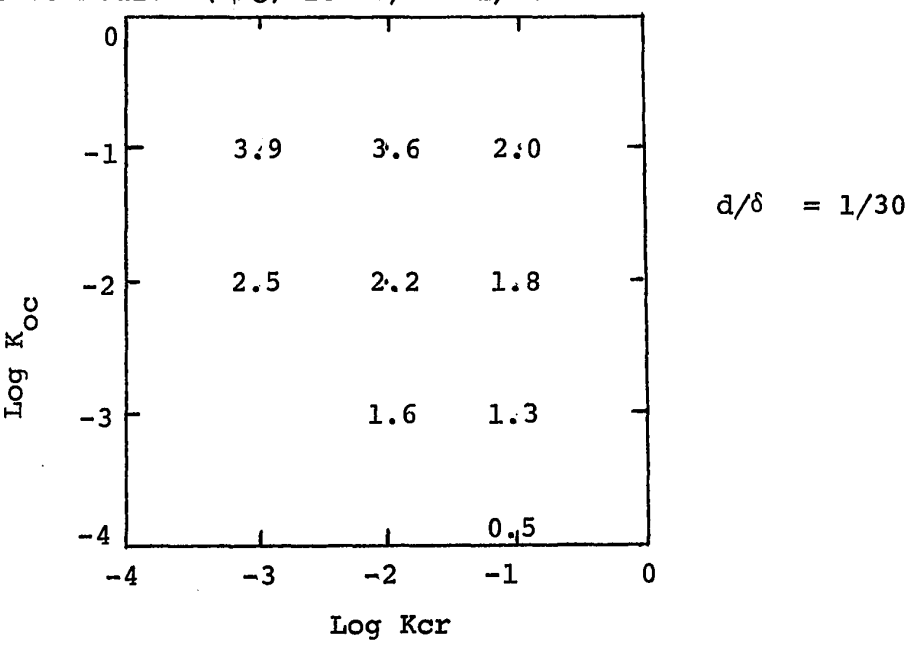
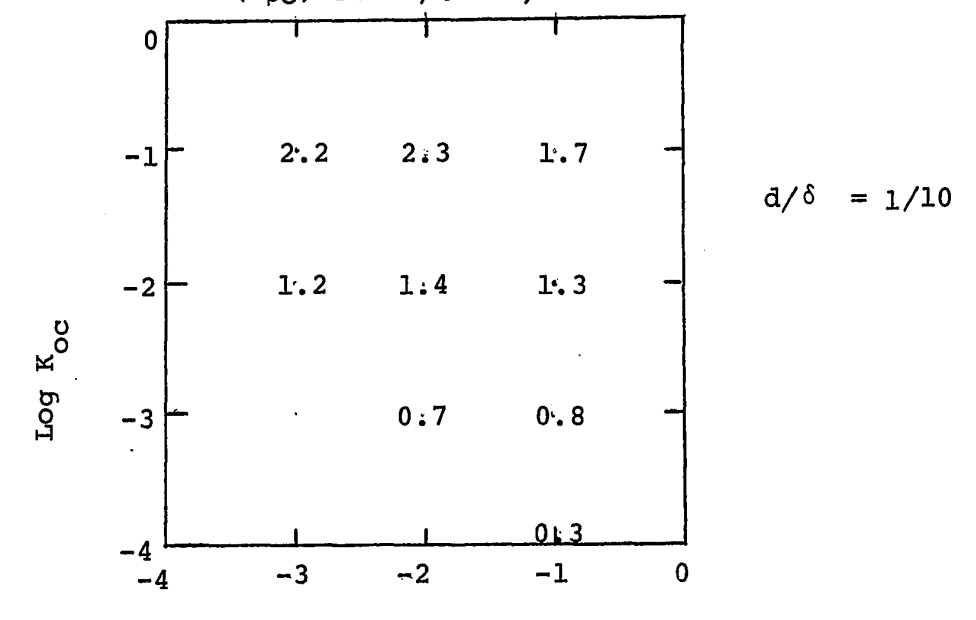


Table 3÷5

Half width of anomaly in terms of Skin Depths (δ) in the more conductive medium ($\rho_{\rm C})$ for d/δ = 1/10



Log Kcr

Table 3-6

Half width of anomaly in terms of Skin Depth (δ) in the more conductive medium (ρ_{C}) for $d/:\delta=1/3$

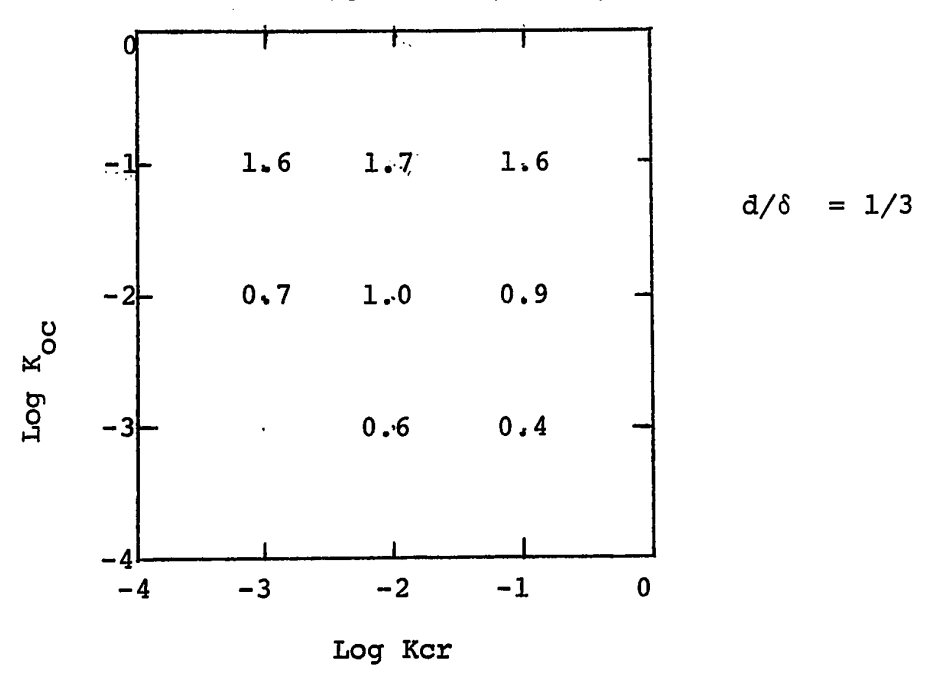
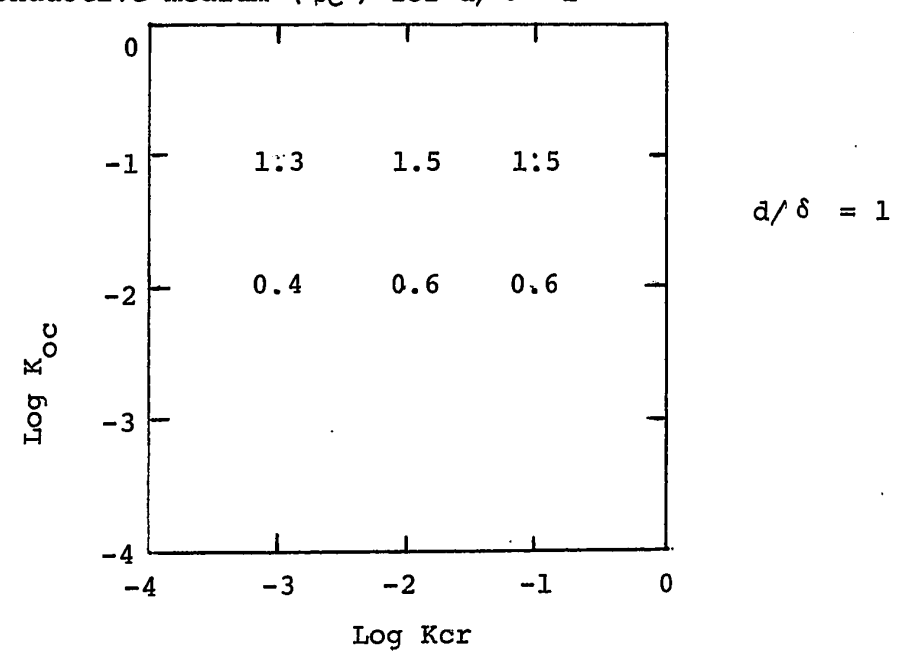


Table 3-7

Half width of anomaly in terms of Skin Depths (δ) is the more conductive medium (ρ_{C}) for d/ δ = 1



CHAPTER IV

INSTRUMENTS

4.1 Geonics EM-16

Designed by Vaino Ronka and manufactured by Geonics Limited, the EM-16 is a Very Low Frequency (VLF) receiver covering the frequency band (15 KHz-25KHz) of the VLF transmitting stations operating for navigation and for communications with submarines. These transmitters use a vertical dipole antenna, which produces a concentric horizontal magnetic field (H_{φ}) around them. When these primary magnetic fields intersect conductive bodies in the ground, there will be secondary fields radiated from the bodies. Then the total magnetic field in the vicinity of the conductor is the resultant of the primary field and the secondary field.

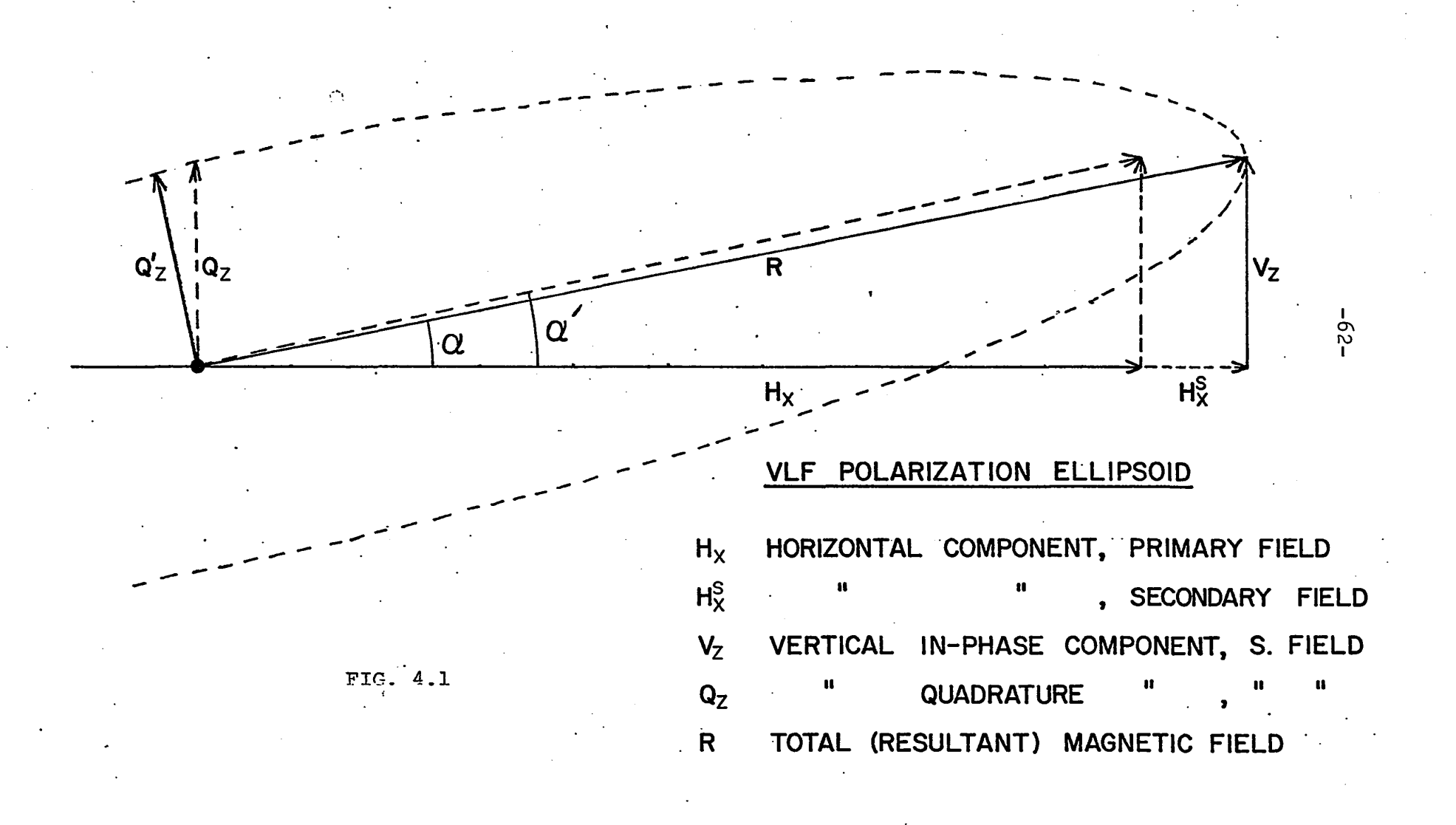
The receiver has two inputs, each with its own receiving coil. One coil normally has a vertical axis while the other is horizontal. The vertical axis receiving coil detects any vertical signal present, while the signal from the horizontal receiving coil, after an automatic signal phase shift of 90 degrees, is fed into a potentiometer in series with the vertical coil. At each station the instrument is initially held horizontal (i.e. the two coils are horizontal) and rotated in azimuth for minimum signal, so that the reference coil (horizontal coil) is aligned with the primary magnetic field.

The instrument is then rotated to vertical, maintaining the horizontal or bottom coil in the primary field direction.

To take a reading, the signal from the vertical coil is first minimized by tilting the instrument. The signal will be a minimum when the vertical coil is at right angles to the total magnetic field direction. The tangent of the tilt angle (angle α in Fig. 4.1) will then be the ratio of the vertical real-component of the secondary magnetic field to the sum of the primary horizontal field and the horizontal component of the secondary field (See Fig. 4.1). If the horizontal component of the secondary field is much smaller than the primary field (and it usually is), then the tangent of the tilt angle (x100) will be a good approximation of the vertical in-phase component expressed as a percentage of the primary field (angle α in Fig. 4.1). The inclinometer dial is calibrated both in degrees and percentage.

The remaining signal in the vertical coil is then balanced out by adjustment of the quadrature potentiometer to provide a part of the signal from the horizontal coil which, as mentioned, is shifted in phase by 90 degrees. The potentiometer thus nulls the vertical quadrature signal in the vertical coil circuit, and its dial is also calibrated in percentage markings. It should be noted that during a reading the horizontal coil will be parallel to the total field. Therefore it is a part of the total field, not just the primary field, which is shifted in phase by 90 degrees. The out of

(j



phase reading is only an approximation (Q_Z') - but generally a good approximation - of the quadrature vertical signal (Q_Z) expressed as a percentage of the primary field.

There are several VLF transmitters which may be detected by the EM-16 receiver in North America. Where possible, a station should be chosen so that the magnetic field lines are approximately at right angles to the main geological strike in the survey area. Stations are selected by means of pre-tuned plug-in units. The instrument normally contains two of these receiver units and an external switch is provided for selection of one or the other.

4.2 Westinghouse VLF Wave Impedance Meter

The apparatus used for measuring the wave impedance was the C-602 VLF Wave Impedance Meter designed and manufactured by the Westinghouse Georesearch Laboratory at Boulder, Colorado. It uses the magnetotelluric method of measuring the impedance of an electromagnetic wave at the earth's surface in the frequency range 10-60 KHz. The instrument has an antenna to sense the tangential electric field (E_r) and another to detect the magnetic field (H_ϕ) from the VLF transmitter being used. A null technique is employed to compare the phase and amplitude of these two fields at the earth's surface (See Fig. 4.2).

The magnetic field $(H_{\dot{\varphi}})$ is detected by a 26 turn air core shielded loop antenna 12-1/2 inches in diameter. The loop circuit, balanced to ground to reject the vertical

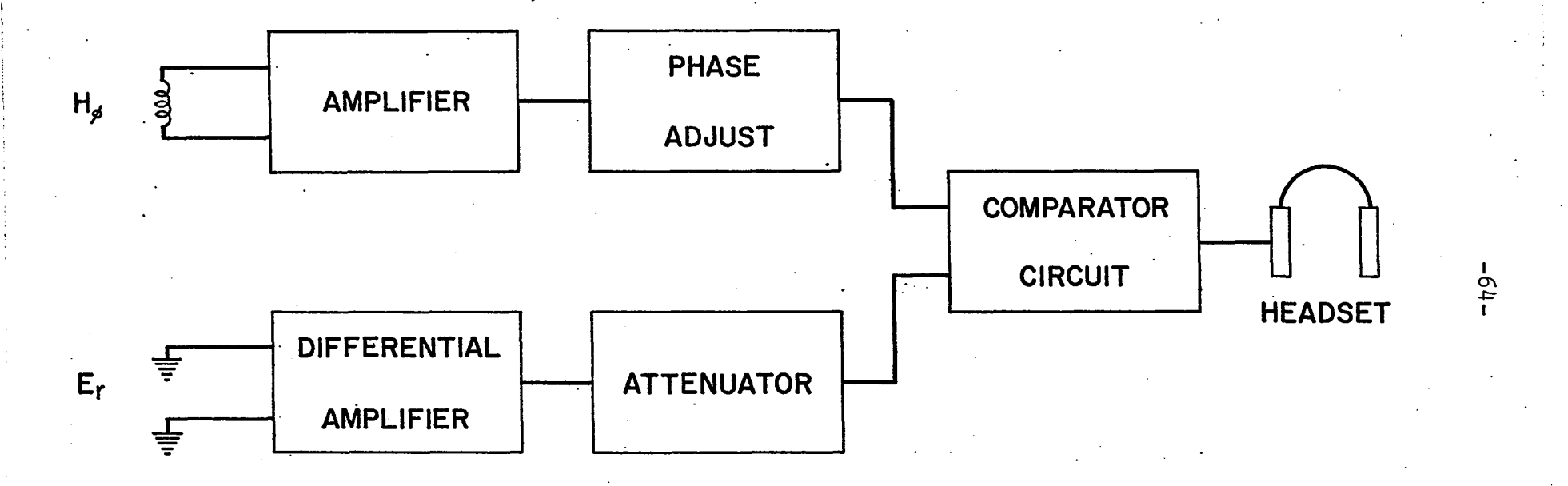


FIG. 4.2 SIMPLIFIED BLOCK DIAGRAM OF WAVE IMPEDANCE APPARATUS

electric field (E_z) from the VLF transmitter antenna, is coupled into the input stage of the H channel amplifier through a step up transformer. The amplifier provides a stable gain and flat response over the desired frequency range. The H_ϕ output from the amplifier is fed to a phase adjust circuit, which provides a means of introducing phase lags in the H channel to assure that the E_r and H_ϕ channels differ in phase by 180 degrees at the comparator input for all normally encountered conductivities. The phase circuit output is coupled into one input of the comparator circuit where it is balanced against the output voltage of the E_r channel.

The tangential electric field (E_p) is sensed by a dipole antenna consisting of a pair of electrodes driven into the earth. These are metal stakes spaced 10 meters apart and fed to the inputs of a differential amplifier. The differential input provides common mode rejection so that only the tangential component of the field (E_p) is detected. The single-ended output of the differential amplifier is fed into a multiplier attenuator. The multiplier attenuates the E signal in 20 dB steps to provide X10, X100, and X1000 multipliers for the wave impedance reading obtained from the potentiometer of the comparator circuit.

The comparator circuit employs a 10 turn linear potentiometer, to balance the output of the ${\rm H_{\phi}}$ circuit against that of the ${\rm E_{r}}$ circuit, calibrated to give a readout of the wave impedance. With equal amplitude signals, 180

degrees out of phase, the output will be zero. In any case, the null condition is indicated either by a pair of earphones or a meter.

(

The apparent conductivity of the ground is then obtained from a graph of wave impedance (as read on the comparator) vs. conductivity (for the particular frequency being used). This graph is provided in the instrument manual, and is shown in Appendix I.

The H channel may be used independently to determine the amplitude of the incident magnetic field (H_{φ}) . The voltage induced in the loop by the magnetic field is measured by a meter, which is calibrated in terms of the equivalent vertical electric field. Thus, the readout is in volts/meter.

CHAPTER V

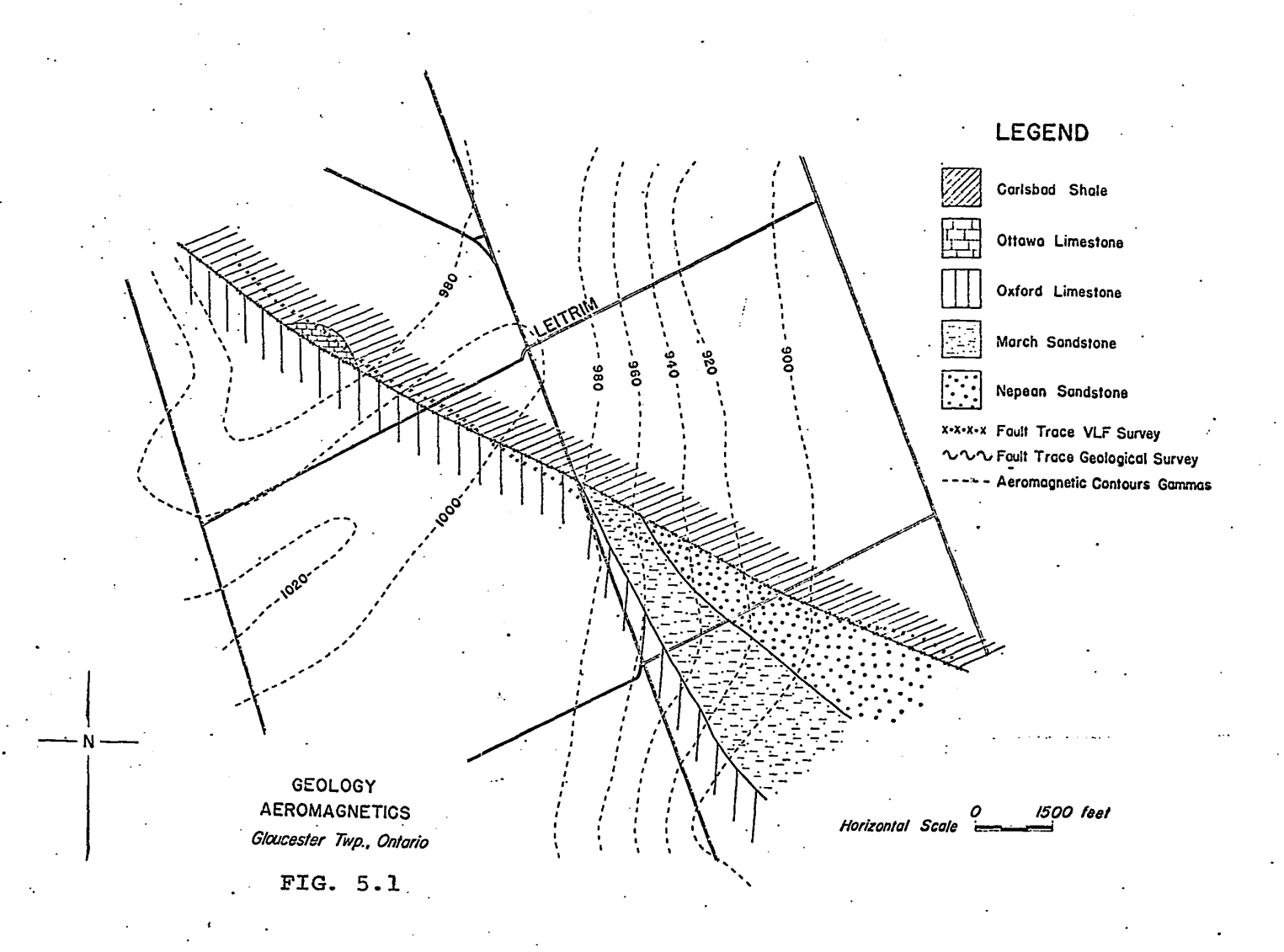
FIELD WORK

- 5.1 Leitrim and Russell Area
- (i) Location and Description of Faults Traversed

The Gloucester fault strikes approximately South-East from Ottawa and has a strike length of roughly 30 miles. The fault is a nearly vertical dip-slip fault which occurs in Precambrian rocks and Paleozoic sediments up to Ordovician in age (See Figs. 5.1 and 5.2). To the North-East the block is downthrown, while to the South-West it is displaced upwards. The Oxford formation, consisting of dolomite and limestone, has been uplifted to lie next to the Carlsbad formation, which consists mainly of grey shale. South of Leitrim, the Nepean formation (sandstone) and the March formation (sandstone and sandy dolomite) also lie in contact with the Carlsbad formation. A representative cross section is shown at the bottom of Fig. 6.6.

Further south, in the vicinity of Russell, several minor faults run parallel to the Gloucester fault for distances up to a few miles, with average distances of about two miles and four miles east of the main structure (See Fig. 5.2). Southeast of Russell a large block of Ottawa limestone lies in contact with the Carlsbad formation to the north, and the Oxford, Rockcliffe, and St. Martin formations to the west.





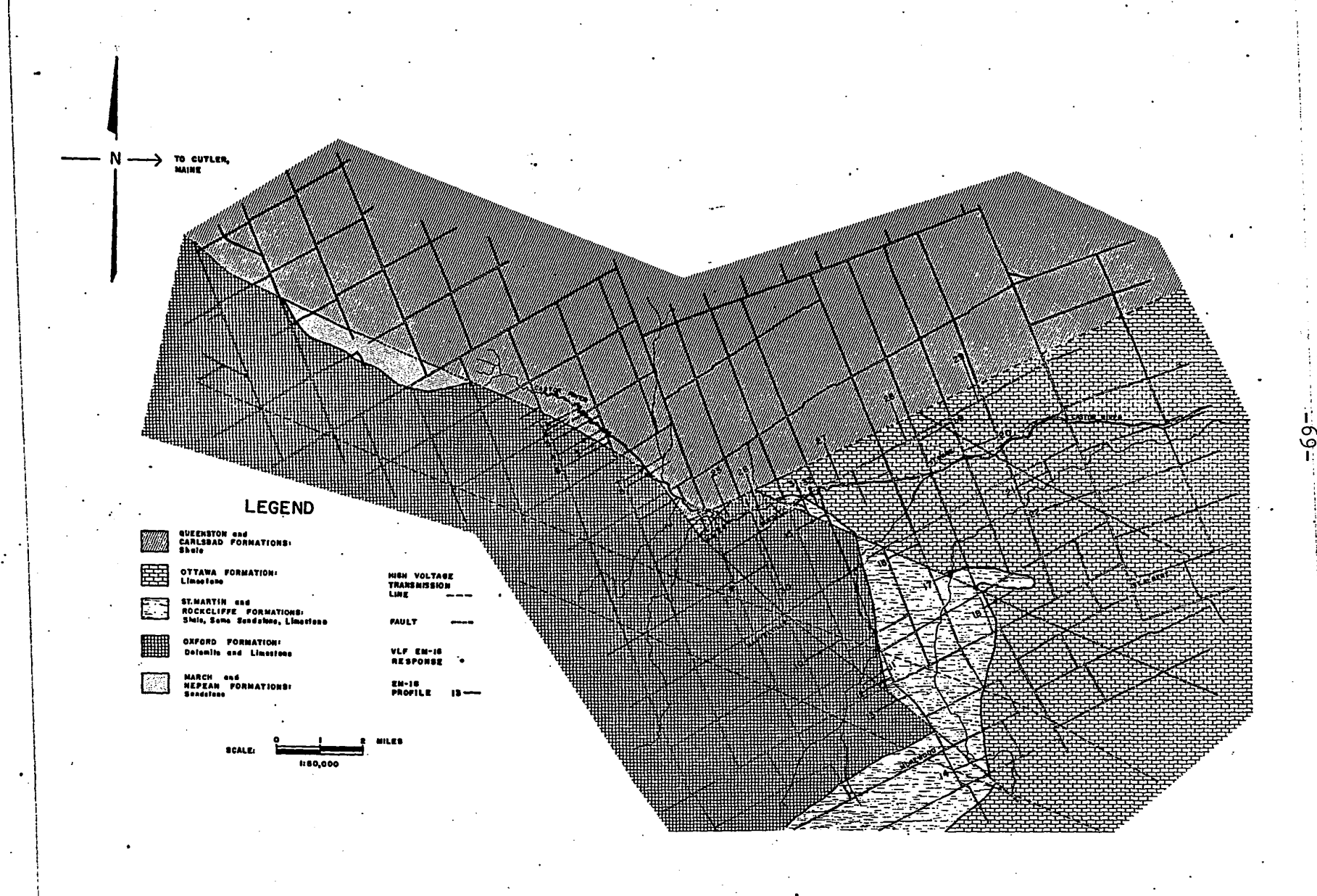


FIG. 5.2 GEOLOGY AND VLF SURVEY LINES, RUSSELL AREA

(ii) Description of Geologic Formations

The Nepean sandstone is mainly composed of coarse quartz sand in a siliceous cement. Andrieux (1971) reports that wherever this formation outcrops, its resistivity is of the order of 1500-3000 ohm meters.

The March formation, lying between the Nepean sandstone and the Oxford dolomite, is comprised of alternating layers of sandstone and dolomite. This formation does not appear as an electrical horizon (Andrieux) but depending on its composition, is considered together with either the underlying or overlying formations.

The Oxford formation is a thick-bedded dolomite, which sometimes changes to limestone. Andrieux found its resistivity to be about 5,000 ohm meters.

The Ottawa formation is mainly limestone with some layers of shale and sandstone, and Andrieux believes that its resistivity is from 2000 to 3000 ohm meters.

The Rockcliffe formation is composed of shale with lenses of sandstones, while the St. Martin formation consists of limestone with some shale and dolomite. Although Andrieux did not carry out any electrical measurements directly on the outcrops of these two shaley formations, he concludes that they exhibit a relatively low resistivity, and may be counted as one unit as far as electrical properties are concerned.

The Carlsbad formation is mainly comprised of shale with some limestone and dolomitic layers. It exhibits a very low

resistivity of about 85 ohm meters (Andrieux). The Russell and Queenston shales are local events northwest of the village of Russell, and have electrical properties almost identical to the Carlsbad Shale.

(iii) Field Procedure

A three mile length of the Gloucester fault was surveyed in detail in the vicinity of Leitrim. Profiles were spaced approximately 500 feet apart and were about one mile long on the average (See Fig. 6.1). The traverse lines had a strike of about ENE-WSW and the VLF transmitter selected for the survey was Cutler, Maine. The strike of this station was almost exactly due east of the survey area, and the station itself was about 400 miles distant. Readings were taken facing north.

The intersection of Leitrim Road and Highway 31 was taken as station 0+00 for this survey. Survey lines are numbered north and south, and stations are numbered east and west from this point.

Pace and compass techniques were used throughout the survey, with aerial photographs providing excellent control for plotting station locations. Remote from the fault a station spacing of 200 feet was used, but approaching the fault this was decreased to 100 feet. Directly over the fault and for several hundred feet on either side of it, a 50 foot station interval was used.

The results were plotted in profile form. In-phase and quadrature components were plotted on one profile, and the total field $(\sqrt{(IP)^2 + (QUAD)^2})$ response was plotted on another.

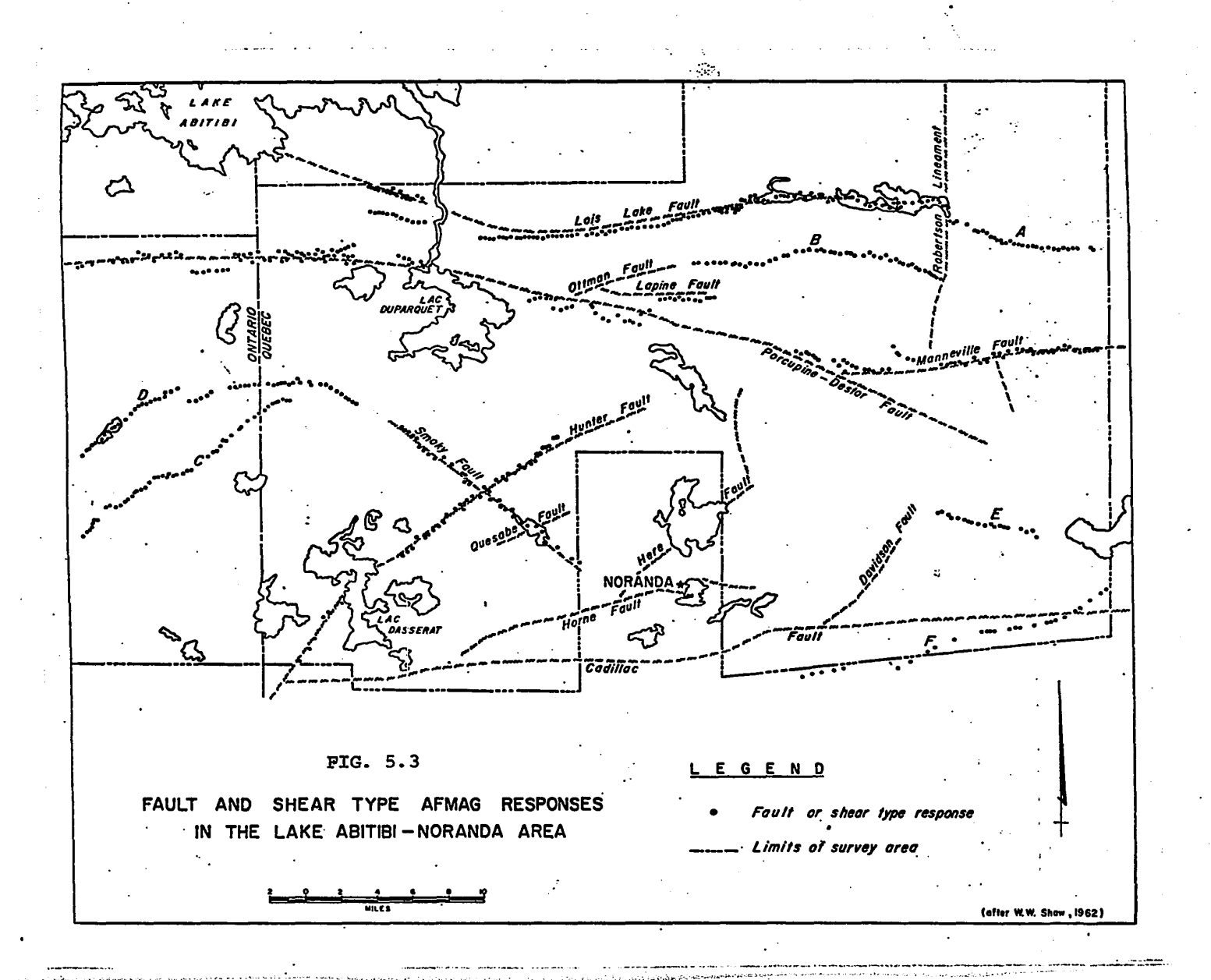
Several profiles were also obtained by traverses with the wave impedance apparatus. These were lines 20+00N, 10+00S, 41+50S, 50+00S, and 60+50S. A station spacing similar to that used with the EM-16 was employed.

The investigation was subsequently extended further south along the Gloucester fault, and to the minor faults in the Russell area. Profiles were arbitrarily selected on the basis of the geological map, but man-made structures also played a role in the selection of a traverse in this area. High voltage transmission lines and buried telephone cables posed a particular problem. It was necessary to avoid such features (if they were close to the fault being surveyed) when choosing traverse lines. Traverse lines were numbered numerically in this area (See Fig. 5.2), and pace and compass techniques with aerial photograph control were once again used. Wave impedance traverses were conducted only along Line 2 and Line 6.

5.2 Noranda Area

Fig. 5.3 shows a general outline of the faults in the Noranda area, where the Smoky Creek, Hunter Creek, and Lois Lake faults were selected for investigation.

The Smoky Creek fault was readily accessible only in

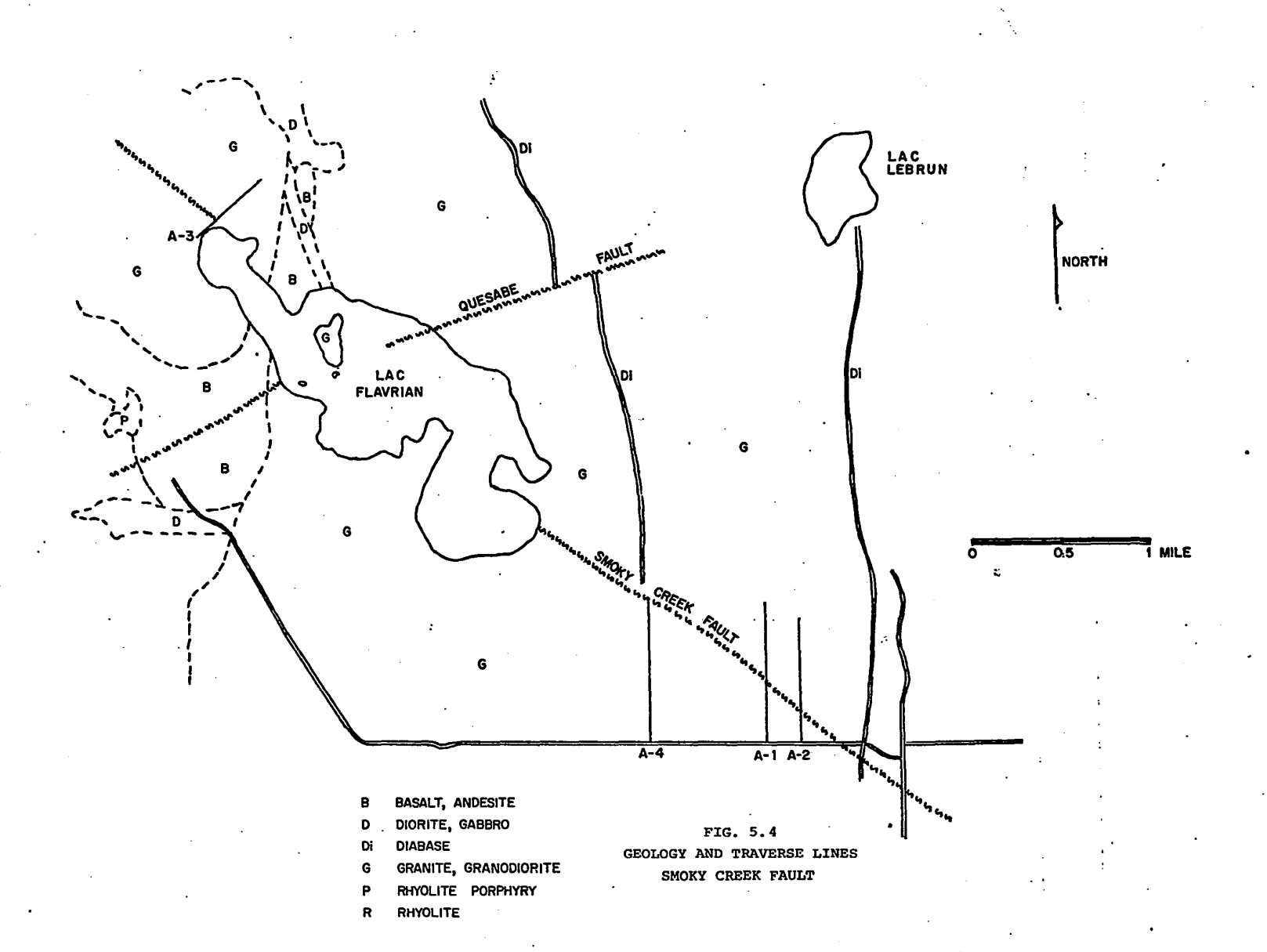


the vicinity of Lac Flavian, where granite and granodiorite appear on either side of the fault. (i.e. there appears to be no change in lithology as the fault is crossed - Fig. 5.4). Four traverses, selected on the basis of aerial photographs, were conducted in this area. These are labelled as A-1 to A-4 on the figure. Pace and compass techniques were once again used. The VLF station used was Cutler, Maine, which has an azimuth of about 110 degrees from the survey area, making it very nearly along strike of the Smoky Creek fault. Traverses with the wave impedance set were conducted along Lines A-1, A-2, and A-3.

The Hunter Creek fault strikes almost 90 degrees from the Smoky Creek fault, and it was hoped that traverses would be conducted across this fault using the VLF transmitter located at Panama. Unfortunately the signal strength was too weak to obtain EM-16 readings, and no traverses were conducted across the Hunter Creek fault.

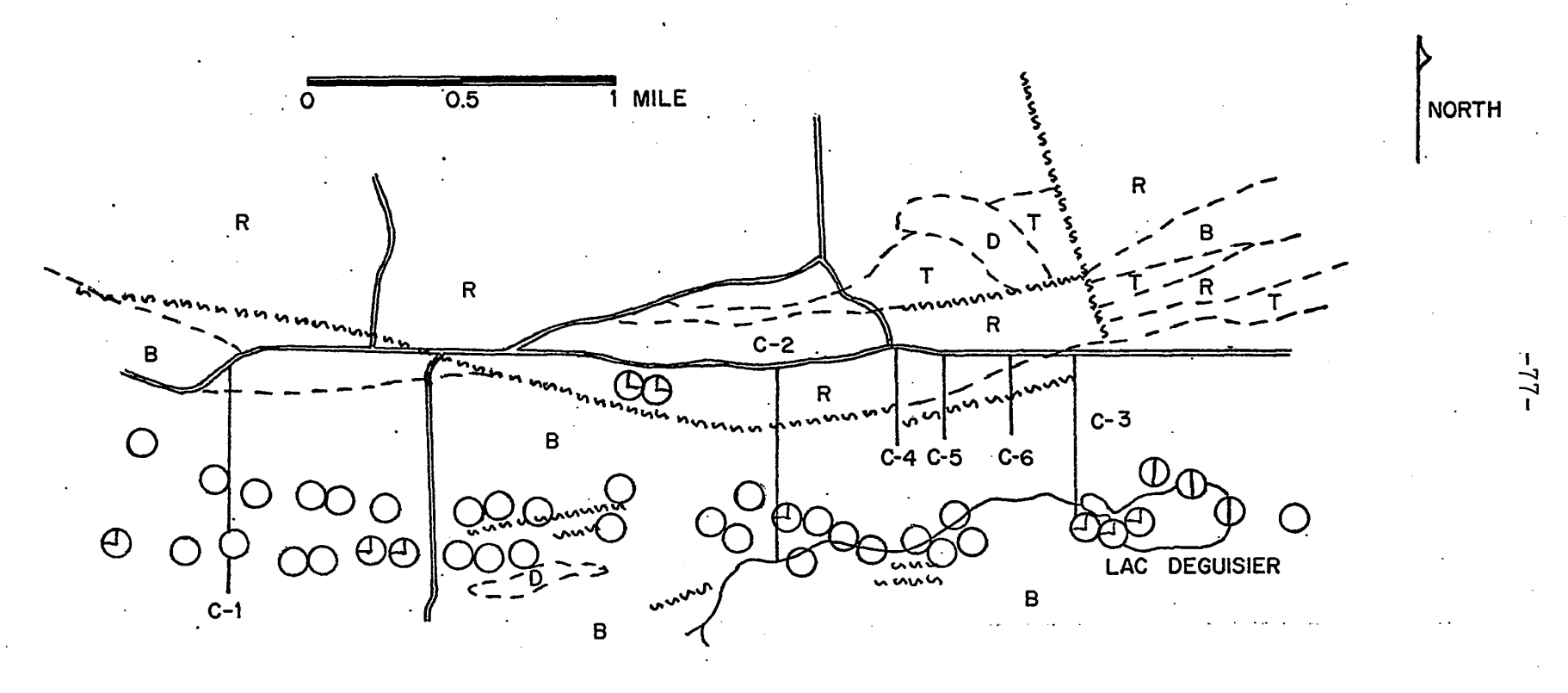
The Lois Lake fault (also known as the Lyndhurst fault) strikes nearly East-West and is generally accessible in the north central part of Duparquet township, about three miles north of the town of Duparquet. Generally speaking, rhyolite occurs on the north side of the fault while basalt and andesite are found to the south. However, according to map no. B-935-N, published by the Quebec Department of Natural Resources, the rhyolite-basalt contact is not always coincident with the





location of the fault (See Fig. 5.5).

Fig. 5.5 shows the area investigated, along with the INPUT anomalies revealed when Barringer Research conducted an INPUT survey in the area in 1967. The INPUT anomalies, like the AFMAG responses observed by Shaw, occur to the south of the fault. Six VLF EM-16 traverses were conducted in this area, again using the transmitter at Cutler, Maine. A traverse was conducted along Line C-1 solely to investigate the INPUT responses along this line. Lines C-2 and C-3 cross the Lyndhurst fault (as it is mapped) and also cross the INPUT anomalies to the south. Lines C-4, C-5 and C-6 are shorter traverses (along claim lines) and cross only the Lyndhurst fault. Wave impedance results were obtained on Lines C-1, C-2 and C-3.



- B BASALT, ANDESITE
- D DIORITE, GABBRO
- R RHYOLITE
- T TUFF, AGGLOMERATE

- O 6 CHANNEL INPUT ANOMALY
- e) 5 " " "
- O 4 " " '
- <u>Ф</u> 3 " "

FIG. 5.5
GEOLOGY AND TRAVERSE LINES
LOIS LAKE FAULT

CHAPTER VI

RESULTS OF FIELD WORK

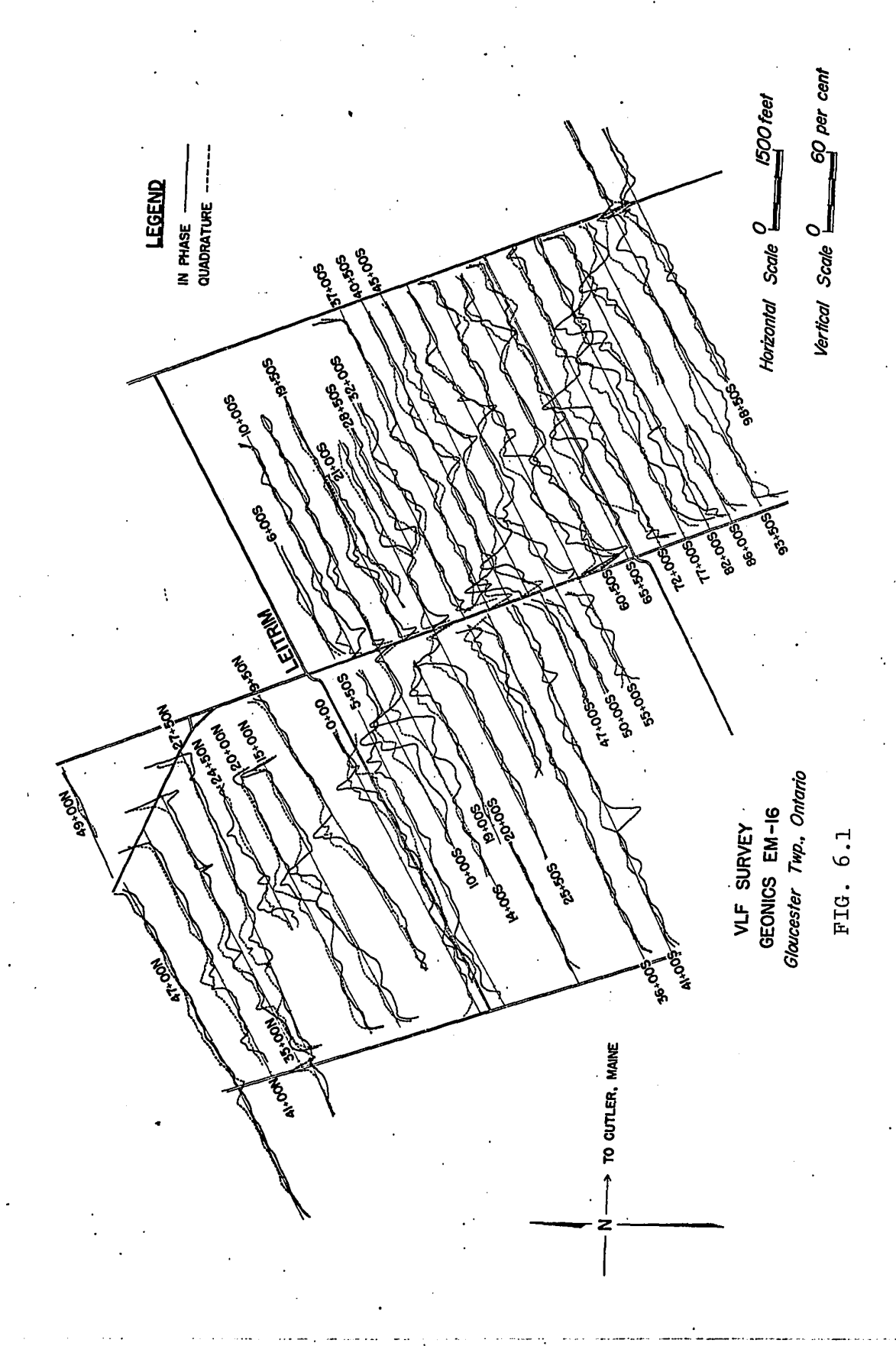
- 6.1 Leitrim Area
- (i) Geonics EM-16 Profiles Across Gloucester Fault

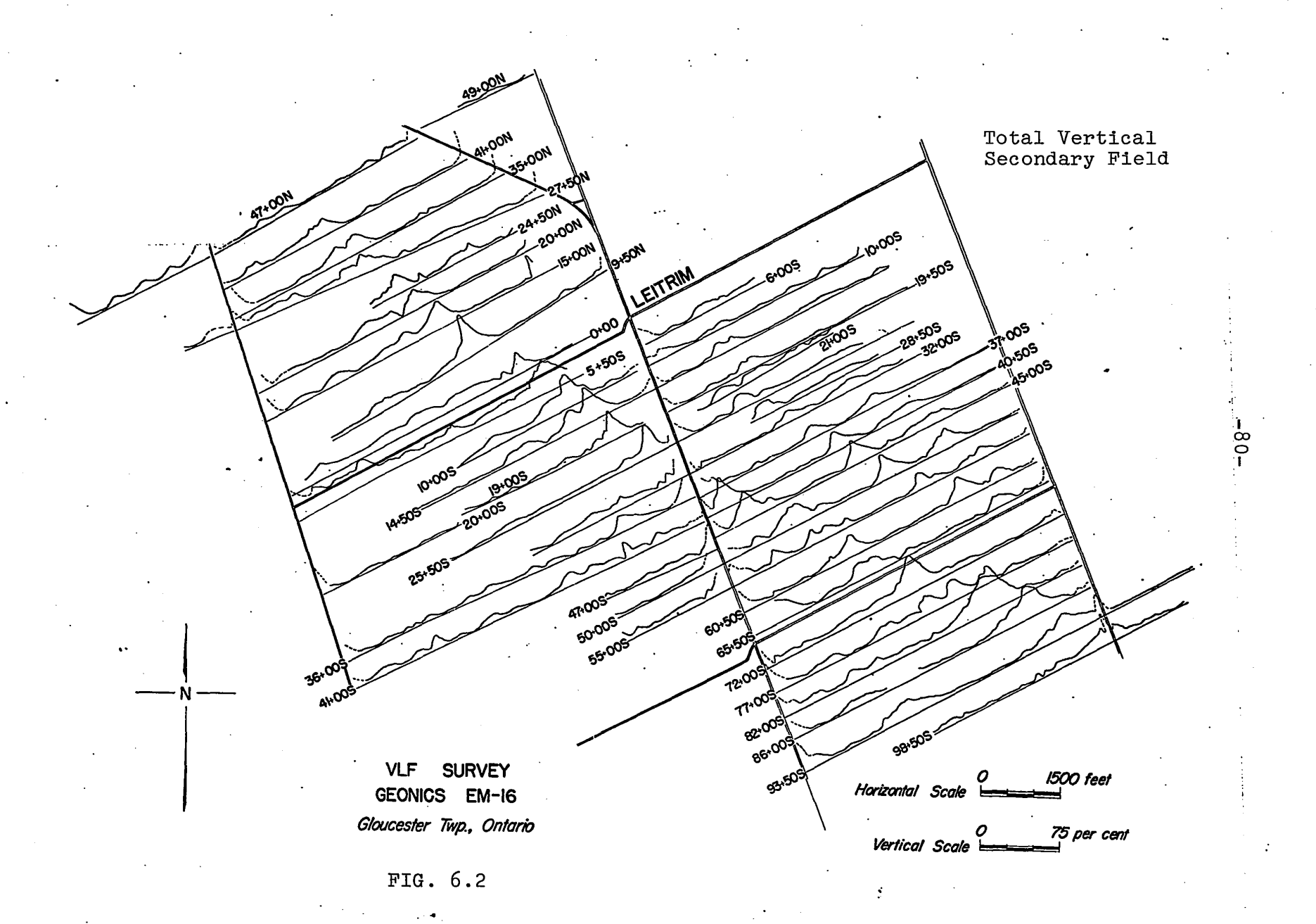
Nearly all the profiles exhibit an anomaly where the Gloucester fault is expected to occur. This anomaly consists of a positive in-phase and quadrature peak, with the latter being generally broader and flatter than that of the in-phase (See Fig. 6.1). However, the quadrature component does not always exhibit a smooth peak over the fault. On many profiles it displays a somewhat lower value (i.e. a local minimum) which generally coincides with the peak of the in-phase response. This is shown particularly well on lines 0+00, 14+00S and 40+50S, but other profiles show this effect as well.

The total field profiles over the Gloucester fault show single, well-pronounced peaks in most cases (See Fig. 6.2). Generally these peaks are slightly asymmetric, having a steeper slope on the eastern side.

These results indicate a contact with the more resistive side to the west.

Several lines (35+00N, 27+50N, 20+00N, 14+50S, 55+00S, 77+00S) exhibit a double peak rather than a single peak on the total field profiles. A fence on line 35+00N greatly distorts the profile near the fault, and this profile should





not be considered typical. The double peaks on the remainder of these lines are caused when the in-phase component takes a negative dip before it becomes a positive peak over the fault.

On lines 21+00S to 65+50S inclusive there is a distinct anomaly parallel to the Gloucester fault but somewhat more than 2000 feet to the east. The character of the anomaly is the same in all the profiles. The in-phase and quadrature components both appear as a negative peak, with the quadrature peak displaced slightly to the west of the in-phase on several of the profiles (notably on line 60+50S). This response is exactly the opposite to that of the Gloucester fault, which exhibits positive in-phase and quadrature peaks. The anomaly appears as a distinct peak on the total field profiles. Once again the peaks are generally asymmetric, but the steeper slope is now on the western side. These results indicate a second contact to the east of the Gloucester fault, but now the resistive side of the contact is on the east. This contact appears to terminate at line 65+50S.

There is a third anomaly somewhat to the east of the one previously described, appearing on lines 32+00S to 60+50S. This anomaly exhibits a positive in-phase and quadrature peak, indicating a contact with the resistive side on the west. The quadrature peak on lines 32+00S to 45+00S is very broad, and this results in a broad peak on the total field profiles. In

fact, the quadrature response seems to dominate that of the in-phase on lines 40+50S, 45+00S and 55+00S. On lines 40+50S and 45+00S there is a small in-phase peak, but this is about 500 feet to the west of the quadrature peak, while on line 55+00S there is a quadrature peak only.

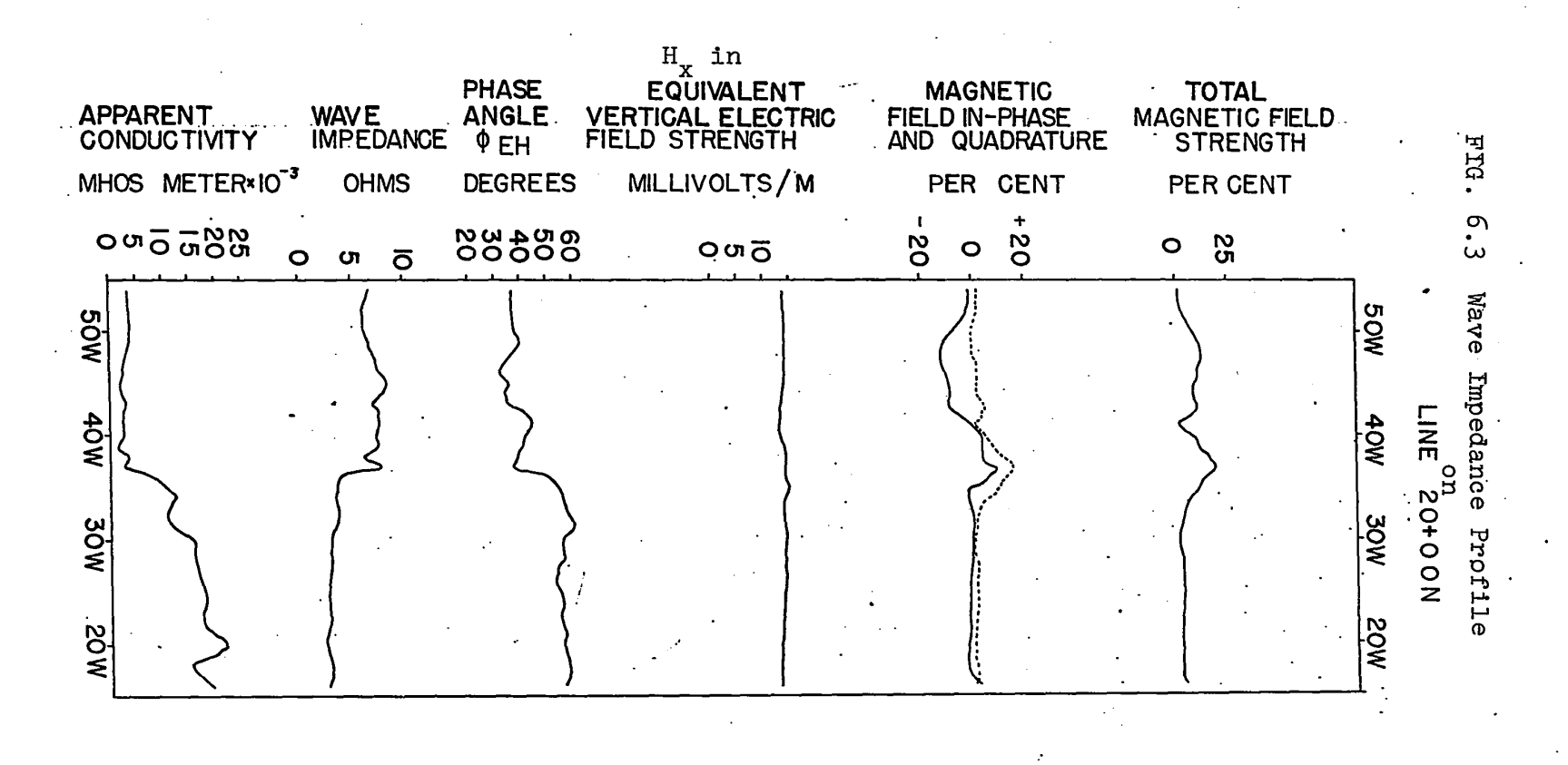
This third contact first appears on line 32+00S about 1300 feet to the east of the second contact, but gradually becomes closer to the second contact as one proceeds south. On line 60+50S these two contacts are only about 800 feet apart, and this results in a cross-over type response on the EM-16 in-phase and quadrature, since the negative peak of the second contact is close to the positive peak of the third.

(ii) Wave Impedance Profiles Across Gloucester Fault

Wave impedance (and hence conductivity) profiles were obtained by traverses on lines 20+00N, 10+00S, 40+50S, 50+00S and 60+50S, and all profiles indicate the location of the Gloucester fault.

Only one feature is apparent on line 20+00N (Fig. 6.3), this being a contact at about station 36+00W. The apparent conductivity is about 3×10^{-3} mhos m.⁻¹ to the west of the contact, while to the east it increases to a maximum of 20×10^{-3} mhos m.⁻¹. The phase angle between the electric and magnetic vectors increases from about 40 degrees on the west side of the contact to about 55 degrees on the east side. This is in agreement with the theoretical profiles, which

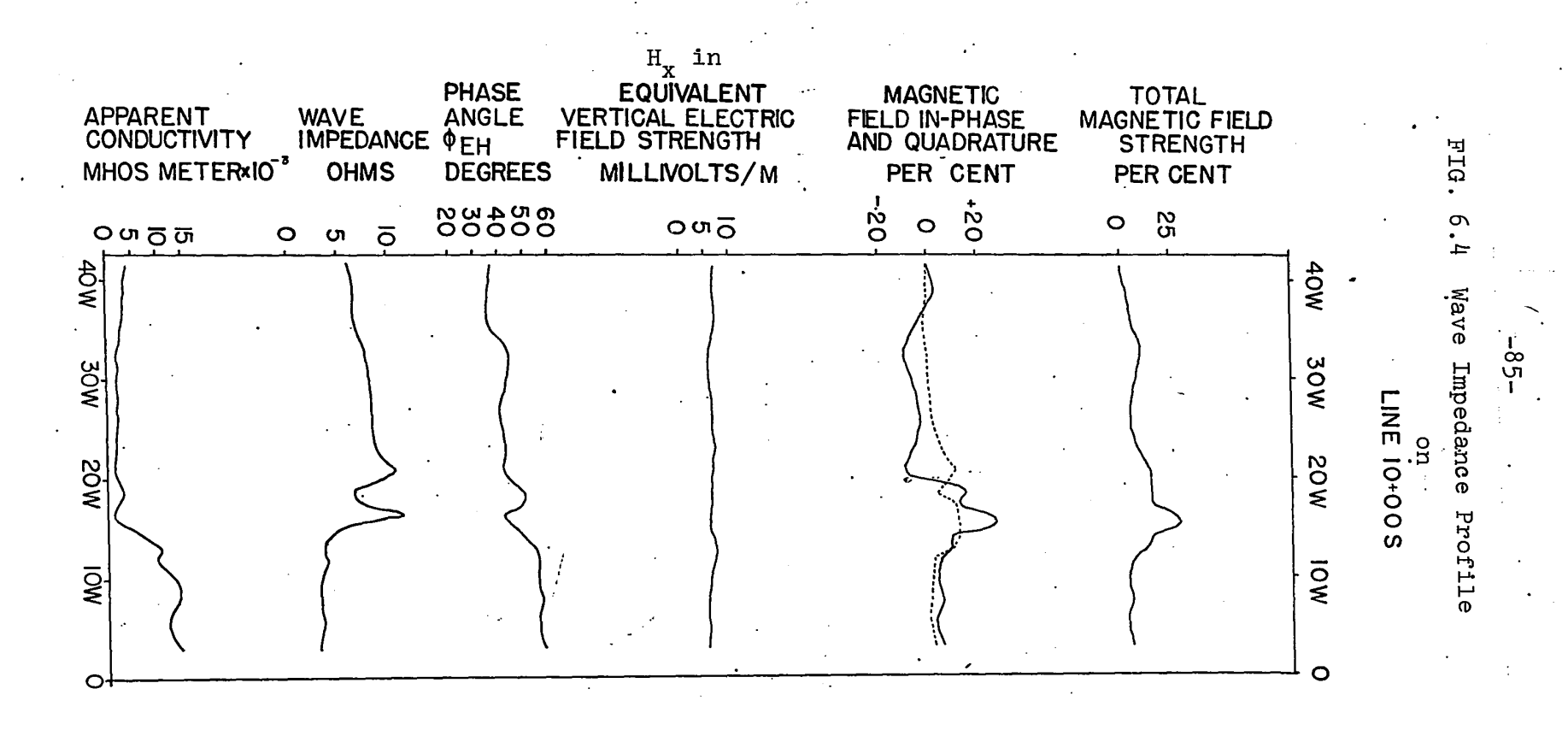
 $\zeta \rightarrow$



indicate that the phase angle (EyAl) should be higher on the more conductive side. The shape of the phase angle profile is also as it should be (Fig. 3.2). Approaching the contact on the resistive side, the phase angle starts to increase (about 41+00W), then decreases slightly in the immediate vicinity of the contact, and then increases on the conductive side. The horizontal magnetic field strength remains essentially constant across the profile. The peak of the total field EM-16 profile occurs at station 36+00W, in excellent agreement with the location of the contact as indicated by the conductivity profile.

The conductivity profile on line 10+00S (Fig. 6.4) is very similar to that of line 10+00N. A contact is indicated at about station 15+00W, correlating very well with the peak of the total field response of the EM-16 which occurs at station 15+50W, The apparent conductivity on the west side of the contact ranges from 2 to 4 x 10⁻³ mhos m. on the east side. The phase angle varies somewhat on the west side of the contact but has a mean value of about 40 degrees compared to about 55 degrees on the opposite side. The shape of the phase angle is in general agreement with theoretical profiles of Fig. 3.2. Once again the magnetic field strength is approximately constant for the length of the profile.

There are three contacts indicated by the conductivity profile on line 40+50S (Fig. 6.5), these being

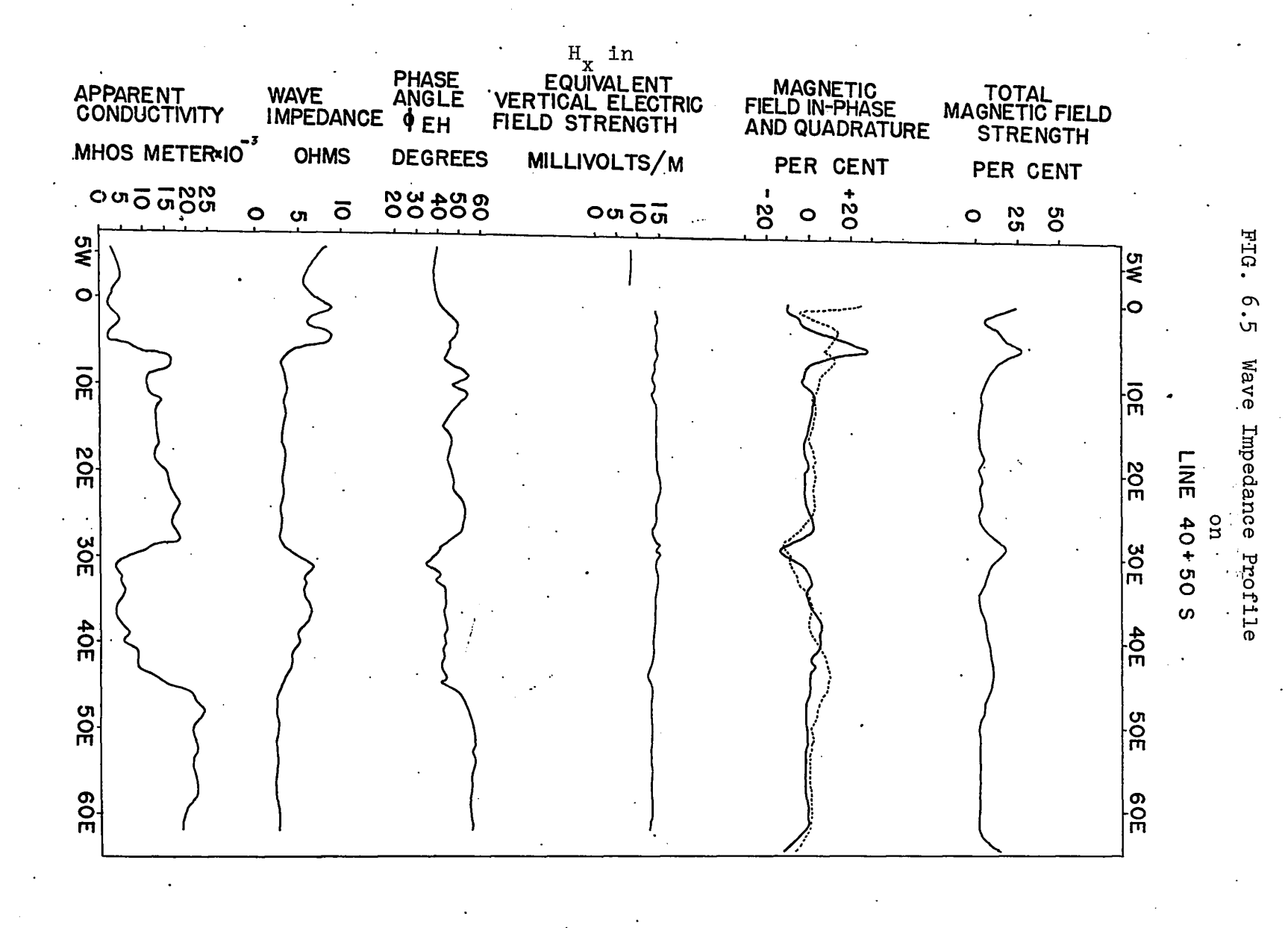


at about stations 6+00E, 29+00E and 44+50E. These results again correlate well with the EM-16 total field results, which show peaks at stations 5+50E, 29+00E and 44+00E. To the west of the first contact (at about 6+00E) the apparencenductivity varies slightly but has a mean value of about 3×10^{-3} mhos m.⁻¹. Between this contact and the one at station 29+00E, the apparent conductivity is about 15×10^{-3} mhos m.⁻¹ making this contact similar to those on the two previous profiles. However, between the contacts at stations 29+00E and 44+00E, the apparent conductivity decreases to about 5×10^{-3} mhos m.⁻¹. East of the third contact it again increases and attains a value of about 22×10^{-3} mhos m.⁻¹. Thus there is a zone of low conductivity about 1500 feet wide which occurs about 2300 feet east of the contact attributed to the Gloucester fault.

The phase angle to the west of the Gloucester fault is about 40 degrees. Between the Gloucester fault and the first contact to the east of it, the phase angle varies considerably but has a mean value of about 45 degrees. Over the sections of low conductivity the phase angle between E_y and H_x is again about 40 degrees, but this increases to about 55 degrees east of the contact at station 49+00E. In general, then, the zones of low conductivity have lower phase angles than the areas of higher conductivity.

The magnetic field strength remains approximately

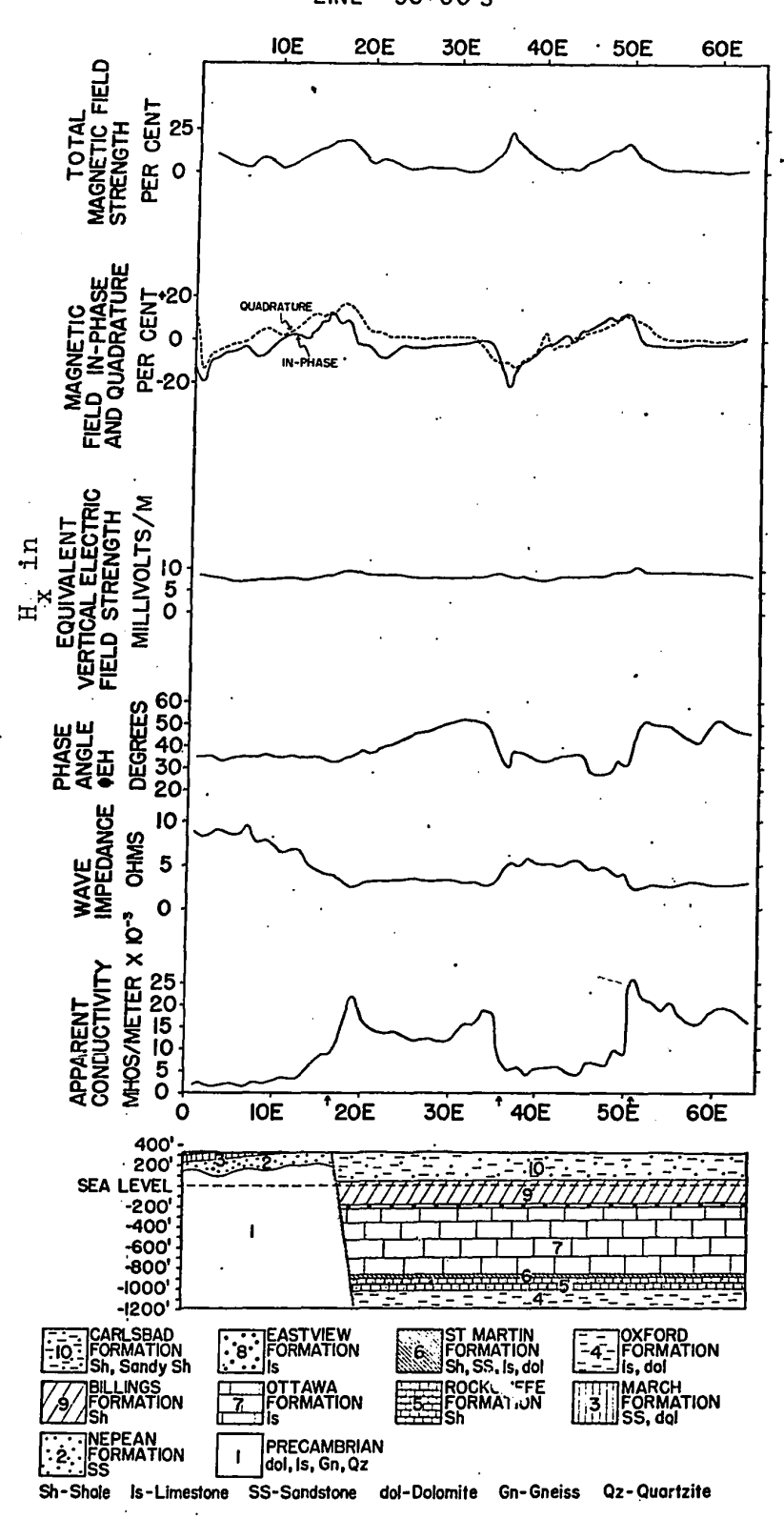
()



constant across the profile. The discontinuity in the profile at station 2+00W occurs because 2+00W, 4+00W, and 6+00W were read on a day that the VLF transmitter was operating at about one-half power (for routine maintenance). The conductivity profile on line 50+00S (Fig. 6.6) is very similar to that of line 40+50S, indicating contacts at about 16+50E, 35+50E, and 50+00E. This is in good agreement with the peaks of the total field profiles, which show these contacts at 16+50E, 36+00E and 51+00E. To the west of the Gloucester fault the apparent conductivity is about 3×10^{-3} mhos m.⁻¹. Between the contacts at 16+50E and 35+50E the apparent conductivity has a mean value of about 15 x 10⁻³ mhos m.⁻¹. but the profile overshoots this value on the conductive side of each contact. The apparent conductivity is about 5×10^{-3} mhos m. -1 between the contacts at 35+50E and 50+00E, but east of 50+00E the conductivity increases to more than 25 x 10^{-3} mhos m. -1 before it decreases to its mean value of about $20 \times 10^{-3} \text{ mhos m.}^{-1}$.

The phase angle is about 35 degrees on the west side of the Gloucester fault. Between the Gloucester fault and the zone of low conductivity to the east of it, the phase angle gradually increases from 35 degrees to a maximum of about 55 degrees just west of the zone of low conductivity. At the contact of this zone the phase angle suddenly decreases and varies somewhat, but has a mean value of just over 30 degrees.

FIG. 6.6 Wave Impedance Profile on LINE 50+00 s

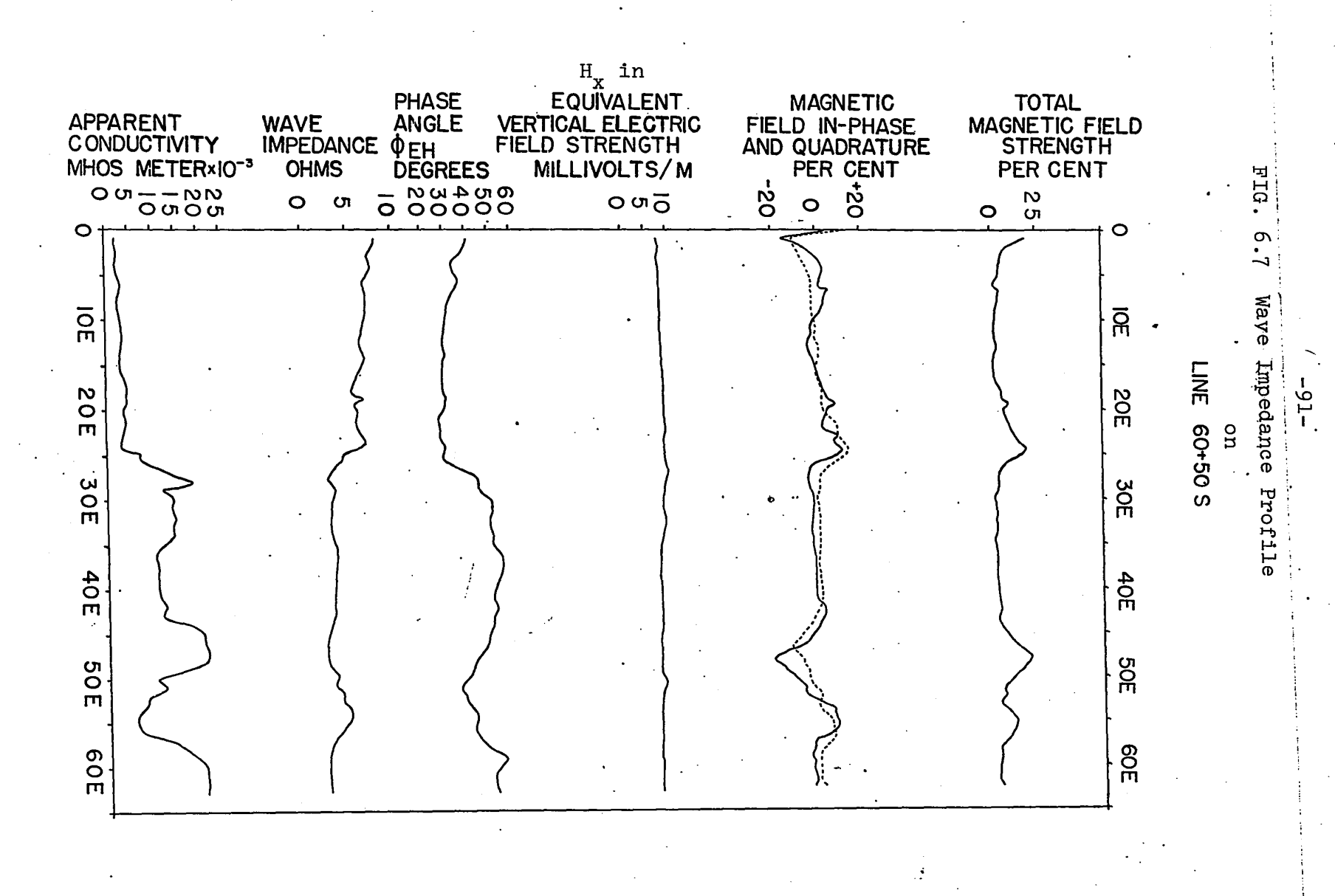


To the east of this low conductivity zone, the phase increases to about 50 degrees.

The horizontal magnetic field strength remains essentially constant.

The conductivity profile of line 60+50S (Fig. 6.7) is quite similar to the previous two profiles except that the zone of low conductivity east of the fault is much narrower. Contacts are indicated at about 25+50E, 49+50E and 57+00E while the EM-16 total field peaks occur at 24+50E, 48+00E and 56+00E. West of the Gloucester fault, the apparent conductivity is about $3-4 \times 10^{-3}$ mhos m.⁻¹. East of the fault the apparent conductivity varies considerably. It increases to 19×10^{-3} mhos m. -1 just east of the contact, and then decreases to about 15×10^{-3} mhos m.⁻¹ between stations 30+00E to 34+00E, and then decreases still further to about 11-12 x 10⁻³ mhos m. -1 between stations 36+00E and 43+00E. The apparent conductivity then increases suddenly to just over 20 x 10^{-3} mhos m⁻¹ from stations 45+00E to 48+00E, and then decreases over the zone of low conductivity. This zone is much narrower (about 750 feet across) on this profile than on lines 40+50S and 50+00S. East of the zone of low conductivity the apparent conductivity increases to about 21 x 10^{-3} mhos m.⁻¹.

The phase angle is about 30 degrees on the west side of the Gloucester fault. Between the Gloucester fault and the zone of low conductivity the phase increases to about 50-55



degrees but decreases to about 38-40 degrees over the zone of low conductivity. East of this zone the phase again increases to more than 50 degrees. Therefore, once again, the zones of low conductivity have lower phase angles associated with them.

As in the previous cases, the horizontal magnetic field strength is approximately constant throughout the profile.

(iii) Discussion of Results

EM-16 responses which closely resemble those of the theoretical profiles in Section 3.2 are observed over the Gloucester fault. This indicates that the contact is between two blocks of different conductivity, and there is no anomalous conductivity associated with the fault itself, as is the case in a water-filled shear or a graphite shear.

The Gloucester fault in the Leitrim area is located by EM-16 measurements very close to its position shown on the geological map. Figure 5.1 shows the location of the fault as Wilson (1946) determined it, and the location as it is determined by the EM-16 survey. There is a little discrepancy between the two, but generally the fault is within 500 feet of where Wilson mapped it.

The wave impedance traverses verified all the contacts indicated by the EM-16. When determined by the two methods, the

location of a contact generally agreed to within 50 feet. Since this is approximately the error inherent in the pace and compass technique, this can be regarded as excellent correlation. The wave impedance traverses showed that the apparent conductivity over the Oxford formation west of the Gloucester fault was about 3 millimhos/meter, while over the Carlsbad shale to the east of the fault it was about 15 millimhos/meter. These correspond to resistivities of 333 ohm m. and 66 ohm m. respectively. It must be remembered that these are apparent conductivities (since overburden is present), and do not represent the true conductivities of these formations.

The phase angle (between E_y and H_x) determined from the wave impedance traverses is higher on the more conductive side of the contacts, as expected from the theoretical profiles in Fig. 3.2. However, over the Gloucester fault, the phase angle does not clearly show an increase in value as the fault is approached from the west, a decrease as it is crossed, then another increase on the conductive side to the east. There seems to be a transition between a low phase angle on the resistive side of the fault to a higher phase angle on the more conductive side. This is probably due to the presence of overburden, but may also be the result of multi-layering on both sides of the fault. The wave impedance apparatus used was not designed to study multi-layered structures. It employed a fixed electrode spacing and a fixed frequency for lateral profiling, rather than for depth probing.

The horizontal magnetic field strength profiles are not very reliable in the Leitrim area. This is due to the fact that sometimes the station (Cutler, Maine) was transmitting a carrier wave (continuous signal) and sometimes Morse code (interrupted signal). When code is being transmitted, the maximum deflection of the needle on the field strength meter can only be guessed at and is usually too low. In addition, the station occasionally operates on half power for maintenance service, usually 12:00 P.M. to 2:00 P.M. on Wednesdays and Thursdays, but other times as well. Nevertheless, there was a continuous signal with the transmitter at full power over most of line 50+00S. This shows that the field strength is slightly higher (Fig. 6.6) on the more conductive side of the Gloucester fault, and is a little lower over the resistive block between 37+00E and 50+00E. This is in agreement with the theoretical results. This is the only line on which the field strength results may be considered consistent enough to give a reliable profile, and it shows that there is very little change in horizontal magnetic field strength across the Gloucester fault in the Leitrim area. This is probably due to the presence of overburden.

The two anomalies east of the Gloucester fault are interesting. These are fault type responses which indicate that a wide resistive zone occurs in the Carlsbad shale, and wave impedous results confirm that this is the case. They

cannot be explained by a bump or hill in the bedrock (resulting in an area of very thin overburden), since the bedrock is the Carlsbad shale which exhibits a very low resistivity (about 85 ohm meters). Possibly there are two faults which have resulted in a resistive block of rock being uplifted into the Carlsbad shale. A likely explanation for this resistive block is the Ottawa limestone, since this formation (which occurs below the Carlsbad and Billings shales) is seen to outcrop north-west of Leitrim. It is not unlikely, then, that this formation is in contact with the Carlsbad formation in other locations, and this would certainly account for the EM-16 and magnetotelluric results. However, this is only a speculative interpretation at best.

6.2 Russell Area

Figures 6.8 - 6.39 show the profiles obtained by traverses in the Russell area. These profiles may be located on the map of Fig. 5.2. Most profiles in this area start and finish on a road, and an anomaly at the end of a profile is due to a power line, unless otherwise explained. The in-phase (solid line) and quadrature response (broken line) appear together at the top of the figure, while the total field appears at the bottom. Uniformity of scale has not been preserved on several of these profiles, for the sake of convenience.

(i) Geonics EM-16 and Wave Impedance Profiles

Profiles were obtained by traverses on Lines 1-14 with the hope of delineating the Gloucester fault further along strike to the south-east.

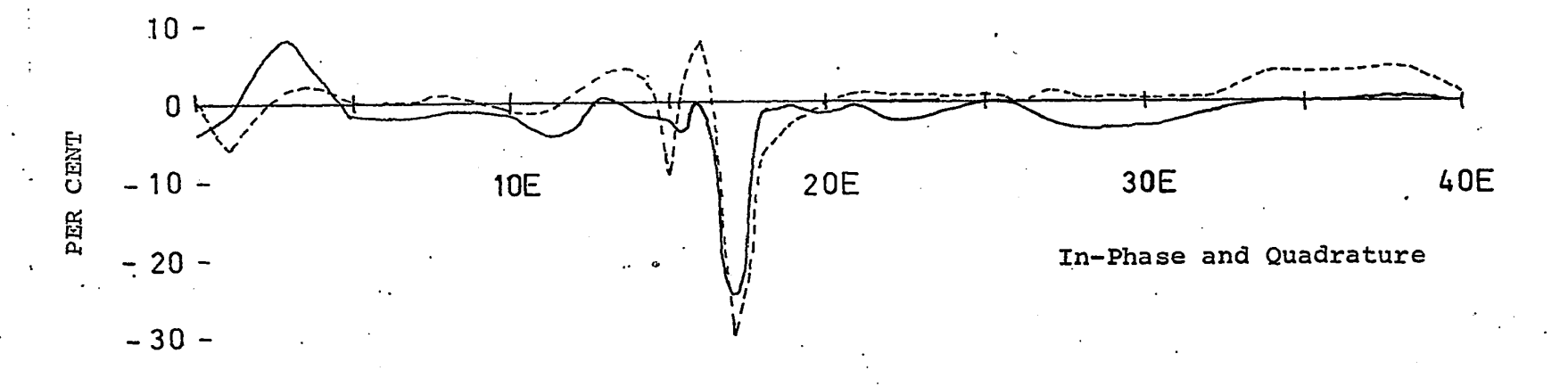
Line l

A buried telephone cable at station 16+90E accounts for the sharp peak of high amplitude at 17+00E. There is a much smaller anomaly at station 3+00E exhibiting a slight in-phase peak, indicating a contact with the higher resistivity on the west side. This is possibly the contact between the Oxford dolomite and the Carlsbad shale but, if so, it is about 1000 feet to the west of this contact as shown by the fault on the geological map.

Line 2

A contact type response occurs in the vicinity of station 10+00E. This is a small in-phase peak with a smaller quadrature peak, indicating a contact at 9+50E with the higher conductivity on the east side. The total field profile shows a distinct peak at 9+50E, although it has a relatively small amplitude. Wave impedance results confirm the existence of a contact at this point. West of the contact the apparent conductivity is about 15 x 10^{-3} mhos m.⁻¹. Between stations 8+00E and 12+00E the apparent conductivity increases from about 13 x 10^{-3} mhos/meter to slightly more than 40 x 10^{-3} mhos/meter (an apparent resistivity of only 25 ohm meters). The apparent conductivity then rapidly decreases to about 25 x 10^{-3} mhos/meter





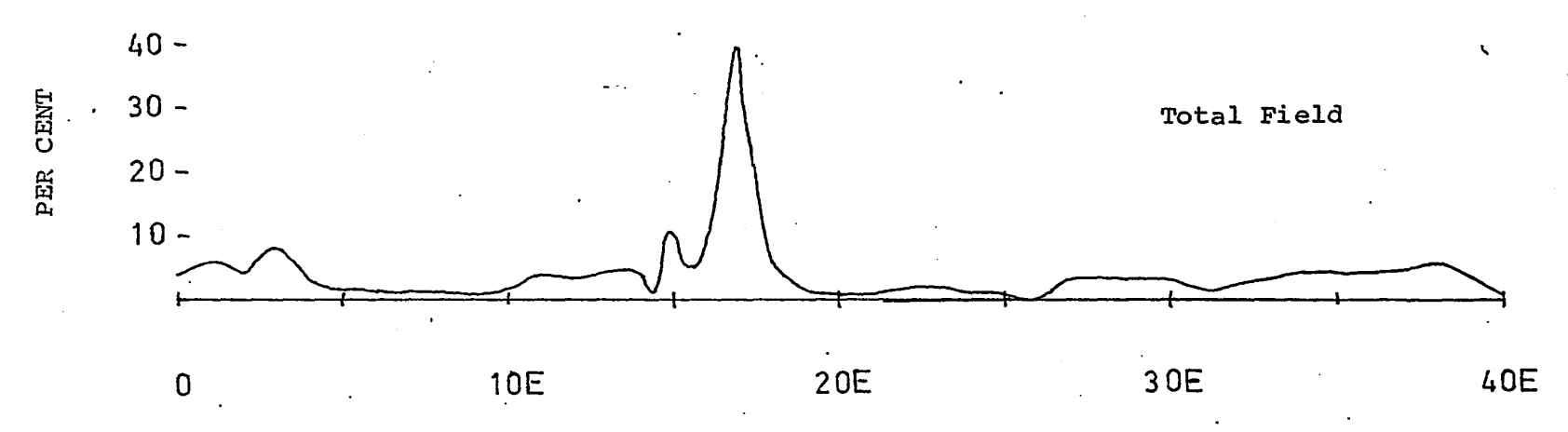
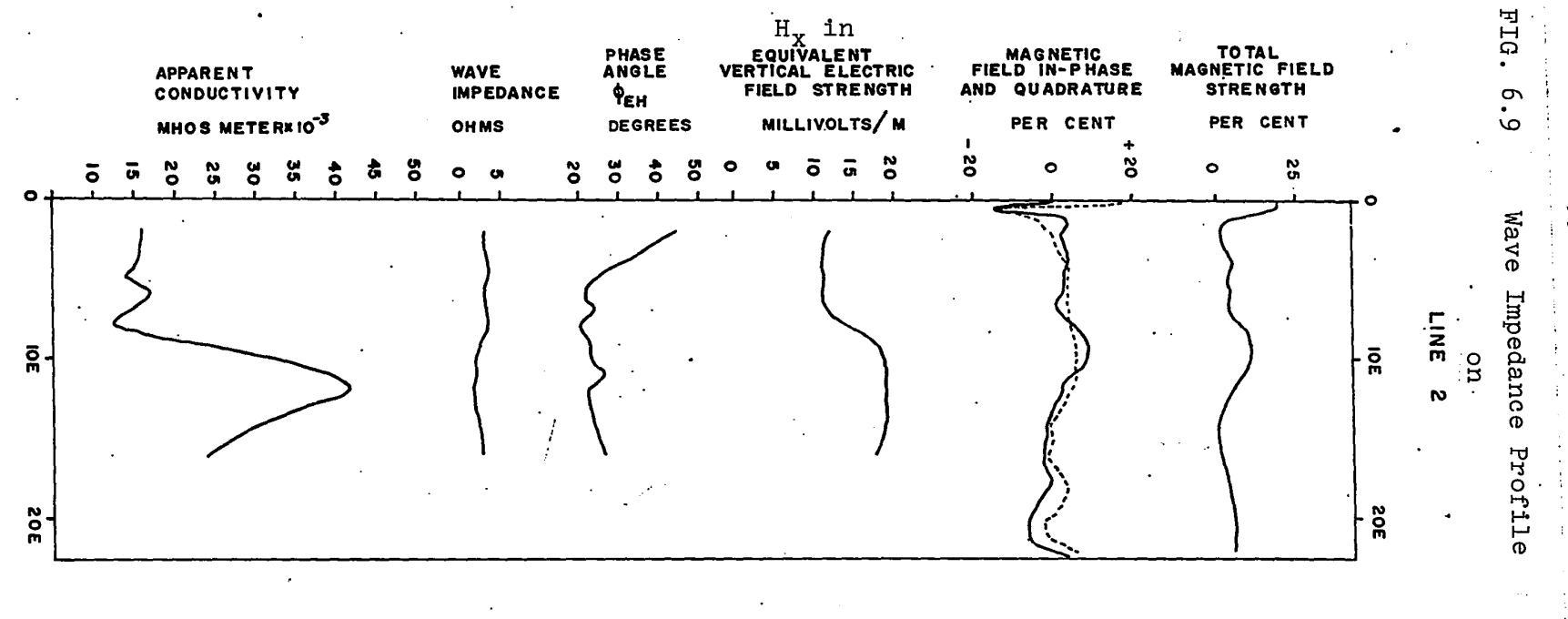


FIG. 6.8 GEONICS EM-16 RESPONSE ON LINE 1

at station 16+00E. The phase varies slightly, but is between 20 and 30 degrees on either side of the contact. It is not known why the phase angle does not change value across the contact in this particular case. The phase decreases rapidly from more than 40 degrees to about 20 degrees at the west end of the profile, but this is possibly due to interference from the overhead power line at 0+20E. The horizontal magnetic field strength increases on the more conductive side of the contact. West of the contact (on the more resistive side) it has an equivalent electrical field strength of about 11 millivolts/meter, while,on the more conductive side of the contact, this value increases to about 19 millivolts/meter. This is in agreement with the theoretical results of Section 3.2 which indicate that the field strength should be higher on the more conductive side of the contact.

There is little doubt that this contact is that between the Oxford dolomite and the Carlsbad shale, although it is about 900 feet west of where the fault is shown on the map. The apparent conductivities on either side of the contact are higher than in the Leitrim area, possibly because the overburden is somewhat thicker on this profile. This could also be the reason that the amplitude of the EM-16 response over the contact is quite low.



-99-

:4

Line 3

The sharp cross-over at station 30+50W occurs right over a ditch, and there is probably a metal drainage pipe running along the ditch, since the response indicated a good, shallow, narrow conductor.

There is a very broad in-phase peak at station 48+00W. This seems to indicate a contact at that point with the higher resistivity to the west. Once again this is probably the contact between the Oxford dolomite and the Carlsbad shale, but about 1200 feet to the west of where it is shown on the geological map. It is not known why this response is much broader than any other over this contact.

Line 4

A response occurs which again indicates a contact with the higher conductivity to the east. There is a positive in-phase and quadrature peak, but the quadrature peak is displaced about 200 feet east of that of the in-phase. In addition, the quadrature shows a local minimum beneath the in-phase peak. Since the in-phase and quadrature peaks do not coincide, the total field response shows a slight depression at its peak. In this case, the contact does not occur at the peak of the total field profile, but at the in-phase peak and local minimum of the quadrature. The in-phase response is quite large and very noisy for a distance of about 1000 feet just to the west of the contact. The overburden is extremely thin (one



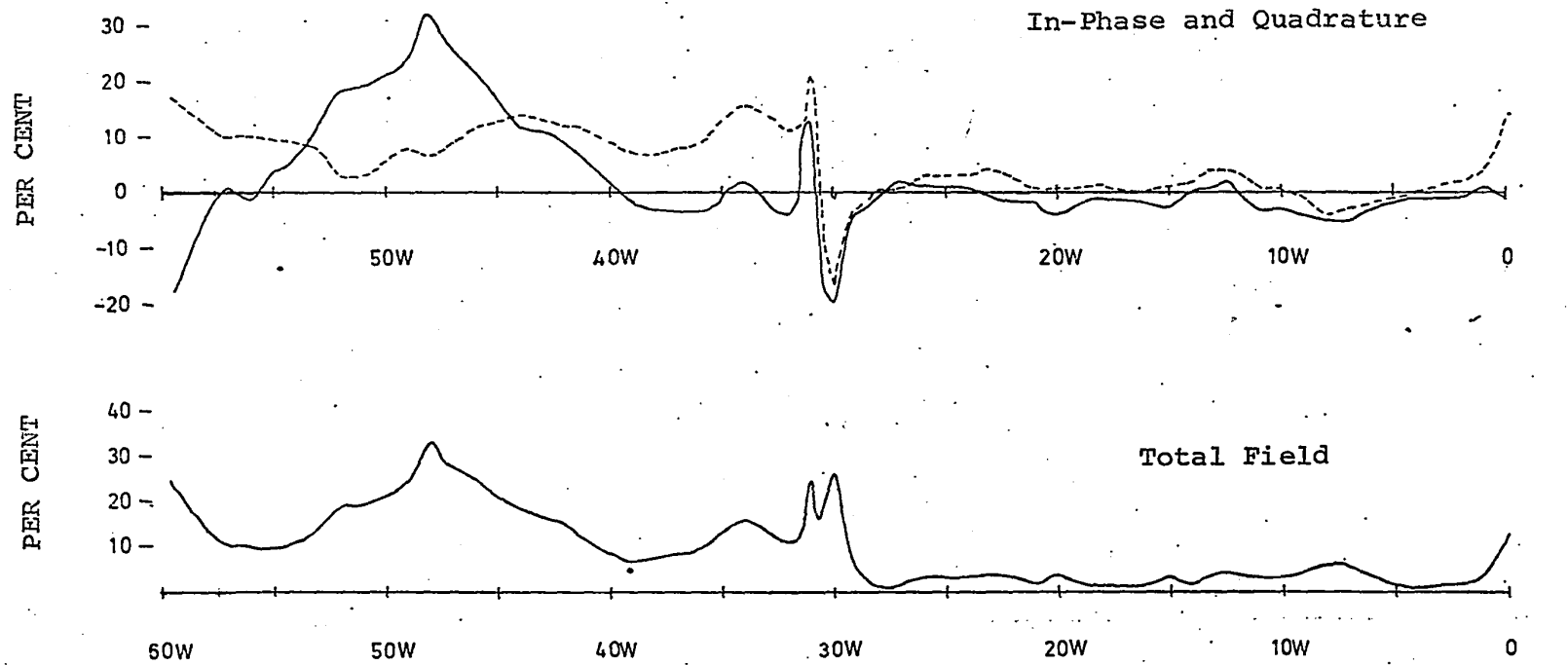


FIG. 6.10 GEONICS EM-16 RESPONSE ON LINE 3

In-Phase and Quadrature

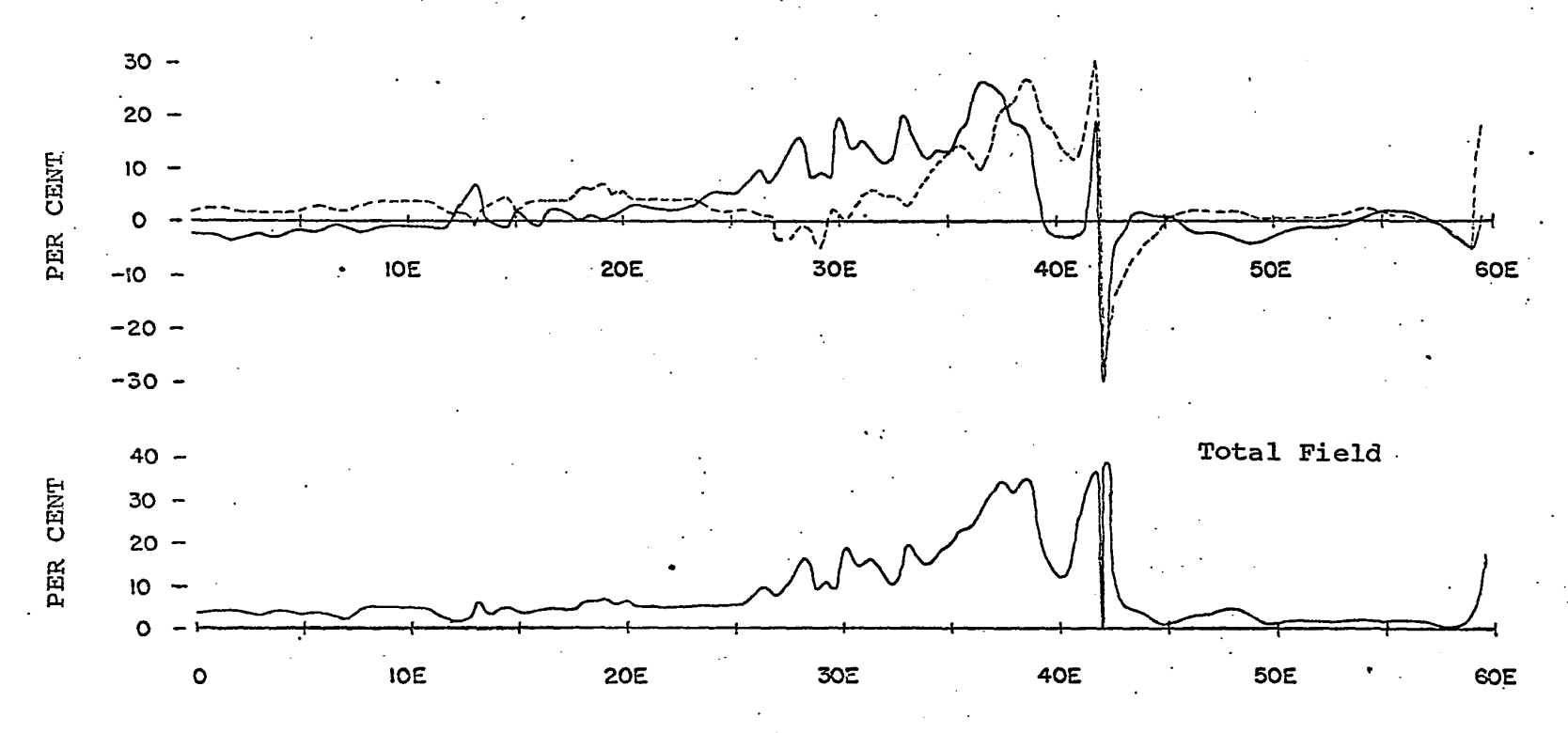


FIG. 6.11 GEONICS EM-16 RESPONSE ON LINE 4

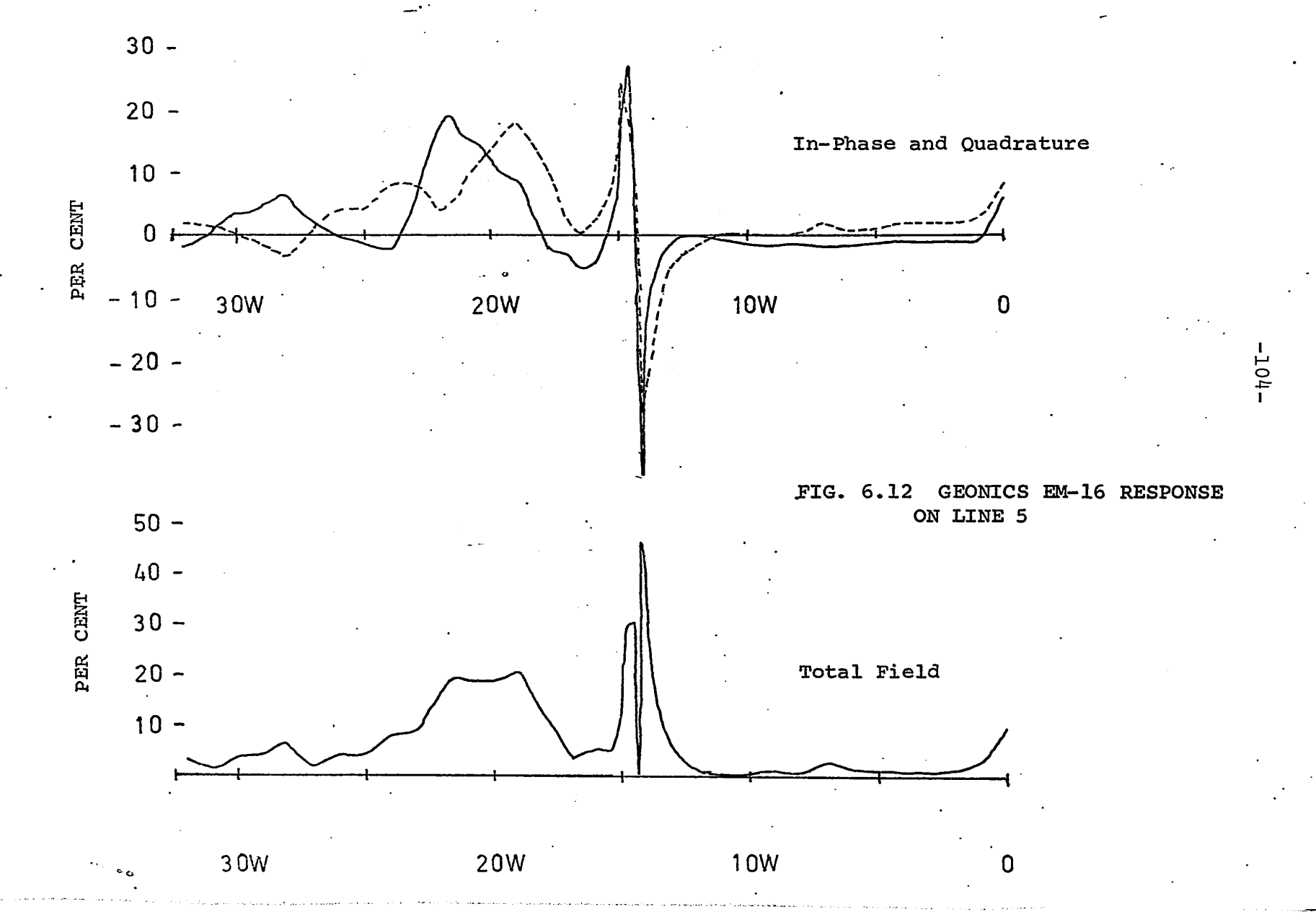
foot or less) in this area, and the Oxford formation outcrops frequently between 25+00E and 35+00E. Since the Oxford dolomite has a relatively high resistivity (about 5000 ohm meters), and is very close to surface, a wide response is to be expected on the more resistive side of the contact. The contact is that between the Oxford dolomite and the Carlsbad (or Queenston) shale, but it is about 500 feet west of where the fault is shown on the map.

The sharp cross-over at 42+00E is caused by a buried telephone cable, and this distorts the east side of the quadrature response over the contact.

Line 5

The sharp cross-over at 14+40W is caused by a buried telephone cable.

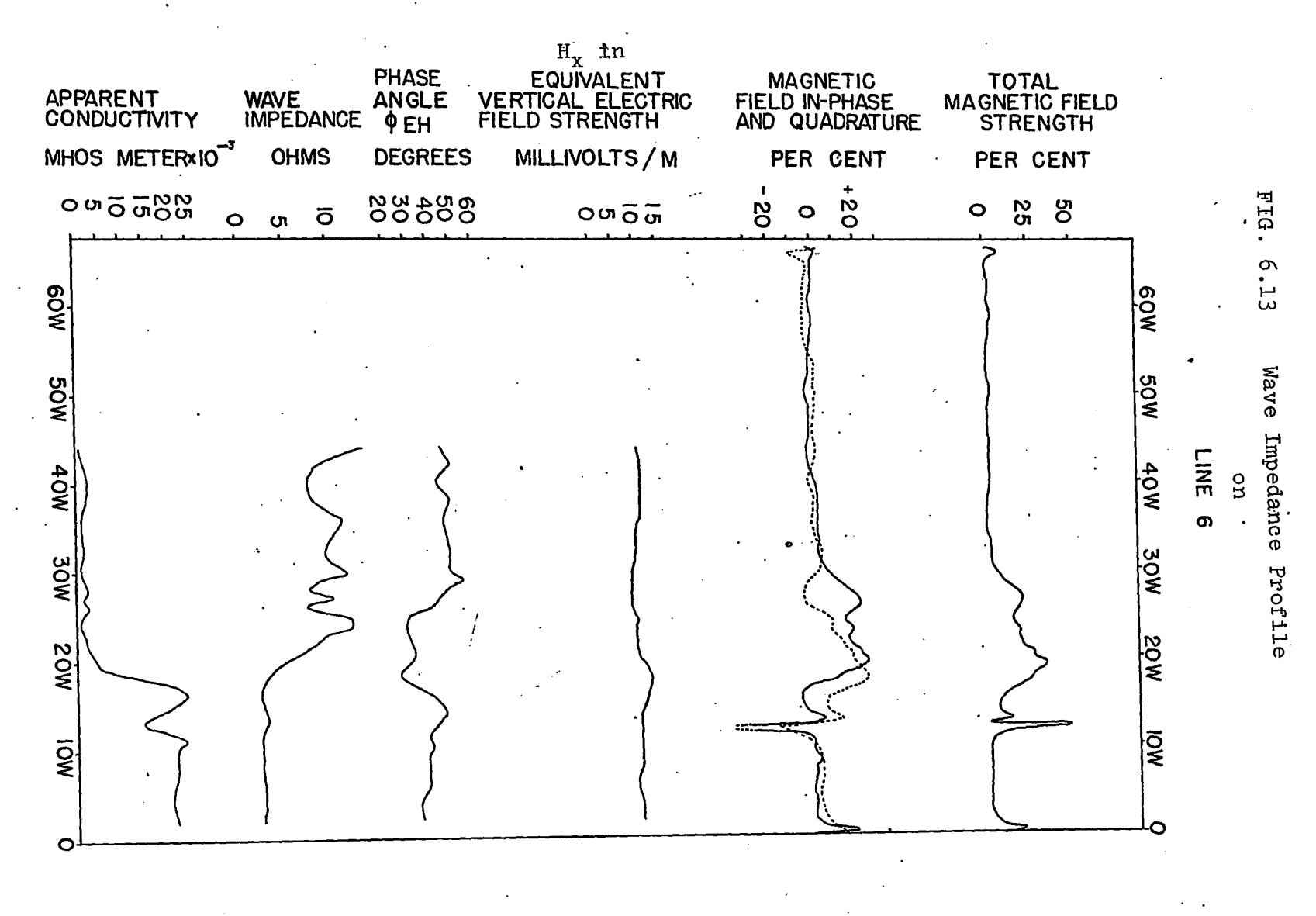
There is a contact type response at 22+00W similar to that of the previous line. The in-phase and quadrature response are both a positive peak, but the quadrature peak is displaced about 250 feet to the east of that of the in-phase (resulting in a wide, flat peak on the total field profile). The quadrature again displays a local minimum beneath the in-phase peak. The contact is that between the Oxford dolomite and the Queenston shale, but about 800 feet west of where it is shown on the map.



Line 6

A buried telephone cable causes the cross-over at 12+50W. The in-phase and quadrature responses over the contact are quite similar to those of the previous two profiles. The in-phase response is very broad on the west side of the contact, which occurs at about 19+50W, and the quadrature peak is once again displaced about 200 feet to the east of the in-phase peak. The total field response is very broad, but peaks at about 19+50W. The peak is very asymmetric, being much steeper on the eastern side of the contact (the more conductive side). As already mentioned, the response is very broad on the west side of the contact. The Oxford formation outcrops frequently between stations 32+00W to 40+00W, as the overburden is shallow in this region. The overburden seemed to be considerably deeper at the east end of the profile.

A traverse was conducted along Line 6 with the wave impedance apparatus and the results confirm the suspicion that the resistivity is considerably higher to the west of the contact. The conductivity profile indicates a contact at station 19+00W, coincident with the peak EM-16 response. West of the contact, the apparent conductivity is very low, roughly 1 to 2 x 10^{-3} mhos/meter, but occasionally even less than that. The apparent resistivity is therefore about 500 ohm meters to slightly more than 1000 ohm meters. This is to be expected,



-106

•

in view of the fact that the Oxford dolomite is very close to surface. East of the contact the apparent conductivity is slightly higher than 20×10^{-3} mhos/meter, although there seems to be a block of more resistive material between stations 11+00W to 15+00W. A reading showing a very high conductivity directly over the telephone cable near 12+00W has been ignored. Readings 100 feet or more away from the telephone cable have been considered reliable.

The phase seems to vary considerably. East of the contact it is about 40 degrees, while over the more resistive block (just east of the contact) it increases to about 45 degrees. Over the contact, the phase decreases to about 30 degrees, where it remains for a space of about 800 feet before suddenly increasing to about 50 degrees, continuing at this level for the rest of the profile. This phase angle curve somewhat resembles that in Fig. 3.2 for the case $d/\delta = 0$. This is not surprising, since there is very little overburden in the area of this profile. However, it is not known why the phase angle is so low (about 30 degrees) for a few hundred feet on either side of the contact.

The horizontal magnetic field strength has an equivalent value of 10-11 millivolts/meter throughout the profile, except in the vicinity of the contact where it appears to increase to about 13 millivolts/meter.

The contact seen here is between the Oxford dolomite

and the Queenston shale, about 800 feet west of where it has been mapped.

Line 7

The very large, sharp cross-over at 20+75E is caused by a buried telephone cable.

There is a contact type response to the east of the response caused by the telephone cable. There is a distinct in-phase peak with a relatively high amplitude, and a quadrature peak with smaller amplitude displaced about 150 feet to the east. The west side of the response is distorted by the presence of the telephone cable, and it is impossible to say how broad the response would have been in the absence of the cable. The total field response shows a well-defined peak over the contact.

This is once again the contact between the Oxford dolomite and the Queenston shale, and is only 300 feet west of where the Gloucester fault is shown on the map.

Line 8

The response on Line 8 is almost identical with that on Line 7. The very sharp cross-over at 24+25E is again due to a buried telephone cable. (The same one that appears on all the previous responses). At station 29+00E there is a positive in-phase peak with a smaller quadrature peak 50 feet to the east.

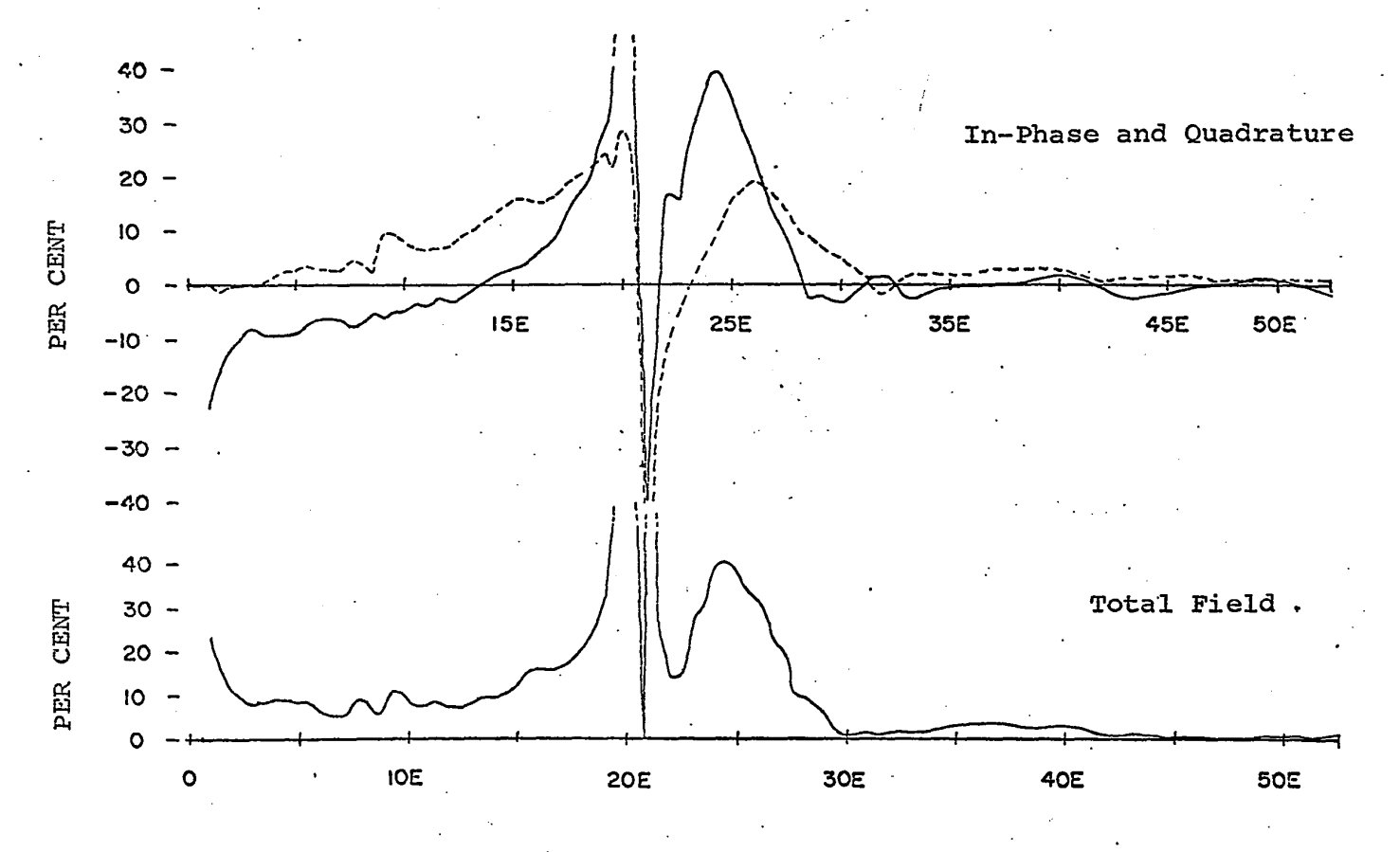


FIG. 6.14 GEONICS EM-16 RESPONSE ON LINE 7

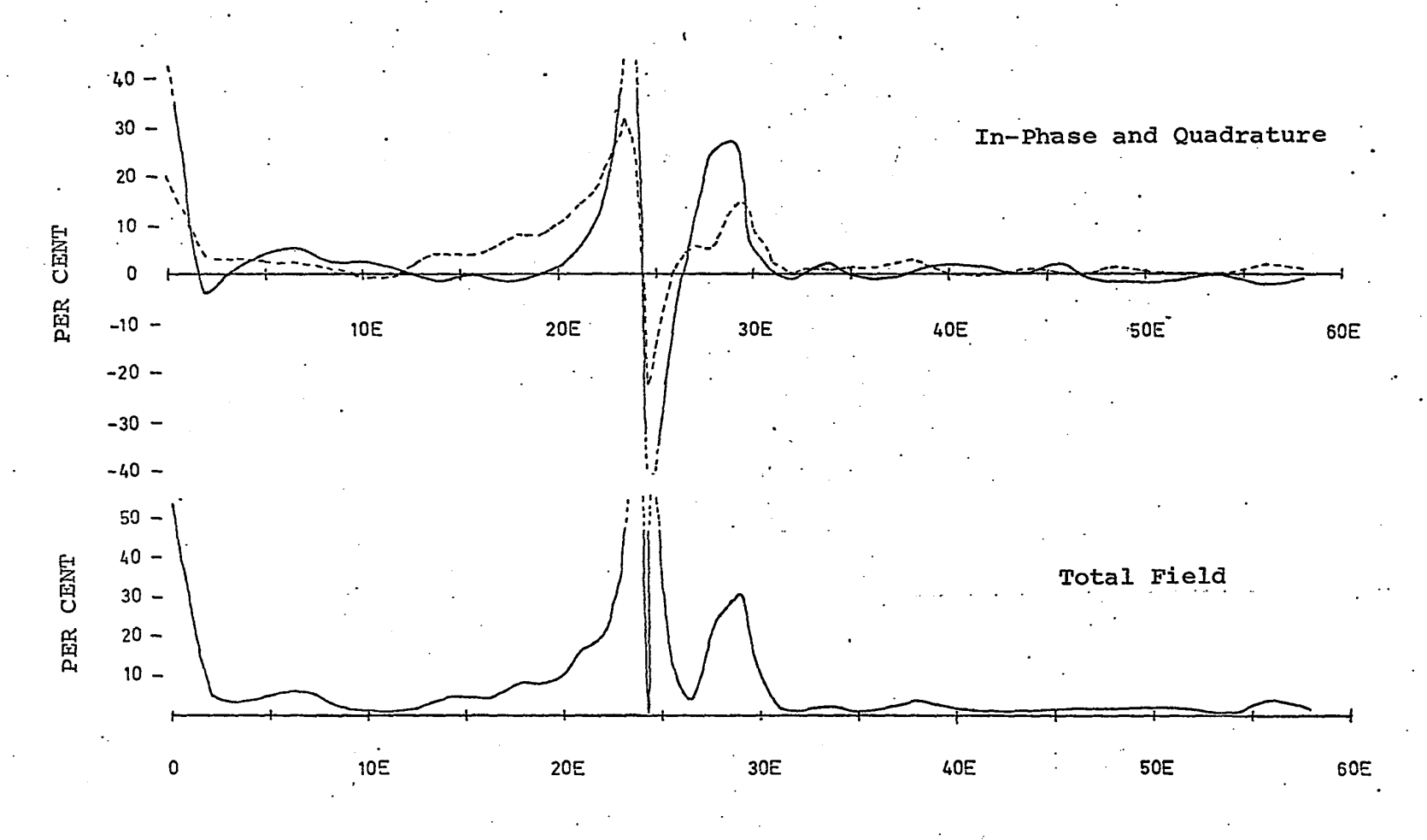


FIG. 6.15 GEONICS EM-16 RESPONSE ON LINE 8

The total field profile shows an asymmetric peak with the steeper slope on the east side, as expected, since the higher conductivity is on the east side of the contact. The contact is again that between the Oxford dolomite and Queenston shale, and is 200 feet west of where the Gloucester fault has been mapped.

Line 9

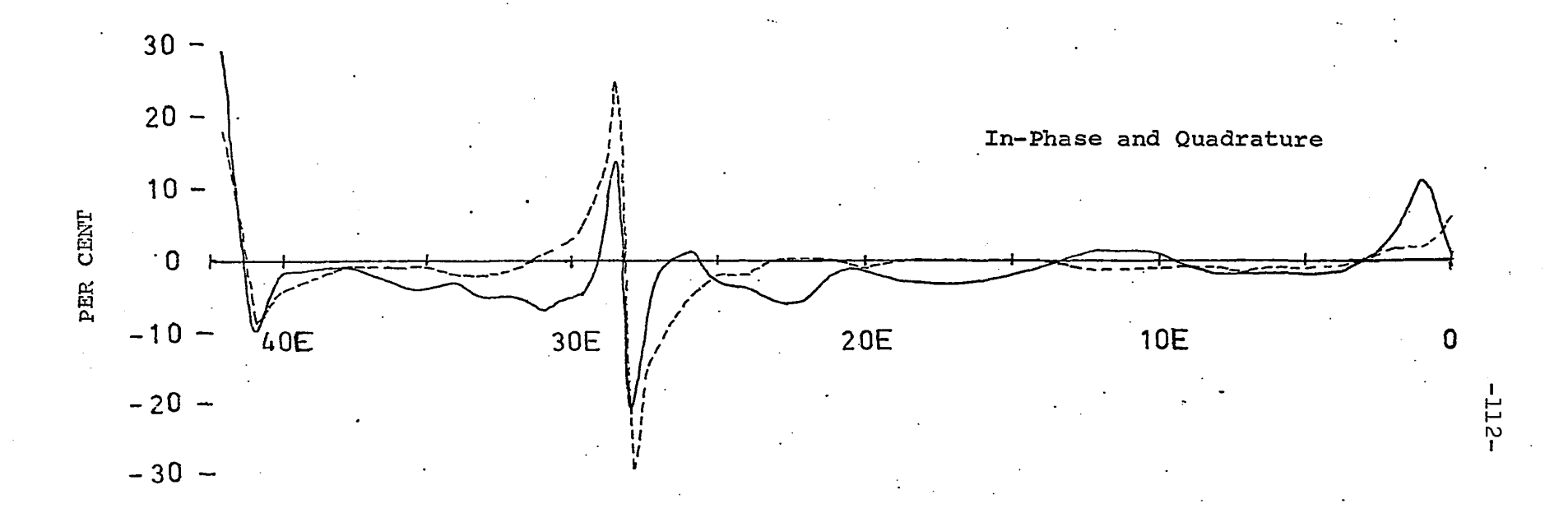
()

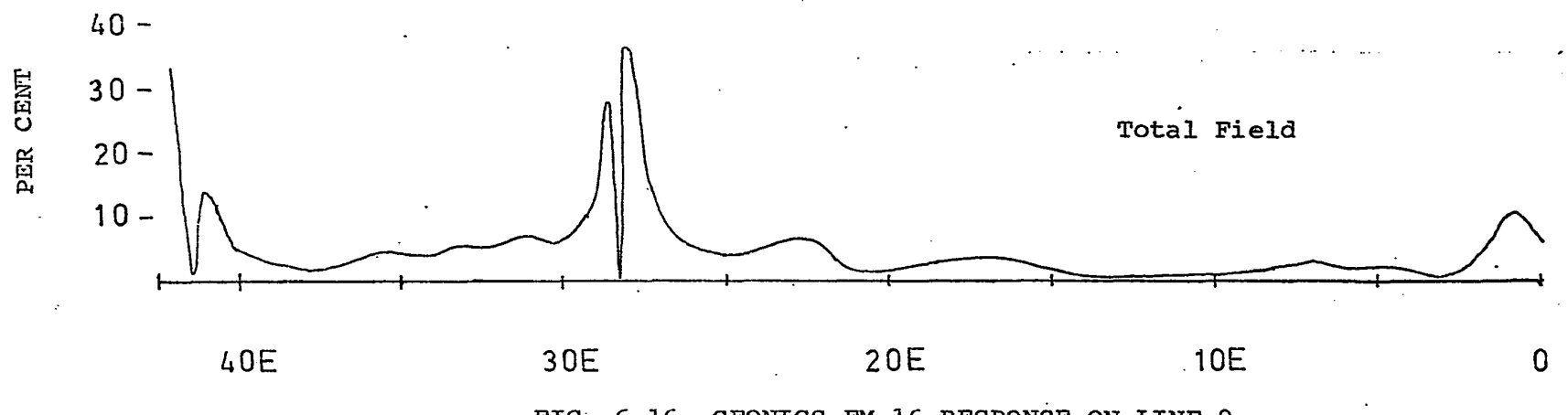
Apart from a buried telephone cable at station 28+25W, there are no other features on this profile.

Line 10

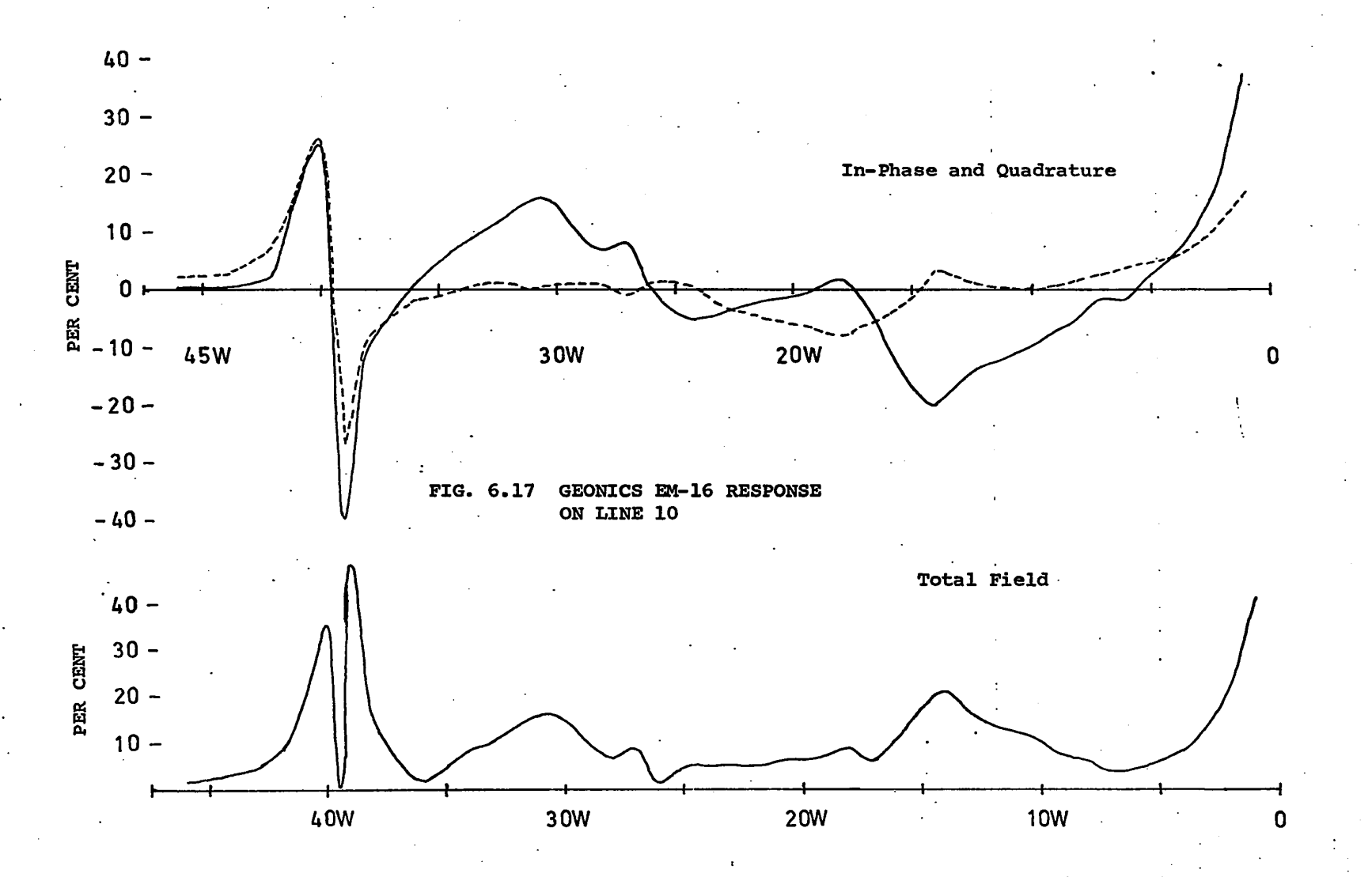
There is a broad, negative in-phase peak and a small positive quadrature peak at station 14+00W. This results in a broad, asymmetrical total field peak, with the steeper slope on the west side, indicating a contact with the more conductive side on the west. This contact occurs about 500 feet east of where the Gloucester fault is shown on the map.

There is a broad, positive in-phase peak at station 31+00W, but the quadrature component beneath the peak remains almost flat. The in-phase component is distorted somewhat by a drainage pipe at station 26+00E, which causes a small cross-over at that point. The total field peak is broad and appears to be asymmetrical, with the steeper slope on the east side, but the drainage pipe distorts the east side of the peak.





GEONICS EM-16 RESPONSE ON LINE 9



This indicates a contact with the more conductive side on the east, but this contact is about 1200 feet west of where the fault is located on the map.

These two peaks are somewhat similar to those seen on lines 37+00S to 60+50S in the Leitrim area. The contact at 31+00W is possibly the contact between the Oxford dolomite and the Ottawa limestone, but the contact at 14+00W is unexplained.

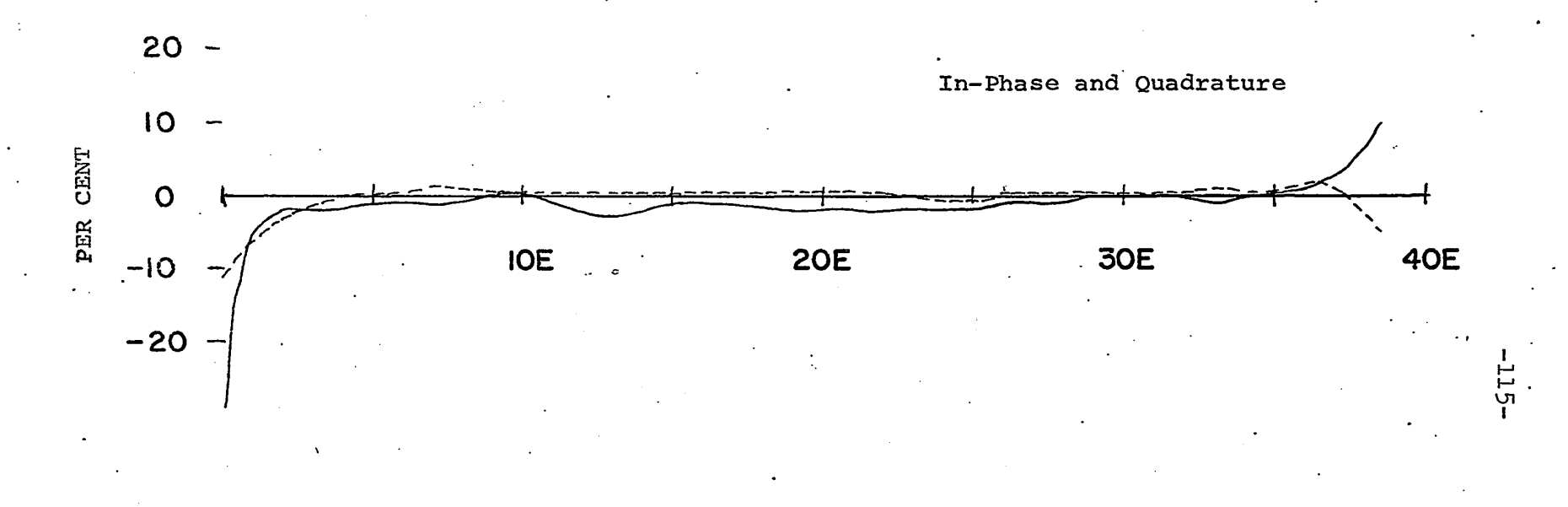
A buried telephone cable causes the cross-over at station 39+50W.

Line 11

There is possibly a negative in-phase anomaly at station 13+00W. It is tempting to regard this as an expression of a contact in the light of the negative anomaly seen on Line 10, and the one which will be seen on Line 12. Unfortunately, it is only a one station anomaly (and a very small one, at that), and is probably only a variation in the background response.

Line 12

There is a small negative in-phase and quadrature anomaly at station 13+00W, which results in a small but distinct peak on the total field profile. This is possibly a contact and, if so, it is about 600 feet east of where the Gloucester fault is shown on the map. This contact seems to



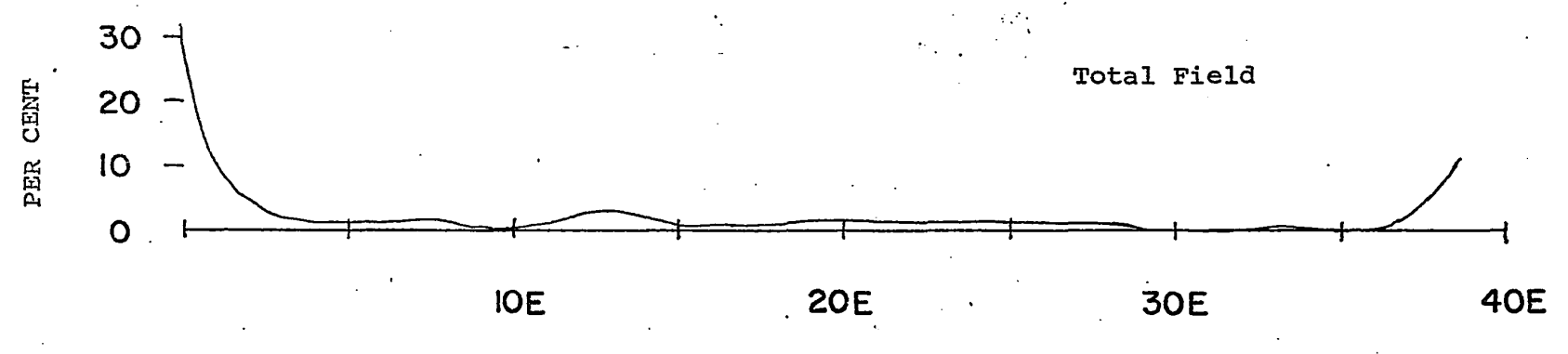


FIG. 6.18 GEONICS EM-16 RESPONSE ON LINE 11

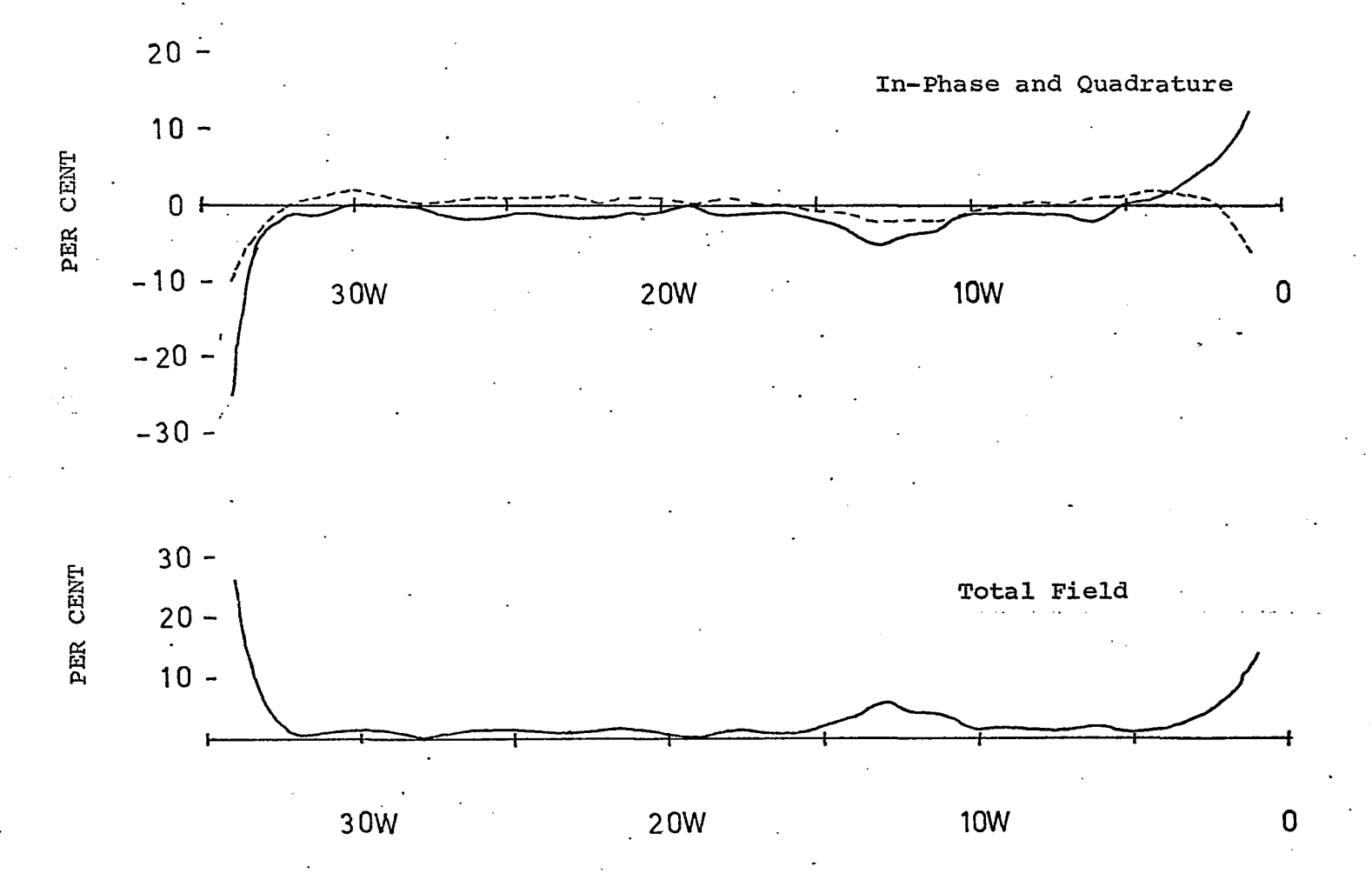


FIG. 6.19 GEONICS EM-16 RESPONSE ON LINE 12

correlate with the one at station 14+00W on Line 10, since it has the more conductive side on the west.

Line 13

The cross-over at station 39+30W is right at a fence, and possibly there is a drainage pipe running along beside the fence. This is the only feature on the profile.

Line 14

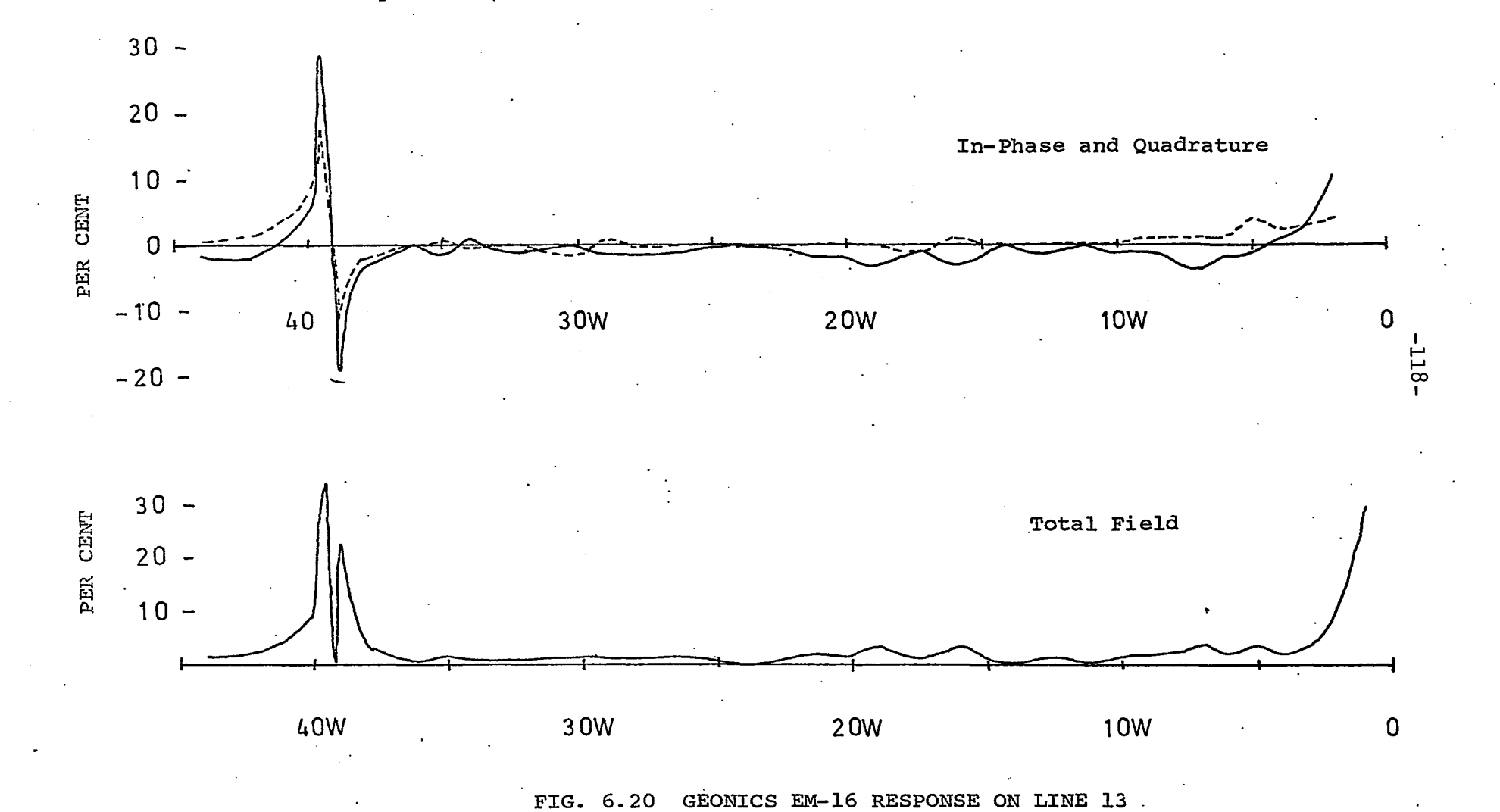
A fence causes a slight response at station 24+00E. There is a drainage ditch at 37+90E, and it probably has a metal pipe running along its length to account for the cross-over at that point. There are no other prominent features on the line.

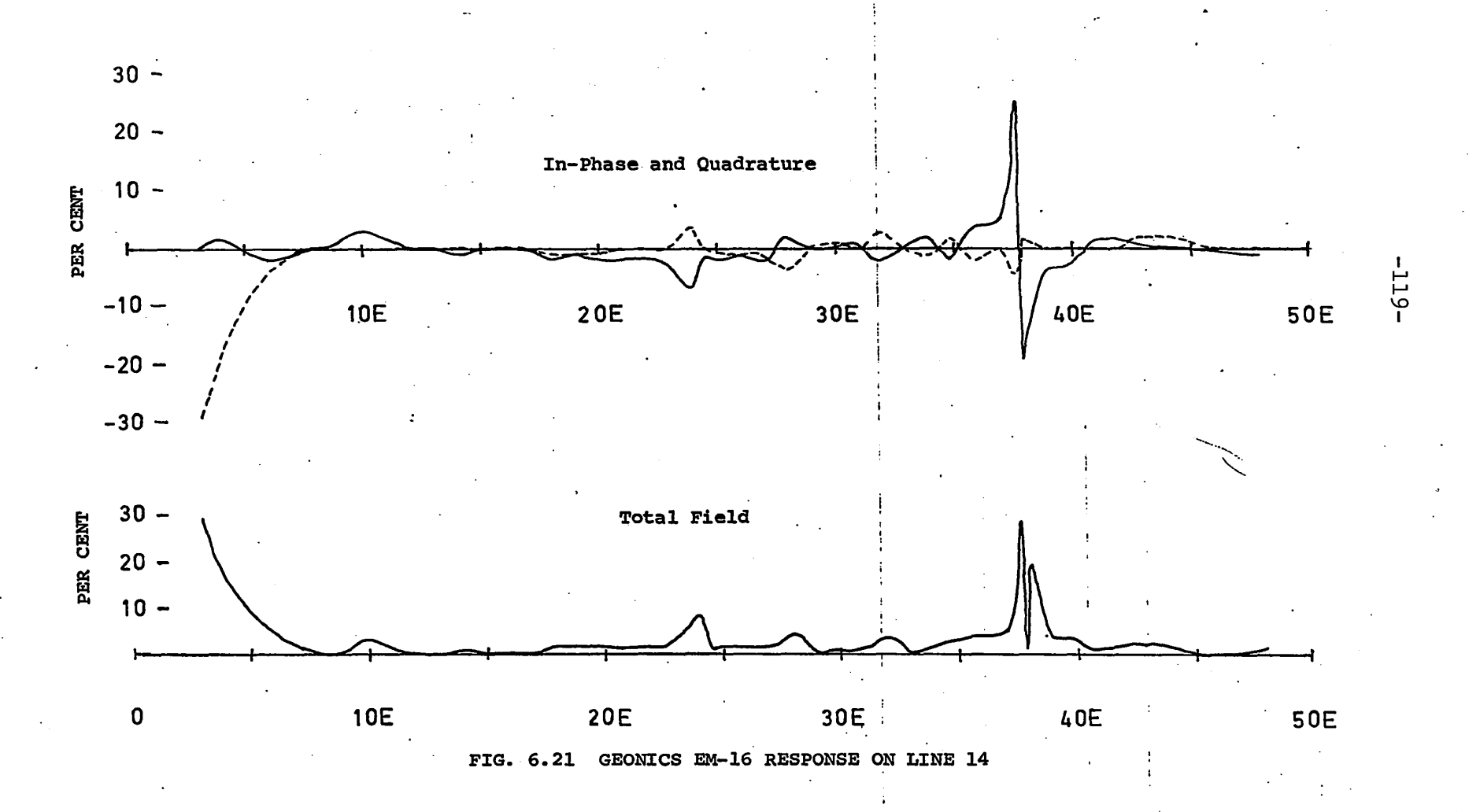
.

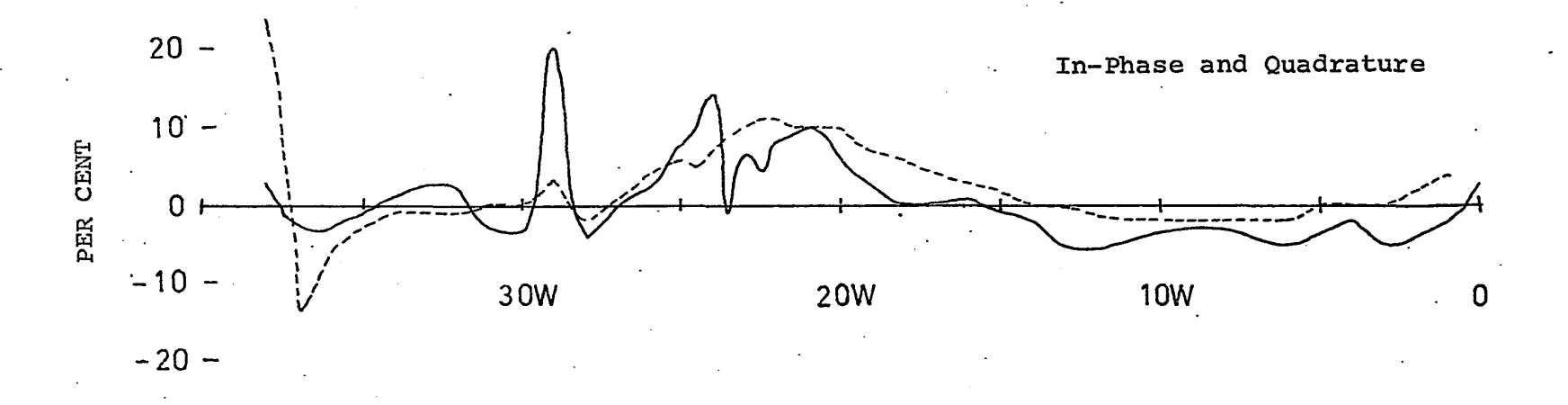
Slightly to the north-west of Russell, another fault appears about two to three miles east of the Gloucester fault (See. Fig. 5.2). This fault runs parallel to the Gloucester fault until both of them are lost in the Ottawa limestone about sixteen to eighteen miles to the south-east. There is very little outcrop in this area, and profiles were conducted along Lines 15 to 18 with the hope of detecting this fault.

Line 15

The anomaly at station 29+00W is caused by a fence at 28+85E.







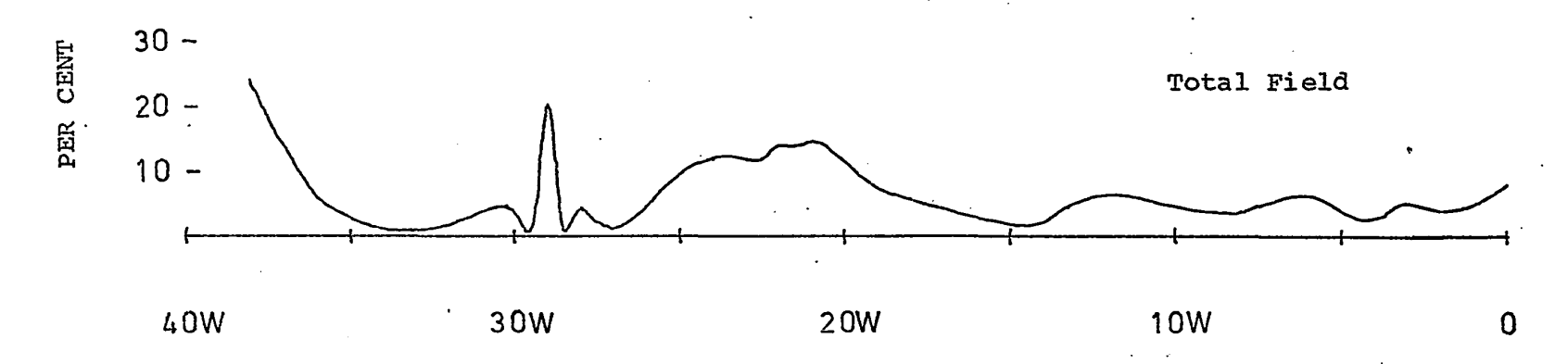


FIG. 6.22 GEONICS EM-16 RESPONSE ON LINE 15

There is a broad, positive quadrature response which peaks at about 22+50W. Unfortunately the in-phase response is distorted by a fence at 23+60W, and exhibits a cross-over at that point. The in-phase displays a positive peak at station 21+00W, but the west side of this response is distorted by the fence. This results in a broad peak on the total field response. A contact is indicated with the higher resistivity on the west. This is probably the contact between the Oxford dolomite and the St. Martin shale, as indicated by the fault on the map. It appears that this contact occurs somewhere between stations 21+00W to 22+50W, although the in-phase response is distorted somewhat.

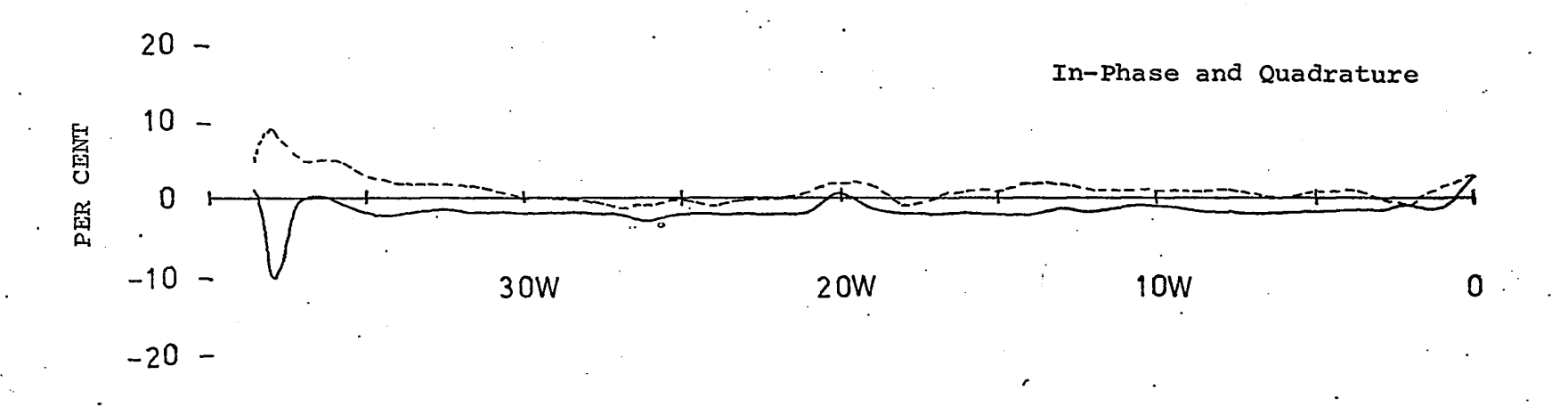
Line 16

Apart from the power lines at 38+15W, there are no definite anomalies on this profile. At station 20+00W where the contact between the Rockcliffe shale and Ottawa limestone is expected to occur, there is a very slight bump on the inphase and quadrature components but this is an extremely minor response. In addition, the conductivity of the Rockcliffe shale is greater than that of the Ottawa limestone, and a negative response would be expected.

Line 17

The anomaly at station 10+00E is caused by a fence.





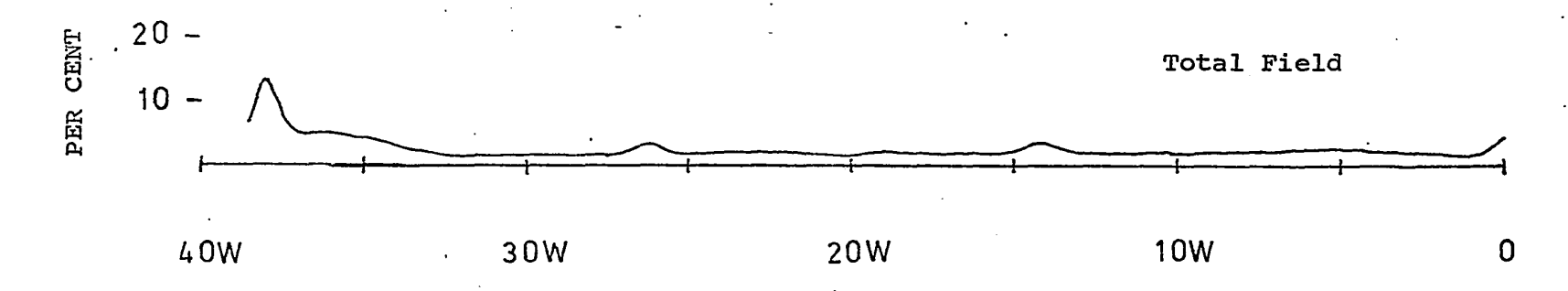


FIG. 6.23 GEONICS EM-16 RESPONSE ON LINE 16

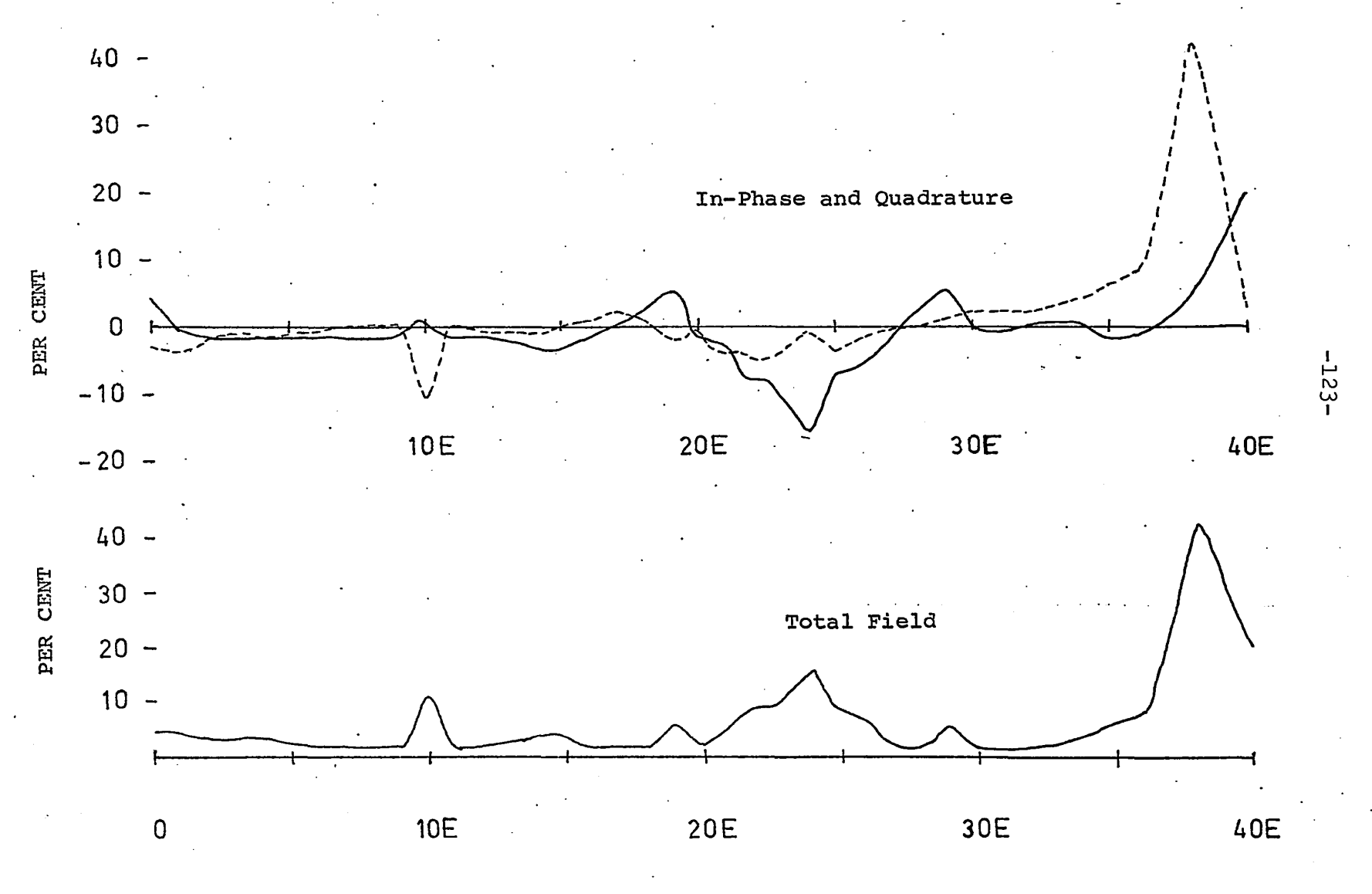


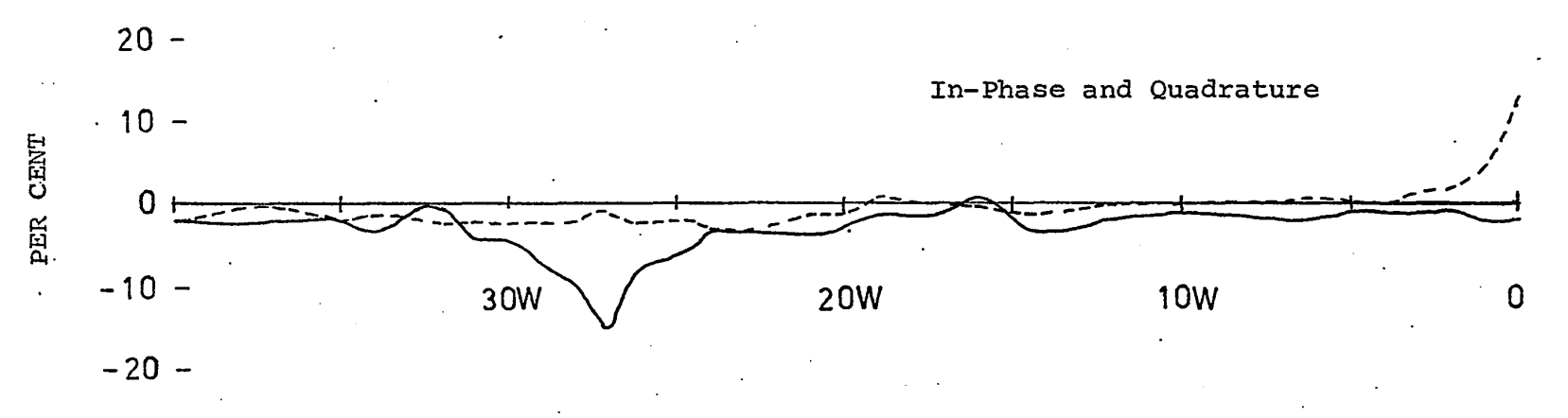
FIG. 6.24 GEONICS EM-16 RESPONSE ON LINE 17.

The in-phase response displays a negative peak at station 24+00E. The quadrature response is also negative, but it shows a local maximum at 24+00E. This response indicates a contact with the higher resistivity on the east, and this is probably the contact between the St. Martin shale and the Ottawa limestone, as indicated by the geological map. The total field response exhibits an almost symmetrical peak at 24+00E, making it impossible to determine which side of the contact has the higher resistivity solely on the basis of the total field response. The in-phase component displays a small positive "shoulder" on either side of the negative peak, but the significance of this is not clear.

The large anomaly at the east end of the profile is caused by a power line at 39+90E.

Line 18

The response on this profile is quite similar to that of the previous line. The in-phase component displays a negative peak at station 27+00W while the quadrature component is slightly negative, but almost flat in the vicinity of the in-phase anomaly. The quadrature does, however, show a slight local maximum directly over the in-phase peak. This response indicates a contact with the higher resistivity on the east. Although the geological map shows the Ottawa limestone on either side of the fault, the more conductive St. Martin shale



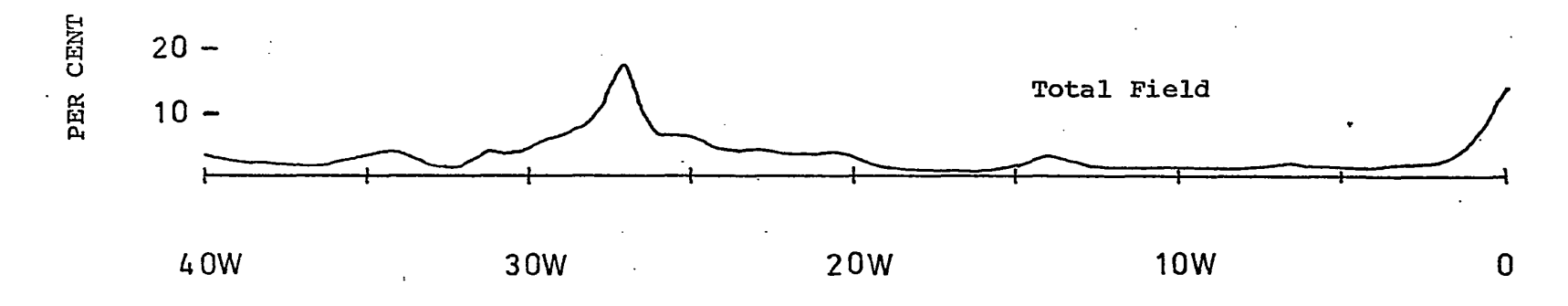


FIG. 6.25 GEONICS EM-16 RESPONSE ON LINE 18

is closer to the surface on the west side of the fault, and the apparent resistivity on that side of the contact can be expected to be lower. The response is, therefore, the expected one. The total field profile, therefore, exhibits a single peak over the fault. Once again the total field peak is quite symmetrical, making it impossible to determine the nature of the contact without looking at the in-phase and quadrature components separately.

.

Approximately four miles to the east of Russell, another fault is shown parallel to the two faults already described. This fault occurs in the Ottawa limestone and is about six miles in length. In spite of the fact that the same formation (Ottawa limestone) occurs on either side of the fault, profiles were conducted along Lines 19 to 22 to determine if this contact could be detected.

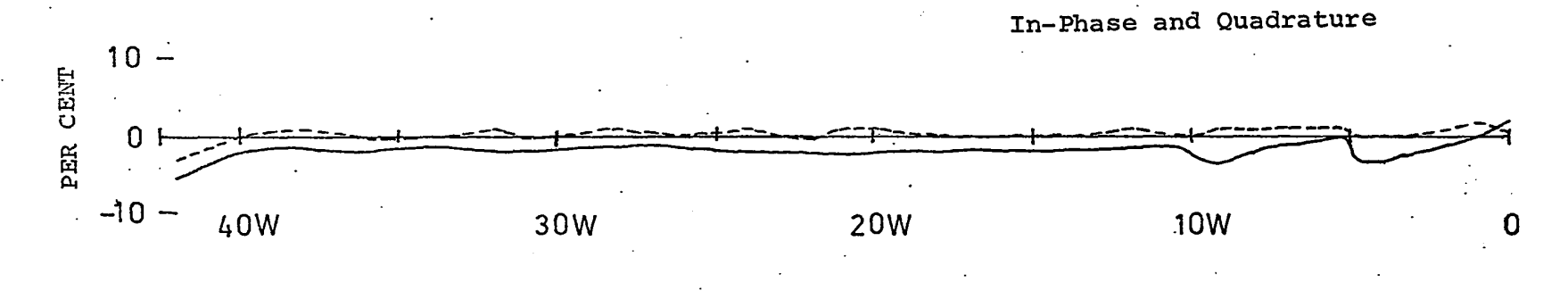
Line 19

There is no anomalous response on this profile.

Line 20

An overhead power line at 35+20W accounts for the very sharp cross-over of high amplitude at that station. There is no other response on the profile.





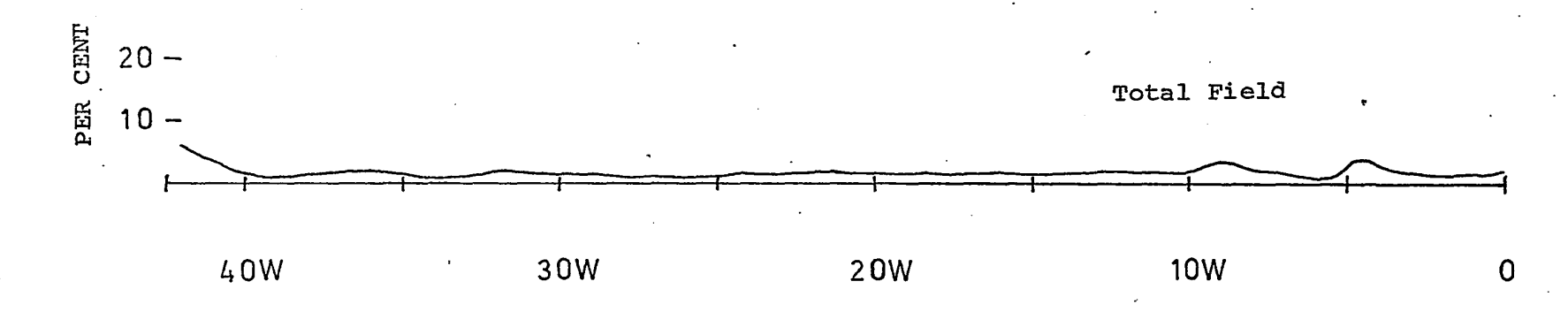
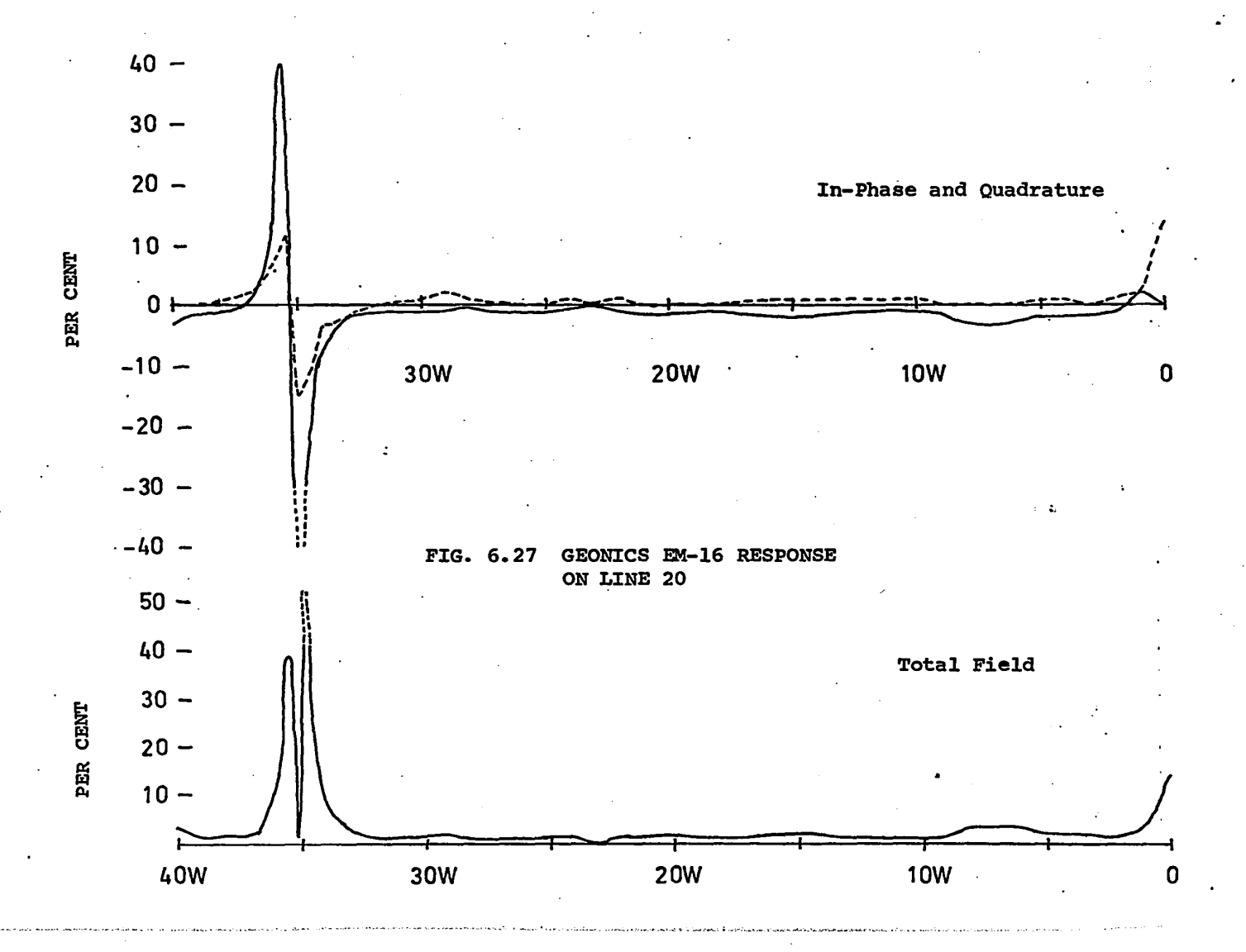


FIG. 6.26 GEONICS EM-16 RESPONSE ON LINE 19

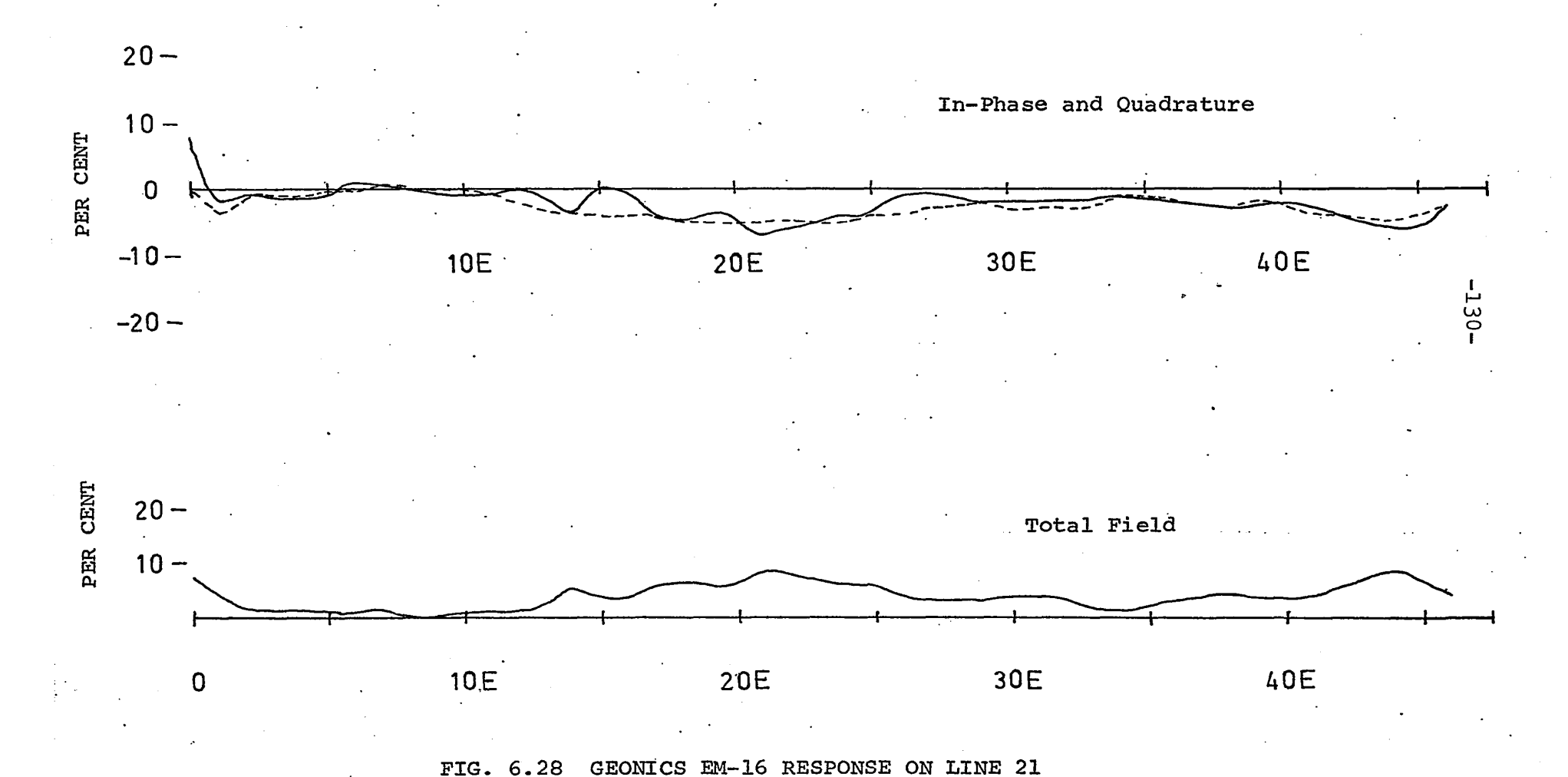


Line 21

There is a broad, low amplitude in-phase and quadrature response in the form of a negative bump centered at about 21+00E, resulting in a broad bump on the total field profile. This response seems to indicate a contact with the higher resistivity on the east. Since it is a low amplitude response, the conductivity contrast between the two sides of the contact cannot be large, although there are at least several feet of overburden in the vicinity of the profile. This is possibly the fault indicated on the geological map. Since the St. Martin shale is closer to surface on the west side of the fault, the apparent resistivity of the Ottawa limestone can be expected to be lower on that side. If this is the case, then the response obtained is to be expected.

Line 22

There is a very broad in-phase response of fairly high amplitude at the west end of the profile. This response is in the form of two positive peaks, one at 50+00W, and a smaller one at 56+00W. The quadrature component displays a broad peak of low amplitude at about 45+00W, and a smaller one at about 53+00W. The total field response therefore exhibits two peaks, one at 50+00W, and the other at 56+00W. This response seems to indicate a contact (or perhaps even two) with the higher resistivity on the west side of the contact. The location of the fault shown on the



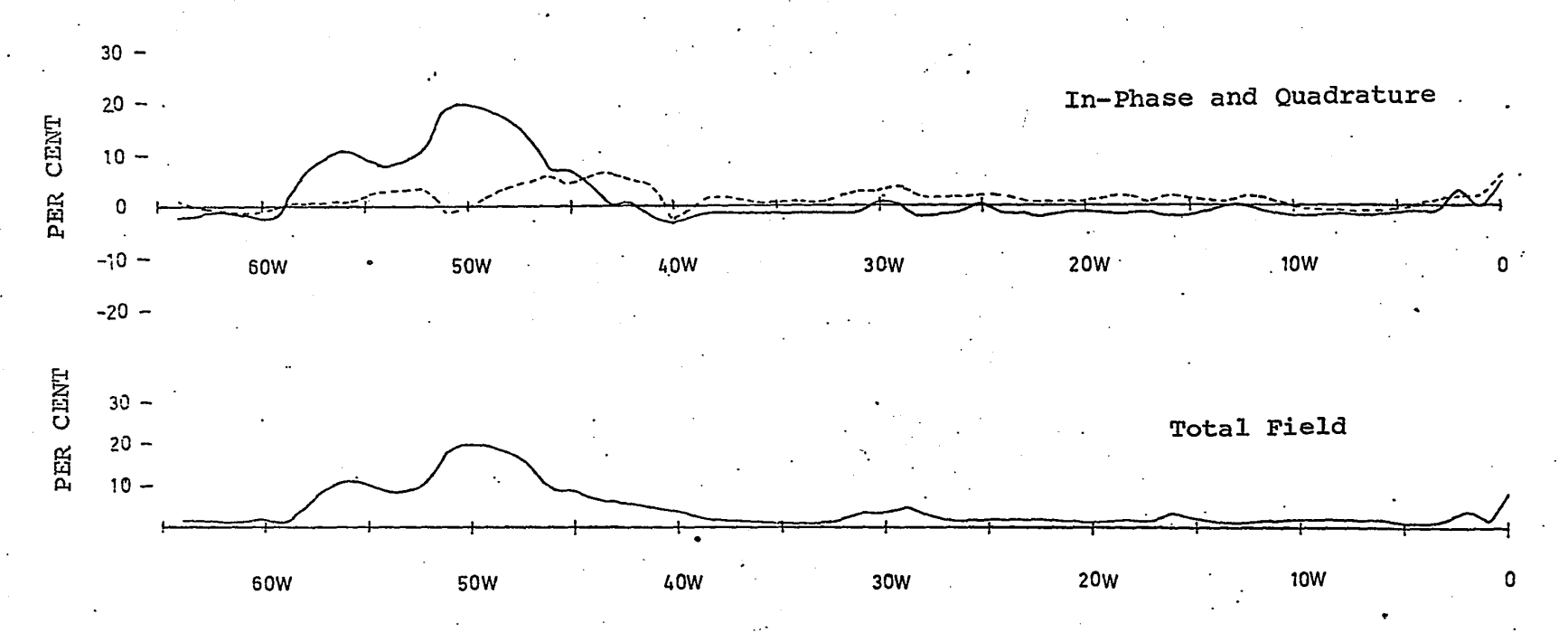


FIG. 6.29 GEONICS EM-16 RESPONSE ON LINE 22

map is slightly more than one-half mile to the east. In addition, a small negative anomaly (if any) is to be expected over the fault. The obtained response is in the middle of an open field covered by, at least, several feet of overburden (and possibly much more). There are no power lines or buried telephone cables in the vicinity, and fences are remote enough to have no influence on the response. The response, therefore, seems to be valid. If this is the case, there is a contact present which is not shown on the map. There is no indication of a similar contact on Lines 19 to 21, but profiles might be conducted parallel to Line 22 and about 500 feet to the north and south of it to see if a contact is in evidence. It is possible that this is only a local feature.

About two miles to the west of Russell, a fault is shown which strikes roughly south-west to north-east. (i.e. perpendicular to the Gloucester fault). This fault passes about a mile north of Russell, and Wilson assumes it continues indefinitely to the north-east, although the area is covered with a heavy mantle of overburden. West of Russell, this fault separates the Oxford dolomite from the Queenstone shale, while east of Russell the contact is between the Ottawa limestone and the Carlsbad shale. Near the west end of this fault, a smaller fault (about a mile in length) is shown branching off to the south-west. This results in a downthrown,

triangular block of Ottawa limestone between the Oxford dolomite and the Queenston shale.

Profiles were conducted along Lines 23 to 29 in order to delineate this system of faults.

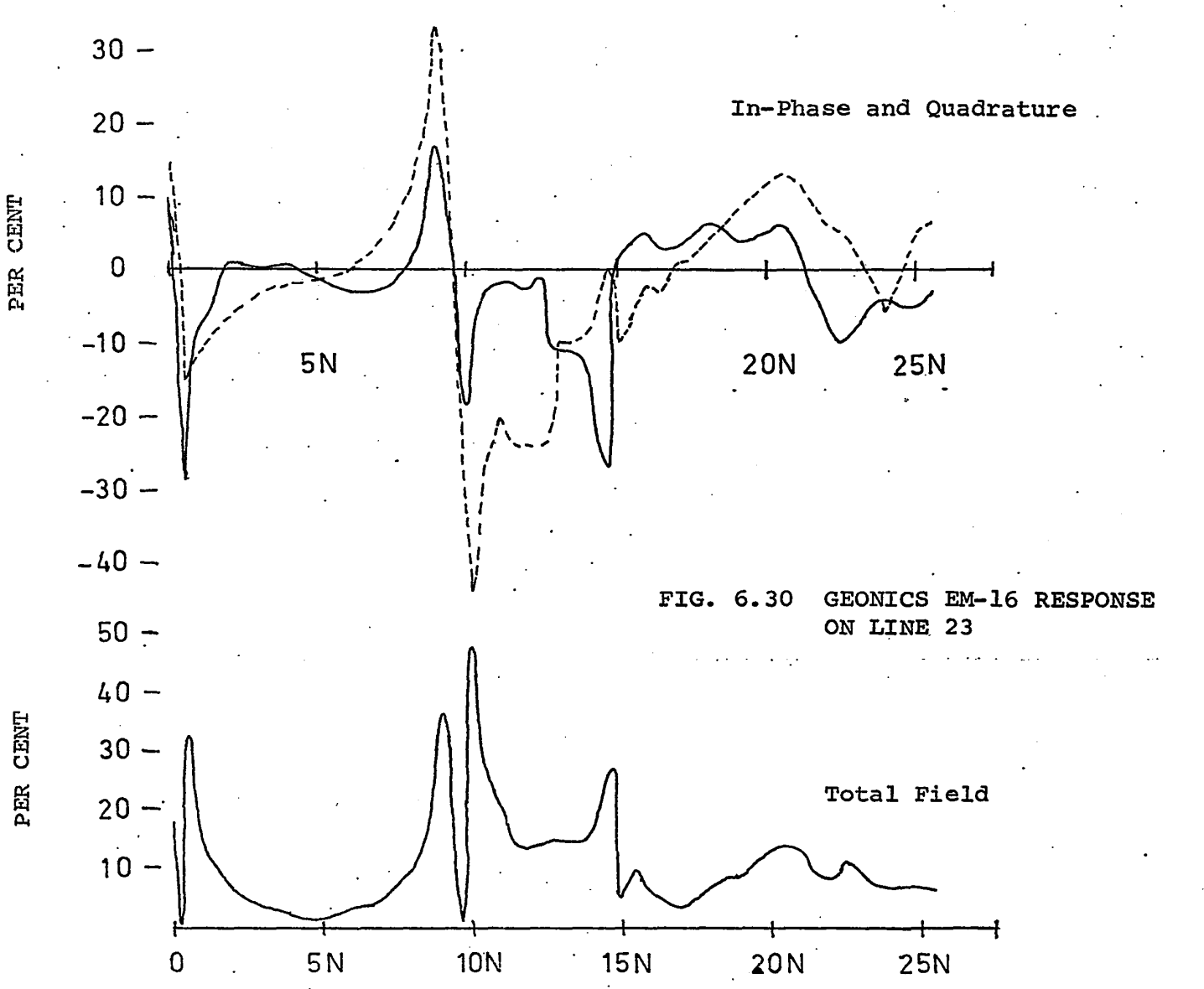
Line 23

(

The large, sharp cross-over at 9+60N is caused by a buried telephone cable.

An unusual response occurs between 13+00N to 15+00N. The in-phase component is in the shape of a negative, sharp asymmetrical peak, while the quadrature component, although also negative, is almost a mirror image of the in-phase. This response occurs very near a small stream (about 60 to 65 feet wide and only 2 to 3 feet deep) which is located at 14+85N to 15+50N on the profile. As the stream is crossed (from south to north) the in-phase component becomes positive (giving the appearance of a false cross-over) while the quadrature becomes negative. This results in a total field profile which looks like a typical cross-over response. i.e. a sharp minimum between two peaks, although the southern peak (corresponding to the large negative in-phase value) has a much higher amplitude than the one to the north. The minimum of the total field profile is directly over the stream. (Similar responses will be encountered later, and will be discussed at that time.)





()

A definite fault type response occurs in the vicinity of station 20+00N. The in-phase component is quite noisy in this vicinity, but the quadrature response seems undistorted. The quadrature component displays a positive, nearly symmetrical peak at 20+50N, while the in-phase also shows a peak at this location, but of smaller amplitude. A cross-over in the in-phase occurs at 21+50N, but the reason for this is not clear. Both components are distorted by a fence at 24+00N. The total field response is a single peak at station 20+50N. This peak appears to have a steeper slope on the north side, although it is distorted somewhat on that side. The response indicates a contact with the more conductive side on the north, and it coincides almost exactly with the fault shown on the map. This contact is undoubtedly that between the Ottawa limestone and the Queenston shale. A few outcrops can be found in this area, particularly along the stream, and Wilson no doubt determined the position of the fault from these.

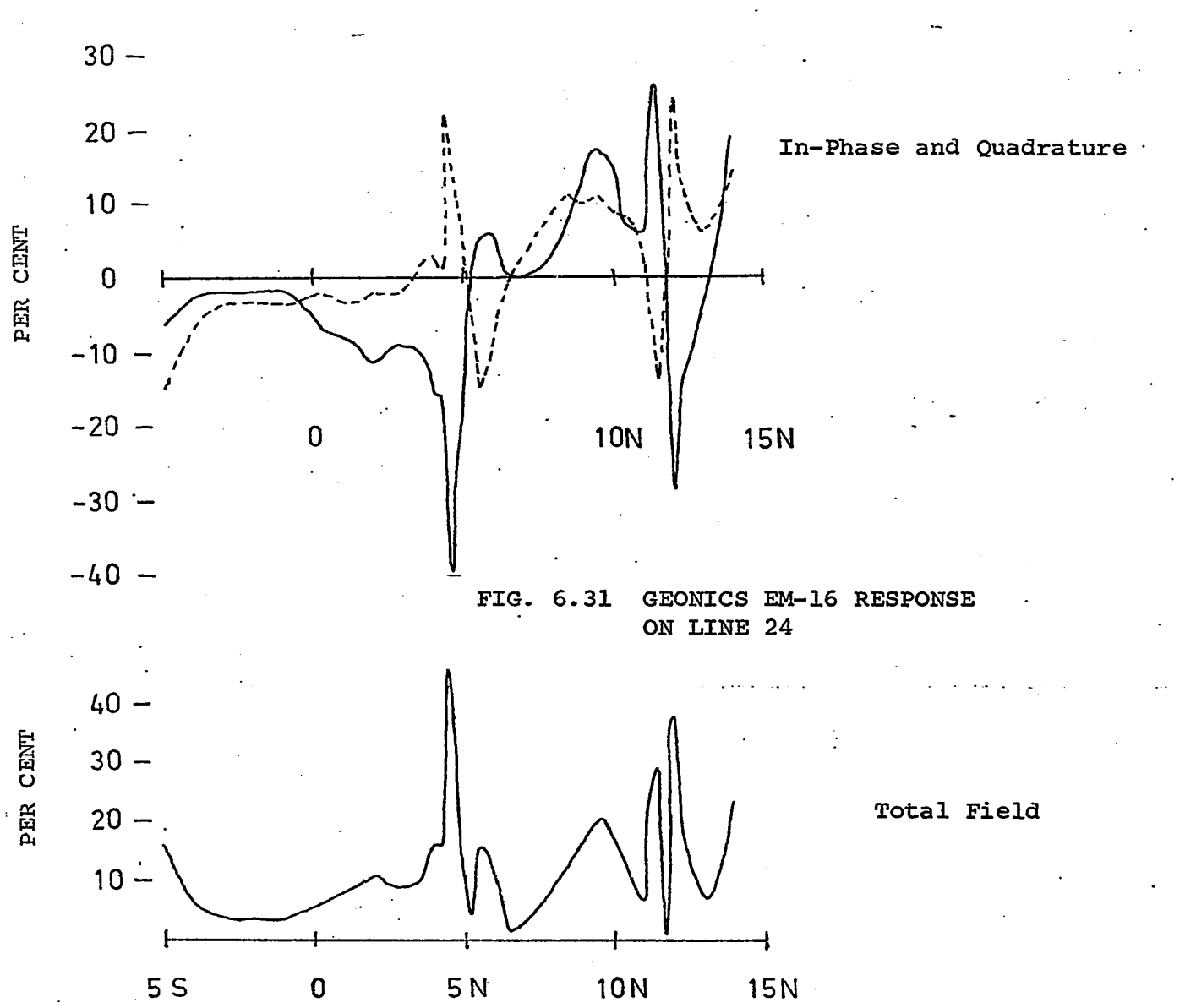
There is no response to indicate the presence of the smaller fault to the south, separating the Oxford dolomite and the Ottawa limestone. However, this fault is shown close to the road at the beginning of the profile, and, if it is present, its response (if any) could be lost due to the interference from the power line.

Line 24

A response similar to the unusual anomaly obtained on Line 23 is observed between stations 3+00N to 6+00N. in-phase component is a very sharp, negative peak while the quadrature component is a sharp, positive peak, being almost a mirror image of the in-phase. There is a stream (the same one which crosses Line 23) between stations 4+75N and 5+50N. As on Line 23, the in-phase component becomes positive and the quadrature negative as the stream is crossed (from south to north). This gives the appearance of a false cross-over on the in-phase. The total field profile again shows a minimum over the stream. This response coincides with the smaller fault shown by Wilson. However, the response that would be expected over this fault is a positive peak similar to the many others already observed, since the contact is between the highly resistive Oxford dolomite and the less resistive Ottawa limestone. This response is not typical of a fault (or a conductor either, for that matter) and it is assumed that it is not due to the fault shown by Wilson. Since this type of response seems to occur in the proximity of a stream, it will be called a "stream response". It will be discussed later in some detail.

A fault type response occurs in the vicinity of station 9+50N. The in-phase and quadrature components are





both in the shape of a peak, with the in-phase having a slightly higher amplitude than the quadrature. A fence at 11+75N causes a very strong cross-over, and this interferes with the response on the north side of the contact. The total field response is a well-defined peak at 9+50N. It appears to be almost symmetrical, but is distorted on the north side by the fence. This indicates a contact at 9+50N with the more resistive side on the south. It is probably the contact between Ottawa limestone and Queenston shale, although it is nearly 500 feet south of where it is shown on the map. There are fewer outcrops as one proceeds east, except along the river, making it more difficult to determine accurately the position of the fault.

River between 12+25N and 13+00N. There appears to be a stream type response associated with the river, although fences at 11+75N and 12+00N distort the in-phase and quadrature response just to the south of the river. However, the sharp, negative in-phase peak and the sharp, positive quadrature peak are present. It is interesting to note that the quadrature shows a false cross-over across the fence at 11+75N, and possibly this is due to the response from the stream. The total field profile indicates the cross-over at 11+75N. An overhead power line at 15+00N greatly distorts the response to the north of the river. The in-phase and quadrature quickly become

positive, and at 14+50N the in-phase component is right off the positive end of the scale. The response over the river is therefore greatly distorted, and cannot be considered reliable.

Line 25

(

The large, narrow anomaly at station 3+00N is caused by a fence at 3+05N. The remainder of the profile shows no anomalies, although the in-phase and quadrature components are a little noisy. If the faults are located where they are shown on the map, they have not been detected.

Line 26

River between 3+50S and 4+50S. There is a distinct response which is spatially associated with the river, but it does not resemble the stream responses already observed. The in-phase component shows a fairly sharp peak on the north bank of the river (3+50S) while the quadrature shows a depressed value at that point. On the south bank of the river (4+50S) the quadrature shows a positive peak while the in-phase displays a negative value. This results in a relatively small peak over the river on the total field profile. Unfortunately, no reading was possible at 4+00S (in the middle of the river). Possibly this may have shown a large negative value for the in-phase component, and a high positive value for the quadrature, similar to previous stream responses. In any event,



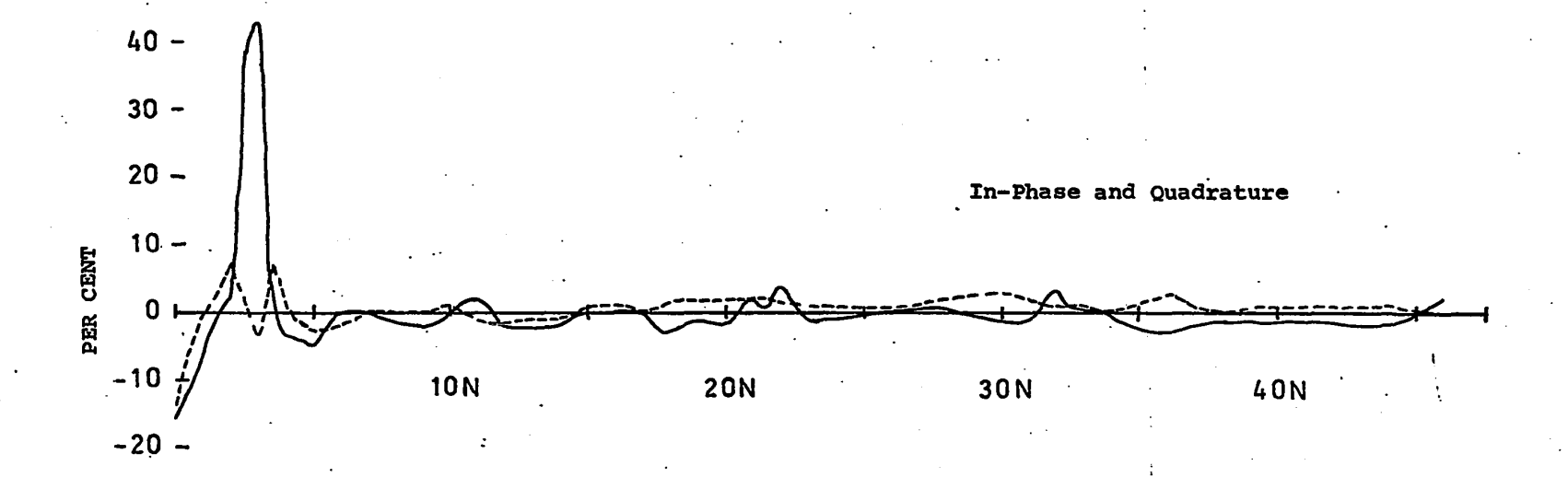
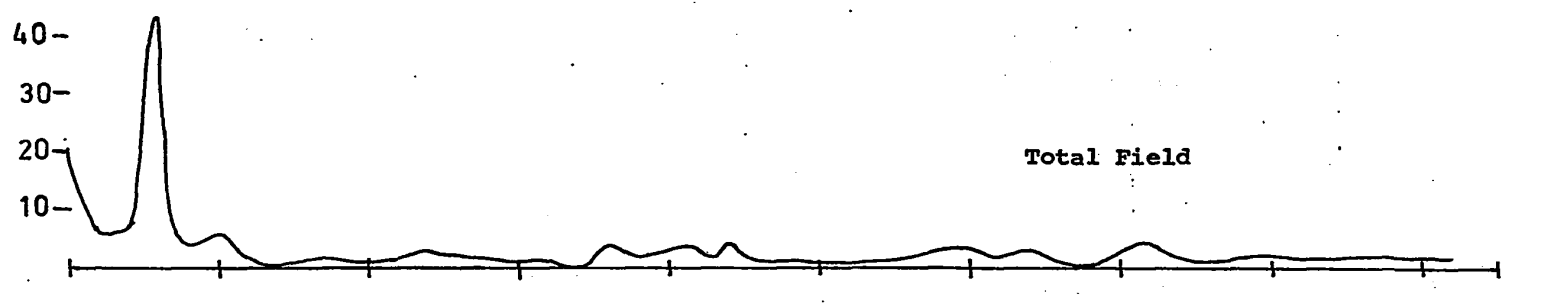


FIG. 6.32 GEONICS EM-16 RESPONSE ON LINE 25

20 N

PER CENT

10 N



30 N

40N

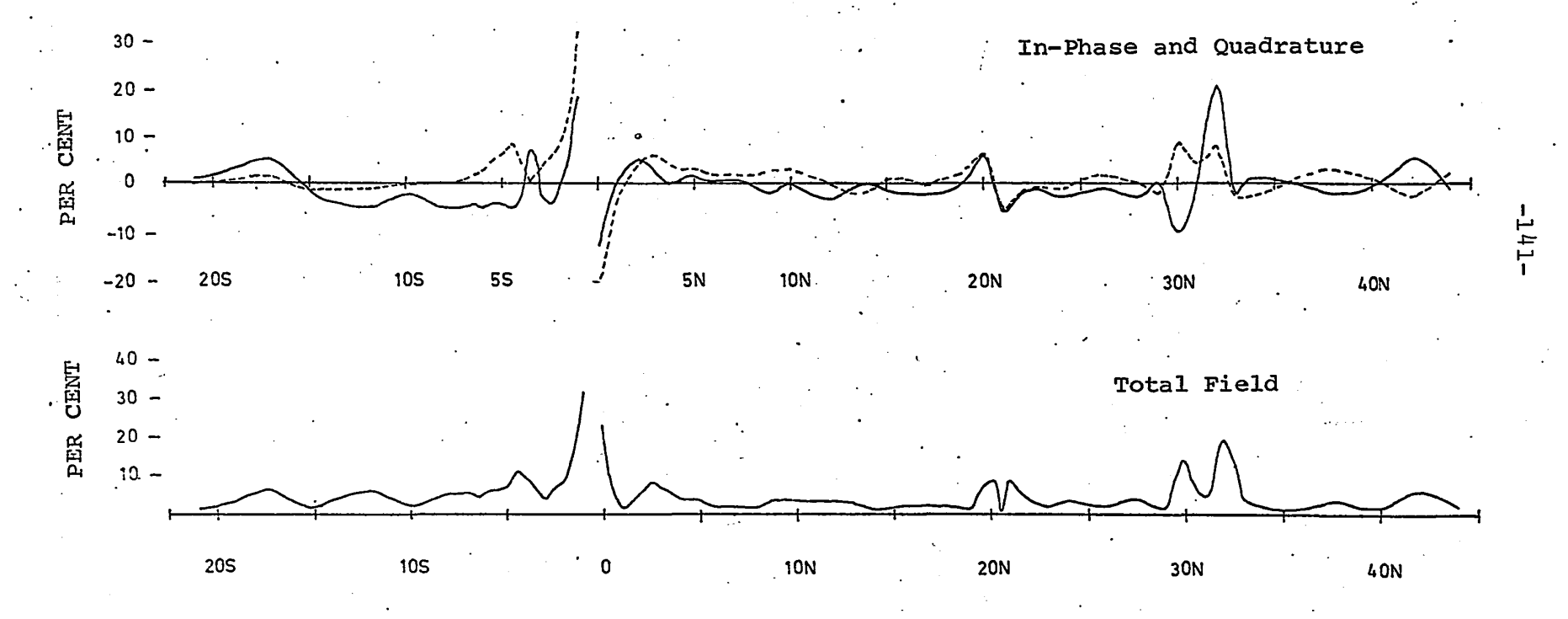


FIG. 6.33 GEONICS EM-16 RESPONSE ON LINE 26

there is definitely a response associated with the river.

This response is distorted to the north by overhead power lines at 0+60S; no reading was possible at 0+50S because of power line interference.

The small cross-over at 20+50N is caused by a fence at that location.

The anomaly at 30+00N is caused by a fence at 29+75N.

The high in-phase and quadrature values at station 32+00N are caused by some man-made structure. The azimuth to Cutler, Maine is distorted by about 20 degrees at this station (i.e. the instrument points east-south-east instead of east when the direction to the station is determined). This is usually indicative of a buried pipe or telephone cable, although there were no markers to indicate a telephone cable. There is probably a metal drain pipe in the ground.

For the most part, the in-phase and quadrature components are generally noisy on this profile.

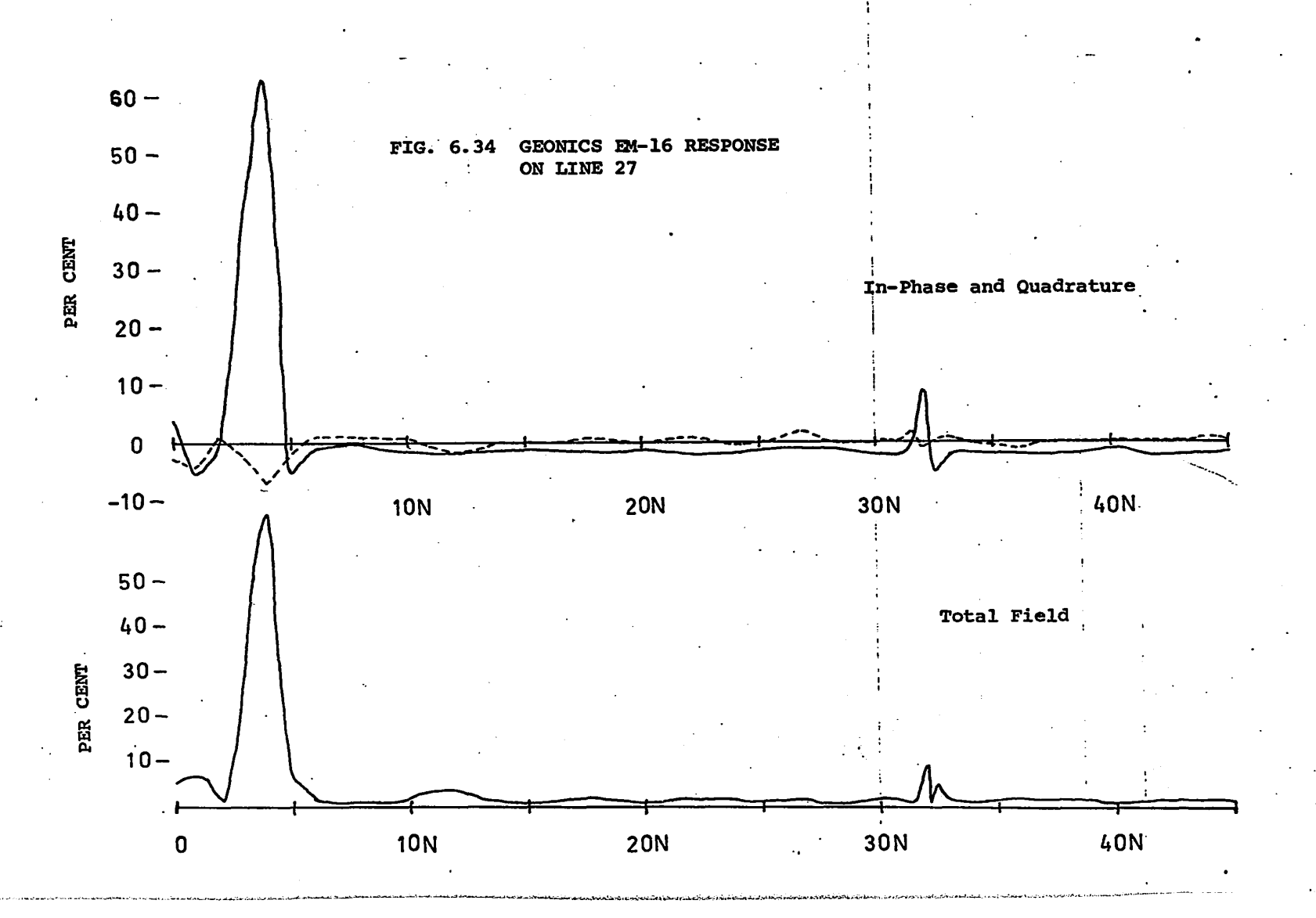
There is no indication of the fault shown on the map.

Line 27

The very high in-phase values at station 3+00N and 4+00N are caused by fences at 3+12N and 4+10N respectively. These readings should have been taken further away from the fences to avoid distortion of the response.

The small in-phase cross-over at 32+25N occurs over





a drainage ditch, and there is possibly a metal drain pipe running along the ditch.

There is no indication of a fault anywhere on the profile.

Line 28

The response on this profile is almost completely flat, with no anomalies at all.

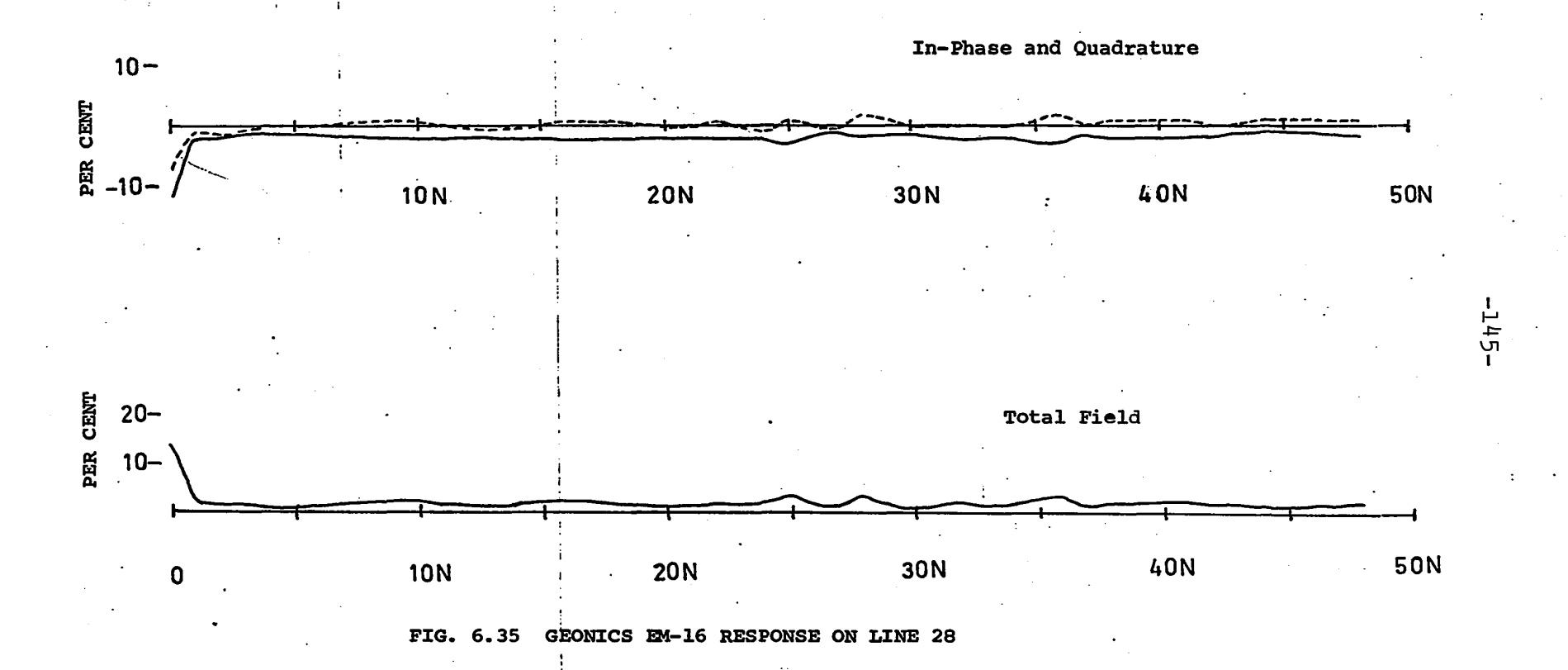
Line 29

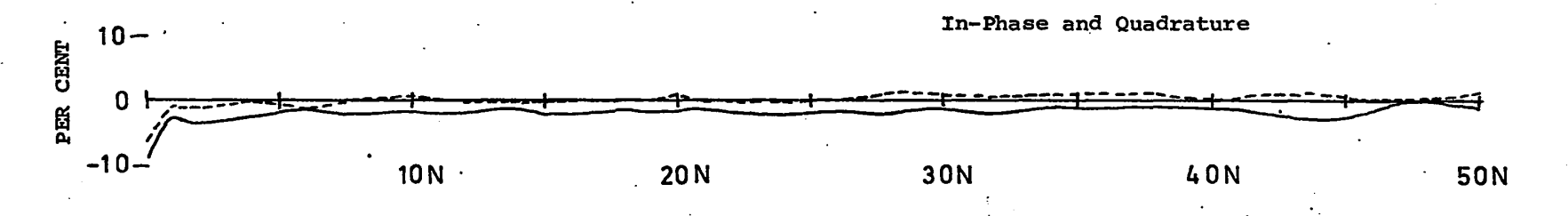
This response is also completely flat. If the fault shown on the map is correctly located, it has not been detected on any of the profiles on Lines 25 to 29. The area around these profiles is completely covered with overburden.

Profiles were obtained on Lines 30 to 32 in order to further investigate the so-called stream response. These three traverses cross the Castor River in the vicinity of Russell.

Line 30

The very sharp cross-over of extremely high amplitude at 19+25S is caused by a fence. This is a very strong response for a fence, and it is not known why this particular fence (apparently quite ordinary), gives such a response. Overhead power lines at 1+10S and 0+20N account for the large cross-overs at those locations, while a fence at 9+50N gives yet





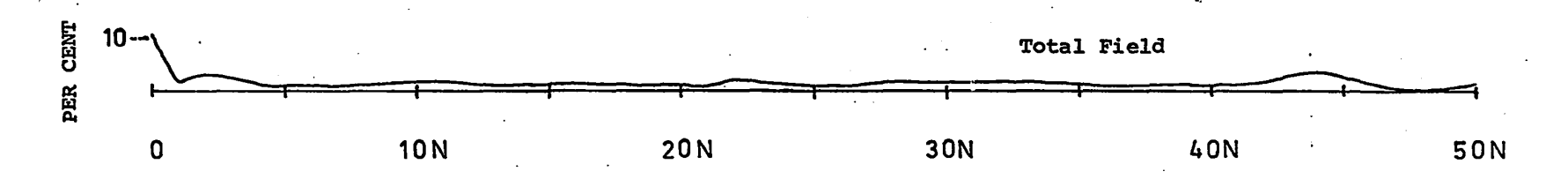


FIG. 6.36 GEONICS EM-16 RESPONSE ON LINE 29

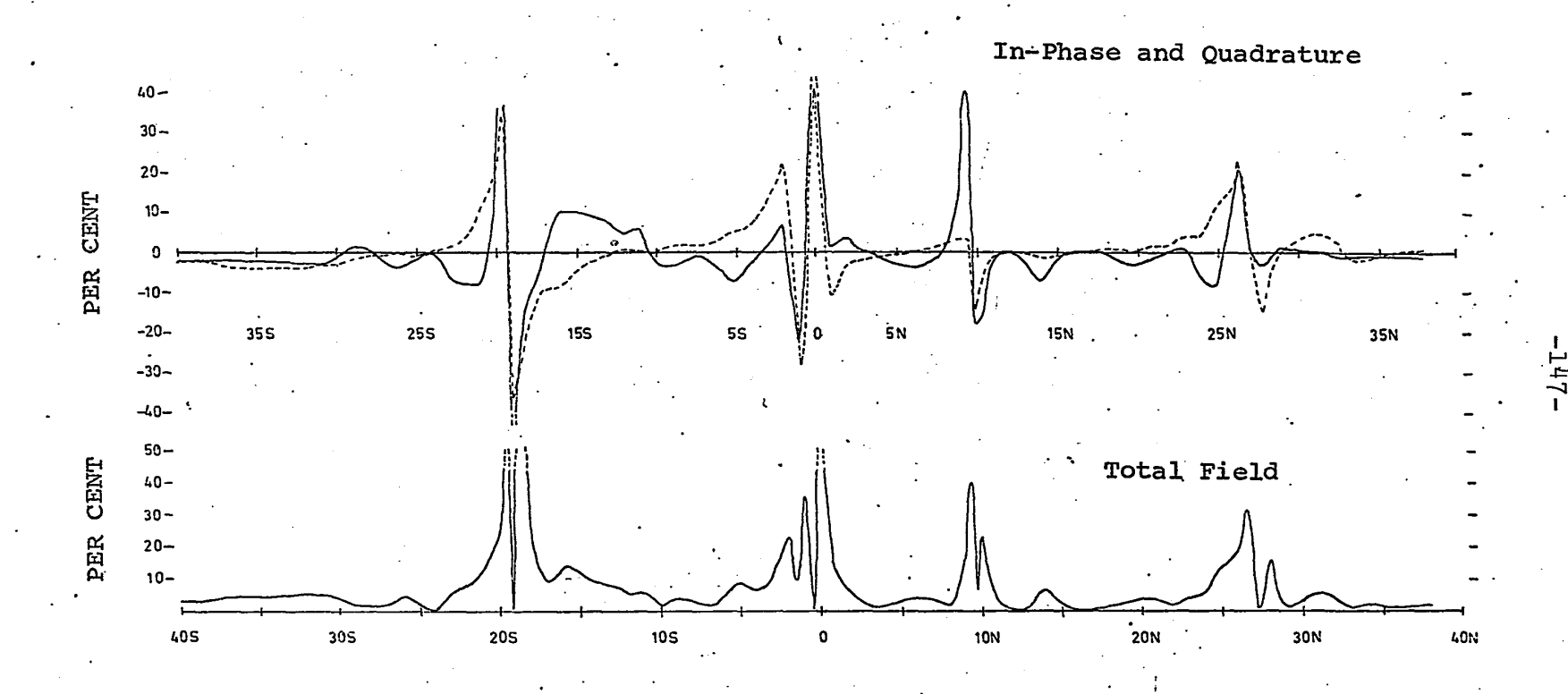


FIG. 6.37 GEONICS EM-16 RESPONSE ON LINE 30

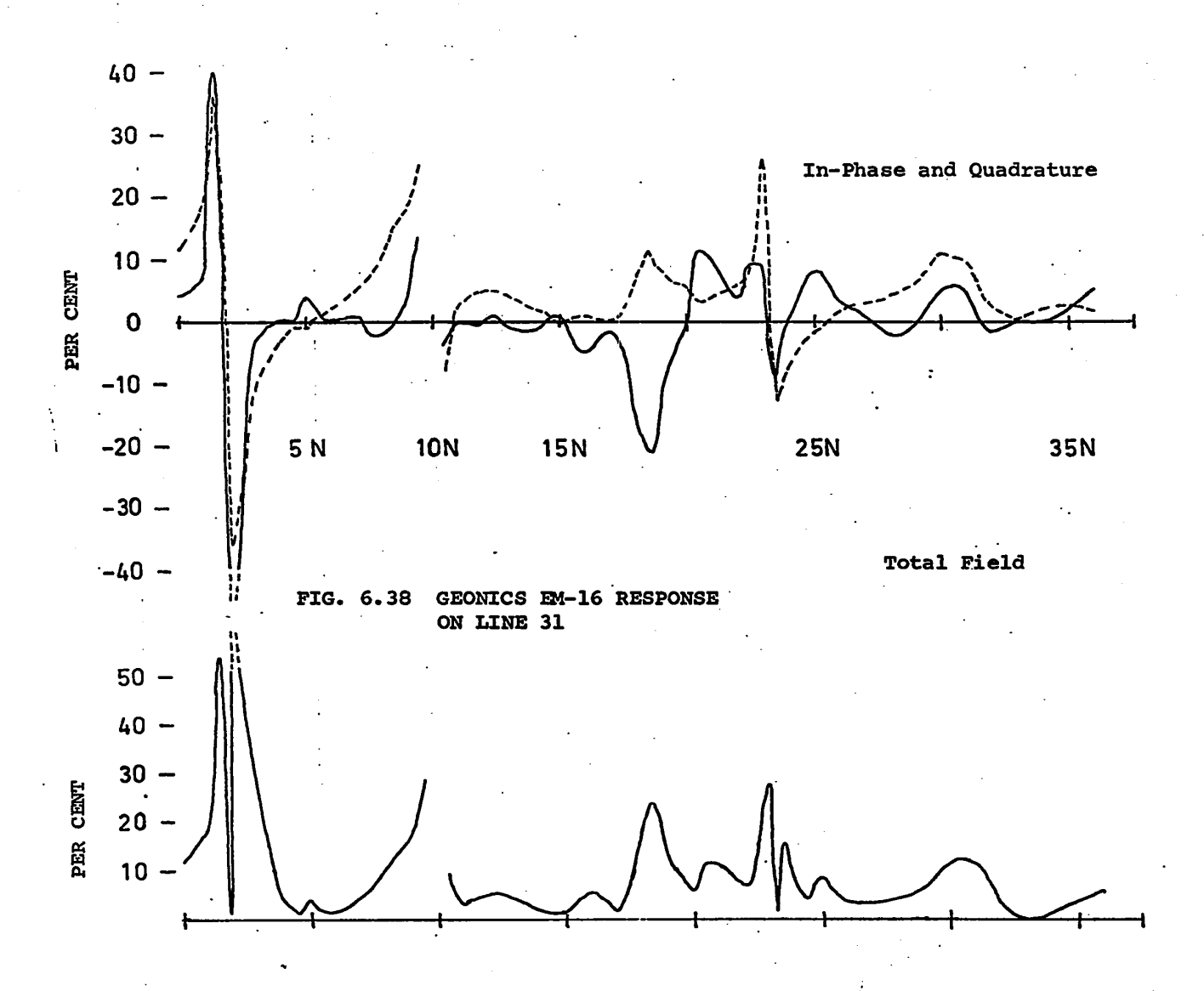
another strong cross-over.

The profile crosses the Castor River between 25+00N and 26+25N. Unfortunately, an overhead telephone line at 27+00N and overhead power lines at 28+00N both give a strong response and their influence is seen immediately at station 26+50N, which shows large positive values for both the in-phase and quadrature. At 25+00N, the in-phase is negative, and the quadrature positive (similar to previous stream responses), but these readings cannot be considered reliable. There may or may not be a response associated with the river.

Line 31

The large, sharp cross-over at 1+75N is caused by a buried telephone cable. A power line at 10+00N causes the anomaly in the vicinity of that station. (It was impossible to get a reading near 10+00N because of power line interference, and that is the reason for the gap in the profile).

The profile crosses the Castor River between 18+50N and 20+00N, and a response similar to those observed previously occurs. The in-phase component shows a negative peak at the south bank of the river, while the quadrature displays a positive peak. As the river is crossed from south to north, the in-phase becomes positive and the quadrature decreases, until 50 feet north of the north bank, the in-phase shows a positive peak and the quadrature is depressed. A false cross-



over occurs in the in-phase component at the north bank of the river. This results in a total field response which displays a minimum value between two peaks. In this case the minimum occurs over the north bank of the river, while in two previous cases it occurred over the river itself.

An overhead power line causes the cross-over at 23+25N.

There is a fault or contact type response at 30+00N. The in-phase and quadrature both display a positive peak, with the quadrature response being somewhat broader and having a higher amplitude than that of the in-phase. This indicates a contact with the higher conductivity on the north side. This is possibly the contact between the Ottawa limestone and the Carlsbad shale, although the fault is shown about 1500 feet to the north.

Line 32

The cross-over at station 9+50N is caused by a fence.

The Castor River crosses the traverse line between 15+50N and 15+80N and shows a response quite similar to the previous streams. The in-phase component shows a large negative peak at the south bank of the river, while the quadrature displays a fairly sharp positive peak. This response is broader than any of the other stream responses. On the north bank of the river, the quadrature does not become negative because of power line interference. The effect of the



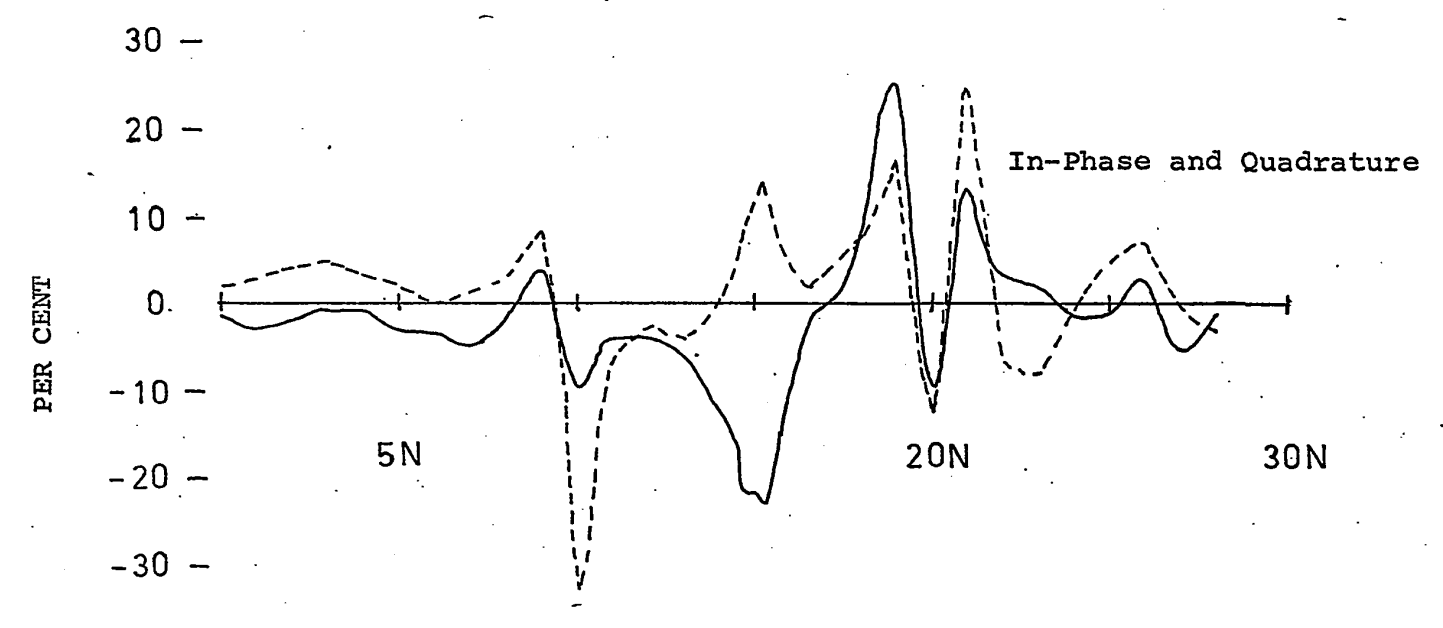
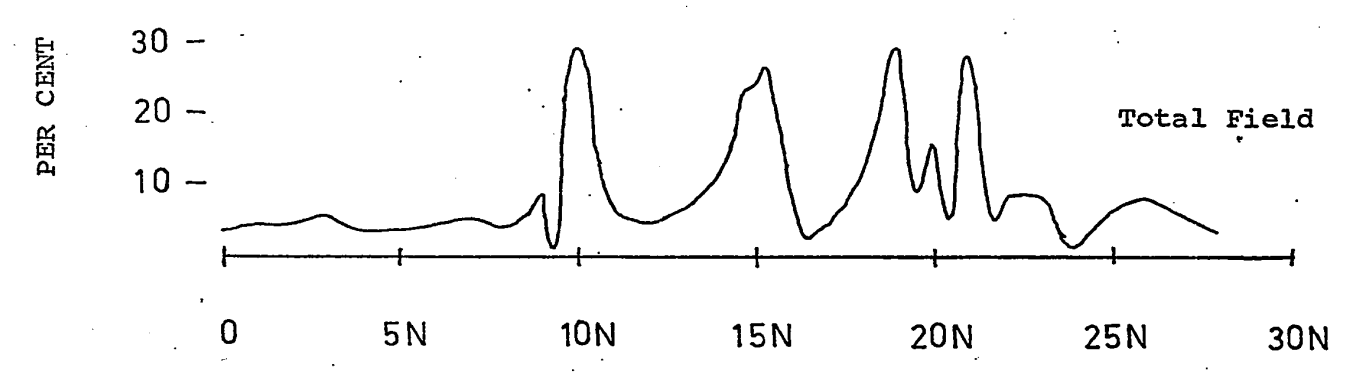


FIG. 6.39 GEONICS EM-16 RESPONSE ON LINE 32



power line at 19+75N can be seen at station 17+00N where the in-phase and quadrature are both starting to become positive. The cross-over at 19+75N and 21+75N are both caused by overhead power lines.

A contact type response similar to that on Line 31 occurs at 26+00N. The in-phase and quadrature are both positive peaks, indicating that the higher conductivity is to the north. The quadrature response has a higher amplitude and is broader than the in-phase. This results in a single peak on the total field profile. This is possibly the contact between the Ottawa limestone and the Carlsbad shale, but is about 2500 feet south of where the fault is shown on the map. This response, and that on Line 31, are quite similar to the response at the northern end of Line 23.

(ii) Discussion of Results

The contact between the Oxford dolomite and the Carlsbad and Queenston shale is easily identified on Lines 1 to 8. The results indicate that, in the vicinity of Lines 1 to 6, the Gloucester fault is as much as 1000 feet west of where it has been mapped. This is undoubtedly due to the lack of outcrop in this area, making it difficult to determine the exact location of the fault solely by geological mapping. On Lines 7 and 8, however, the location of the fault on the map nearly coincides with the EM-16 anomalies on those lines.

(")

The results are not as good further south along the Gloucester fault, where the contact is between the Oxford dolomite and the Ottawa limestone. In fact, four of the traverses (Lines 9, 11, 13, 14) show no response at all. only profile that shows the type of response to be expected over this contact is Line 10, but the anomaly occurs 1200 feet west of where the fault is mapped. Since the other lines show no similar responses, it is impossible to say whether this contact is due to the fault or not. Lines 10 and 12 show a contact about 500 feet east of where the Gloucester fault has been mapped, but the higher conductivity is on the west; presumably this is not the Gloucester fault. It is difficult to say what causes these two responses, but they appear to be local events. Since the true resistivity contrast between the Oxford dolomite and the Ottawa limestone is only of the order of 2 to 1, it is not surprising that the contact between these formations cannot be delineated.

The results are satisfactory over the fault which is parallel to, and immediately to the east of, the Gloucester fault. This fault has been detected on Lines 15, 17 and 18 quite close to where it is mapped. A very minor response (not having the right sign to be caused by the fault) occurs on Line 16. There are no wave impedance traverses to substantiate the EM-16 results, but, nevertheless, the location of the contact can be inferred on the basis of the EM-16 responses alone.

(T)

The fault parallel to, and farthest to the east of, the Gloucester fault was not detected. A minor contact type response on Line 21 cannot be definitely attributed to the fault. Line 22 exhibits an anomaly west of the fault, but presumably not associated with it. The same formation (Ottawa limestone) occurs on either side of the fault, and the conductivity contrast is not large enough to give a good response.

No evidence was found to support the short fault (striking roughly NE-SW, about a mile west of Russell) separating the Ottawa limestone and the Oxford dolomite. However, fault type responses occur north of the Castor River on Lines 23, 31, and 32, and these are believed to be caused by the contact between the Ottawa limestone and the Carlsbad shale. This seems to support the long fault, striking roughly SW-NE indicated by Wilson. However, the responses on Lines 31 and 32 indicate that the fault should be further south, about 1000 feet north of the Castor River. The only outcrop in this area occurs along the river, and Wilson probably only estimated the location of the fault. Since Lines 25 to 29 do not detect the fault at all and since, east of Russell, it is only shown as assumed, it is probably safe to conclude that the fault is not where it is shown on the map. In the vicinity of Russell, it is possibly just north of the Castor River, but east of Russell its location is unknown.

One of the more interesting results of the survey in the Russell area are the stream responses (so called because they are all associated with streams or rivers) which appear on Lines 23 to 26 and Lines 30 to 32. These responses seem to be stronger when they occur over streams which pass through the Ottawa limestone (Lines 23, 24, 31, 32). responses over the streams on Lines 26 and 30 are not as well defined, and these occur in the Oxford formation. It is difficult to account for these responses. If the stream was flowing along a fault, one would expect either a fault type response or a conductor type (cross-over) response (due to a water-filled shear) over the stream. However, these stream responses are neither fault type nor conductor type responses. Perhaps the response is due to the presence of the stream itself. One would expect the stream water to have a higher conductivity than the surrounding bedrock and therefore a conductor type response should occur. However, there seems to be a false cross-over (not a true cross-over) on the in-phase component which either occurs in the middle of the stream, or near the north bank of the stream, and the quadrature component is really a mirror image of the in-phase. It is known that conductive overburden can reverse the sign of the quadrature component (ref. EM-16 manual), and perhaps this effect is somehow involved. In any event, these stream responses are not well understood.

- 6.3 Noranda Area
- (i) Geonics EM-16 and Wave Impedance Profiles Across the Smoky Creek Fault

Line A-3

This traverse was conducted at the side of a road at the north-west end of Lac Flavrian. The geological map (Fig. 5.4) shows granodiorite on both sides of the Smoky Creek fault. The EM-16 profile (Fig. 6.40) has a negative in-phase peak of high amplitude (~100%) at station 15+50N, indicating a contact with the higher resistivity on the north-east side. The quadrature displays a local maximum over the negative in-phase peak. Wave impedance results confirm such a contact (See Fig. 6.41). Between stations 0+00 and 12+00N the apparent resistivity varies from 100 to 150 ohm m., while between stations 13+00N and 16+00N it rapidly increases to more than 6,000 ohm m. Between stations 16+00N and 25+00N, the apparent resistivity generally varies from 5,000 to 8,000 ohm m., while at 25+00N it has a somewhat lower value of about 3300 ohm m.

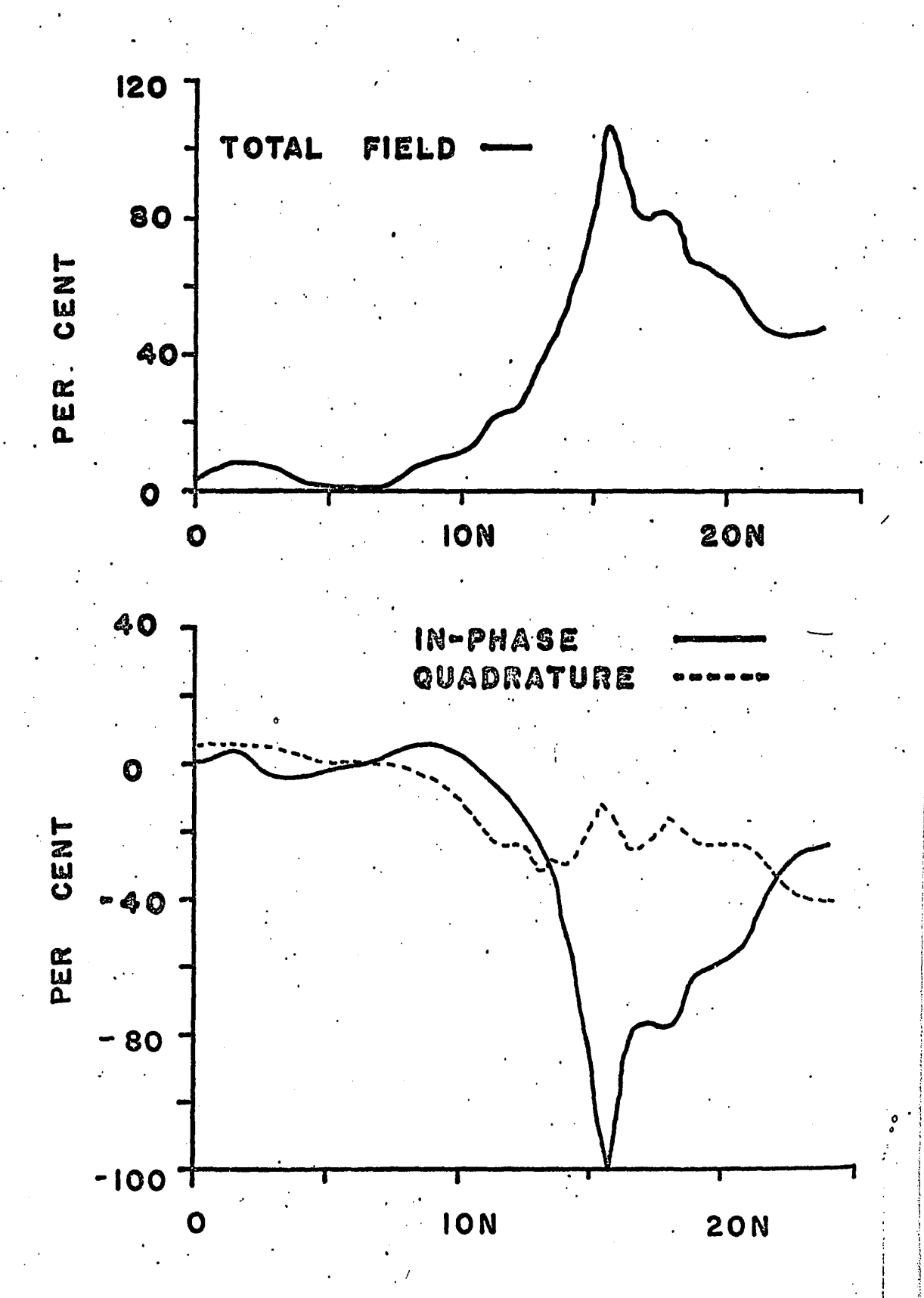
It appears that this contact is indeed the Smoky Creek fault. On the south-west side of the fault the apparent resistivity is about 100 to 150 ohm m., while on the north-east side of the fault it is roughtly 5,000 ohm m.

The horizontal magnetic field strength, as shown by the equivalent vertical electric field strength in Fig. 6.42, is clearly lower on the more resistive side of the fault. In fact,

the field strength on this particular profile clearly illustrates the behaviour shown by it in the theoretical profiles in Fig. 3.9. Approaching the contact on the less resistive side, the field strength increases (8+00N to 13+00N), then suddenly decreases as the fault is crossed (say around 14+00N), and then assumes a distinctly lower value on the more resistive side of the fault. The very high resistivity contrast and the thin overburden (meaning a small value for d/δ) is undoubtedly the reason why this traverse best demonstrates the expected behaviour of the horizontal primary magnetic field strength.

The phase angle $(E_y^{-H}_x)$ does not illustrate the behaviour shown in Fig. 3.2. The phase angle is relatively high in the more conductive zone between 1+00N and 10+00N (as expected), and decreases somewhat as the contact is approached, but then increases rapidly on the resistive side of the contact. The phase angle is, in fact, extremely high at station 22+00N (so high that it is off the conversion table in the wave impedance manual) and, although there were no power lines in the immediate vicinity of the station, this reading must be considered unreliable.

DC resistivity (depth probing) profiles were obtained at stations 7+50N, 13+50N, and 16+50N. An expanding Wenner array was used, and the interpretation was done by the method of asymptotes, described by Keller and Frischknecht (p. 122).



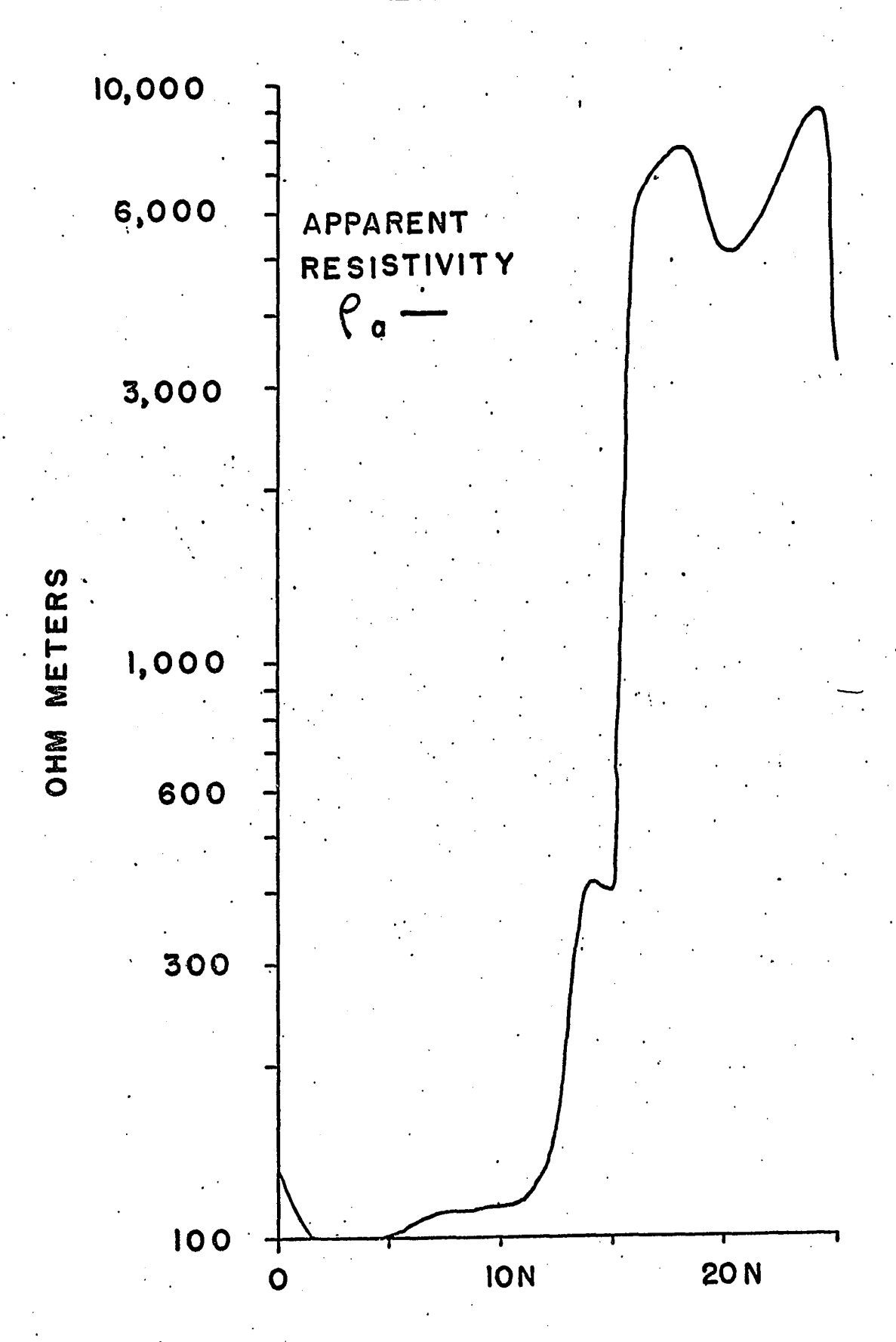
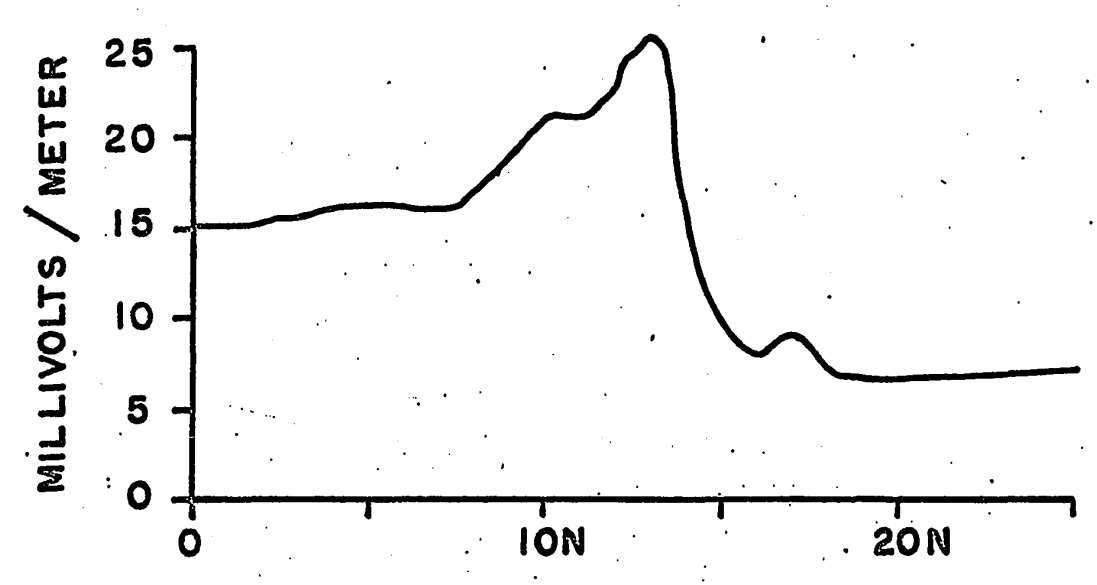
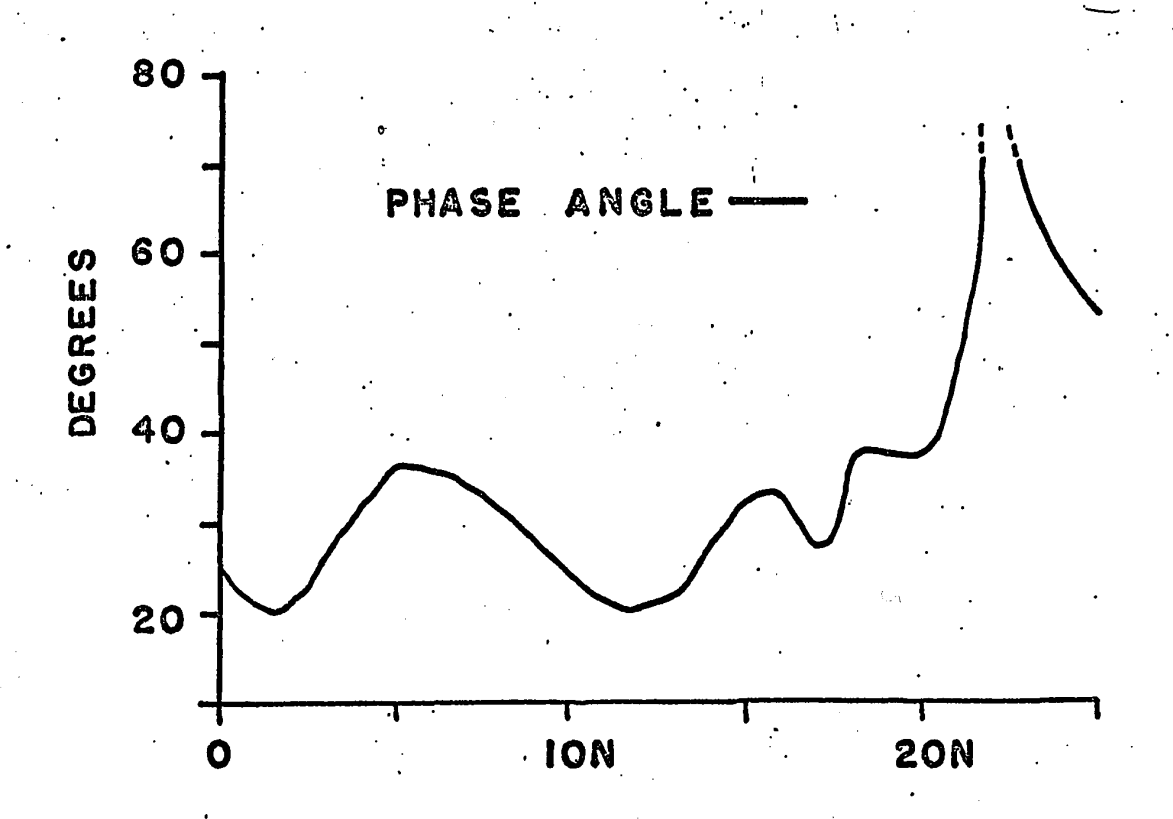


FIG. 6.42 - LINE A-3







This method assumes a single layer of overburden overlying resistive basement rocks, and points on the profile obtained with very short electrode spacings are ignored, since they reflect resistivity variations within the first few feet of the surface. The method can be used to estimate the minimum depth of overburden even if the electrode array is not expanded to the point where the high resistivity basement affects the sounding curve appreciably. The DC resistivity profiles are shown in Appendix III and reveal that the dramatic change in apparent resistivity on Line A-3 is caused by a change in the thickness of overburden, and not by a contact between two formations with different resistivities.

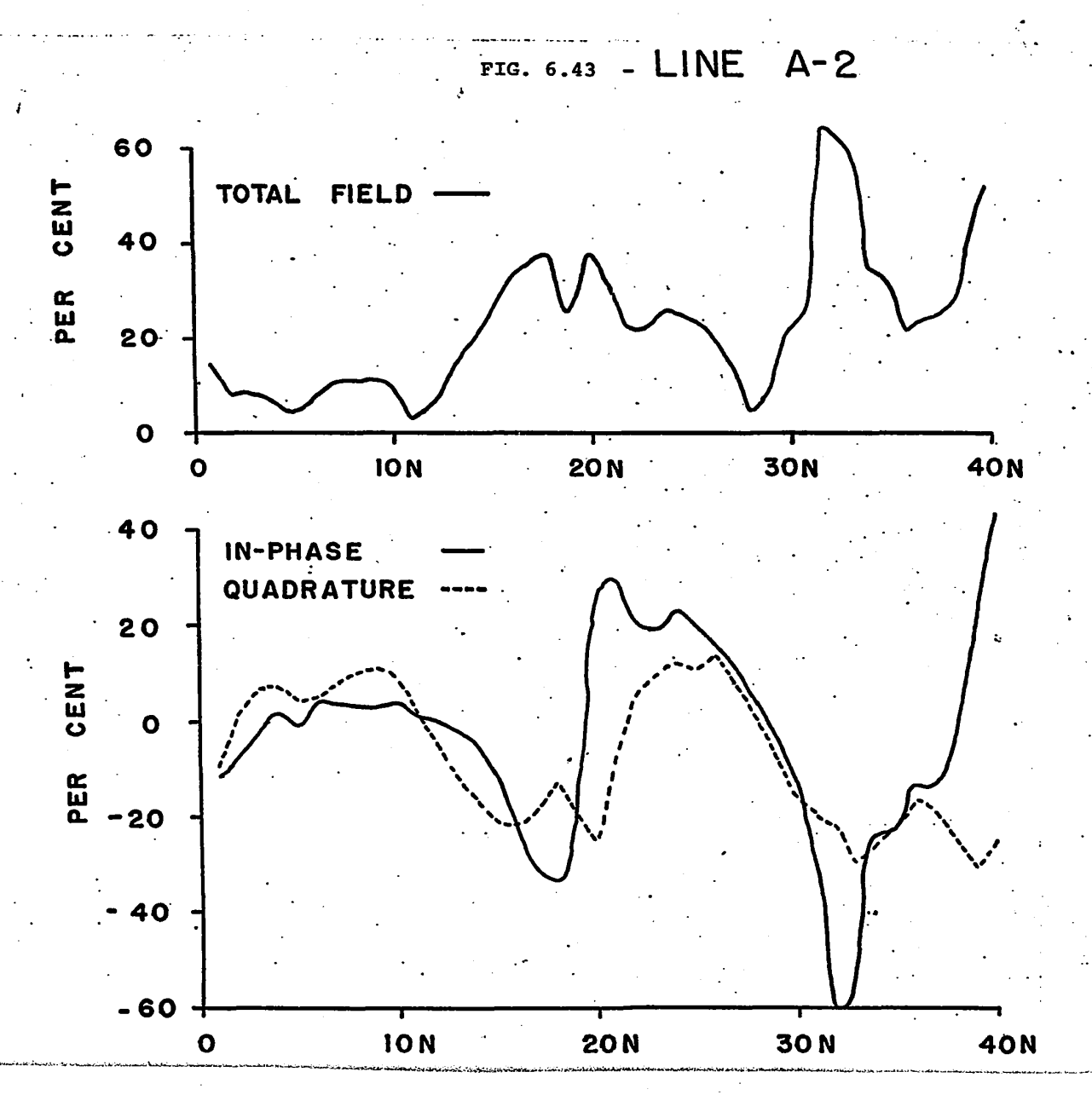
The overburden is at least 57 feet thick at station 7+50N, and at least 43 feet thick at 13+50N. However, the overburden thickness at station 16+50N is only about 6 feet. At the latter station, this is probably a maximum figure, since the shape of the curve makes it difficult to draw the asymptote. Since the overburden resistivity is only about 50 to 60 ohm meters (as seen from the DC resistivity curves), such a rapid thinning of overburden is critical. The abrupt change in apparent resistivity appears as a contact on the wave impedance and EM-16 profiles, even though there is no change in the bedrock lithology. (Actually, this may be regarded as a vertical contact between the overburden and the bedrock). A change in overburden thickness from about 50 feet to about 5 feet in a very

short lateral distance possibly indicates that the bedrock is extremely undulatory. On the other hand, this thinning is possibly due in some way to the Smoky Creek fault, in which case the fault is the indirect cause of the observed anomaly. It is very tempting to say that the fault is somehow related to the change in bedrock topography, since the EM-16 anomaly occurs exactly where the fault is mapped. There is, however, no evidence to support this argument.

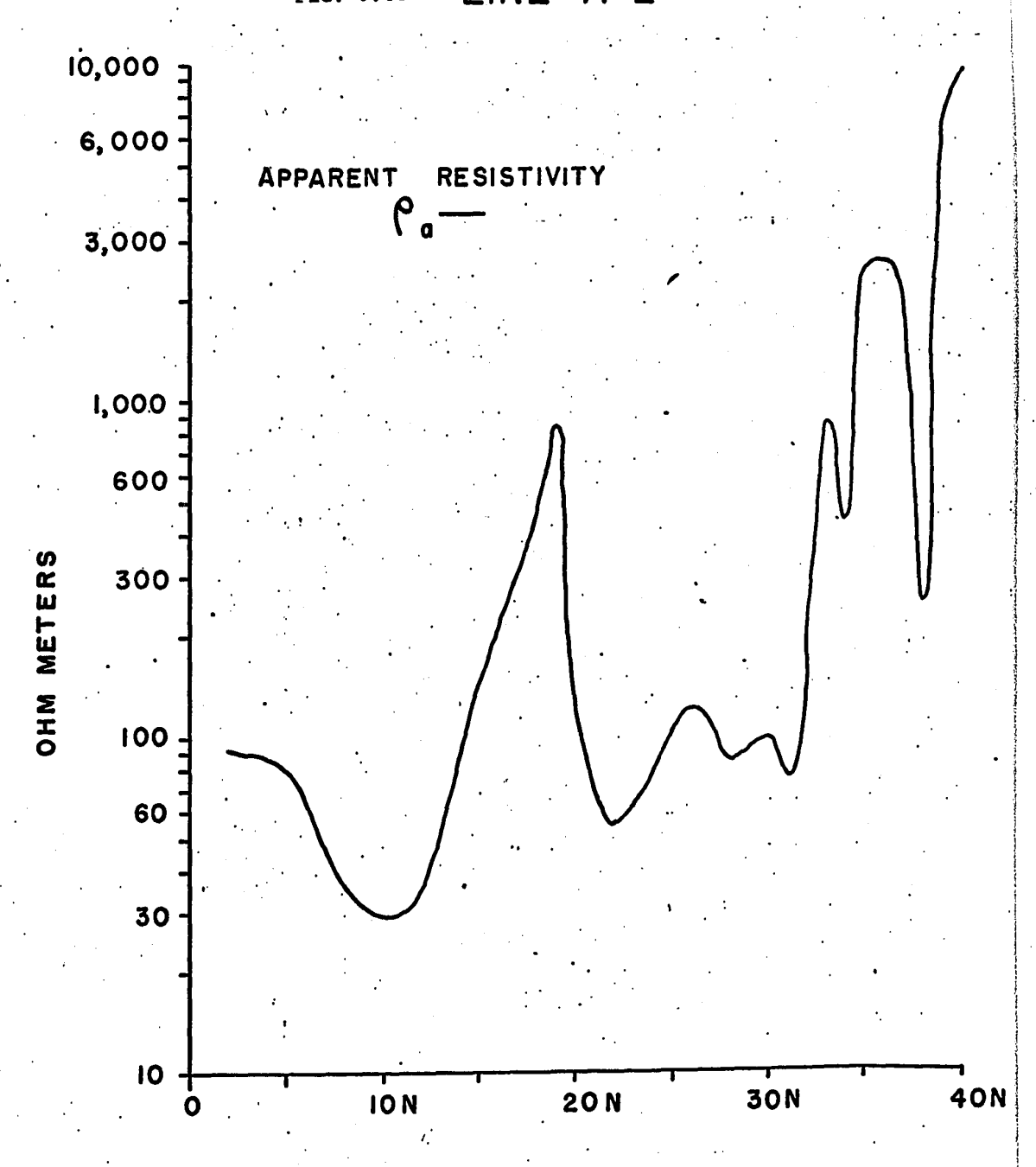
Line A-2

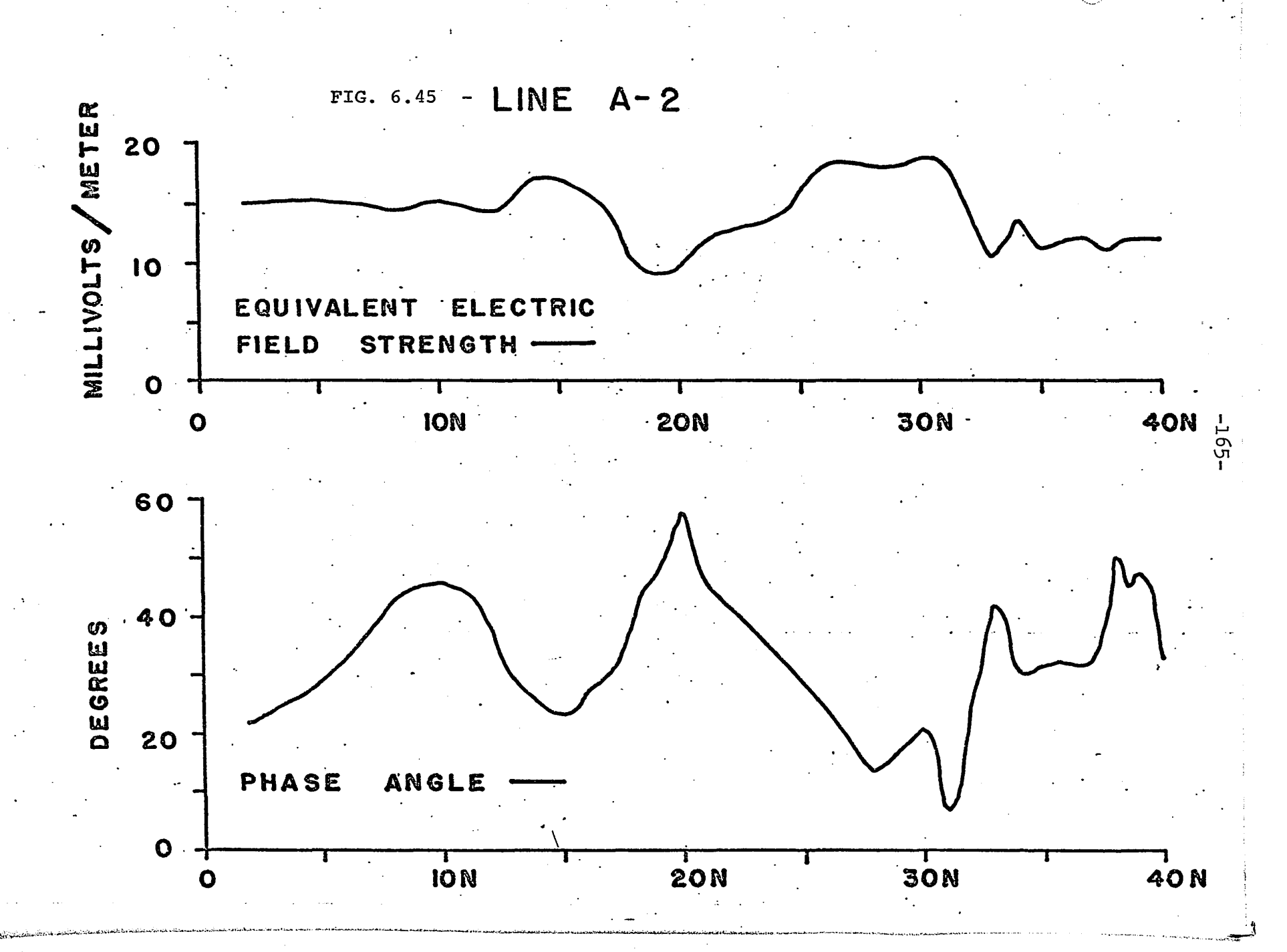
 $\langle \overline{} \rangle$

According to the geological map. (Fig. 5.4), the fault should occur at about 8+00N on the profile. Granodiorite occurs on both sides of the fault. There is no anomalous response in the vicinity of 8+00N. However, the EM-16 in-phase component shows a negative peak at about 18+00N, and the quadrature component displays a local maximum at that point (Fig. 6.43). This indicates a contact with the higher resistivity on the north side. At 21+00N, the in-phase component shows a positive peak, while the quadrature displays a local minimum at 20+00N. This indicates a contact at about 20+00N or 21+00N with the higher resistivity on the south side of the contact. The EM-16 results, therefore, indicate a zone of higher resistivity between 18+00N and 20+00N. Wave impedance results confirm the existence of this zone of high resistivity (Fig. 6.44). The apparent resistivity is less than 100 ohm m. between stations









()

0+00 and 14+00N, but increases from about 130 ohm m. at station 15+00N to about 830 ohm m. at 19+00N. The apparent resistivity then suddenly decreases to 130 ohm m. at 20+00N. According to wave impedance results the zone of higher apparent resistivity occurs from about 16+00N to 19+00N or 19+50N. DC resistivity depth sounding curves were obtained at stations 5+00N, 15+00N, and 20+00N, indicating that the overburden resistivity in the area is about 40 ohm meters, on the average. These curves reveal that the overburden is at least 30 feet thick at station 5+00N and at least 36 feet thick at 15+00N. However, at station 20+00N (which appears to be very near the northern boundary of the resistive zone) it is only about 11 feet thick. It is unfortunate that a depth sounding curve was not obtained at station 18+00N or 19+00N, for the overburden is probably very thin over those stations. The narrow zone of high apparent resistivity between stations 16+00N and 19+00N is therefore due to a bump in the basement topography, and the flanks of the bump (where there is an abrupt change in the apparent resistivity) appear as contacts on the EM-16 and wave impedance profiles.

An EM-16 response somewhat similar to that between 18+00N and 20+00N occurs further north on the profile. There is a negative in-phase peak at station 32+00N, while at 40+00N the in-phase component displays a high positive value. This indicates a contact at about 32+00N with the more resistive side on the

north, and possibly another contact at about 40+00N (or possibly slightly farther north) with the more resistive side on the south of the contact.

Thus the EM-16 results seem to indicate a fairly wide zone (at least 800 feet) of higher resistivity between 32+00N and about 40+00N. Wave impedance results once again confirm the EM-16 results. Between stations 21+00N and 31+00N, the apparent resistivity varies from about 50 ohm m. to slightly more than 100 ohm m. At station 32+00N, the apparent resistivity suddenly increases to about 250 ohm m. and then to more than 800 ohm m. at 33+00N. The apparent resistivity decreases somewhat to slightly more than 400 ohm m. at 34+00N, increases suddenly to more than 2,000 ohm m. at 35+00N and 36+00N, and decreases to less than 300 ohm m. at 38+00N. apparent resistivity then suddenly increases to almost 7000 ohm m. at 39+00N and to slightly more than 9000 ohm m. at 40+00N. There is clearly a zone of higher resistivity from 32+00N to at least 40+00N, containing two small bands of lower resistivity, at 34+00N and 38+00N. It is not possible to say where the high resistivity zone terminates, but the high EM-16 in-phase component at 40+00N seems to indicate that it ends slightly north of 40+00N. DC resistivity depth sounding curves at stations 27+00N and 34+00N once again indicate that the apparent contact is caused by bedrock topography. There are

near surface resistivity variations within the first 10 feet of overburden at station 27+00N, but it is apparent that there are at least 40 feet of overburden at this location. However, there are only about 6 feet of overburden at station 34+00N, indicating that the overburden abruptly thins between these two stations. Thus we have another bump in the bedrock which occurs at about station 32+00N. This appears as a contact on the EM-16 profiles.

Again the horizontal primary magnetic field strength (as shown by the equivalent vertical electric field in Fig. 6.45), is distinctly lower over the two resistive zones (i.e. between about 17+00N and 21+00N, and between 32+00N and 40+00N) as expected.

The phase angle (Fig. 6.45) varies considerably, as can be expected in an area where there are several zones where the apparent resistivity varies. The very low value exhibited by the phase angle is not very indicative in cases where there are many zones of different apparent resistivity fairly close together.

Line A-1

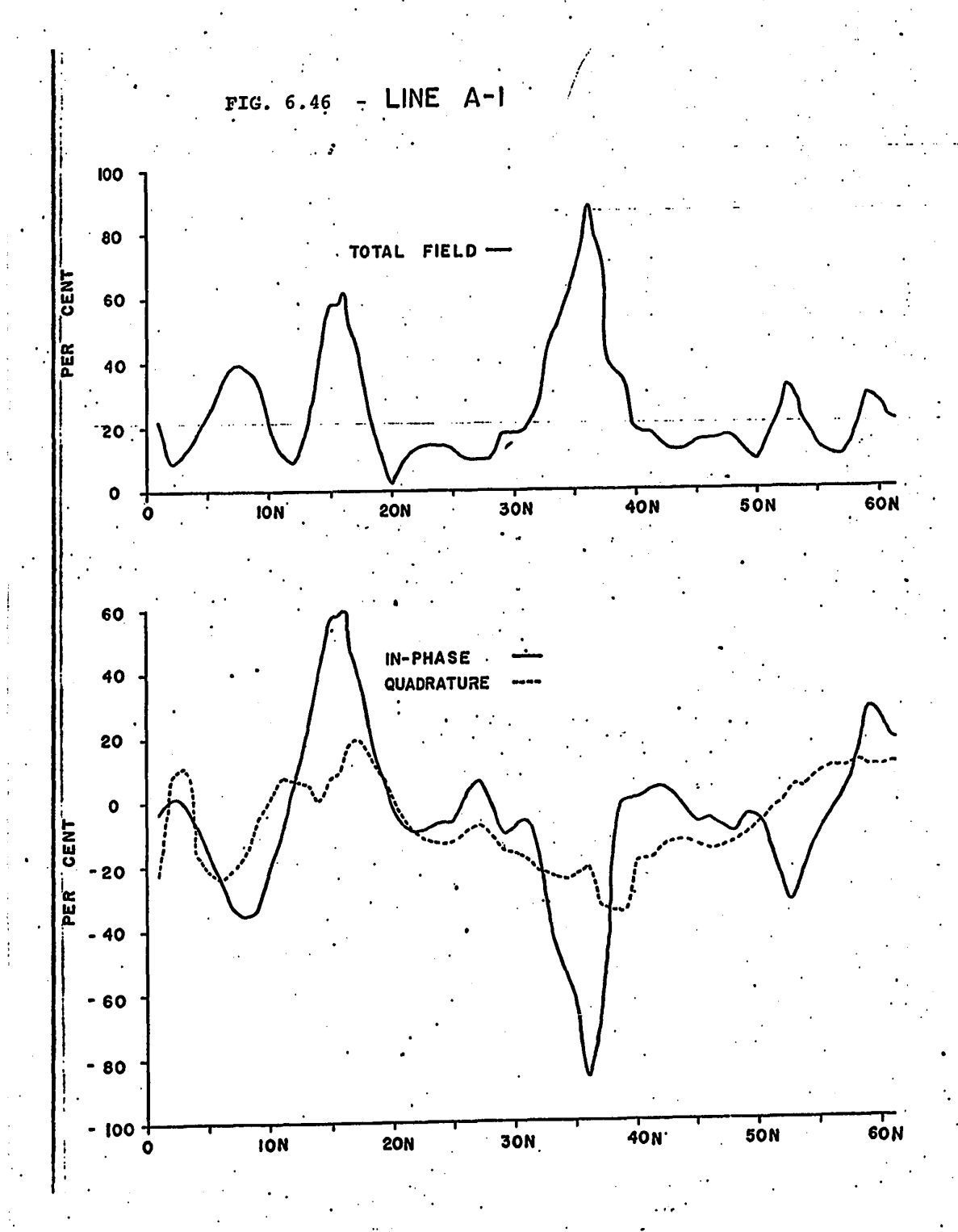
()

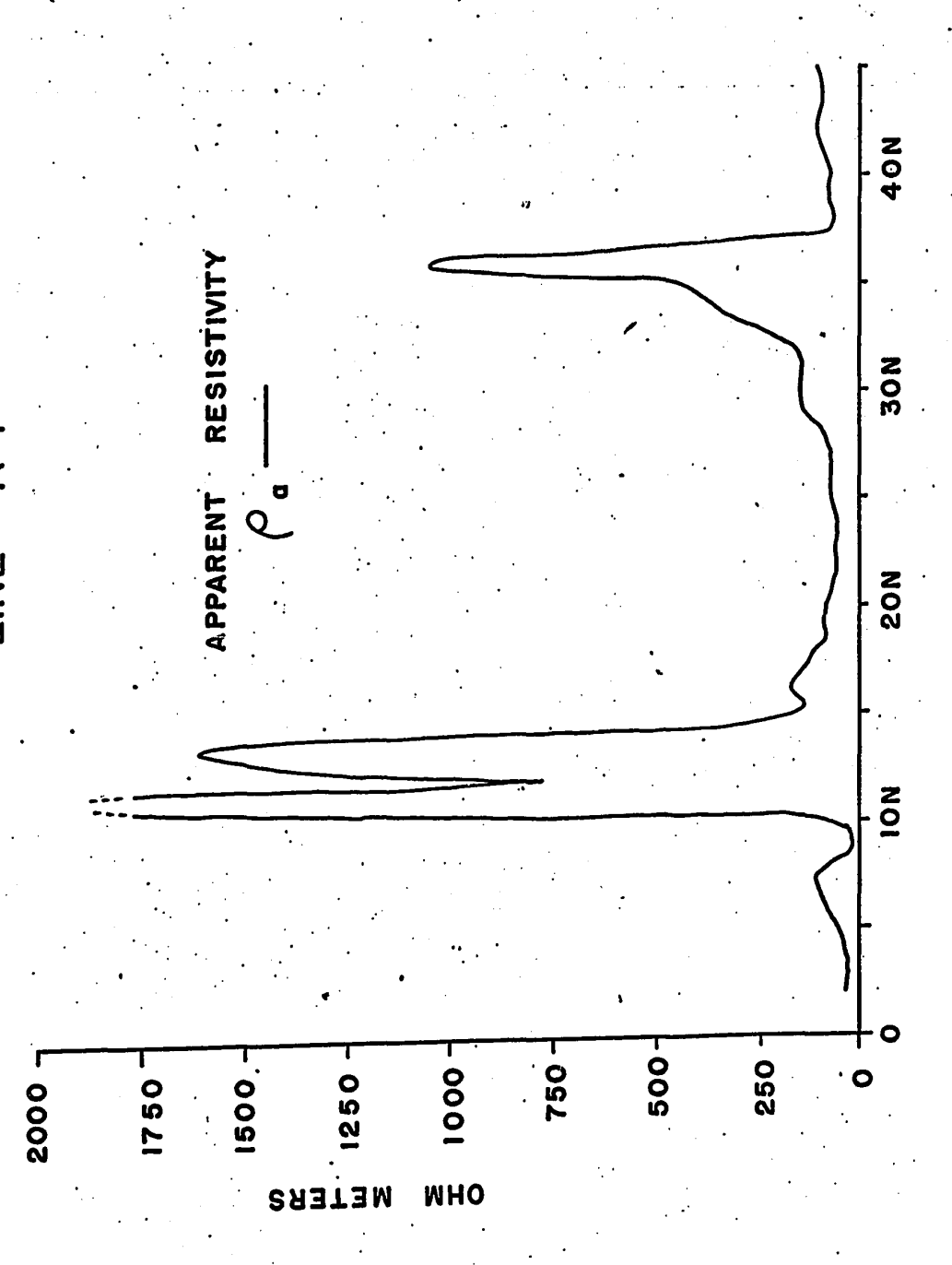
()

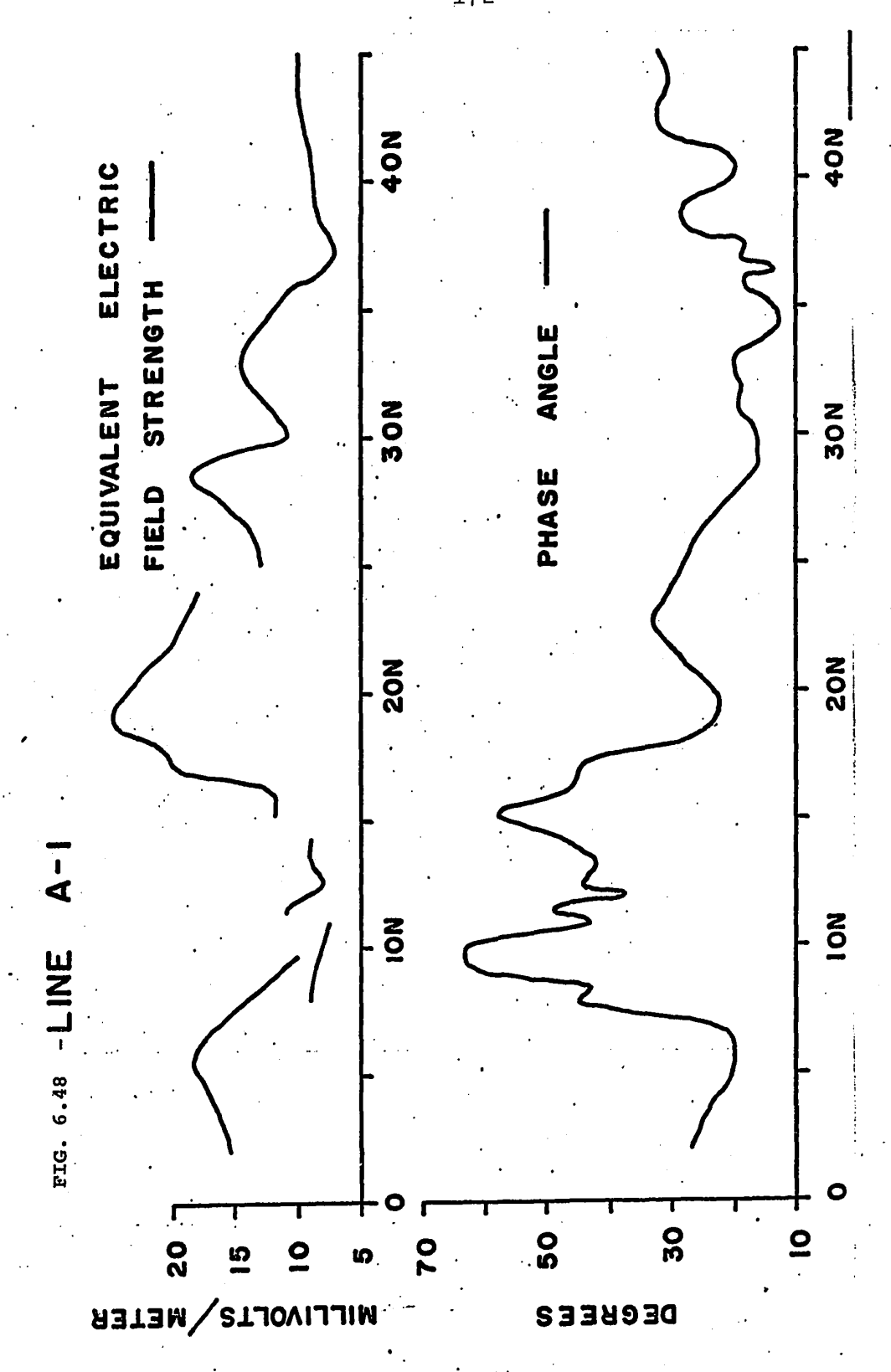
This traverse was conducted approximately 1000 feet to the west of A-2. According to the geological map in Fig. 5.4, granodiorite occurs on both sides of the Smoky Creek fault, which should occur at about 18+50N on the profile.

 (\cdot)

The responses on this profile are quite similar to those on Line A-2. A negative in-phase peak occurs at about 8+00N or 9+00N and a positive in phase peak occurs at about 15+00N or 16+00N (See Fig. 6.46), A local minimum in the quadrature response occurs at 14+00N. Unfortunately, the south end of the profile is distorted by a power line at 0+10N. The EM-16 results indicate a zone of higher resistivity between stations 8+00N and 15+00N (approximately). Wave impedance results substantiate this (Fig. 6.47), although the zone of high apparent resistivity is somewhat narrower than the EM-16 results indicate. Between stations 2+00N and 10+00N the apparent resistivity varies from about 25 to 100 ohm m., and then suddenly increases to almost 9000 ohm m. at 11+00N. The apparent resistivity then decreases to slightly less than 800 ohm m. at 12+00N, increases to about 1600 ohm m. at 13+40N and suddenly decreases to slightly less than 150 ohm m. at 15+25N. The zone of high resistivity therefore occurs between about 10+50N and 14+50N, with a narrow band of lower resistivity at 12+00N. Unfortunately, there are no DC resistivity results on Line A-1, but it is assumed that the zone of high apparent resistivity is again caused by a bump in the bedrock. Apparently this bump has very steep flanks, since the apparent resistivity changes abruptly in a very short lateral distance. The extremely high apparent resistivity at 11+00N probably indicates that the bedrock is almost at surface at that station.







(

A very large negative in-phase peak, accompanied by a local quadrature maximum, occurs at 36+00N. This indicates a contact with the higher resistivity on the north side. wave impedance results show a zone of higher resistivity between stations 34+00N and 37+00N. This high resistivity zone should result in an EM-16 in-phase response similar to those already observed. i.e. there should be a negative in-phase peak at the southern edge of the zone and a positive in-phase peak at the northern limit of the zone, resulting in a false cross-over approximately over the center of the zone. There is no positive in-phase peak, in spite of the fact that there seems to be a sharp contact at about station 37+00N between the resistive zone to the south and the more conductive zone to the north. The apparent resistivity is slightly more than 1000 ohm m. at 36+00N and decreases rapidly to less than 100 ohm m. at 37+50N. The contact on the south side of the resistive zone seems to be at about 34+00N or 35+00N, while the EM-16 in-phase component locates it at 36+00N. It is once again assumed that this zone of high apparent resistivity is caused by a high in the bedrock topography. There are no DC resistivity curves to support this, but similar responses on Lines A-3 and A-2 are caused by bumps in the bedrock.

A negative in-phase peak at 52+50N and a positive in-phase peak at 59+00N indicate a third zone of high resistivity between those points, but there are no wave impedance

results to substantiate this.

(

The wave impedance results on Line A-1 were obtained at three separate times, with stations 2+00N to 10+00N, 8+00N to 24+00N, and 25+00N to 45+00N being read on different days. This accounts for the discontinuities in the equivalent electric field strength (Fig. 6.48) at 16+00N and 24+00N, since it is not uncommon for the VLF transmitter at Cutler to broadcast at slightly different power levels from day to day. discontinuity at 11+50N is due to the fact that the transmitter increased power at that point while the traverse was being conducted, and again at 15+00N. For this reason, it is difficult to determine the behaviour of the horizontal magnetic field strength over the resistive zone between 10+00N and 15+00N. Nevertheless, it can be seen that the field strength is decreasing from 5+00N to 10+00N, and increasing from 15+00N to 20+00N, and it is safe to conclude that the field strength is considerably lower over the resistive zone. The field strength varies considerably between 25+00N and 45+00N. The low value at 30+00N does not coincide with a zone of high resistivity, but the field strength is definitely lower over the resistive zone between 35+00N and 38+00N.

The phase angle (E_y-H_x) varies considerably on Line A-1. (N.B. - changing the power output of the transmitter affects only the field strength readings, and not those of phase angle and wave impedance). However, it is relatively lower over the

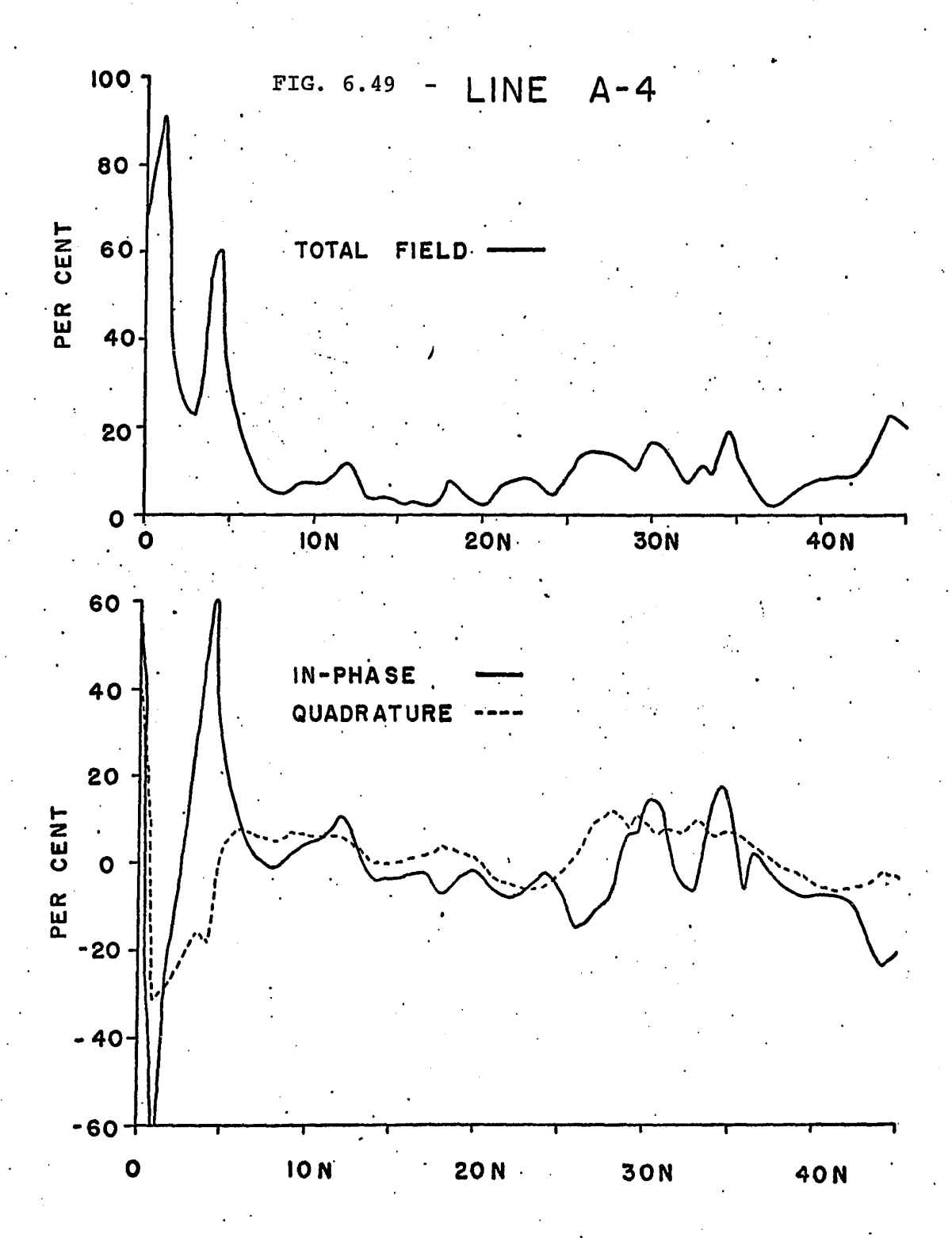
resistive zones between 10+00N and 15+00N, and between about 32+00N and 38+00N.

Line A-4

()

This traverse was conducted approximately 3400 feet to the west of A-1. Granodiorite occurs on both sides of the fault, which should occur at about 43+00N, which is at the extreme north end of the profile.

The traverse crosses a large granodiorite outcrop between 0+00 and 4+50N. This outcrop is about 1000 feet long in the east-west direction, and 450 feet wide in the northsouth direction (along the traverse). The outcrop displays considerable relief (about 20 feet high) and has steep flanks. This is visual proof that the bedrock surface is very hilly. Unfortunately, the EM-16 response (Fig. 6.49) over the south flank of the outcrop is distorted by a power line at 0+50N, which causes a large cross-over at that station. However, a very large positive in-phase peak occurs at 4+50N, where the north flank of the outcrop abruptly disappears beneath the overburden. This response indicates a contact with the resistive side on the south, which is exactly the case. clearly shows that it is possible to have a large EM-16 response over the flanks of a hill in the bedrock, where the apparent resistivity changes abruptly if overburden is present.



There appear to be alternating zones of low and high resistivity between 25+00N and 35+00N. A negative in-phase peak at 26+00N and a positive one at 30+50N indicate a zone of higher resistivity between those points while a negative in-phase peak at 33+00N seems to indicate a zone of lower resistivity between 30+50N and 33+00N. Another positive in-phase peak at 34+50N indicates a second narrow zone of higher resistivity between 33+00N and 34+50N. These alternating zones of high and low resistivity probably reflect the undulating nature of the surface of the bedrock in this area. The quadrature component is generally positive over all these zones, but varies slightly.

The in-phase component displays high negative values (-20%) at the north end of the profile. The Smoky Creek occurs at 45+00N, and this is where the Smoky Creek fault is supposed to lie. It was impossible to cross the creek and complete the profile.

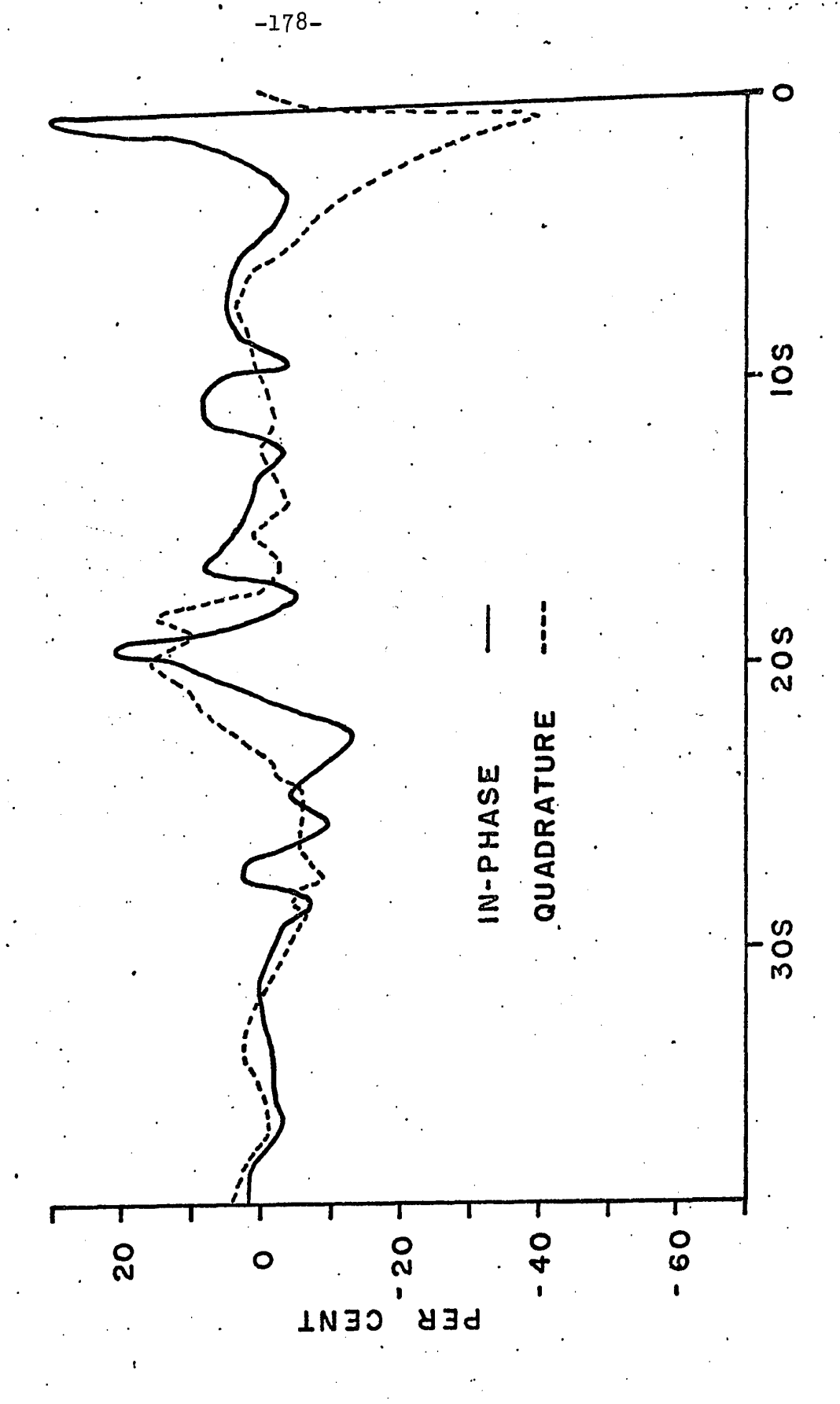
Wave impedance readings were not conducted on this traverse.

(ii) Geonics EM-16 and Wave Impedance Profiles
Across the Lois Lake Shear Zone

Line C-1

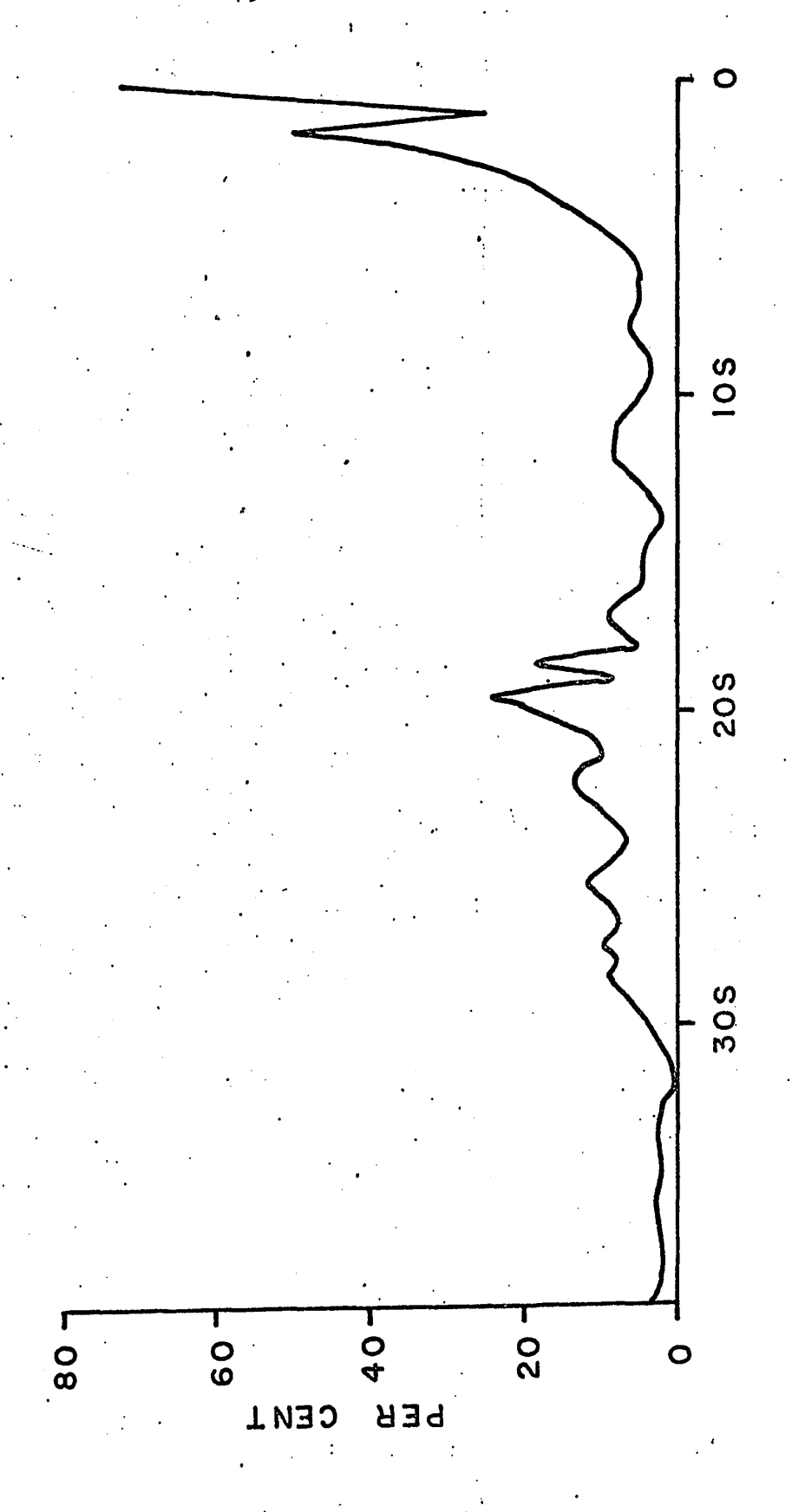
()

This traverse crosses two INPUT anomalies, which should appear on the profile at about 21+00S and 31+50S respectively (Fig. 5.5).

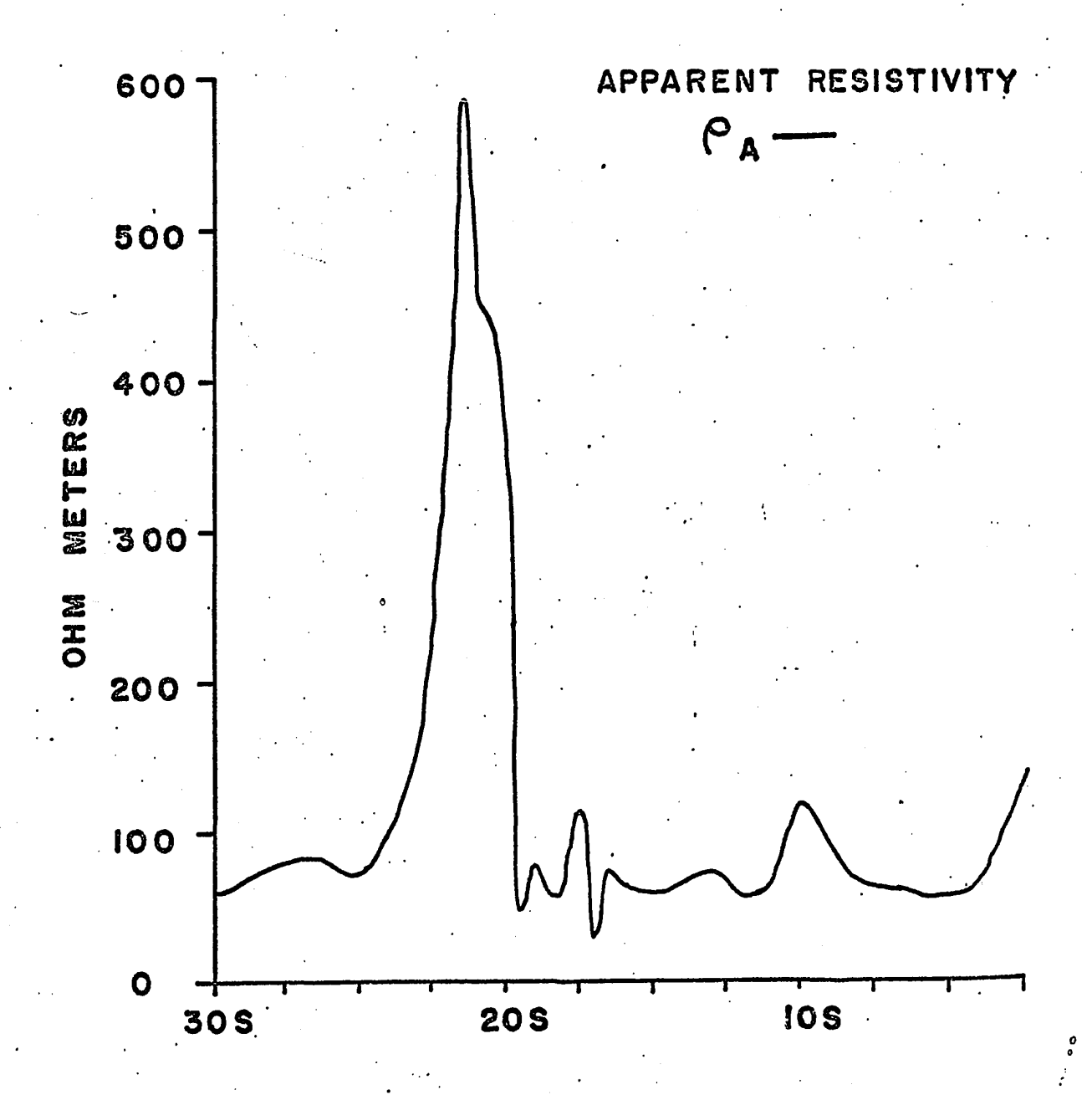


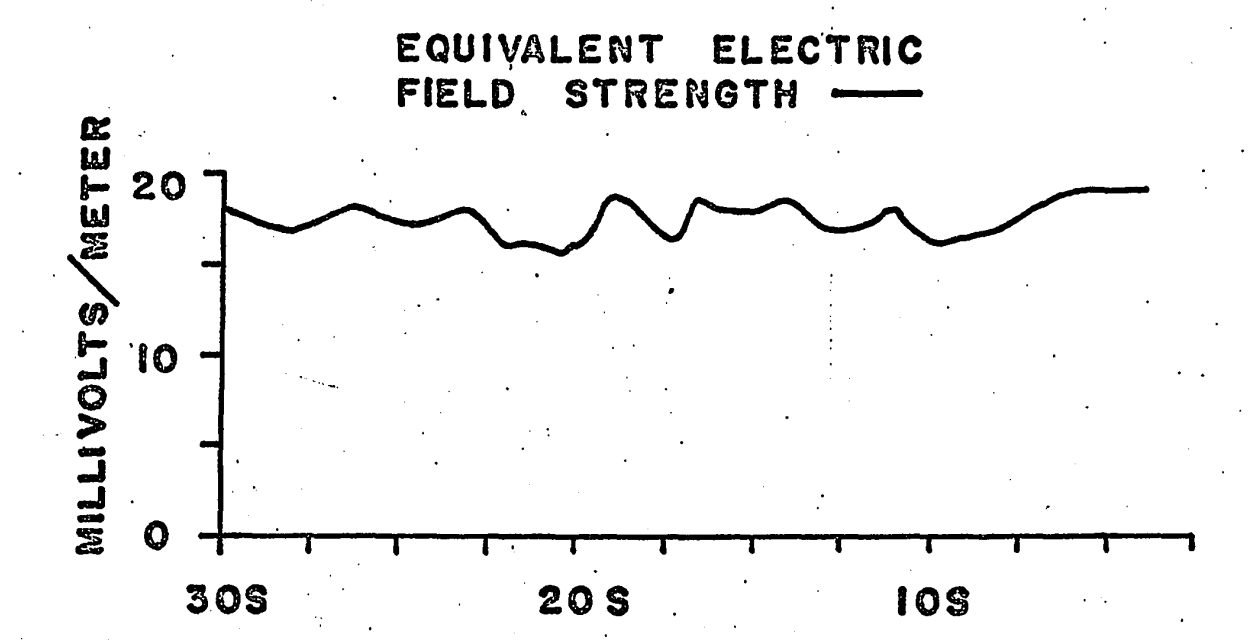
TOTAL FIELD

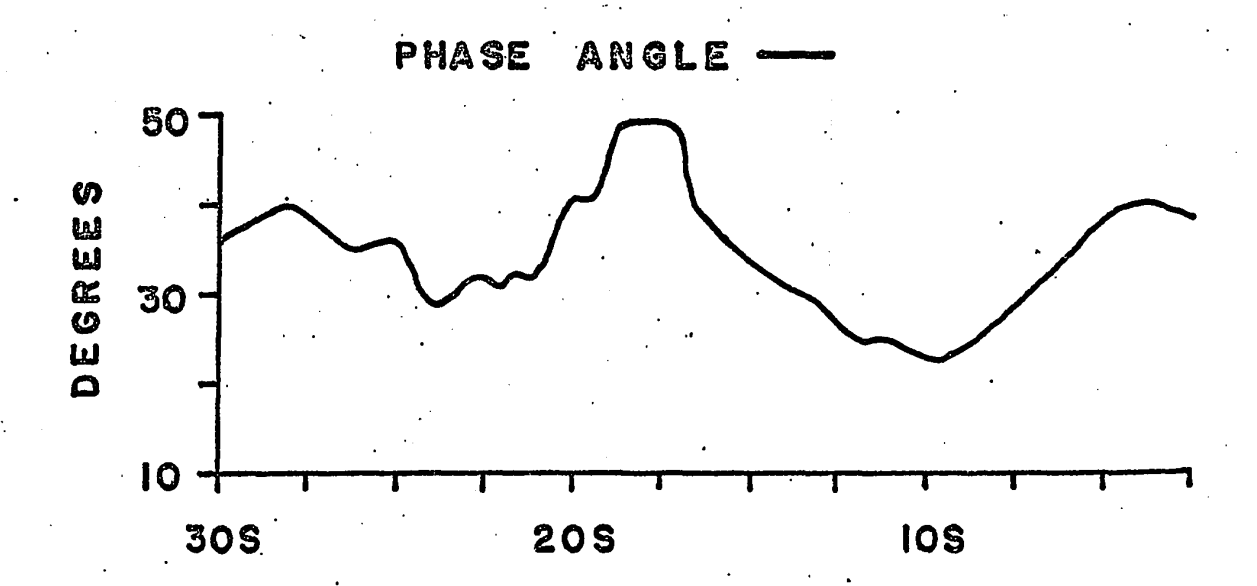
FIG. 6.51



(







The large EM-16 anomaly (Fig. 6.50 and 6.51) at the beginning of the profile is caused by a power line at 0+15S, and another at 1+05S.

There is a distinct in-phase peak at 19+50S, and a local quadrature minimum at 19+00S. This indicates a contact at about 19+00S with the more resistive side on the south. There is also a negative in-phase peak at 22+50S, indicating a contact at that point with the more resistive side to the north. The EM-16 results therefore indicate a zone of high resistivity between about 19+00S and 22+50S. Wave impedance results once again bear out the EM-16 interpretation (See Fig. 6.52). There is a zone of high apparent resistivity between 19+50S and 23+00S. On either side of this zone the apparent resistivity is generally less than 100 ohm m., while at the center of the zone at 21+50S, it approaches 600 ohm m. This resistive zone seems to be the feature which causes the INPUT anomaly at 21+00S. Bearing in mind the results from the Smoky Creek area, this zone of higher apparent resistivity is possibly caused by a bump in the bedrock topography. However, there are no DC resistivity results for the Lois Lake area, and it is impossible to prove or disprove this conjecture. The remainder of the EM-16 profile is devoid of features out to 39+00S, and the INPUT anomaly at 31+50S remains unexplained.

The horizontal primary magnetic field strength which varies between 15 and 20 millivolts/meter is distinctly lower

over the slightly more resistive zone between 8+00S and 11+00S. It is also lower at 17+50S, which corresponds to a narrow zone of slightly higher resistivity.

The phase angle (E_y-H_x) shown in Fig. 6.53 varies considerably along Line C-1. It decreases from about 35 degrees at 0+00 to about 20 degrees over the slightly more resistive zone at 10+00S, increases to almost 50 degrees at about 18+00S and then decreases to about 30 degrees over the resistive zone between 20+00S and 24+00S. It increases to around 40 degrees over the low resistivity zone between 25+00S and 30+00S.

Line C-2

 $(\)$

A fault is shown on the geological map in Fig. 5.5, corresponding to station 0+00 on the profiles of Figs. 6.54 to 6.58. Basalt and andesite occurs south of the fault, while rhyolite occurs on the north side of the fault. An INPUT anomaly occurs at about 17+50S on the profile, and a second is shown at about 25+00S, at the creek. (0+00 is about 900 feet south of the road).

The EM-16 in-phase and quadrature (Fig. 6.54) are both negative from about 10+00S to 9+00N (i.e. for almost 2000 feet). There is a distinct negative in-phase peak at 1+00N with the more resistive position on the north side of the contact. Wave impedance results tend to confirm this (Fig. 6.56). Between

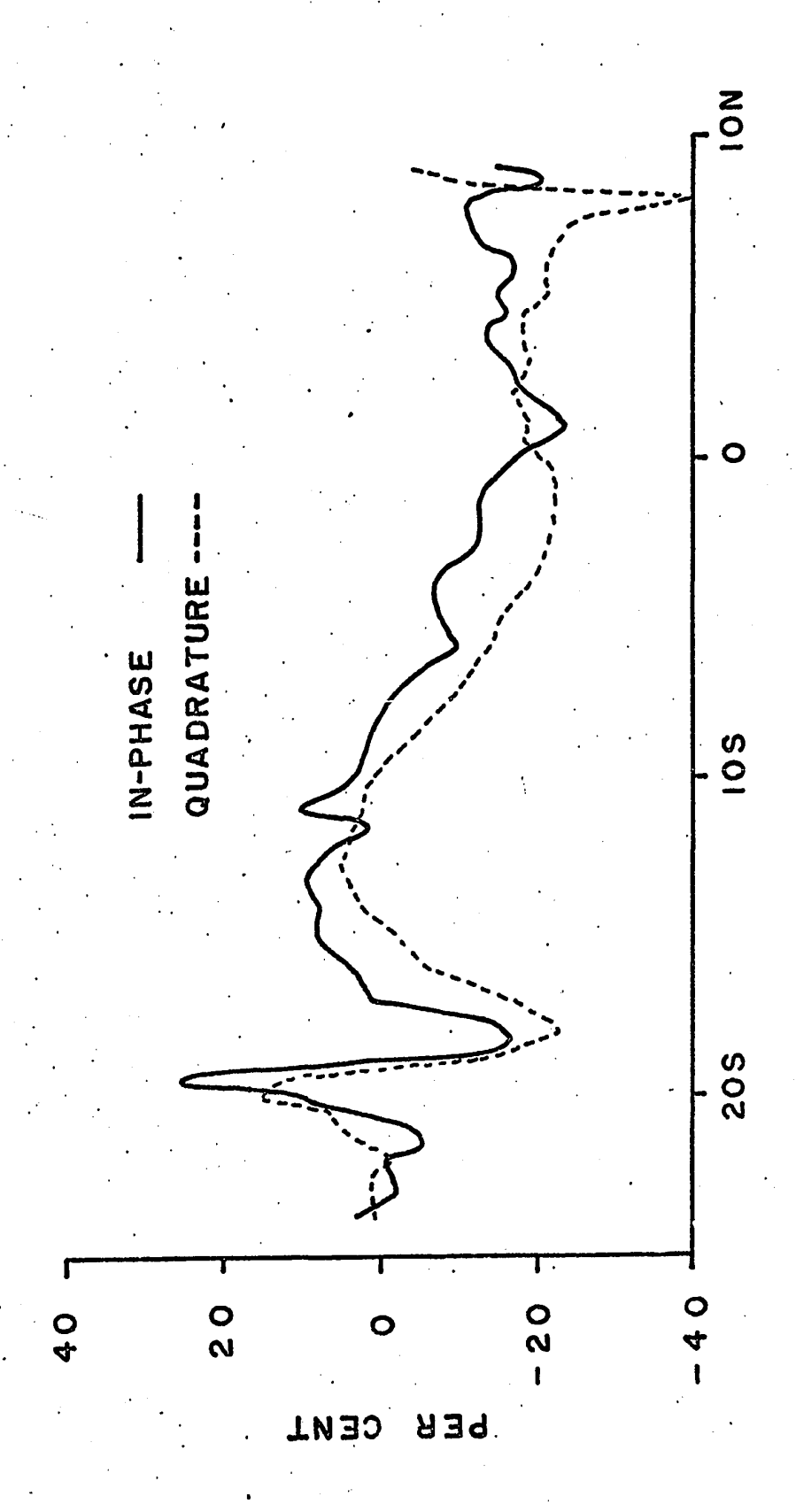


FIG. 6.54 - LINE C-2

()

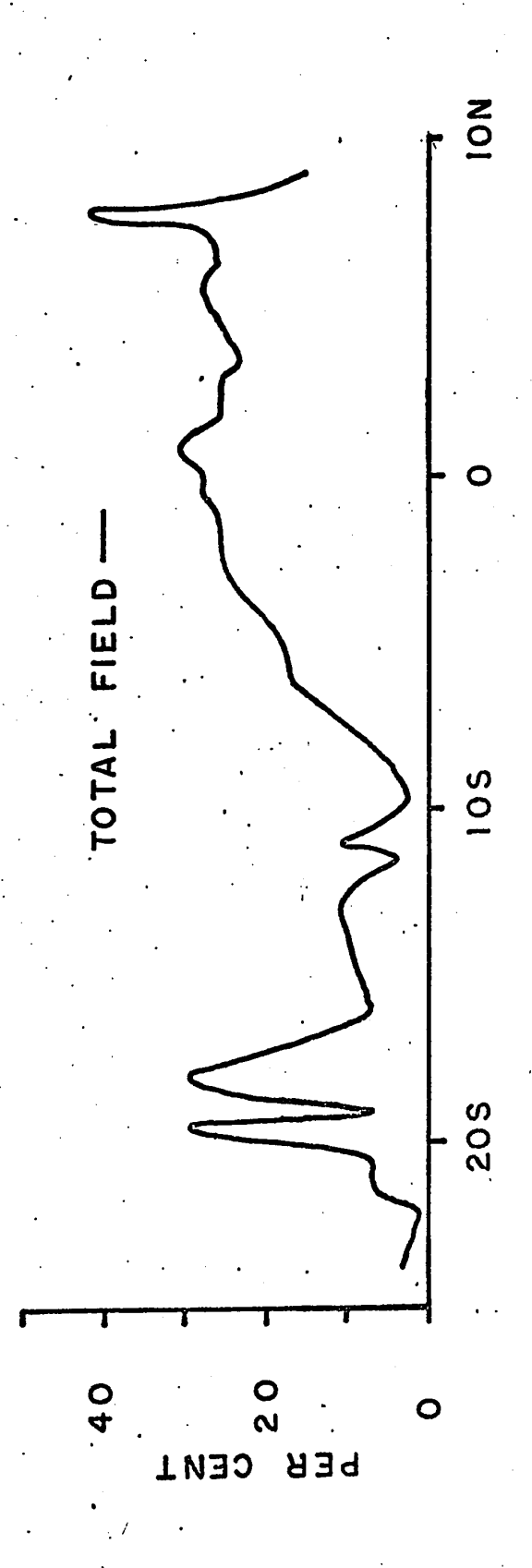
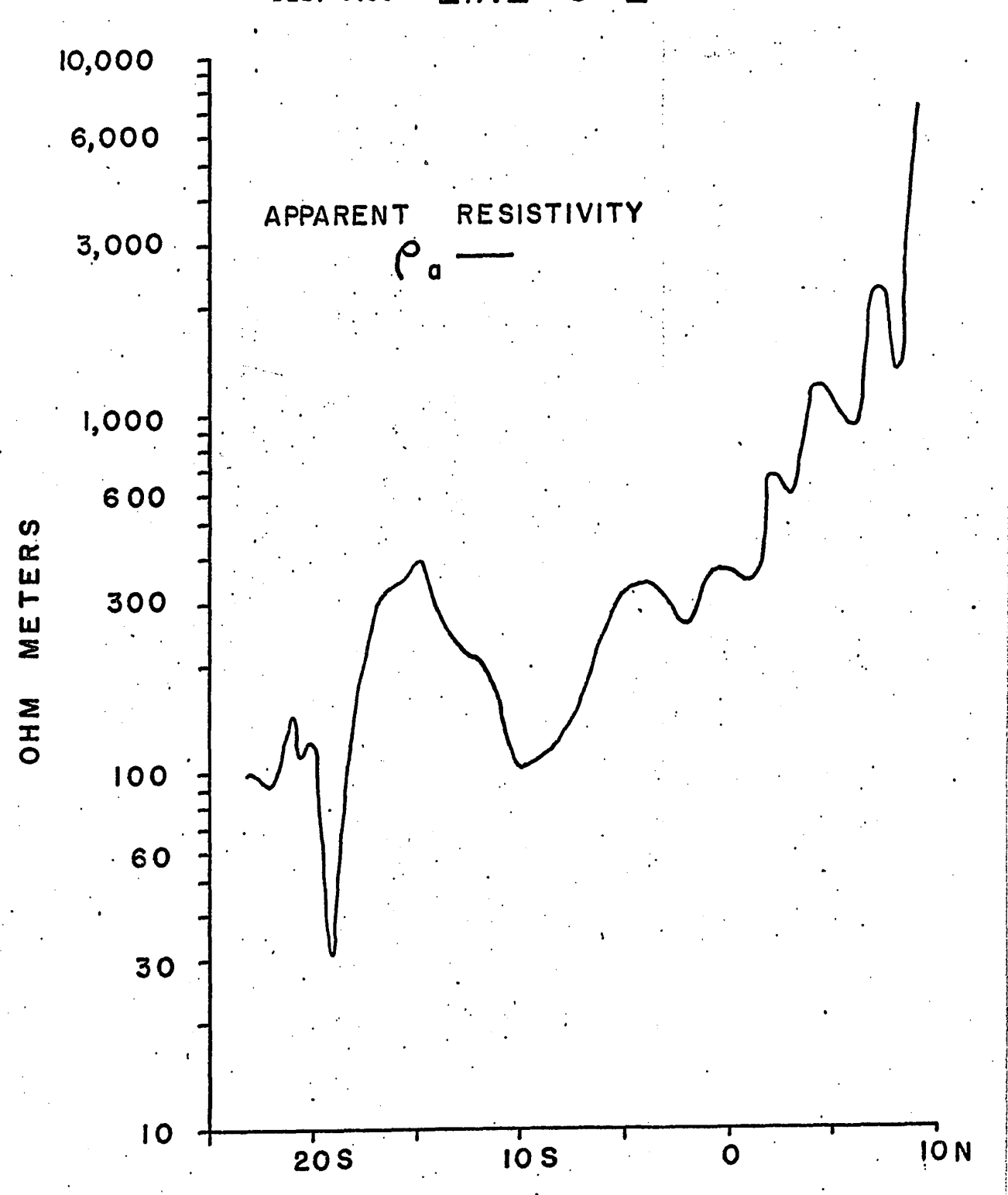


FIG. 6.55 - LINE G-2

FIG. 6.56 -LINE C-2



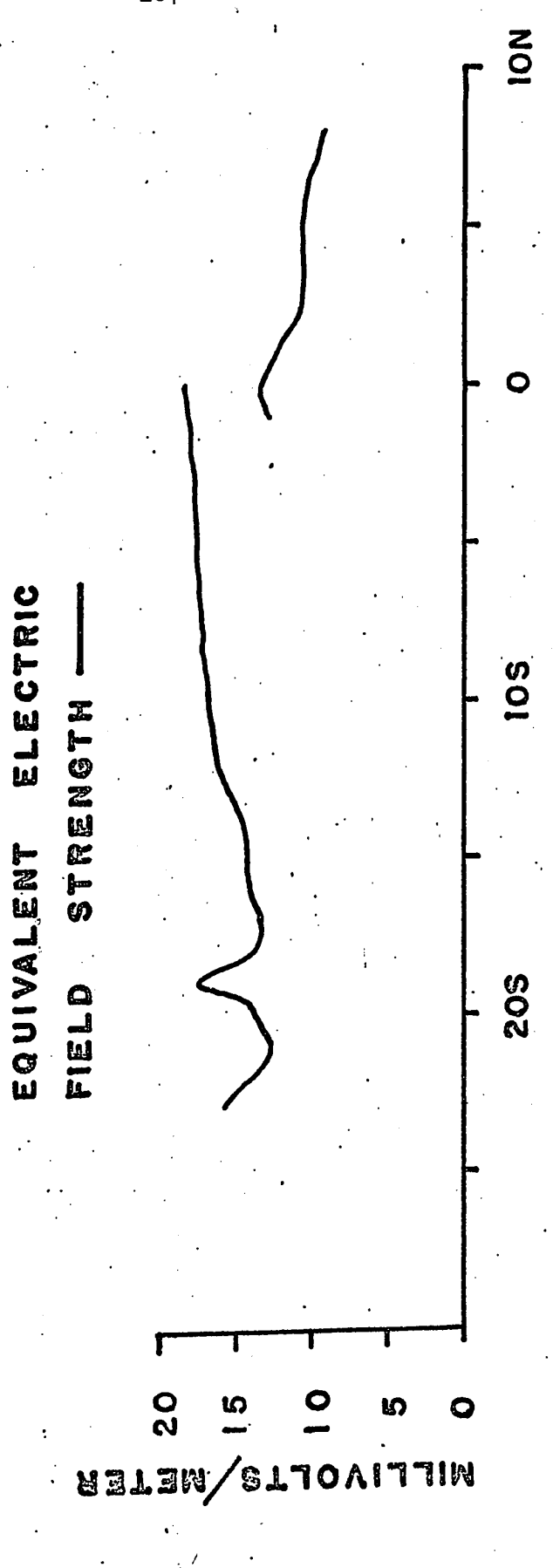
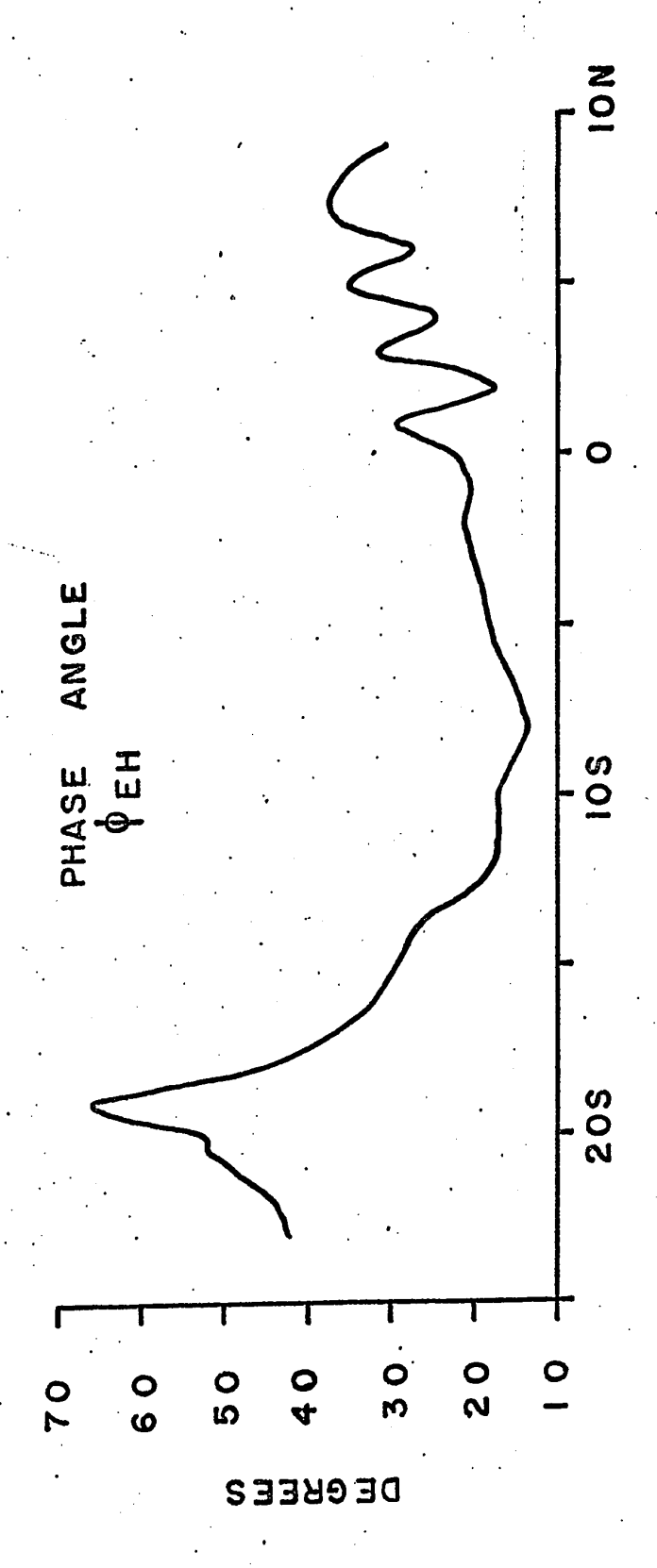


FIG. 6.57 - LINE C-2



LINE C-2

5+00S and 1+00N the apparent resistivity is approximately 300 ohm m. From 2+00N to 9+00N the apparent resistivity increases greatly, although it varies considerably. The contact seems to be between 1+00N and 2+00N, where the apparent resistivity increases from just over 300 ohm m. to almost 700 ohm m. This contact is probably the fault shown on the geological map, since the spatial correlation is excellent. Nevertheless there are no DC resistivity depth sounding curves to determine the overburden thickness, and it is possible that the overburden is much thicker south of the apparent contact. However, since the response occurs almost exactly where the fault is mapped, and different formations occur on either side of the fault, it is improbable that the response is caused by bedrock topography, in this case.

A cross-over type response occurs at 19+00S, indicating a narrow conductor at that point. This is confirmed by wave impedance results. A narrow band of low resistivity occurs at 19+00S. The apparent resistivity decreases rapidly from almost 300 ohm m. at 17+00S to 31 ohm m. at 19+00S. At 18+00S and 20+00S the apparent resistivity is about 100 ohm m. This band of low resistivity, no greater than 100 feet in width, causes the EM-16 cross-over at 19+00S and accounts for the northernmost INPUT anomaly on the profile. It is probably a graphite shear zone, since it has a long strike length according to the INPUT results.

()

(

The creek occurs at 23+75S, and up to this point there is no indication of an anomaly south of the previous one. The southern INPUT anomaly must therefore occur just south of the creek, which could not be crossed.

The horizontal magnetic field strength as shown by the equivalent electric field strength in Fig. 6.57 is considerably higher over the low resistivity zone at 19+00S. The gap in the profile near 0+00 is due to the fact that stations 0+00 to 23+00S and stations 1+00S to 9+00N were read on different days, and the VLF transmitter was operating at a lower power when the latter stations were read. Nevertheless, it can be seen that the magnetic field strength (H_X) between 0+00 and 9+00N is decreasing as the apparent resistivity is increasing.

The phase angle (Ey-Hx) shown in Fig. 6.58 is extremely high over the low resistivity zone at 19+00S. Between 0+00 and 10+00S, the phase angle is generally low, varying from 15 to 25 degrees. It increases to almost 70 degrees at 19+00S and then decreases further south, away from the low resistivity zone. The phase angle, like the apparent resistivity, varies considerably between 0+00 and 9+00N. There appear to be narrow bands of varying resistivity in this part of the traverse (probably associated in some way with the fault), and this accounts for the varying phase angle.

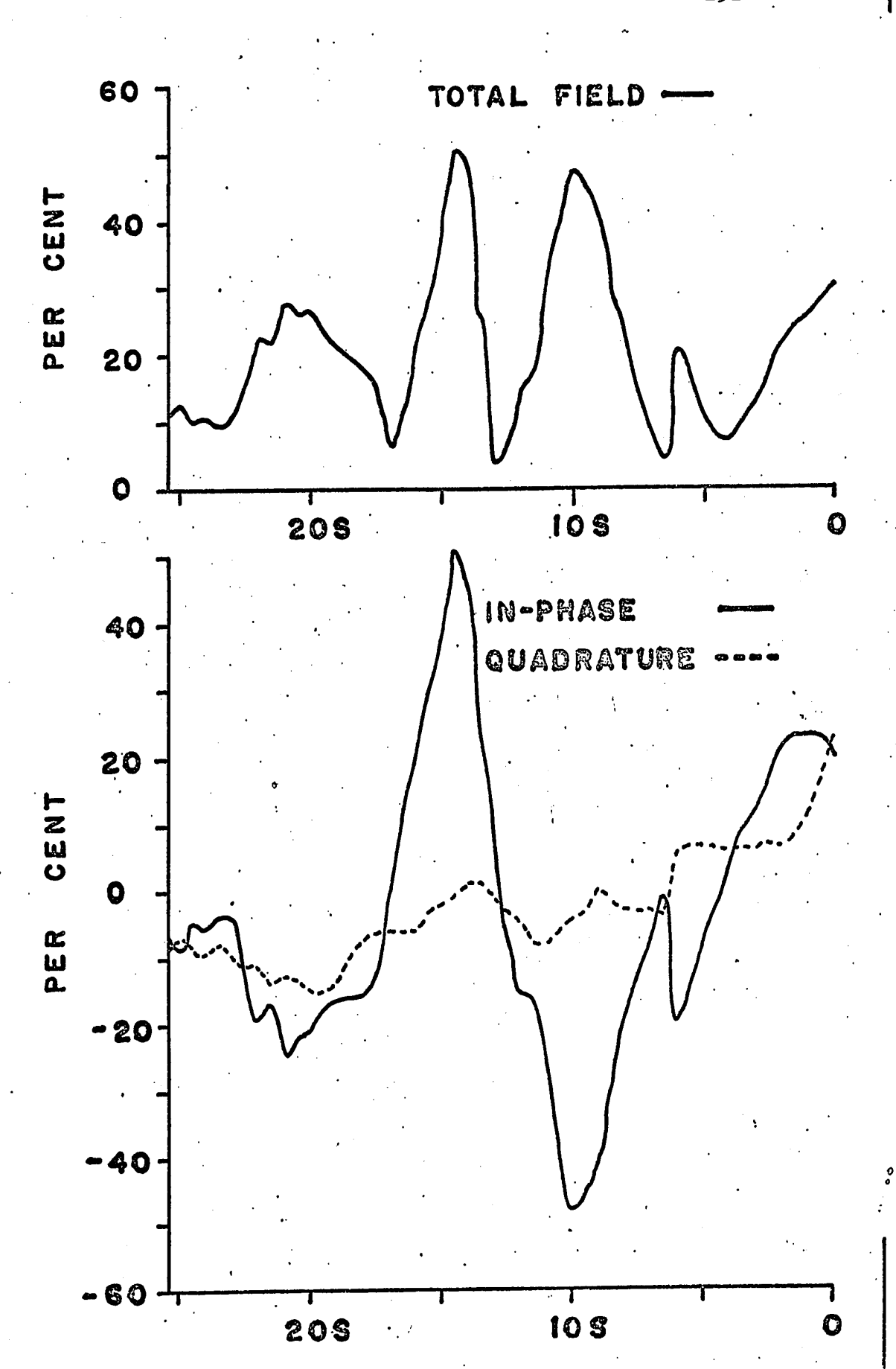
Line C-3

()

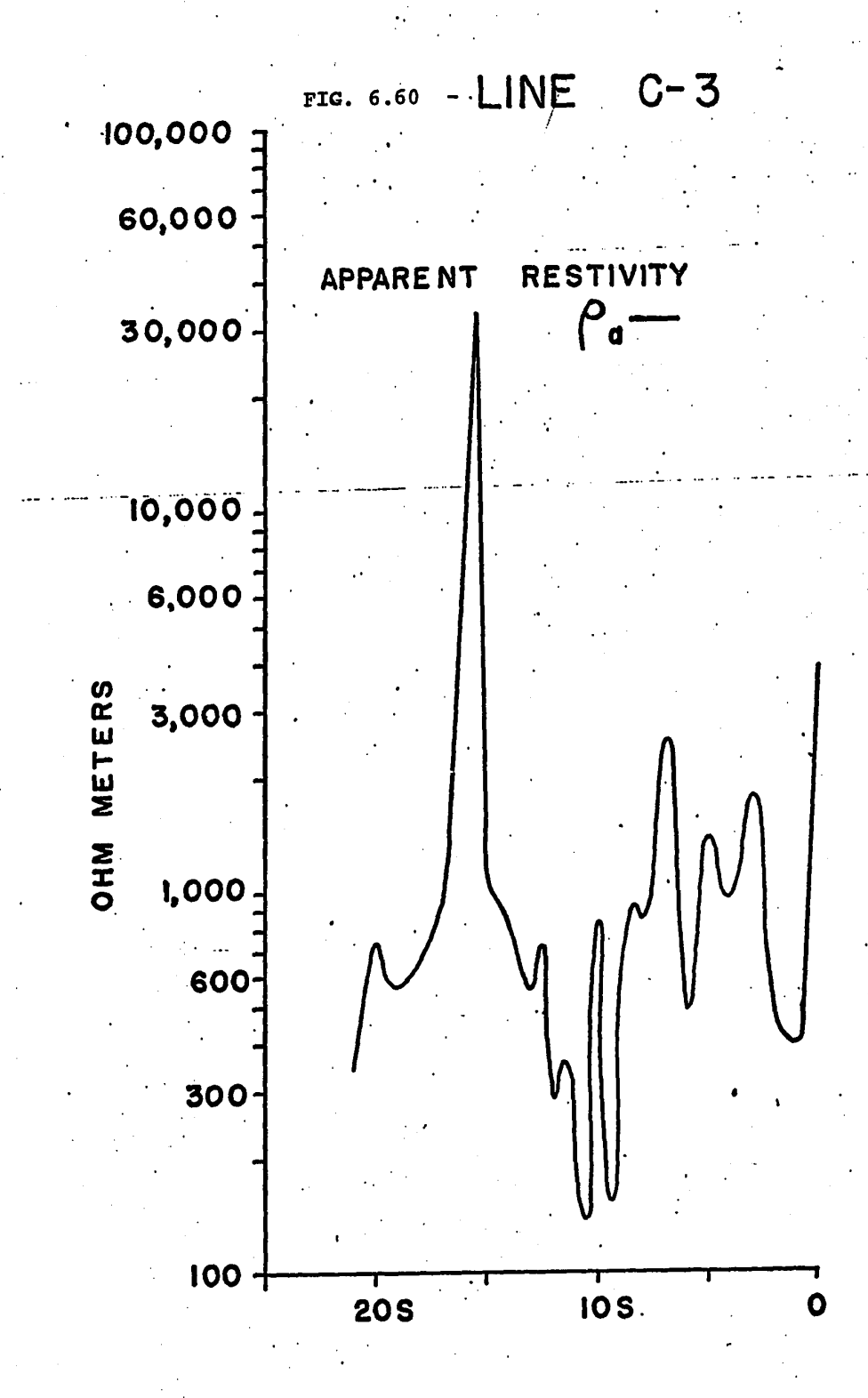
The traverse possibly crosses an east-west fault at about 4+00S (Fig. 5.5). An INPUT anomaly appears at the southern end of the traverse (near the south shore of Lac Deguisier), but apparently is not crossed by the traverse.

A large cross-over type response occurs at 12+75S, and seems to indicate a conductor at that point (Fig. 6.59). How-ever, wave impedance results reveal that the apparent resistivity along the profile varies greatly, and the situation is quite complex (Fig. 6.60).

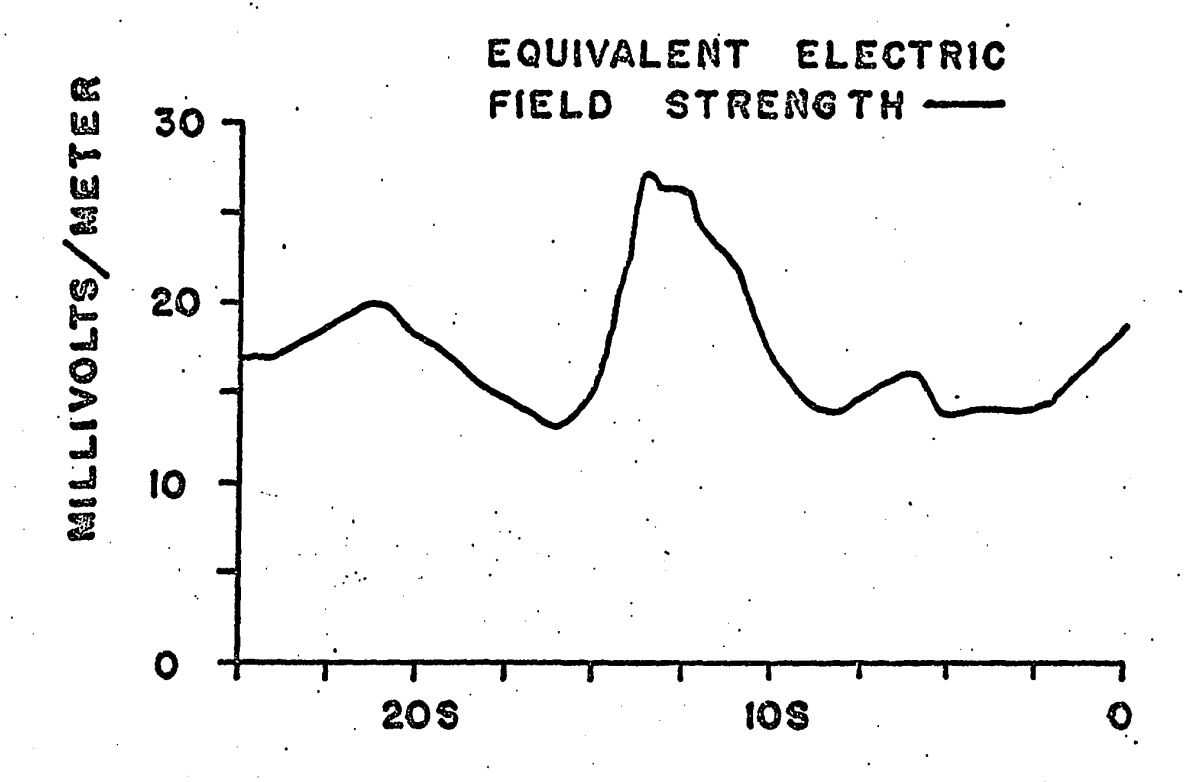
A zone of very high resistivity occurs between 15+00S and 17+00S. As in previous cases, a large, positive in-phase peak occurs at 14+50S (i.e. almost directly over the northern edge of this zone.) Just north of this highly resistive zone, there is a zone of low resistivity, located approximately between 12+00S and 9+00S. There seems to be a narrow band of more resistive material at 10+00S, in the middle of this zone of low resistivity. The negative in-phase peak at 10+00S indicates a contact with the higher resistivity on the north side. There is a contact at about 9+50S between the low resistivity zone (150 to 300 ohm m.) and a zone of higher resistivity to the north (1000 to 2000 ohm m. between 8+50S and 7+00S) and this is probably the source of the negative in-phase peak. It is not known why the apparent resistivity

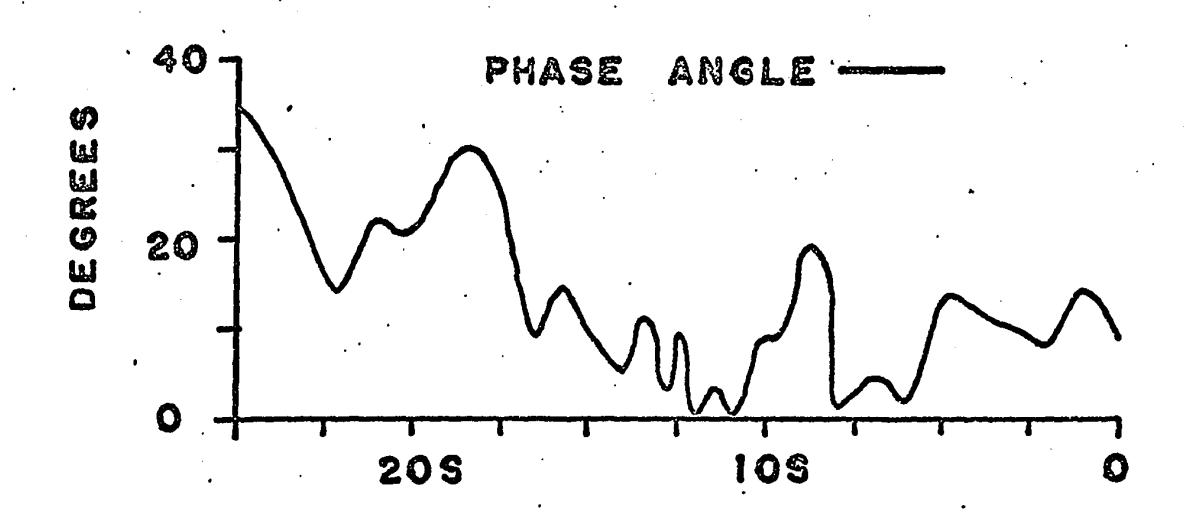


 $(\underline{\ })$



()





varies so erratically along this profile. Extreme (and closely spaced) undulations in the bedrock topography are a possibility.

The horizontal magnetic field strength (Fig. 6.61) varies greatly. As expected, the equivalent electric field strength is high over the zone of low resistivity between 10+00S and 13+00S, and lower over the high resistivity zone between about 15+00S and 18+00S.

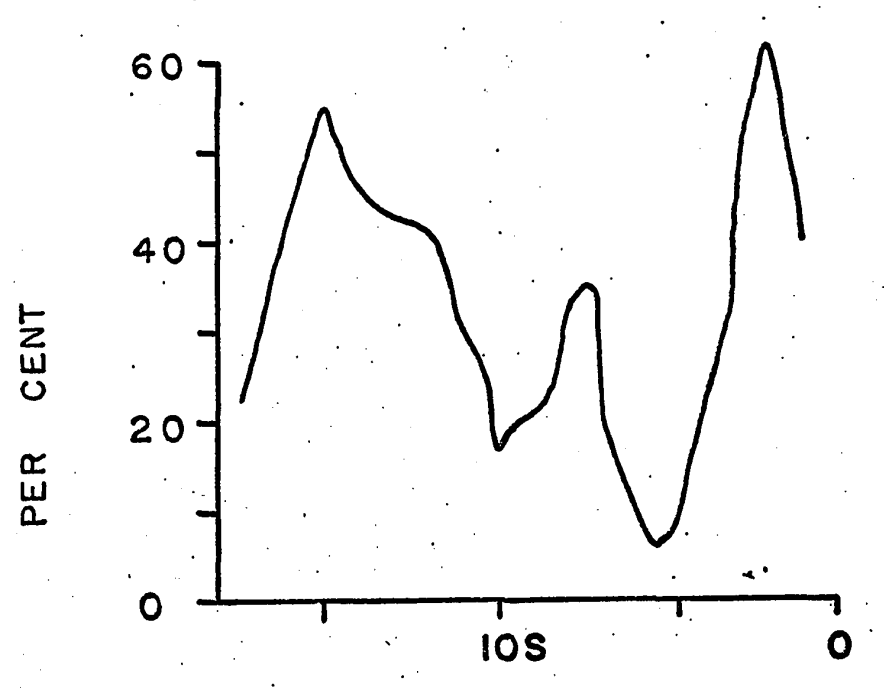
The phase angle (E_y-H_x) also varies greatly, but it is considerably higher over the resistive zone between 15+00S and 20+00S than over the less resistive zone between 10+00S and 13+00S. If anything, this is just the opposite of what would be expected. It definitely seems that the phase angle cannot be relied upon to show any characteristic behaviour in complex areas where there are closely spaced, narrow zones of varying resistivity.

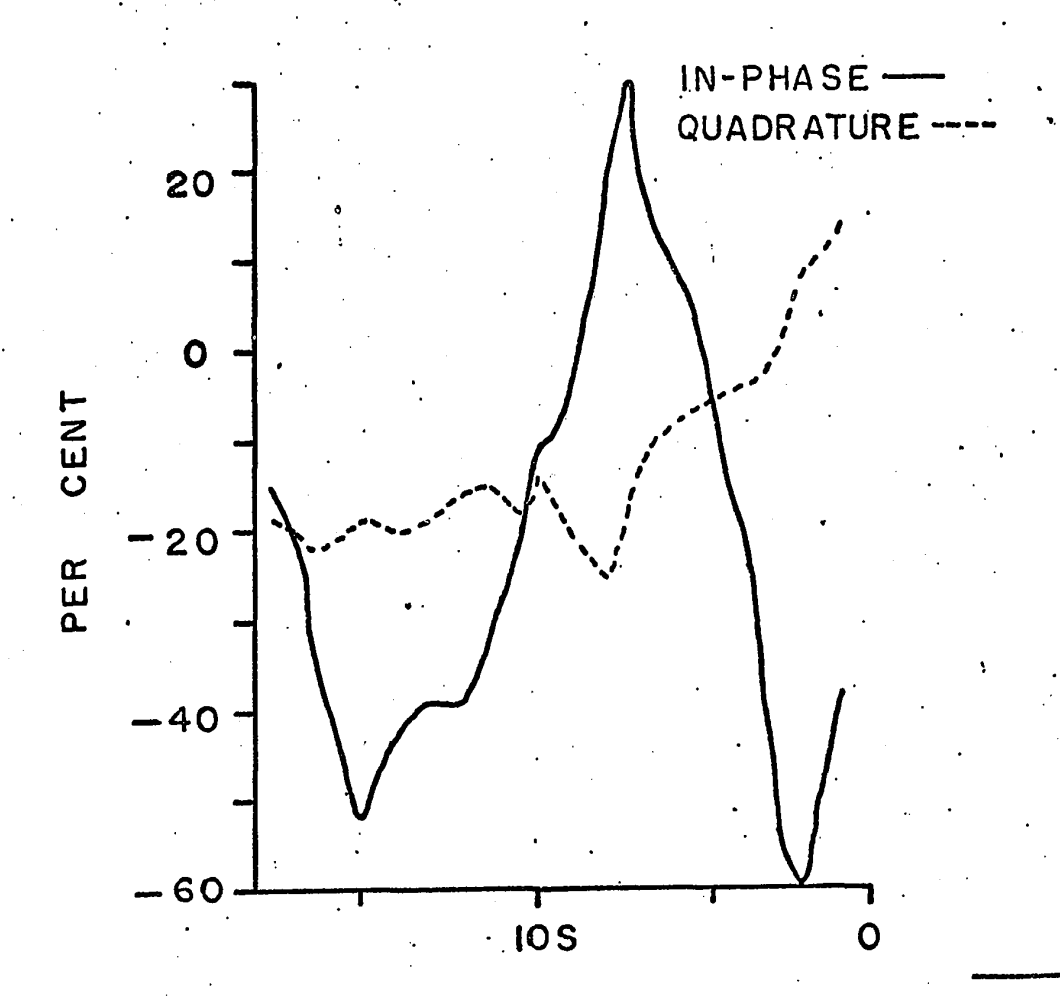
Line C-4

The geological map in Fig. 5.5 shows a fault corresponding to station 10+00S on the profile of Fig. 6-62. Rhyolite occurs on the north side of the fault, while basalt occurs on the south side.

The EM-16 response is difficult to interpret (Fig. 6.62). There is a negative in-phase peak at 14+50S and a positive peak at 7+00S, which seems to indicate a resistive zone somewhere







between those two points. There is another negative in-phase peak at about 2+00S, but a power line at 0+50S influences the in-phase and quadrature readings (making them more positive) approximately as far as station 2+00S, and it is impossible to say exactly where the negative in-phase peak occurs. This seems to indicate a more conductive zone somewhere between 7+00S and 2+00S. (The cross-over occurs at about 5+00S).

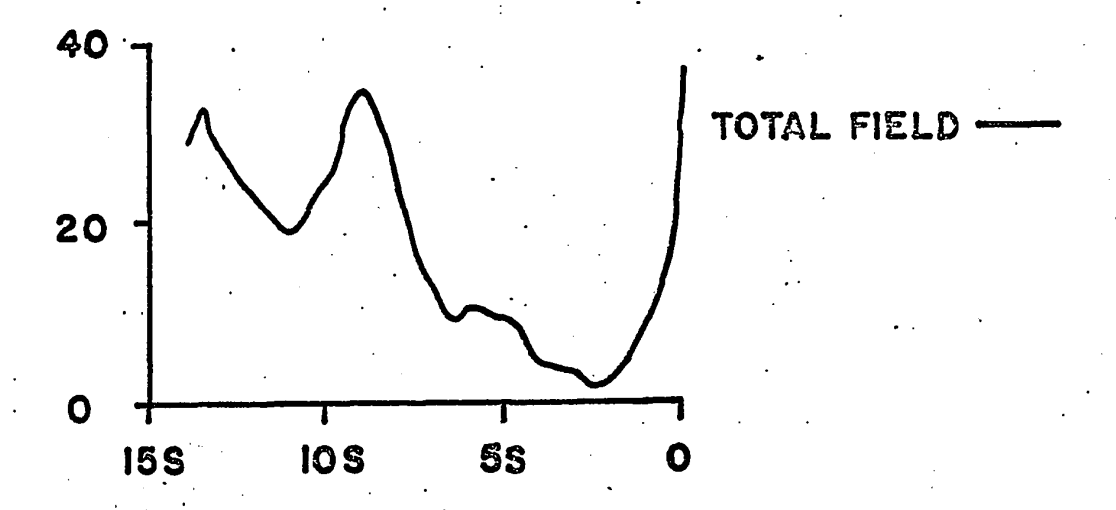
It is difficult to say how these zones are associated with the fault. There are no wave impedance results for this line. It is possible that one of the contacts is the fault shown on the map.

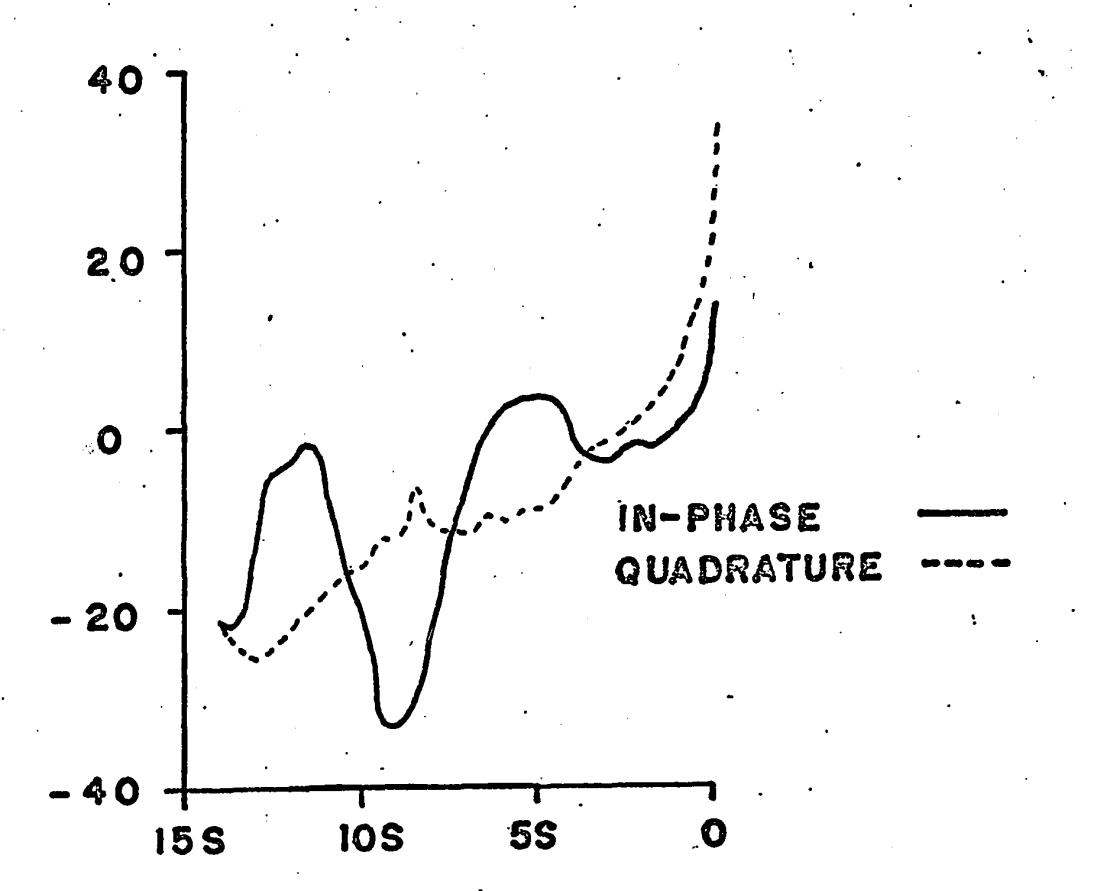
Line C-5

 $(\tilde{})$

The geological map shows a contact between rhyolite and basalt located approximately at 7+00S on the traverse (Fig. 5.5). A fault occurring in the basalt is shown south of the contact at about 10+00S.

A power line at 0+80N distorts the in-phase component until about station 1+00S, and the quadrature as far as about 4+00S (Fig. 6.63). (The readings become positive as the power line is approached). However, a good contact type response occurs at about 8+50S or 9+00S. This is a negative in-phase peak accompanied by a local quadrature maximum, indicating a contact with the higher resistivity to the north. This—response is possibly due to the contact shown on the map



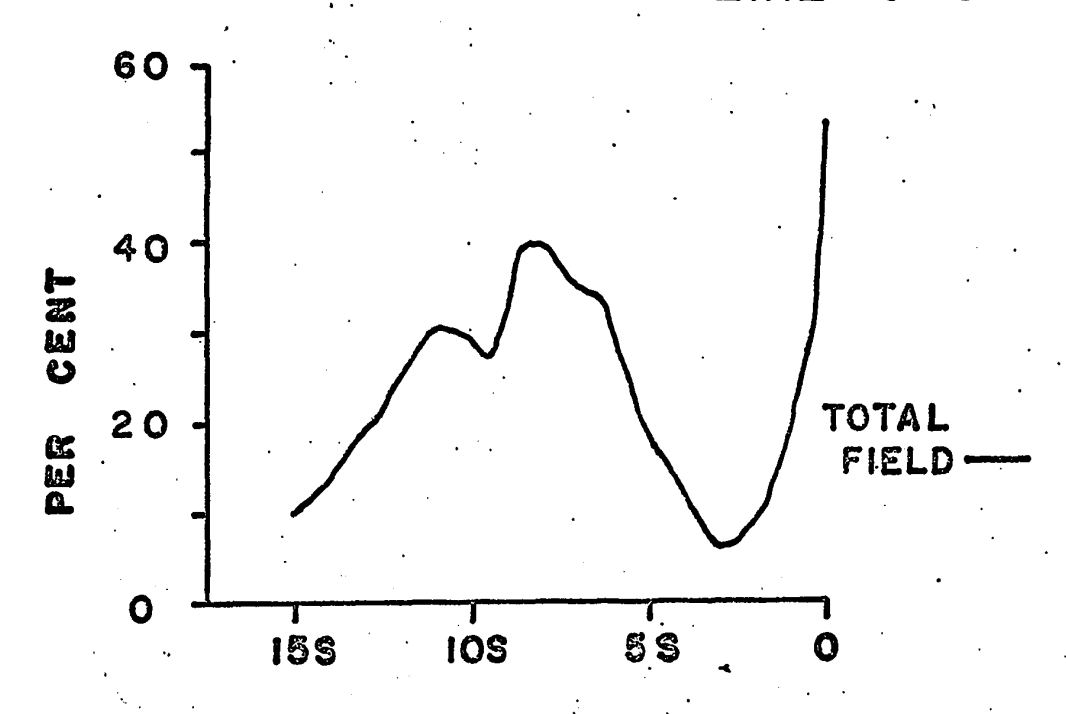


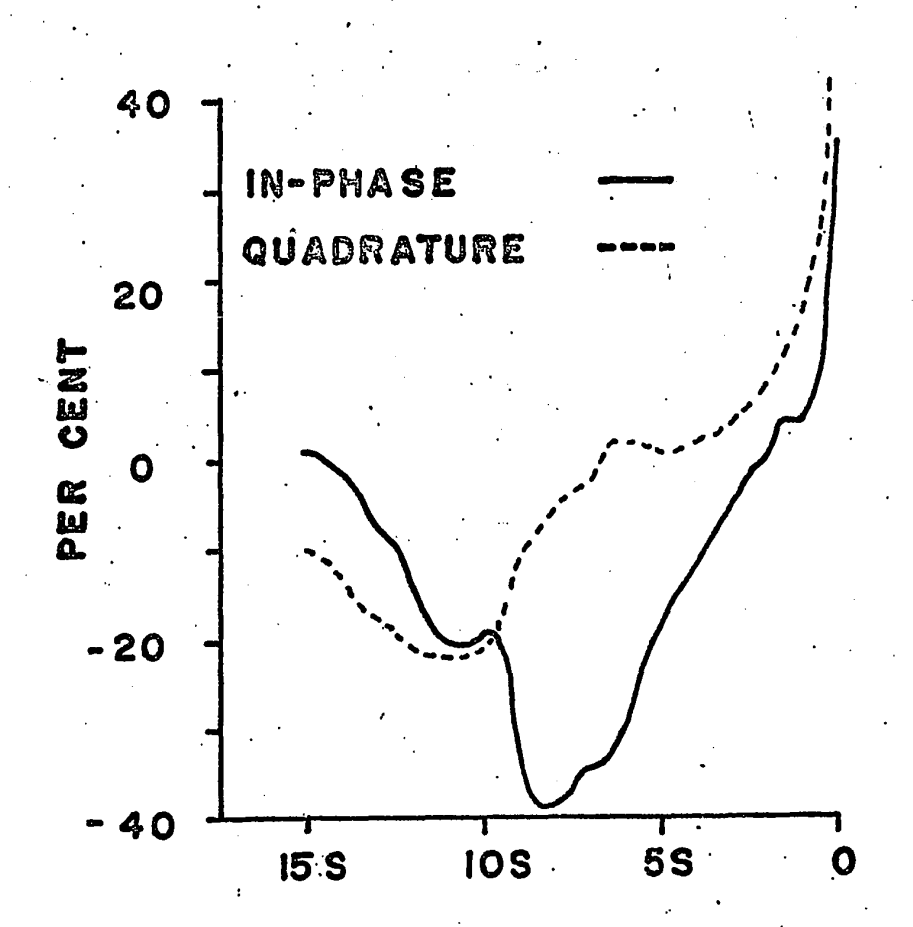
(between rhyolite and basalt), or may be associated with the fault shown south of the contact. The fault is accompanied by a slight rise in the topography and is easily identified when mapping. Unfortunately, the relationship (if any) between the fault shown in the basalt and the rhyolite-basalt contact is not known.

Line C-6

The geological map in Fig. 5.5 shows a contact between rhyolite and basalt at about 2+50S on the traverse. A fault is shown occurring in the basalt at about 8+00S.

Once again the in-phase and quadrature components become highly positive at the north end of the profile because of a power line at 0+80N (Fig. 6.64). There seems to be a contact type response at about 8+00S. The in-phase component is a negative peak, while the quadrature seems to be a maximum in the vicinity of this negative peak, but is unfortunately distorted by the power line from about 5+00S to 0+00. The response coincides with the location of the fault shown on the map, and indicates higher resistivity on the north side of the fault. This response somewhat resembles that of Line C-5, and seems to indicate that the response on that line is due to the fault shown on the map. Line C-5 and Line C-6 do not extend far enough to the south to give a clear picture of what is really happening here.





(ii) Discussion of Results

The Noranda area is situated in the Canadian Precambrian shield, and the geology of the area is vastly different from that of the St. Lawrence Basin, where the basement is covered by hundreds of feet of flat-lying Paleozoic sediments. In the Noranda area, the metamorphosed igneous rocks of the basement are covered by a maximum of several tens of feet of overburden (generally glacial drift), and they often outcrop. Thus bedrock is close to surface, and it apparently exhibits rugged topography. This greatly affects VLF responses in the area.

all the EM-16 responses in the Smoky Creek area are caused by bedrock topography. The overburden is generally from 30 to 50 feet thick, and has a resistivity of about 40 ohm meters. However, the bedrock surface is very hilly. The hills are a few hundred feet wide and apparently have very steep flanks. This results in an abrupt (and often very large) increase in apparent resistivity over these hills, which come to within several feet of the surface. These hills are apparently unrelated to the Smoky Creek fault, since there are at least two such hills on Lines A-2 and A-1, neither of which correlate with the location of the fault. One of these hills in the bedrock outcrops on Line A-4, but at least 4000 feet south of the fault. Only the abrupt change in bedrock topography on

 $(\bar{})$

Line A-1 may possibly be related to the Smoky Creek fault.

For these reasons, the attempts to locate the Smoky Creek fault by means of VLF measurements may be regarded as unsuccessful.

In the Lois Lake area, one of the INPUT anomalies on Line C-l is due to a zone of high apparent resistivity abou-300 feet wide (possibly another hill in the bedrock, while no response was obtained over the southernmost INPUT anomaly on this line. There is a relatively good response over the Lois Lake fault on Line C-2, while a graphite shear zone is the cause of the INPUT anomaly about 1800 feet south of the fault. The apparent resistivity on Line C-3 varies so much (possibly due to rugged bedrock topography) that it is impossible to determine the location of the fault by either the EM-16 or The EM-16 profile on Line C-4 shows wave impedance profiles. three contacts, but it is not possible to say if any of them are caused by the fault. However, the EM-16 profiles on Line C-5 and C-6 show a single contact type response, probably due to the fault, but possibly due to a basalt-andesite contact.

CHAPTER VII

CONCLUSIONS

The field results in many cases agree very well with the theoretical results of Section 3.2. The theoretical profiles show the type of EM-16 response to be expected over a vertical fault, and this type of anomaly is observed over the Gloucester fault. In fact, in all three of the areas investigated, distinct contact type responses are observed over nearly all abrupt changes in apparent resistivity. vertical secondary field components (in-phase and quadrature) behave as predicted over such changes. The wave impedance data show that the horizontal magnetic field strength is lower over areas of relatively high apparent resistivity, in agreement with the theoretical results. The phase angle (between E_v and H_x) seems to vary considerably along any given profile. This is probably because there are several zones of different apparent resistivity on most of the traverses investigated with the wave impedance apparatus. Nevertheless, the phase angle is generally lower over zones of relatively high apparent resistivity than it is over zones of low resistivity. This behaviour is essentially correct from a theoretical viewpoint.

The field results definitely confirm that the VLF method is a useful technique to supplement geological mapping

in areas covered by overburden. In all cases where there are both EM-16 and wave impedance data available on a given profile, the EM-16 responses correlate with changes in the apparent resistivity. All resistive and conductive zones indicated by the EM-16 are verified by the apparent resistivity profiles.

In areas where the geology is relatively uncomplicated (such as sedimentary basins, like the St. Lawrence), it is relatively easy to map structural features such as faults and shears, provided that there is a sufficient resistivity contrast across these features. In such regions it is possible to map the features using only EM-16. All interpretation of the EM-16 profiles should be done by examining both the inphase and quadrature responses. Calculating the total vertical secondary field ((IN-PHASE)2 + (QUADRATURE)2) simplifies the results for graphical presentation, but interpretation should not, in general, be based upon the total field profile.

The main disadvantage of mapping with the EM-16 alone is that little quantitative information, other than which side of the contact exhibits a higher resistivity, can be obtained. This is true, however, of most EM induction methods. For this reason it is occasionally desirable to supplement the EM-16 data with wave impedance profiles to obtain information on apparent resistivity, phase angle, and primary magnetic field

strength. Since wave impedance data take much longer to obtain than EM-16 data, it is desirable to keep wave impedance traverses to a minimum if the survey is to be conducted as rapidly as possible.

()

()

EM-16 results are more difficult to interpret in areas where the bedrock exhibits rugged topography. High spots in the bedrock (thin overburden) and low spots in the bedrock (thick overburden) will appear as zones of higher and lower apparent resistivity, respectively. Using only EM-16 and wave impedance data, it is impossible to determine whether or not these zones are, in fact, due to bedrock topography, or whether they are due to a change in lithology. In these cases it is necessary to obtain DC resistivity depth sounding curves to determine the thickness of the overburden. This is a major disadvantage to the VLF method, since one of the features of the EM-16 is the speed with which a survey can be conducted. Clearly if the VLF data must be supplemented with DC resistivity data, the speed of the survey is greatly reduced.

Finally, if one is contemplating use of the EM-16, a little prior knowledge of the nature of the overburden would be very helpful. The theoretical curves of Figure 3.12 will prove extremely useful if the approximate resistivity and thickness of the overburden are known.

BIBLIOGRAPHY

- Andrieux, P., Applications of the DC electrical resistivity method in the Ottawa area, in preparation, 1971.
- Becker, A., Radio-wave mapping of ground conductivity anomalies, Geological Survey of Canada Paper 67-1, Part A, p. 130, 1967.
- Becker, A., personal communication, 1970.

()

- Collett, L.S., Resistivity mapping by electromagnetic methods, in Mining and Groundwater Geophysics, edited by L.W. Morley, p. 615, Department of Energy, Mines and Resources, Ottawa, Canada, 1967.
- d'Erceville, I., and G. Kunetz, The effect of a fault on the earth's natural electromagnetic field, Geophysics, 27, p. 651, 1962.
- Frischknecht, F.C., Application of electromagnetic surveying to geologic mapping in northern Maine, in Mining Geophysics, Volume I, edited by the SEG Mining Geophysics Volume Editorial Committee, p. 10, Society of Exploration Geophysicists, Tulsa, Oklahoma, 1966.
- Frischknecht, F.C., and E.B. Ekren, Mapping conductive strata by electromagnetic methods, United States Geological Survey Professional Paper 400-B, p. Bl21, 1960.
- Geonics Limited, "EM-16 Operating Manual", 27 pp., 2 Thornecliffe Park Drive, Toronto 17, Ontario.
- Grant, F.S., and G.F. West, Interpretation Theory in Applied Geophysics, 584 pp., McGraw-Hill, New York etc., 1965.
- Heiland, C.A., Geophysical Exploration, 1013 pp., Prentice-Hall, New York, 1946.
- Keller, G.V., and F.C. Frischknecht, Electrical Methods in Geophysical Prospecting, 517 pp., Pergamon Press, Oxford etc., 1966.

- Madden, T.R., and C.M. Swift, Magnetotelluric studies of the electrical conductivity structure of the crust and upper mantle, in The Earth's Crust and Upper Mantle, Geophysical Monograph 13, edited by P.J. Hart, p. 469, American Geophysical Union, Washington, D.C., 1969.
- Paterson, N.R., and V. Ronka, Five years of surveying with the VLF-E.M. method, paper presented at the 1969 Annual International Meeting of the Society of Exploration Geophsicists, Calgary, Alberta, 1969.
- Shaw, W.W., Regional AFMAG fields and their effects, Ontario-Quebec, paper presented at the 1961 Annual International Meeting of the Society of Exploration Geophysicists, November, 1961.
- Shaw, W.W., The use of airborne AFMAG to map shears and faults, paper presented at AIME meeting, New York, February, 1962.
- Slankis, J.A., personal communication, 1969.

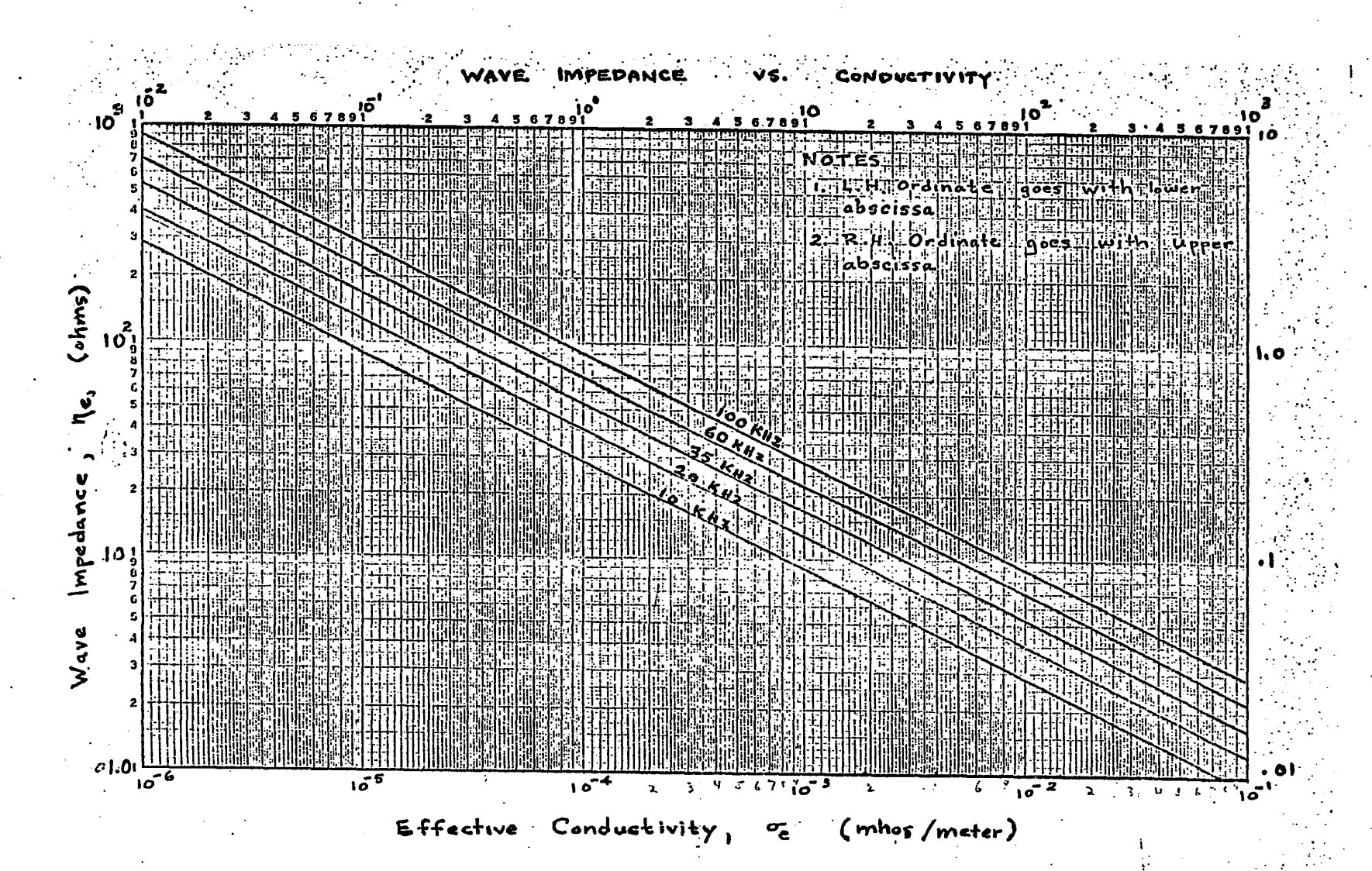
()

()

- Slankis, J.A., Telluric and magnetotelluric studies at 8 Hz, Ph.D. thesis, McGill University, Montreal, July, 1970.
- Strangway, D.S., and K. Vozoff, Mining exploration with natural electromagnetic fields, in Mining and Ground-water Geophysics, edited by L.W. Morley, p. 109, Department of Energy, Mines and Resources, Ottawa, Canada, 1967.
- Sutherland, D.B., AFMAG for electromagnetic mapping, in Mining and Groundwater Geophysics, edited by L.W. Morley, p. 228, Department of Energy, Mines and Resources, Ottawa, Canada, 1967.
- Swift, C.M., A magnetotelluric investigation of an electrical conductivity anomaly in the southwestern United States, Ph.D. thesis, Massachusetts Institute of Technology, Cambridge, Massachusetts, 1967.
- Wilson, A.E., Geology of the Ottawa-St. Lawrence Lowland, Ontario and Quebec, Geological Survey of Canada Memoir 241, 65 pp., 1946.

Appendix I

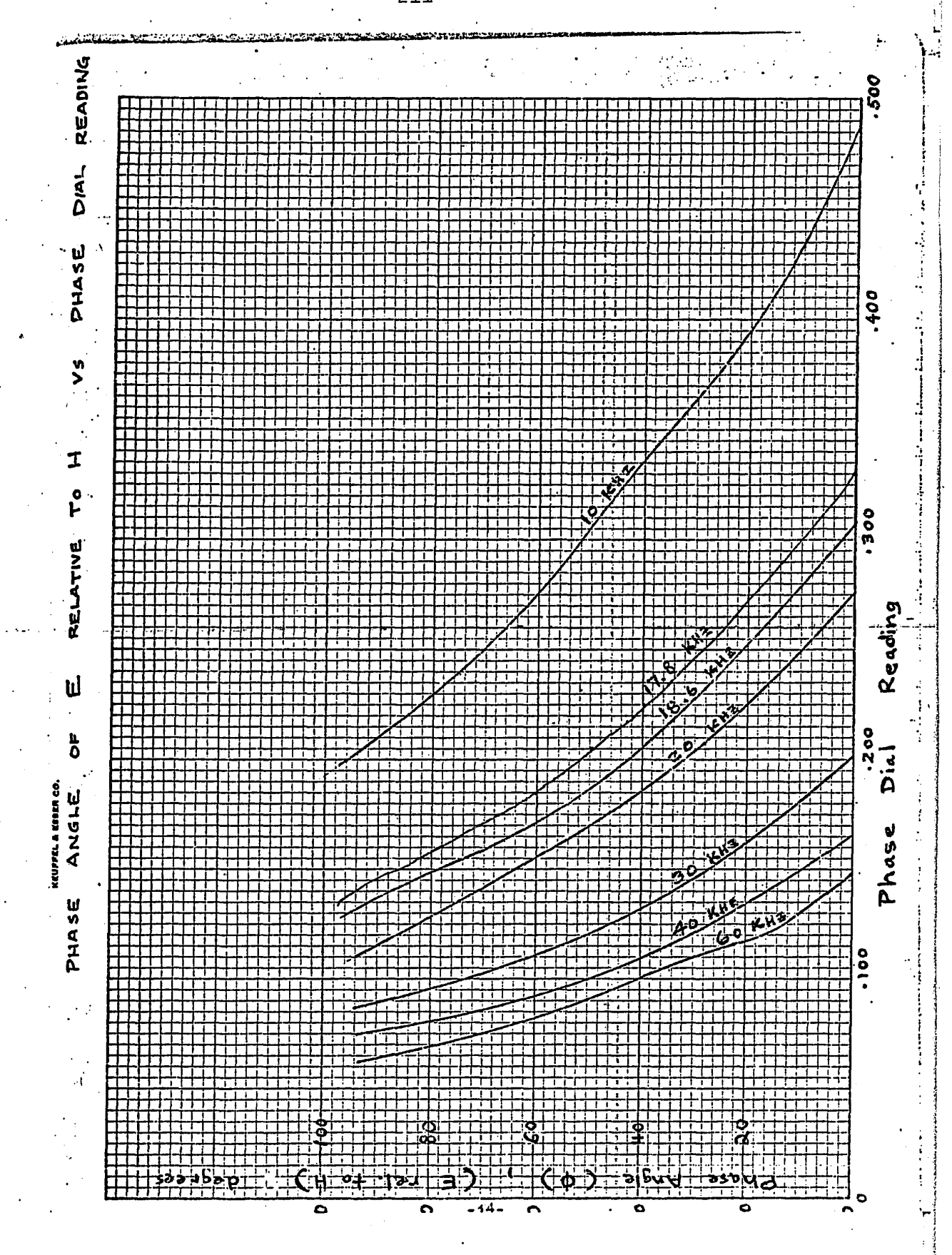
Conversion of Wave Impedance Dial Reading (in ohms) to Apparent Conductivity (in mhos/meter).



()

Appendix II

Conversion of Phase Dial Reading to Phase Angle Between Ey and Hx.



Appendix III

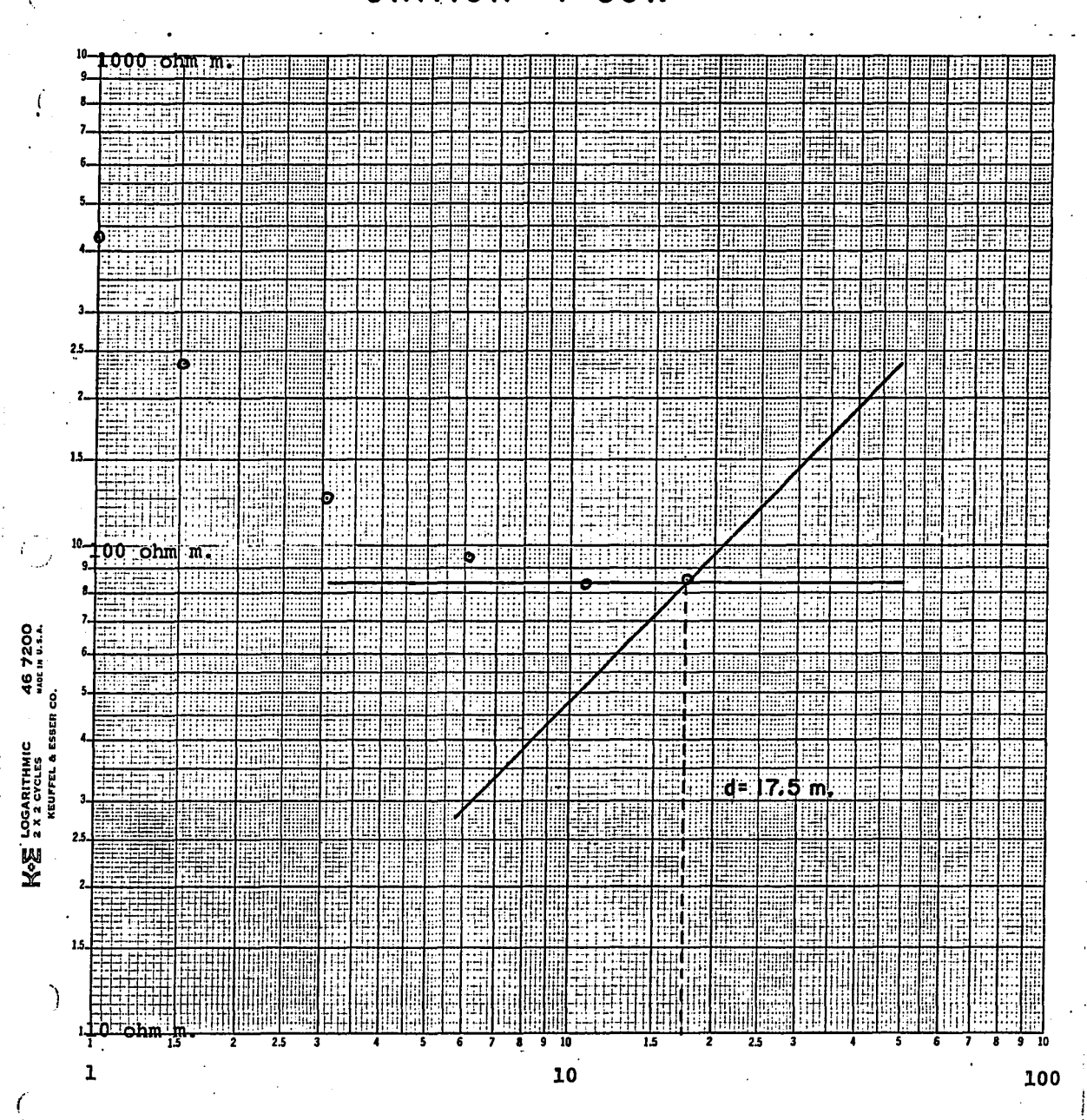
DC Resistivity Depth Sounding Profiles for the Smoky Creek Area (Wenner Array).

Line	A-3	Station Station	13+50N
Line	A-2	Station Station Station Station	15+00N 20+00N 27+00N

(

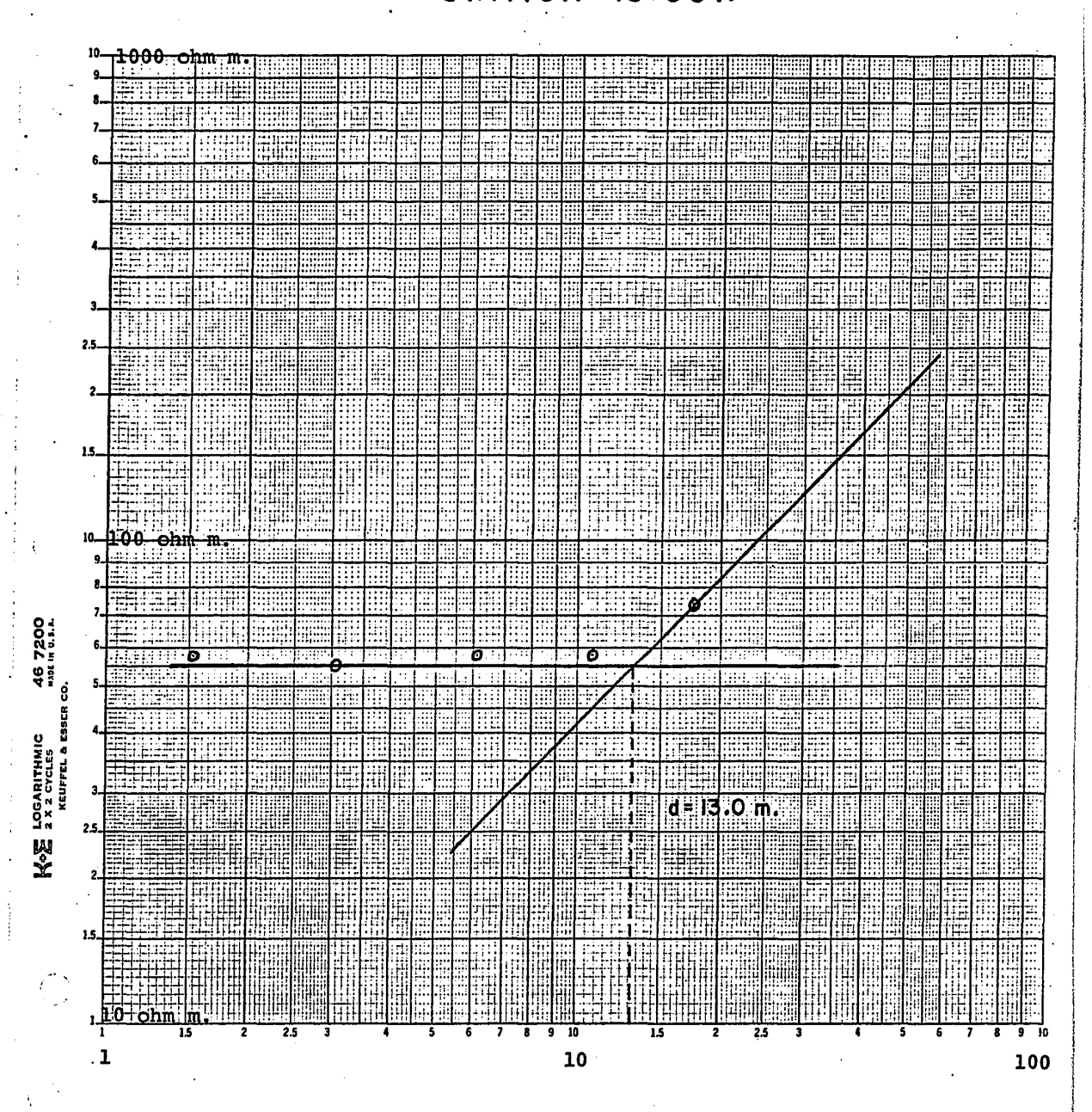
()

LINE A-3
STATION 7+50N



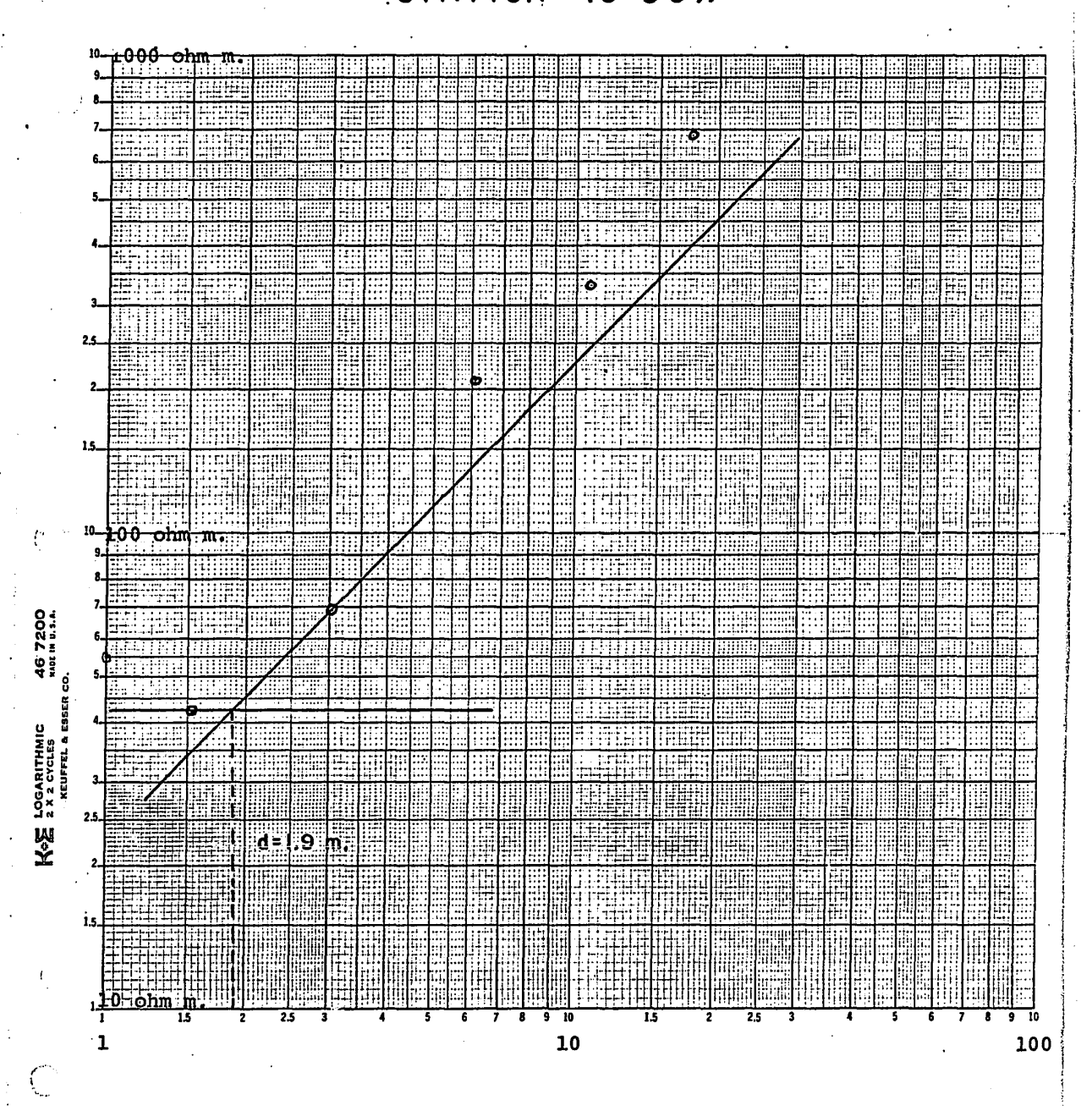
Electrode Spacing in Metres

LINE A-3 STATION 13+50N



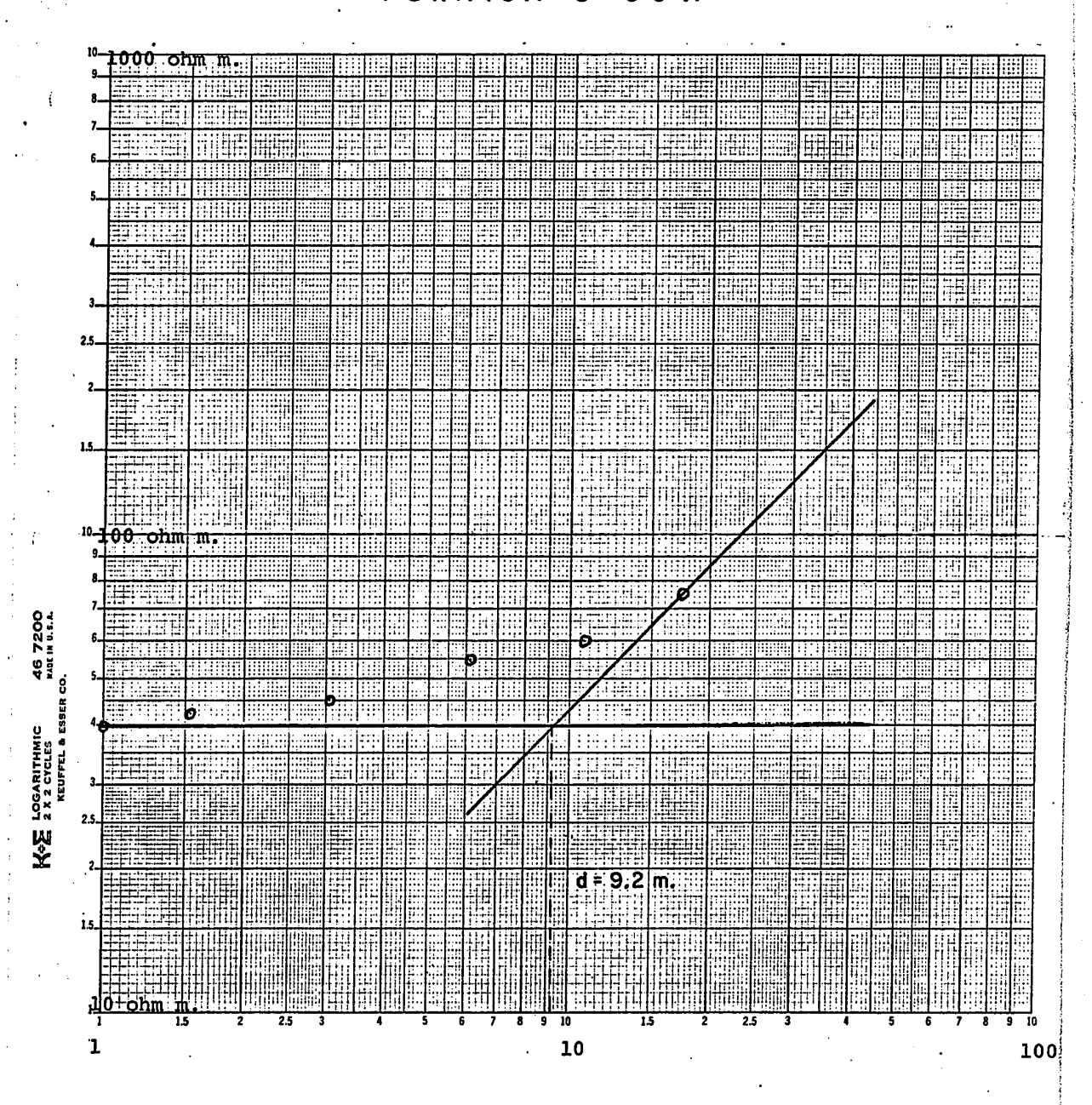
Electrode Spacing in Metres

LINE A-3 STATION 16+50N



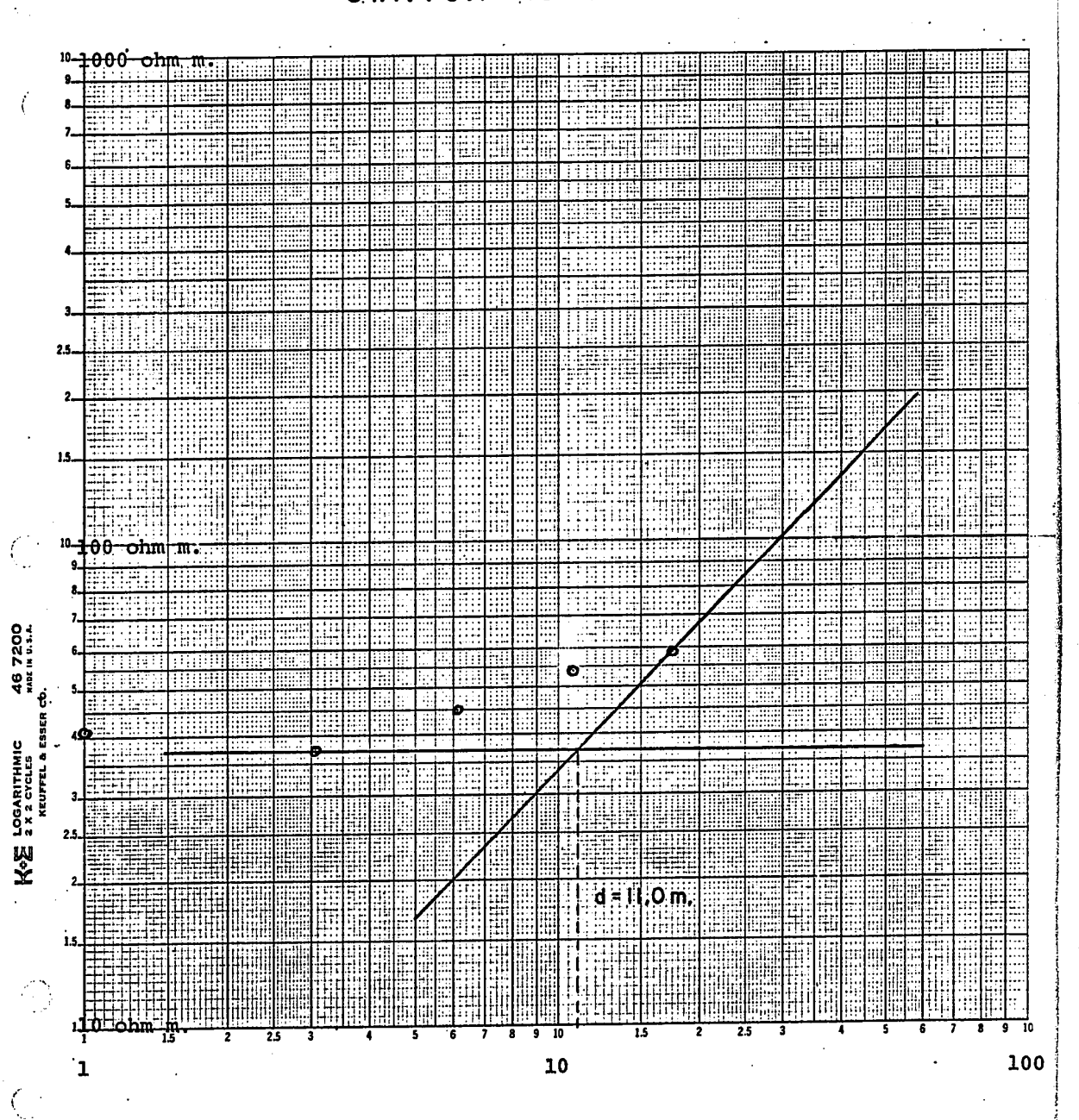
Electrode Spacing in Metres

LINE A-2 STATION 5+00 N



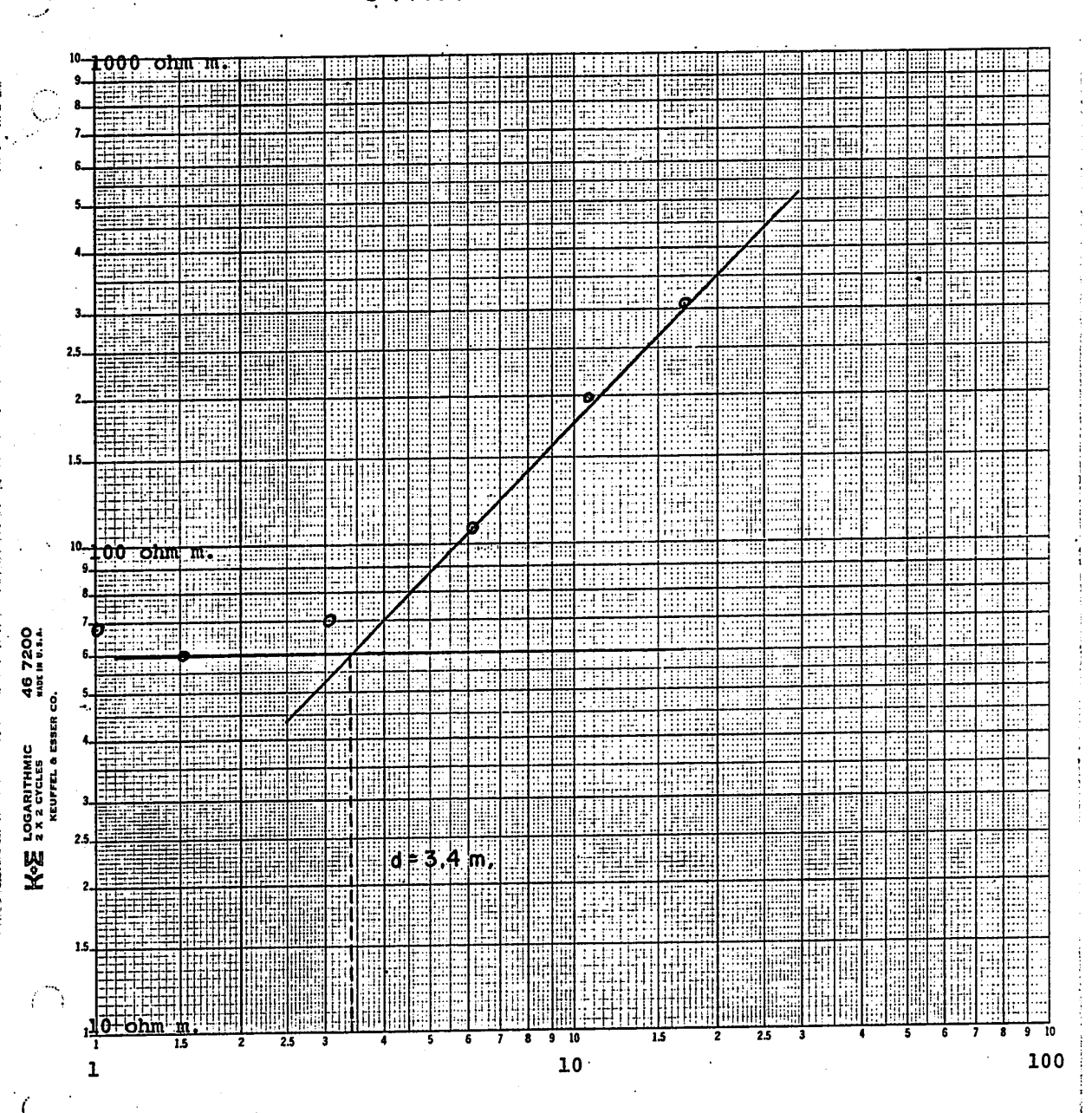
Electrode Spacing in Metres

LINE A-2 STATION 15+00N



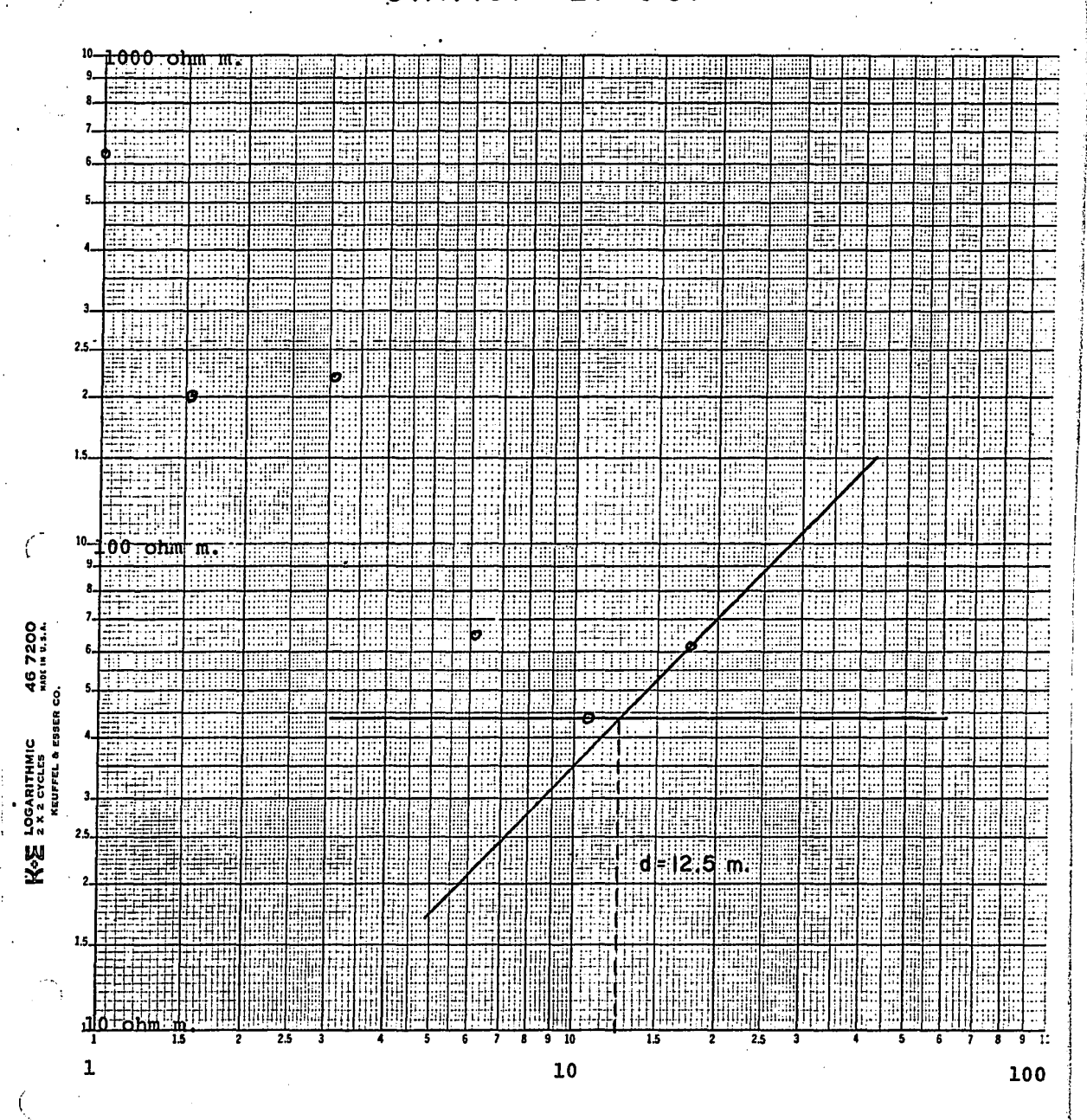
Electrode Spacing in Metres

LINE A-2 STATION 20+00 N



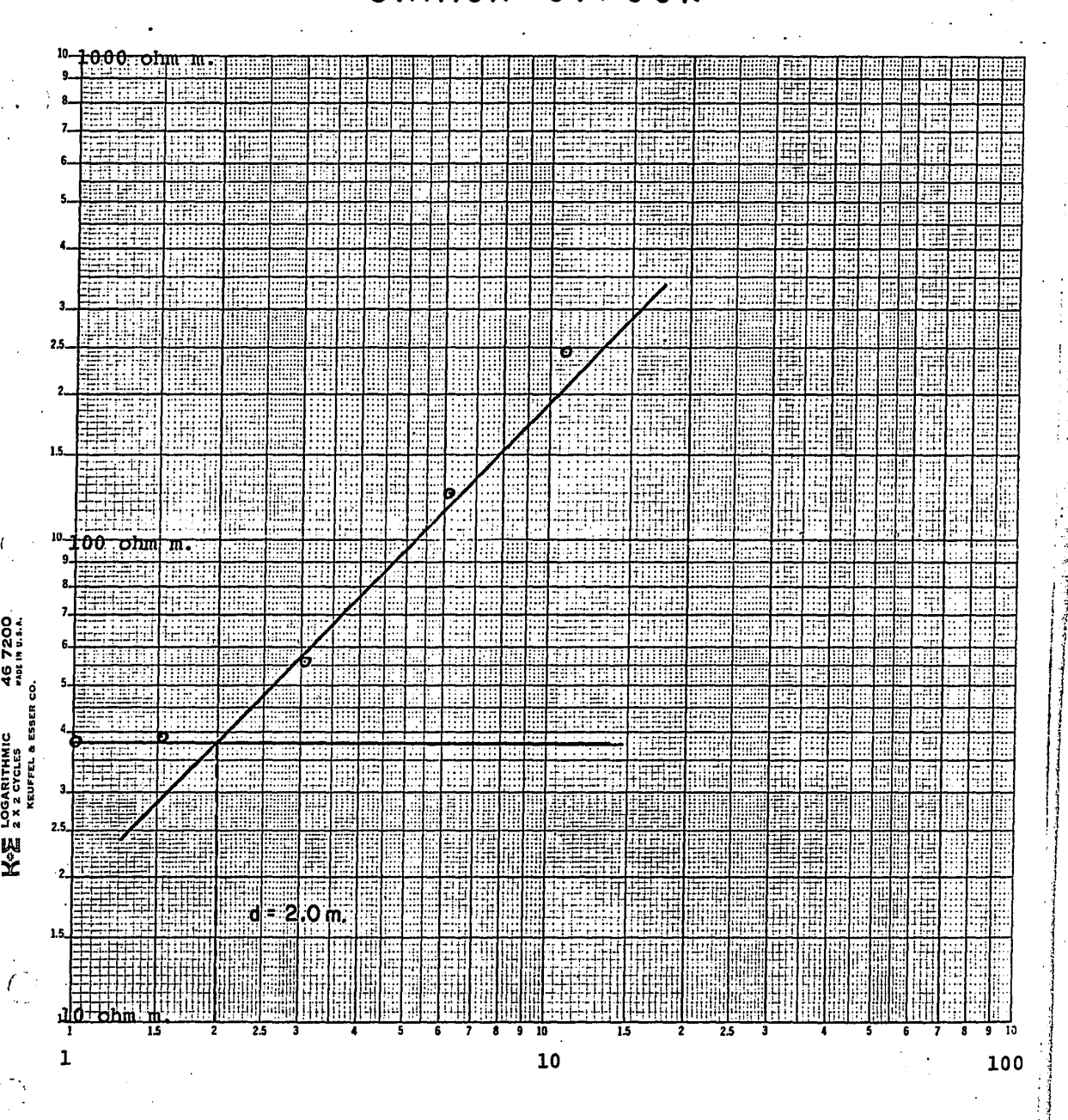
Electrode Spacing in Metres

LINE A-2 STATION 27+00N



Electrode Spacing in Metres

LINE A-2 STATION 34+00N



Electrode Spacing in Metres